Year : 2013

Assessing sedimentary evolution by means of Sr-isotope ratios – 3 case studies on the Caribbean Plate (Cretaceous: Nicoya Peninsula, Costa Rica, Tertiary: Hess Rise, and La Désirade, Guadeloupe, France)

Weber Philippe

UNIL | Université de Lausanne

Faculté des géosciences et de l'environnement
Institut des Sciences de la Terre

Assessing sedimentary evolution by means of Sr-isotope ratios – 3 case studies on the Caribbean Plate (Cretaceous: Nicoya Peninsula, Costa Rica, Tertiary: Hess Rise, and La Désirade, Guadeloupe, France)

Thèse de doctorat

présentée à la faculté des géosciences et de l'environnement
de l'Université de Lausanne

pour l'obtention du grade de

Docteur ès Sciences

par

Philippe Joseph Nicolas Weber

Maîtrise universitaire ès sciences - Géologie

Jury:

Prof. Eric Verrecchia - Président du jury
Prof. Peter O. Baumgartner - Directeur de thèse
Prof. André Strasser - Expert externe
Dr. Laszlo Kocsis - Expert interne

LAUSANNE, 2013

UNIL | Université de Lausanne
Décanat Géosciences et de l'Environnement
bâtiment Géopolis
CH-1015 Lausanne

IMPRIMATUR

Vu le rapport présenté par le jury d'examen, composé de

Président de la séance publique :	M. le Professeur Eric Verrecchia
Président du colloque :	M. le Professeur Eric Verrecchia
Directeur de thèse :	M. le Professeur Peter Baumgartner
Expert externe :	M. le Professeur Andreas Strasser
Expert interne :	M. le Docteur Laszio Kocsis

Le Doyen de la Faculté des géosciences et de l'environnement autorise l'impression de la thèse de

Monsieur Philippe Joseph Nicolas WEBER

Titulaire d'une
Maîtrise universitaire ès sciences – géologie
Université de Lausanne

intitulée

ASSESSING SEDIMENTARY EVOLUTION BY MEANS OF SR-ISOTOPE RATIOS – 3 CASE STUDIES ON THE CARIBBEAN PLATE (Cretaceous : Nicoya Peninsula, Costa Rica, Tertiary : Hess Rise, and la Désirade, Guadeloupe, France)

Lausanne, le 7 juin 2013

Pour le Doyen de la Faculté des géosciences et de l'environnement

Professeur Eric Verrecchia, Vice-doyen

Acknowledgements

I would like to thank the Swiss National Science Foundation for supporting this thesis (project 125130).

I hereby would like to sincerely thank Prof. Peter Oliver Baumgartner for accepting me as a PhD student. He encouraged, advised and motivated me during the last 4 years. I also would like to thank him for giving me the opportunity to travel to the field and conferences. It was a great experience.

A warm "thank you" to Prof. André Strasser and Dr. Laszlo Kocsis for accepting to be member of the jury of this thesis.

I thank Claudia Baumgartner-Mora. She did most, if not all the determinations of foraminifers that appear in this thesis.

I appreciated the availability, friendliness and patience of Dr. Massimo Chiaradia who helped me for the preparation of samples for TIMS measurements in the laboratory of Prof. Urs Schaltegger in Geneva, many thanks to him.

I am grateful to Dr. Jorge Spangenberg for his help in the Lausanne stable isotope laboratory. He was available when asked and always had a good advice.

A special thank to Dr. Follkmar Hauff and Dr. Werner Reinhard, for giving Erika and myself the opportunity to join the R/V Sonne cruise SO-208. Furthermore I also would like to thank him for the measurements on the TIMS device at the IFM-Geomar in Kiel.

I also would like to thank my colleagues, who helped me during the writing of this thesis and gave me great advices. These are Dr. Alexis Godet, Dr. Brice Lacroix and Dr. Antoine Quilichini.

A thought goes to Goran Andjic. We shared a lot of good moments in the field in La Désirade and in Costa Rica, now he takes over. Good luck!

I would also like to thank my family, especially my mother and my sister who encouraged me during all my studies. I would like to thank my father he encouraged me in the beginning of my studies and has always been a good example to me. He would have been glad to see me nowadays.

Abstracts

Assessing sedimentary evolution by means of Sr-isotope ratios – 3 case studies on the Caribbean Plate (Cretaceous: Nicoya Peninsula, Costa Rica, Tertiary: Hess Rise, and La Désirade, Guadeloupe, France)

Philippe Joseph Nicolas Weber - Université de Lausanne - Faculté des géosciences et de l'environnement - Institut des Sciences de la Terre

The understanding of sedimentary evolution is intimately related to the knowledge of the exact ages of the sediments. When working on carbonate sediments, age dating is commonly based on paleontological observations and established biozonations, which may prove to be relatively imprecise. Dating by means of strontium isotope ratios in marine bioclasts is the probably best method in order to precisely date carbonate successions, provided that the sample reflects original marine geochemical characteristics. This requires a precise study of the samples including its petrography, SEM and cathodoluminescence observations, stable carbon and oxygen isotope geochemistry and finally the strontium isotope measurement itself.

On the Nicoya Peninsula (Northwestern Costa Rica) sediments from the Piedras Blancas Formation, Nambi Formation and Quebrada Pavas Formation were dated by the means of strontium isotope ratios measured in Upper Cretaceous *Inoceramus* shell fragments. Results have shown average $^{87}Sr/^{86}Sr$ values of 0.707654 (middle late Campanian) for the Piedras Blancas Formation, 0.707322 (Turonian-Coniacian) for the Nambi Formation and 0.707721 (late Campanian-Maastrichtian) for the Quebrada Pavas Formation. Abundant detrital components in the studied formations constitute a difficulty to strontium isotope dating. In fact, the fossil bearing sediments can easily contaminate the target fossil with strontium mobilized form basalts during diagenesis and thus the obtained strontium isotope ratios may be influenced significantly and so will the obtained ages. The new and more precise age assignments allow for more precision in the chronostratigraphic chart of the sedimentary and tectonic evolution of the Nicoya Peninsula, providing a better insight on the evolution of this region.

Meteor Cruise M81 dredged shallow water carbonates from the Hess Rise and Hess Escarpment during March 2010. Several of these shallow water carbonates contain abundant Larger Foraminifera that indicates an Eocene-Oligocene age. In this study the strontium isotope values ranging from 0.707847 to 0.708238 can be interpreted as a Rupelian to Chattian age of these sediments. These platform sediments are placed on seamounts, now located at depths reaching 1600 m. Observation of sedimentologic characteristics of these sediments has helped to resolve apparent discrepancies between fossil and strontium isotope ages. Hence, it is possible to show that the subsidence was active during early Miocene times.

On La Désirade (Guadeloupe France), the Neogene to Quaternary carbonate cover has been dated by microfossils and some U/Th-ages. Disagreements subsisted in the paleontological ages of the formations. Strontium isotope ratios ranging from 0.709047 to 0.709076 showed the Limestone Table of La Désirade to range from an Early Pliocene to Late Pliocene/early Pleistocene age. A very late Miocene age ($^{87}Sr/^{86}Sr$ =0.709013) can be determined to the Detrital Offshore Limestone. The flat volcanic basement had to be eroded by wave-action during a long-term stable relative sea-level. Sediments of the Table Limestone on La Désirade show both low-stand and high-stand facies that encroach on the igneous basement, implying deposition during a major phase of subsidence creating accommodation space. Subsidence is followed by tectonic uplift documented by fringing reefs and beach rocks that young from the top of the Table Limestone (180 m) towards the present coastline. Strontium isotope ratios from two different fringing reefs (0.707172 and 0.709145) and from a beach rock (0.709163) allow tentative dating, (125ky, ~ 400ky, 945ky) and indicate an uplift rate of about 5cm/ky for this time period of La Désirade Island. The documented subsidence and uplift history calls for a new model of tectonic evolution of the area.

Etude de l'évolution sédimentaire par le biais des isotopes du Sr – 3 cas d'étude sur la plaque Caraïbe (Crétacé: la Péninsule de Nicoya, (Costa Rica) ; Tertiaire: Hauts-fonds de Hess et La Désirade, Guadeloupe (France))

Philippe Weber - Université de Lausanne - Faculté des géosciences et de l'environnement - Institut des Sciences de la Terre

Les datations par isotopes du strontium permettent de déterminer l'âge de roches carbonatées ainsi que de fossiles calcitiques et aragonitiques. Diverses études effectuées depuis une trentaine d'années sur des roches d'âge connues ont permis d'établir des courbes de référence montrant l'évolution des ratios des isotopes du strontium à travers le temps. Dès lors, si un ratio est mesuré, il suffit de le comparer avec ces courbes pour obtenir un âge. Cette méthode est très délicate car des contaminants, ayant des caractéristiques chimiques variables peuvent interférer et influencer les valeurs. Leur présence peut induire une mauvaise datation d'un échantillon.
Durant cette étude, cette méthode a été appliquée à des échantillons provenant de trois régions différentes des Caraïbes : de la Péninsule de Nicoya au nord-ouest du Costa Rica du haut fond de Hess et de La Désirade en Guadeloupe (France), afin de mieux comprendre les évolutions de ces régions.
Les différentes couches géologiques présentes sur la Péninsule de Nicoya au nord ouest du Costa Rica sont étudiées depuis plusieurs décennies. Leur contexte géologique est complexe: plusieurs entités géologiques de nature différente ont été accrétés depuis le Crétacé supérieur; l'accrétion de ces entités étant liée à la subduction de la plaque tectonique pacifique sous la plaque tectonique des Caraïbes. Cette étude a été effectuée afin de conforter et d'étendre des âges préalablement attribués par du microplancton siliceux et par des mesures radiogéniques. La présence de grands bivalves calcitiques, les Inoceramides, permet de dater les roches étudiées aux Crétacé supérieur. Finalement, la présence de matière siliceuse et de couches d'origine volcanique, constituant les contaminants, restreint les datations des isotopes du strontium, celles-ci étant très facilement influencé par leur présence. Néanmoins il a été possible de dater 3 formations, celle de Nambi, de Piedras Blancas et de Quebrada Pavas.
L'escarpement de Hess ainsi que le haut fond de Hess sont des structures géologiques peu étudiées. Ceci est lié à leur situation, des profondeurs de 2000 - 4000 m rendent un échantillonnage très difficile. Les échantillons sédimentaires étudiés sont des calcaires qui ont été formés dans de faibles profondeurs d'eau. Il s'avère que ces calcaires se sont déposés sur des volcans sous-marins. Connaître l'âge de ces calcaires est donc le premier pas vers une compréhension des événements qui ont placés ces roches à leur emplacement actuel. Cette étude a permis de contraindre l'âge de ces roches à l'Oligocène, il y a quelques 24-30 millions d'années. De plus, il a été possible d'indiquer qu'un affaissement ait eu lieu au plus tard au Miocène inférieur il y a quelques 20-22 millions d'années.
Le dernier sujet discute les calcaires de La Désirade en Guadeloupe, située à quelques encablures de la zone de subduction des Antilles. Sur base de mesures des isotopes du strontium, des âges précis ont pu être attribués aux couches géologiques de cette île. De plus, des récifs frangeants situés aujourd'hui à des niveaux d'élévation différents ont pu être datés. La datation de ces récifs permet de calculer la vitesse à laquelle cette île est sortie de la mer. Ayant déterminé un âge Miocène tardif à Pléistocène (5.20 - 2.40 millions d'années) des roches de La Désirade, il est possible de présenter un nouveau modèle d'ascendance et de subsidence qu'a du subir cette île. Cette étude montre que le sous-bassement de l'île se trouvaient un jour au fond de la mer, puis a été remontée à un niveau proche de la surface. Par la suite l'île dû subsidier afin de créer de l'espace pour la mise en place des roches calcaires. Finalement des contraintes géologiques ont fait remonter La Désirade à sa position actuelle.

INDEX

Figures

Tables

1. Introduction

The Caribbean tectonic plate is located between the North- and South- America. It is bordered by two subduction zones, one eastward tilting on the western part and an eastward tilting one on the eastern part. The northern and southern limits, two major overlapping/strike slip faults, separate this tectonic plate from the Americas (Pindell & Kennan, 2009). The subduction zones are characterized by two arcs, the Antilles Arc that initiated during the Early Cretaceous and the Central American Arc, which initiated during the Late Cretaceous (Buchs, *2008*).

This thesis focuses on different geologic topics, on the Nicoya Penisnsula, (Costa Rica), the Hess Rise and La Désirade Island (Guadeloupe) (Figure 1). These three case studies are common in their geographic localization, the Caribbean tectonic plate, and the applied method of strontium isotope dating. The method of $^{87}Sr/^{86}Sr$ dating has been applied because the known paleontological ages are either relatively poor or show wide age intervals, which can be refined by $^{87}Sr/^{86}Sr$ ratios measured on target fossils.

Figure 1: General overview map of the Carribbean Tectonic Plate with the locations of the three study areas, the Nicoya Peninsula (North-Western Costa-Rica), the Hess Rise and La Désirade (Gouadeloupe, France).

In Chapter 2 an introduction to the strontium isotope dating and Strontium Isotope Stratigraphy (SIS) presents the history of the method, its general aspect and principles. It also outlines the sample screening methods in order to confirm ages obtained by the $^{87}Sr/^{86}Sr$ ratios. This chapter is based on the different aspects that can be read in recent publications that have commonly been accepted in the field of strontium isotope geochemistry.

Chapter 3 presents the methods that were used during this study.

The first case study is presented in Chapter 4, which deals with the geology of the Nicoya Peninsula in northwest Costa Rica. Many studies done in this region concluded ages based on radiolarian assemblages, which provide rather large age intervals because of the absence of biostratigraphical assemblages in the Upper Cretaceous. In this case strontium isotope dating was used in order to better constrain and refine the ages of the formations that occur in the Southern Nicoya Peninsula and better understand the geology of the region. This work has been done in collaboration with Goran Andjic and is based on the former works of A.N. Bandini (2008), K. Flores (2003, 2003a, 2003b) and D. Buchs.

Chapter 5 synthesizes an age vs. facies correlation at the Hess Rise. Sediment samples collected by Prof. Peter O. Baumgartner during a scientific cruise organized by IFM-GEOMAR in Kiel during spring 2009 (Baumgartner and Baumgartner-Mora, 2010) have been described and dated by the means of strontium isotopes. The shallow water carbonates are supposed to be linked to the presence of seamounts, on which they deposited and once formed atolls. In this chapter are presented strontium isotope ages of the samples and a possible age of the initiation of the subsidence.

The Chapter 6 treats the local geology and tectonics of La Désirade, Guadeloupe (France). It shows the geologic features of this island and the methods that have been used in order to solve two different problems. The first one is the ages given to the carbonate sediments. According to the different groups working on La Désirade, different conclusions of ages through paleontological data have been obtained. Here, the strontium isotopes permit to date the La Désirade carbonates. Furthermore, the second problem, as to know the subsidence/uplift history of La Désirade, can be quantified through the ages given by strontium isotopes. This chapter is complementary to Baumgartner-Mora & Baumgartner (2011).

Chapter 7 is a general conclusion on the $^{87}Sr/^{86}Sr$ dating method used in this thesis. This Chapter presents how the common $^{87}Sr/^{86}Sr$ method was applied in this thesis and were major difficulties of strontium ratio dating can be encountered.

References

Bandini, A. N., Flores, K., Baumgartner, P. O., Jackett, S.-J. & Denyer, P., **2008**. Late Cretaceous and Paleogene Radiolaria from the Nicoya Peninsula, Costa Rica: a tectonostratigraphic application. Stratigraphy, 5, 3-21.

Baumgartner and Baumgartner-Mora, **2010**. Chapter 5.5, Sedimentary Rocks pp. 29-34; in Meteor-Berichte 11-8, CLIP - Origin of the Caribbean Large Igneous Province (CLIP) in connection with the geodynamic evolution of the Central Caribbean 78 pp.

Baumgartner-Mora, C., Baumgartner, P.O., **2011**. Latest Miocene-Pliocene Larger Foraminifera and depositional environments of the carbonate bank of La Désirade Island, Guadeloupe (French Antilles). Revue de micropaléontologie, 54, p.183-205.

Buchs, D. M., **2008**. Late Cretaceous to Eocene geology of the South Central American forearc area (southern Costa Rica and western Panama): Initiation and evolution of an intra-oceanic convergent margin. PhD thesis, Université de Lausanne, 1 - 230.

Flores, K., **2003**. Propuesta tectonoestratigráfica de la región septentrional del golfo de Nicoya, Costa Rica. Licenciatura thesis, University of Costa Rica, 1-176.

Flores., K., Denyer, P. & Aguilar, T., **2003a**. Nueva propuesta estratigráfica: Geología de las hojas Matambú y Talolinga, Guanacaste, Costa Rica. Revista Geológica de América Central, 28, 131-138.

Flores, K.., Denyer, P. & Aguilar, T., **2003b**. Nueva propuesta estratigráfica: Geología de la hoja Abangares, Guanacaste, Costa Rica. Revista Geológica de América Central, 29, 127-136.

Pindell, J.L., & Kennan, L., **2009**. Tectonic evolution of the Gulf of Mexico, Caribbean and northern South America in the mantle reference frame: an update, *in* James, K., Lorente, M.A., & Pindell, J., eds., Origin and evolution of the Caribbean Region: Geological Society of London, Special Publication, 328, 1–55.

2. $^{87}Sr/^{86}Sr$ in carbonate rocks and fossils

2.1. Strontium Chemistry

Strontium (Sr) is the 38th element of the periodic table and is a member of alkaline earths group (along with Be, Mg, Ca, Sr, Ba and Ra). The ionic radius of Sr^{2+}, which is about 1.13 Å, is close to the one of Ca^{2+} that is around 0.99 Å. Consequently strontium can replace calcium in minerals. The replacement of Ca^{2+} by Sr^{2+} is restricted by the strontium's favour for eightfold coordinate sites, whereas calcium can be incorporated in six and eightfold coordinate sites because of its smaller size (Faure and Mensing, 2004).

Strontium has four naturally occurring stable isotopes (^{84}Sr: 0.56%; ^{86}Sr: 9.87%, ^{87}Sr: 7.04% ^{88}Sr: 82.53%) from which only ^{87}Sr is radiogenic and derives from ^{87}Rb (Faure, 1986; Veizer, 1989). The abundance of the ^{87}Sr isotope can slightly vary because of this radiogenic decay (Capo *et al.*, 1998) and the strontium isotopic composition of a mineral or rock containing Rb then depends on its age and Rb/Sr ratio (Faure and Mensing, 2004).

The decay of ^{87}Rb produces his daughter isotope, ^{87}Sr, by emission of a Beta particle (electron), which has a half-life period of 58.8 Ga. ^{87}Rb is incompatible in the mantle; this is why the upper crust is enriched. Commonly old cratons have relatively high ^{87}Rb, hence $^{87}Sr/^{86}Sr$ ratios contents compared to the average sea-water strontium ratio (Faure, 1986; Veizer, 1989; Faure and Mensing, 2004).

2.2. Strontium cycle in marine waters

Because of the radiogenic decay, which produces ^{87}Sr, the alteration product of cratons will provide a $^{87}Sr/^{86}Sr$ influx that is above the marine average, between 0.710 (McArthur, 1998) and 0.7116 (Banner, 2004). It is admitted that high $^{87}Sr/^{86}Sr$ ratios are characteristic for a stream or river influx, but they depend on the mineral composition of bedrock and climatic factors (Palmer and Osmond, 1992). The chemical composition of the river influx depends on the chemical and isotopic composition of drainage basins. If rocks with different isotopic compositions are crossed, the resulting composition will be a mix of these drained basins (McArthur, 1994, 1998; Faure and Mensing, 2004). Variations in the strontium isotope composition of rivers or lakes can be explained by the spontaneous deposition of ash layers or lava extrusion in the drainage basin, the exposure or removal of isotopically different rock

formations by erosion and deposition of glacial or eolian sediments from a distal origin (Faure and Mensing, 2004).

On the contrary, mid ocean ridge activity, where the exchange between seawater and ocean crust generally occurs (Shields, 2007), will considerably lower the average marine $^{87}Sr/^{86}Sr$ ratios, the inherited strontium isotopic signature will tend towards the ratios of the depleted mantle (Spooner, 1976) (Figure 2). Consequently, the average strontium isotopic ratios ranges between 0.703 (McArthur, 1998) and 0.7037 (Banner, 2004).

Also, the diagenesis of marine carbonates is considered as being important to the general $^{87}Sr/^{86}Sr$ variations in seawater. The average value of this source is ~0.708 (McArthur, 1994), because these carbonates already have an average $^{87}Sr/^{86}Sr$ that is put back into the system when they get dissolved (Figure 2).

Another source that can be separately discussed is the dissolution of carbonate rocks and evaporitic sulphates, which may be considered as the major source for strontium in the oceans because of their high strontium content and high solubility (Brass, 1976; Shields, 2007). The strontium isotope ratio resulting from this dissolution (~0.708) is close to that of Phanerozoic seawater ($\sim 0.708 \pm 12 * 10^{-6}$) (Peterman *et al.*, 1970) and is not taken into account when interpreting $^{87}Sr/^{86}Sr$ trends (Veizer and MacKenzie, 2003, in Shields, 2007)(Figure 2).

The two main poles for strontium isotopic ratio variations are then the hydrothermal exchange with oceanic crust and the continental weathering because of their extreme low and high strontium isotope ratio, respectively. If diagenesis of marine carbonates provides a negligible input of $^{87}Sr/^{86}Sr$ compared to the two main sources (Figure 2), its average value will not change significantly the worldwide ratio (Banner, 2004; Faure and Mensing, 2004, McArthur, 1994, 1998). The same remark is true for the dissolution of carbonate rocks and evaporitic sulphates.

An exact influx cannot be quantified, i.e. it is impossible to measure the exact riverine input, even the 200 largest rivers in the world as they only account for 60% of the global input (Lasaga and Berner, 1998). The river input also depends on the global climate, the isotopic evolution of the crust, the susceptibility to weathering, the age of the rocks and the strontium content of the exposed parts of the crust (Shields, 2007).

The input quantities do not vary significantly according to the different authors that mention them; they are around 1×10^6 tons/year (1.2×10^{10} mol Sr/y) for the hydrothermal input, 0.3×10^6 tons/y (0.34×10^{10} mol Sr/y) for the diagenetic input and 3×10^6 tons/y (3.4×10^{10} mol Sr/y) for the river input (McArthur, 1998, Banner, 2004) (Figure 2).

The mixture of alteration/erosion and volcanic/mid ocean ridge activity has a direct effect on marine $^{87}Sr/^{86}Sr$, as erosion increases the strontium isotopic ratio and hydrothermal volcanic activity at mid ocean ridges lowers the strontium isotopic ratio. The strontium isotope ratio is considered to be the same worldwide for a given time, because the residence time of Sr is about 10^6 years, far longer than the mixing time of the ocean waters, in the order of 10^3 years (Raymo *et al.*, 1988, Palmer and Edmond, 1989; Holland, 1984; Hodell *et al.*, 1989; Berner and Rye, 1992; McArthur 1994; Banner, 2004). Additionally, the strontium records show a cyclicity of about 60-70 Ma throughout the Phanerozoic (Prokoph *et al.*, 2008).

Consequently, irregular variations of the strontium isotope ratio can be observed through time (Prokoph *et al*, 2008; McArthur, 1994, 1998; Faure and Mensing, 2004). A strontium isotope curve may therefore have a chaotic appearance. Variations can always be explained by major volcanic/tectonic/orogenic events (Figure 4,
Figure 5), (McArthur, 1994; Hochard *et al.*, 2011; Vérard *et al.*, 2011).

As a consequence, strontium isotope ratios for age determinations can only be measured in marine sediments, preferably carbonates because they are exceptionally rich in strontium, up to 7000 ppm, (Faure *et al.*, 1978, Shields, 2007). Also biominerals are very important to $^{87}Sr/^{86}Sr$ dating because they precipitated in equilibrium with seawater and should therefore reflect the original marine seawater $^{87}Sr/^{86}Sr$ ratio. In general, for a given age, there is a "unique" value of strontium isotope ratio, which makes it possible to use strontium isotope ratios as a rock-dating tool. The other way around, for a given strontium ratio, multiple ages are possible. This has to be considered when working with $^{87}Sr/^{86}Sr$.

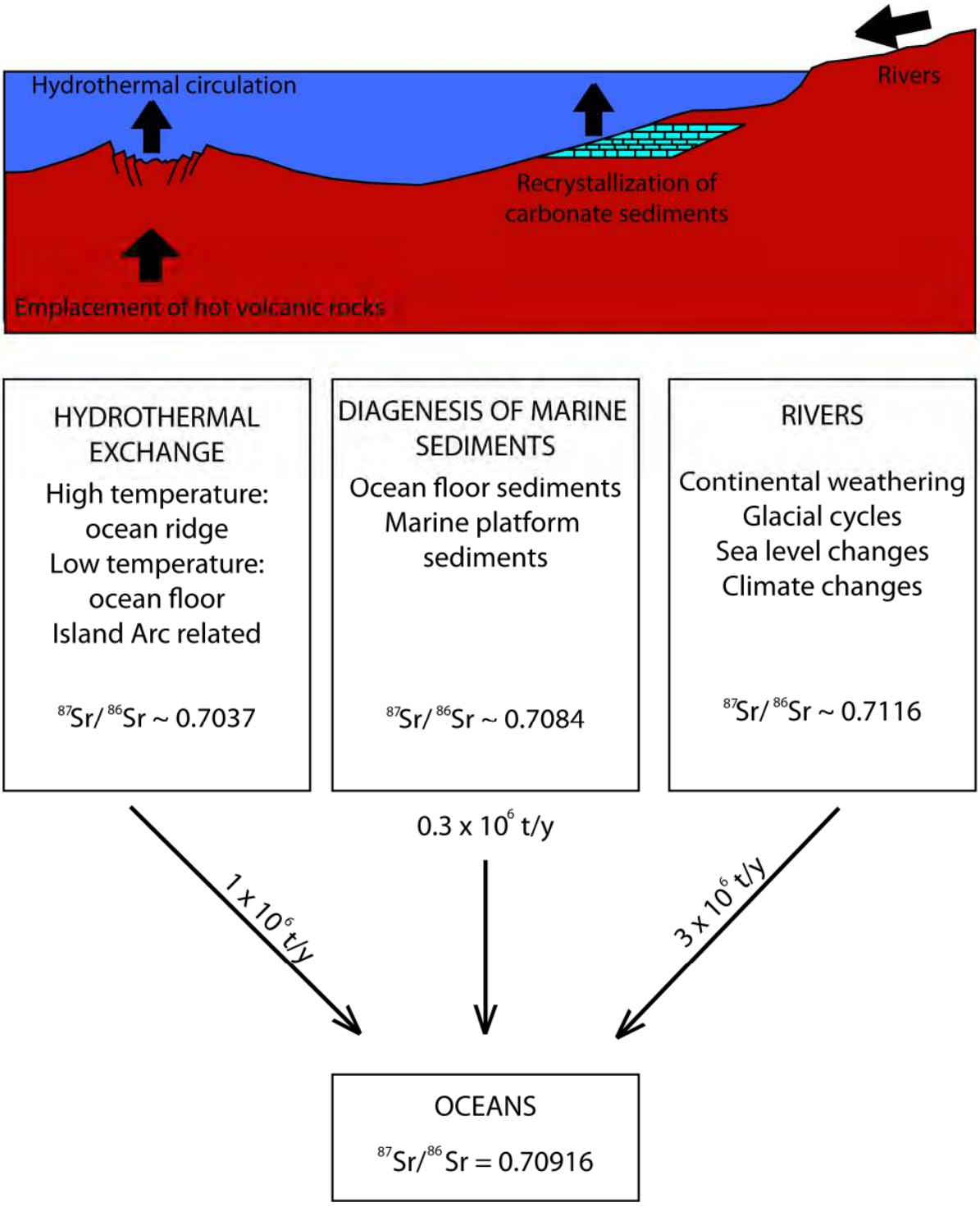

Figure 2: Strontium cycle with the corresponding quantities of the marine, river and diagenetic input (after Banner, 2004 and McArthur, 1998). In general, ridge activity will lower the strontium isotope ratio, whereas a continental influx will increase the ratio. The marine values of strontium isotope ratios are an average of these two main sources.

2.3. **Strontium Isotope Stratigraphy (SIS)**

Strontium Isotope Stratigraphy (SIS) has known a considerable improvement over the last three decades and has made its proofs as a high-resolution method for sediment dating and correlation between different sedimentary series (Burke *et al.*, 1982; De Paolo and Ingram, 1985; Elderfield, 1986; McArthur 1994; Smalley *et al.*, 1994; Veizer *et al.*, 1997; Frijia and Parente, 2008; Prokoph *et al.*, 2008, Hodell *et al.*, 1991).

A detailed history of the use of SIS has been described by McArthur (1994), and completed by McArthur (1998), Veizer *et al.* (1999), Banner (2004) and Prokoph *et al.* (2008).
Wickman (1948) suggested a linear increase of strontium isotope ratios, as the oceans are the depositary of continental weathering input, which includes strontium isotope ratios, that are greater than the marine $^{87}Sr/^{86}Sr$, and are reflected in precipitated sediments (in McArthur, 1994). This idea was contradicted later, because positive and negative variations of $^{87}Sr/^{86}Sr$ through Phanerozoic times have been observed (Faure *et al.*, 1967; Peterman *et al.*, 1970, in Brass, 1976).

Some early works were made on the sources of the strontium isotope ratio. Positive ratio trends have been related to a chemical weathering possibly due to orogenic tectonics, while negative trends have been explained as hydrothermal activity related to tectonic/mid-ocean ridge activity (Brass, 1976; Raymo *et al.*, 1988, Palmer and Edmond, 1989; Hodell *et al.*, 1989; Berner and Rye, 1992; Jones and Jenkins, 2001). Worldwide strontium isotope ratio curves have been compiled in order to date marine sediments with strontium isotope ratios (Burke *et al.*, 1982, McArthur *et al.*, 2001, Veizer *et al.*, 1999, Prokoph *et al.*, 2008 amongst others).

The average strontium isotopic ratio measured in marine sediments has never reached the high $^{87}Sr/^{86}Sr$ of the continental crust neither the low values of the oceanic crust (Banner, 2004). This in fact proves that strontium in the oceans is continuously mixed and the influx of the sources has considerably varied during time (Banner 2004; McArthur, 1994, 1998; Veizer *et al.*, 1999).
A strontium isotope ratio curve shows major negative and positive variations (e.g.,Figure 4,

Figure 5), which may be attributed to major tectonic events (orogeny or mid ocean ridge activity). Minor fluctuations can be related to climate changes that would increase/lower the chemical weathering and/or glacial weathering (Banner, 2004).

2.4. **Strontium curves**

Two worldwide and long-term strontium isotope ratio curves are presented here. The first one is based on the work of McArthur *et al.* (2001) and the second one is based on the work of Prokoph *et al.* (2008). Both curves range from the actual marine strontium ratios to an age of 509 and 500 Ma for McArthur *et al*. (2004) and Prokoph *et al.* (2008), respectively (Figure 4, Figure 5).

2.4.1. McArthur Curve

The LOWESS curve from McArthur et al. (2001) is based on works of different authors. The strontium vs. age data used for this thesis is from the "SIS LOOK-UP TABLE: Version 4: 08 / 04",(Howarth and McArthur, 1997; McArthur et al., 2001) that has kindly been given by J.M. McArthur (Figure 3, Figure 4
Figure 5). McArthur and co-workers integrated original Sr isotope data, and obtained a curve that can globally be used to date marine carbonate sediments and calcitic or aragonitic fossils with their strontium isotope ratios. This curve has some advantages and limits.
The first advantage is the covered time interval that ranges through the entire Phanerozoic. In fact there are no gaps in the curve (Figure 3, Figure 4), as regressions allow having strontium isotope values between two data points, and therefore a given ratio always has a corresponding age. The different calculated ratios are separated by 50 Ka intervals, which lead to a very high precision. Another advantage is the 95% confidence interval that allows considering the main curve with an upper and lower error bar (Figure 3). When plotting data on the curve, this error in addition with the analytical error provides a total age error of the geologic samples. All the data points are normalized to the same standard (NBS 987 standard of 0.710248), which leads to an input data that is homogenized. Furthermore, samples measured for strontium isotope dating have to be adjusted to this value in order to define correct ages of a sample.

Disadvantages of the curve appear when the original data on which regressions are based on are sparse. The general aspect of the curve can questioned when just few data points define the curve (e.g., Eocene). In fact, the confidence interval is then wider and the ages that can be read on the curve have a higher error. Of course in times where large amounts of data exist, the curve can be considered as very trustful. The Neogene for instance is very suitable because the number of measured ratios is impressive. When working on old rock formations, the data points defining the curve are sparse, deducted ages might then have a lower precision due to the higher alteration degree of an old rock compared to a younger rock (McArthur and Howarth, 2004).

One has to keep in mind that when building the curve, the authors selected data they evaluated as trustful and useful, hence scientific subjectivity has to be taken in account as well.

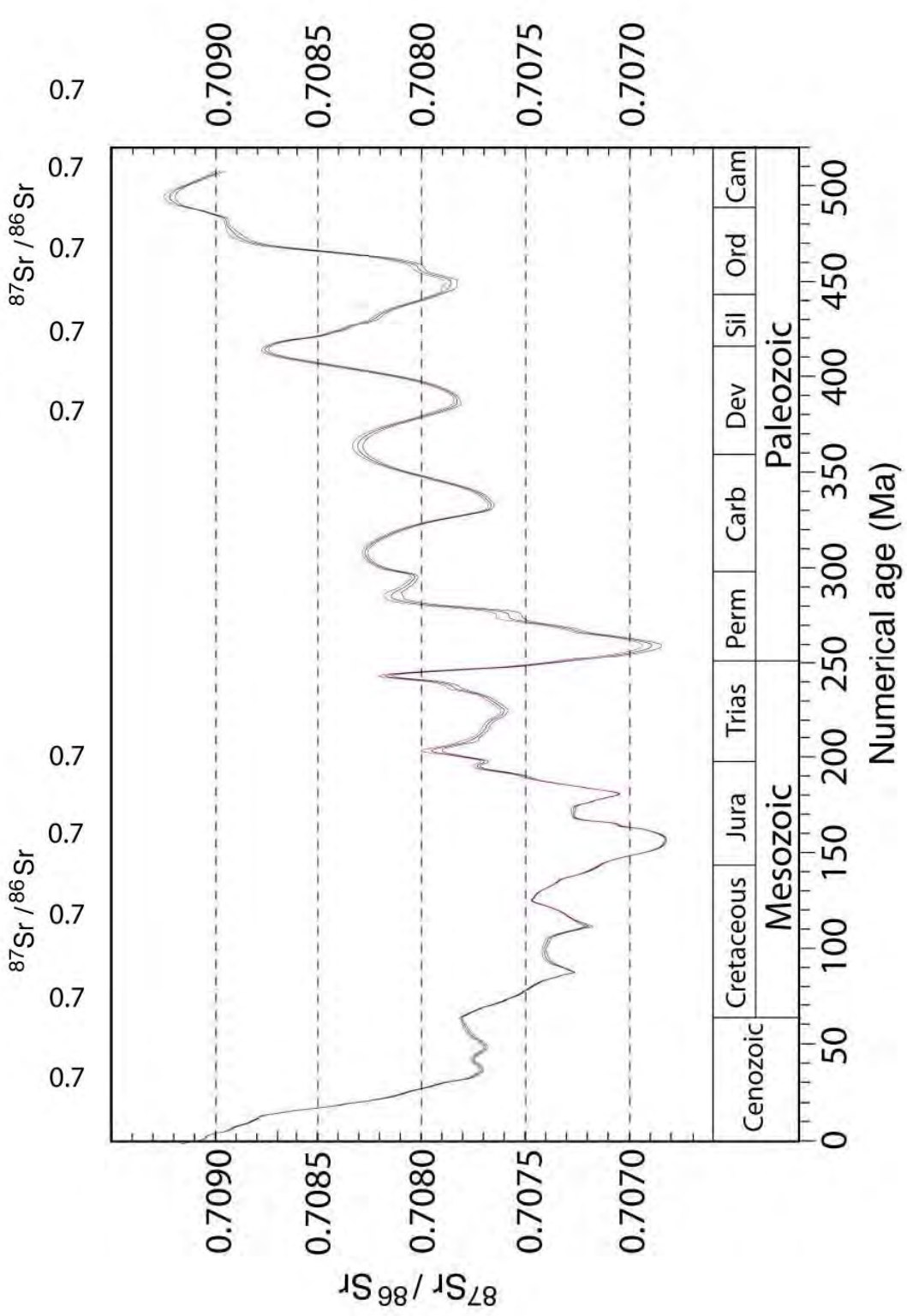

Figure 3:Mc Arthur LOWESS curve with 95% confidence interval (represented by blue and red line)

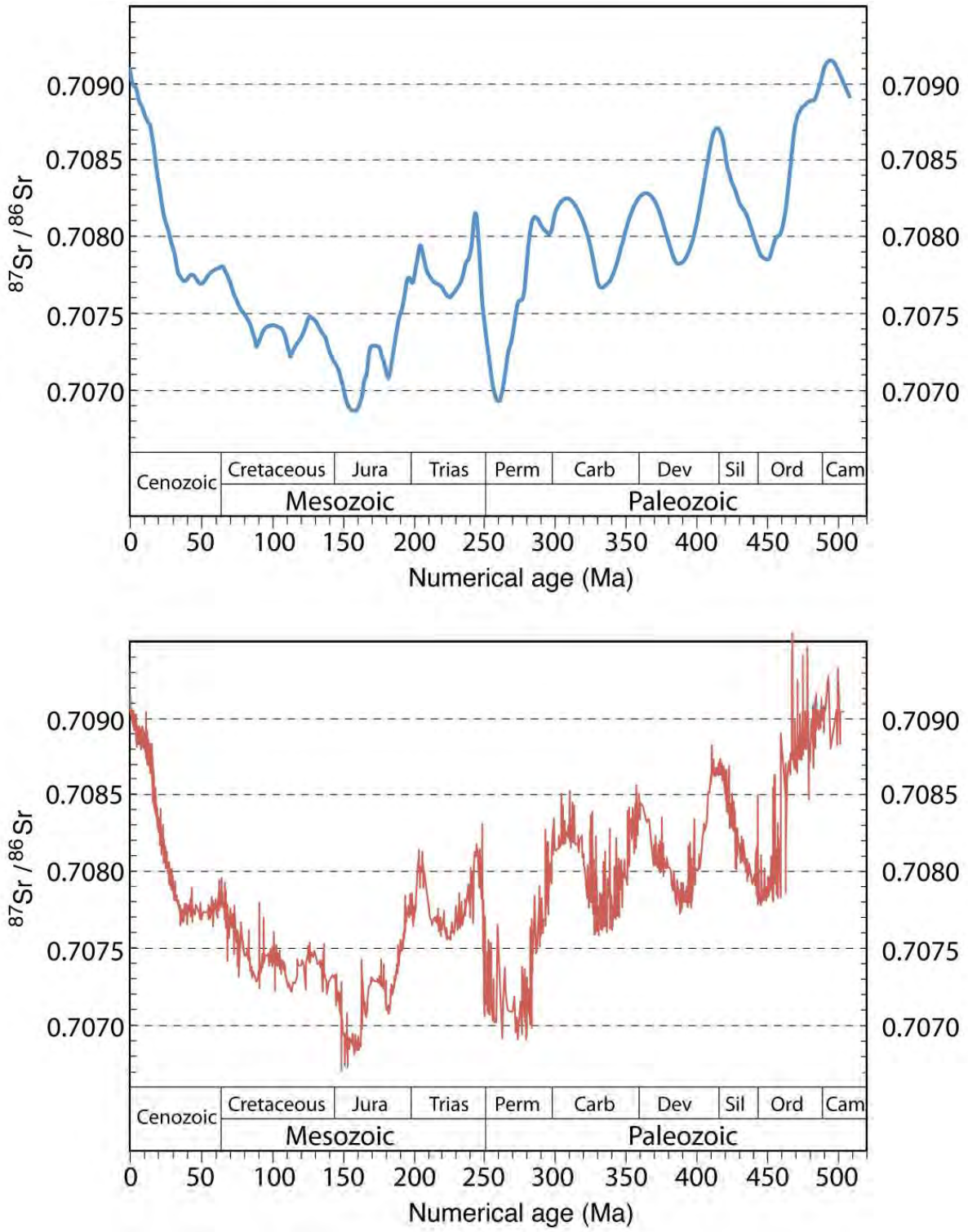

Figure 4: McArthur LOWESS curve (on top), Prokoph curve (on bottom). Both curves show the same general trends. The LOWESS curve is smoothened, based on the values of various authors. The Prokoph curve has a more hacked aspect, no smoothing has been applied to these values.

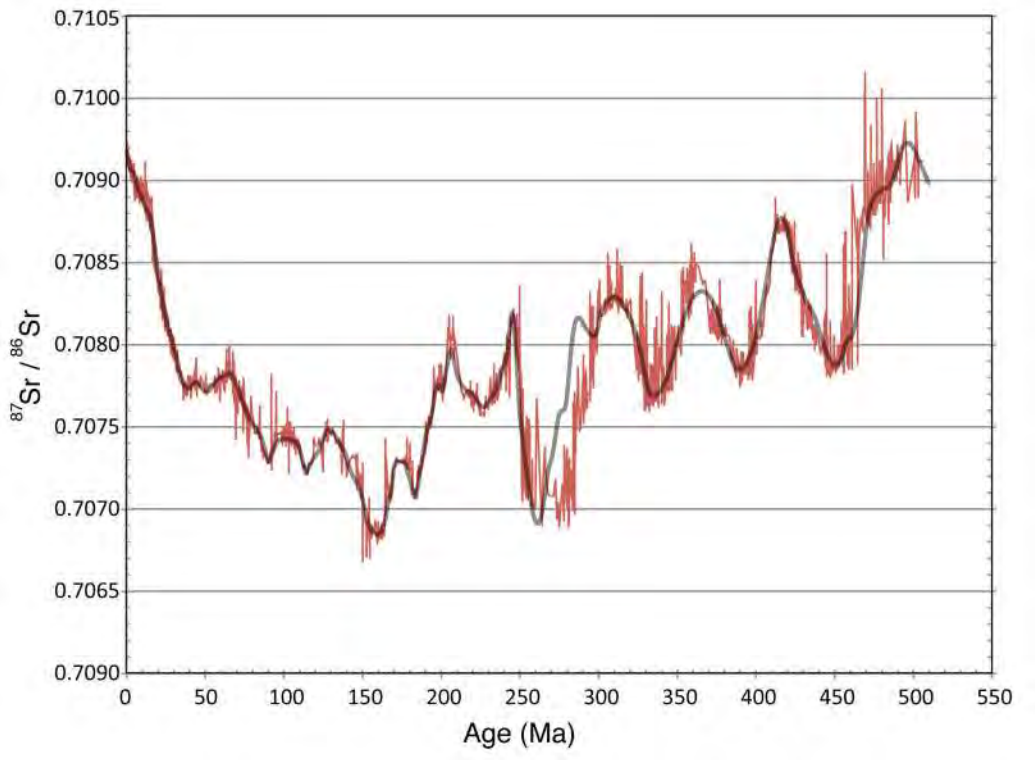

Figure 5: McArthur (blue) vs. Prokoph (red) curve plotted on same graph, the general trends are the same, except in the 280-260 Ms interval, where the values of Prokoph are significantly lower than those of the LOWESS curve. No reason for this difference could be assigned.

The differences between these two global curves on strontium isotopic ratios explained above, lead to the conclusion that the "SIS LOOK-UP TABLE: Version 4: 08 / 04",(Howarth and McArthur, 1997; McArthur *et al.*, 2001), is the most appropriate tool to date with SIS. Of course it has some disadvantages (see 1.4.1) that have to be considered when using it, but it remains the most suitable curve for SIS.

2.5. Example of the Neogene

Hodell *et al*. (1989b) observed a sharp increase of $^{87}Sr/^{86}Sr$ over the last 40 Ma, which they linked to the Himalayan orogeny. An orogeny such as the Himalaya affects the climate and consequently the weathering (Evans *et al.*, 2001). Furthermore, the Himalaya is known to be constituted of rocks with various Sr isotope compositions that influence positively the Sr isotope ratio of its draining rivers (silicates, carbonates and evaporites) (Singh *et al.*, 1998; Karim and Veizer, 2000). According to Banner (2004), the increases that can be observed during the Late Eocene and Early Miocene are related to the uplift of the Tibetan Plateau. He

mentions the implications on the weathering rates and climate changes (minor or major) induced by such an orogeny. Also, the strontium isotopic composition of the draining rivers has influences on the global strontium isotopic ratio (see also Raymo *et al.*, 1988; Raymo and Ruddiman, 1992; Edmond, 1992; Richter *et al.*, 1992; Richter and Turekian, 1993; Raymo, 1994; Derry and France-Lanord, 1996; McCauley and DePaolo, 1997; Zachos *et al.* 1999). McArthur (1998) on his side rejects this idea, because the Himalayan Mountains were not significant before the Miocene and the rapid rise in $^{87}Sr/^{86}Sr$ started in the late Eocene. However, he does not suggest any other alternative.

2.6. **Terminology**

The term of Strontium Isotope Stratigraphy (SIS) may be misleading, because it implies a stratigraphic work. This may not be true for every study because single outcrops or samples can be dated with strontium isotope ratios. Some authors use the term of radiogenic dating, which is also inappropriate, because it implies a calculation of half-life period. Therefore, the term of $^{87}Sr/^{86}Sr$ ages or $^{87}Sr/^{86}Sr$ deduction (because the resulting ages are derived) may be more appropriate. Strontium isotope ratios are measured and then compared to the existing worldwide strontium isotope curves in order to obtain meaningful ages.

2.7. **Problems of the relativity of ages**

Farrel *et al.* (1995) already describe the problematic of SIS due to stratigraphic, chronostratigraphic, alteration and analytical problems. The best way for obtaining a strontium curve is to combine multiple deep sea records of foraminifera and bulk rock calcium carbonates (Hess *et al.*, 1989; Hodell *et al.*, 1991; Richter *et al.*, 1992; in Farrel *et al.*, 1995). These authors point out the importance of the erroneous chronostratigraphic correlations among sites.

The problem lies in the fact that a geologic timescale is in some cases based on relative ages of First Appearances and Last Occurrences of a certain species. From the moment where biozonation interferes with absolute ages, the numerical age obtained is consequently also relative. Of course with the ongoing paleontological works, biozonations are constantly renewed and the derived ages also change; therefore, strontium isotope ratios calibrated on a

relative age, might then be shifted. The derived age in the global strontium curve should be constantly reevaluated.
Of course this has to be considered when dealing with $^{87}Sr/^{86}Sr$, but permanent progress from the part of paleontologists in order to define precisely foraminifera biozones should facilitate this work. If ages derived from strontium isotopic ratios are based on wrongly interpreted biozones, shifts have to be considered for the absolute age too. On the other hand, most of the ages from the International Stratigraphic Chart are derived from radiometric dating.

2.8. **Problems encountered with the curve**

The question of the age of a sample, that most of the people would like to answer through strontium isotope dating, has to be addressed in a larger manner, before strontium isotope ratios are measured. The origin of this problem lies in the fact that a single strontium isotope ratio can have multiple ages. It is important to constrain the age of the sample before measuring any values. The better the age is constrained before, the easier it gets to date with strontium isotopes. Some examples of this problem are shown in Figure 6 where, for a relatively short period of time, two or in some cases even more ages can be derived from the same $^{87}Sr/^{86}Sr$ value. Of course while working with strontium isotope ratios, it is very useful to define the age range before dating with $^{87}Sr/^{86}Sr$. This may be done by any other geological method or technique available.

The precision of the curve, the slopes of the curve and the analytical quality have an influence on the derived age (McArthur, 1998).
Generally and independently of which curve is used, the steeper the general trend is, the easier it is to put an age on a value. In contrary, if the curve is flat, the age of a sample will be less constrained, even with a very low analytical error (Figure 7).
The analytical error combined with the error of the curves will give an age with a numerical age error. The more precise an analysis is, the better the age constrain will be, in the case of a steep curve. If the curve is relatively flat, the error of the ages will be defined mostly by the curve.

Another problem of a curve is the number of measured points for a given time period. In general, when a large number of data-points define the line, the curve can be assumed as very

precise, because the interpolation of data between two points is very close to the original value (e.g. Neogene). In contrary, when just few points define the curve care has to be taken when interpreting the strontium isotope ratios because the interpolation between two points defines a line which in some way is out of control. In this case, the interpretation of ages has to be discussed precisely and carefully (Figure 8).

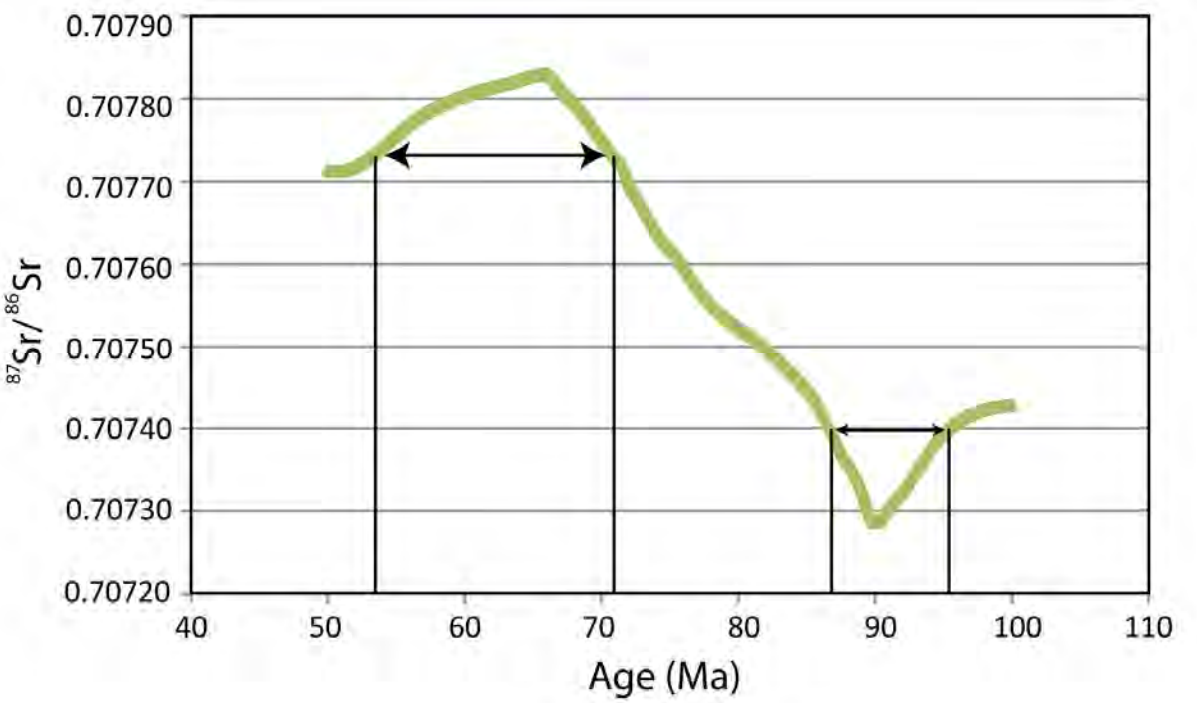

Figure 6: Graph showing the possibility of multiple ages for one single strontium isotope ratio depending on general aspect of the curve, which occurs often during the Phanerozoic. Unfortunately a difference can only be made if an age constrain exists prior to the strontium isotope age determinations. When facing this kind of problem, the strontium isotope ages provide a relatively wide time range and lose precision.

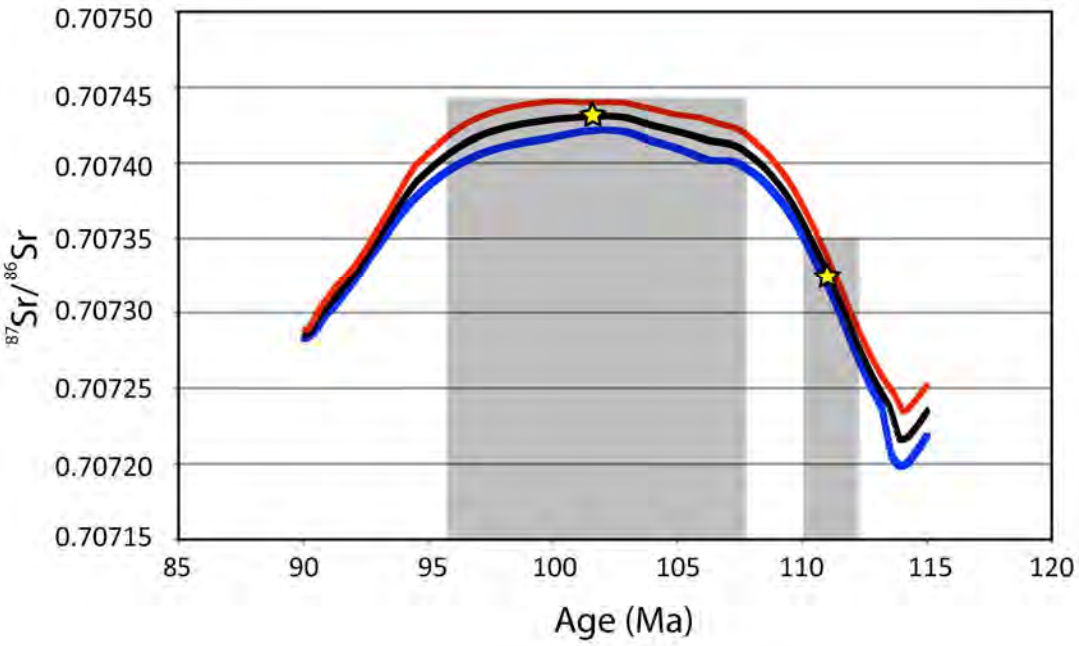

Figure 7: Problem of steep vs. flat curve (the red and blue line define the 95% Confidence Limits). This graph shows that depending on the aspect of the curve, a precise age determination cannot be done, because the curve itself determines the age interval. Even with a very good measurement, with very small deviations, the resulting dating can have a wide time range, defined by the curve.

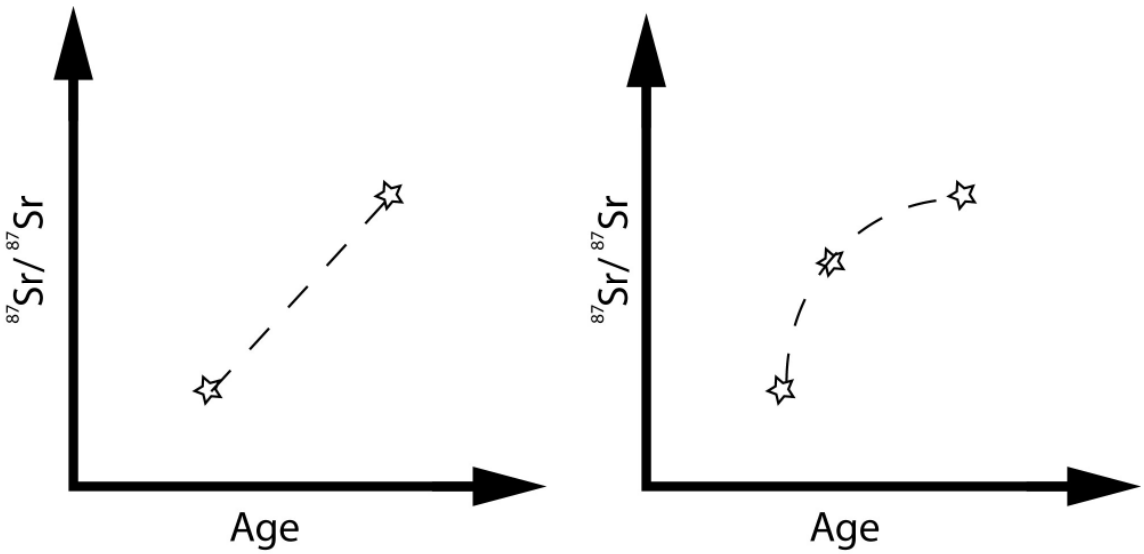

Figure 8: Simplified illustration of the problem of the number of defining data. It is commonly accepted that a regression between two points that are in a 5 Ma time interval can be used to define the curve (McArthur et al, 2005), This case shows that an additional strontium isotope ratio plotted on such a regression might considerably change the aspect of the strontium isotope curve.

2.1. **Sample types**

For fossils, the first point to take care of is the sampling. Different criteria have to be considered depending on the type of samples. Bulk rock studies have been controversial for many years but more and more of published data include bulk-rock analyses using appropriate dissolution techniques (McArthur, 1998; Bailey *et al.*, 2000; Li *et al.*, 2011).

Biogenic samples may include:

- Foraminifera are unsuitable to use, as they are small, and no separation of an original shell and a contaminant or alteration coating can be done properly (McArthur, 1998). Also, in some time lapses, ages are well constrained with planktonic foraminifera, and consequently strontium isotope ratios would be measured in order to calibrate the curve. Microfossils are also difficult to drill and even when possible, the amount of drilled powder is relatively low. Often a same specimen cannot be used for multiple purposes ($^{87}Sr/^{86}Sr$, stable isotopes, major and trace element evaluation in liquid mode). Foraminifera from a same species have to be picked from a same sample in order to perform analyses.

- Macrofossils or Low-Mg calcite (LMC) are very suitable for SIS, as they are easy to handle due to their size. Often it is possible to do thin sections through fossils and observe parts of remains with a Scanning Electron Microscope (SEM) in order to check the preservation of the shell. Another advantage with macrofossils is the possibility to gain a high amount of powder and so measure the same homogenized powder with different techniques. LMC is very useful for strontium isotope dating, because it is resistant to alteration and can give hints on a potential diagenesis (McArthur *et al.*, 1994; Veizer *et al.*, 1997, Boix *et al.*, 2011).

- According to McArthur (1998), apatite is very suitable for $^{87}Sr/^{86}Sr$ study because it is very resistant to alteration. However, Martin and Scher (2004) explain that for many time intervals, $^{87}Sr/^{86}Sr$ values of fish teeth have an offset both, from the global seawater ratios and contemporaneous foraminifera, towards the pore fluid $^{87}Sr/^{86}Sr$. This offset presumes a continuous reprecipitation and exchange between the apatite

and the pore fluid during burial. Dating is only possible when using the enamel because it is made of fluor-apatite, which is the most resistant part to alteration (Posner *et al.*, 1984, Venneman *et al.*, 2001). Strontium isotope ratios measured in apatite can be used either for an environmental study or for dating (e.g. Vennemann *et al.*, 2001; Kocsis *et al.*, 2009a,b).

- Based on Whittacker and Kayser, (1993) and McArthur *et al.*, (1994), McArthur (1998) recommends that aragonitic samples such as cephalopods are best to be avoided; "one can have the Devil's own time with these beasts" (McArthur, 1994, p.333).
  (N.B.; In fact, e.g. gastropods can be very tricky, not only because of the aragonitic shell but also because of the terrestrial and/or marine habitat of those animals).
  But, aragonite often is a very good marker of alteration in the field and if the preservation is confirmed, there should be no opposition for SIS dating.

Bulk rock analyses can be done either on a powdered sample of whole rock or a selected mineral:

- Barite is suitable for strontium isotope dating, because it is very robust to diagenetic effects. It can be used in carbonate-free abyssal sediments, as it is the only mineral that can preserve the marine isotopic ratio of strontium in these environmental conditions (Paytan *et al.*, 1996, in McArthur, 1994; McArthur, 1998, Paytan *et al.*, 2002). Barite is rarely preserved in sediments accumulated in shallow settings. Consequently, dating sequences on continental margins is then very limited (McArthur, 1998). It cannot replace calcite as a tracer but it might be useful when calcite is rare or affected by diagenesis (Martin *et al.*, 1995a). Care has to be taken because barite can have hydrothermal origins and the $^{87}Sr/^{86}Sr$ isotope ratio would then be much lower than the seawater ratio (Martin *et al.*, 1995a). The origin is reflected in the strontium and sulfur isotopic composition of barite (Paytan *et al.*, 2002).

- Bulk rock samples often have lower strontium concentration than e.g. fossils, but the ratio should correspond to the original marine value; the measured ratio reflects the average $^{87}Sr/^{86}Sr$ ratios of its composing minerals. Special care should be given when

measuring strontium isotope ratios on bulk rock because there is no control on the dissolution of contaminants (e.g. secondary calcite) that can considerably alter the $^{87}Sr/^{86}Sr$ value (McArthur, 1998; Bailey *et al.*, 2000). On the other hand, if there is any possibility to separate minerals in a bulk rock sample, and using a proper sampling and dissolution method, the success rate for bulk rock analyses can be relatively high (Li *et al.*, 2011). The right washing method of e.g. chalk, carbonate ooze and phosphorite may remove contaminants (McArthur, 1998; Bailey *et al.*, 2000). Early marine sediments should not alter the isotopic ratio as it is assumed the isotopic ratio of pore fluid should be the same or close to the overlying marine value (McArthur, 1998). In some cases, strontium isotope ratios of bulk rock analyses were used in order to date cementation phases (e.g., Brigaud *et al.*, 2009).

McArthur (1998) presents foraminifera as easily contaminated because of their hollow shell and their small size, which make them difficult to be properly cleaned. An important fact he points out is the reprecipitation of foraminifer's shells and the presence of clay; reprecipitation shells can be used in the case of carbonate rich sediments, the measured strontium isotopic ratio is generally derived from the encasing sediment and should then be close or equal to the original one. The presence of clay is considered as a contaminant as it can have a major influence on the ratio.

The statement of McArthur (1998) about reprecipitation might be true for every sample and not only for foraminifers. If there is any control on the reprecipitation of samples, it is then possible to consider the ratio as homogenized within one layer and should not vary significantly.

Independently on what is described above, in the field there is often no choice on what sample and what fossil is collected and no perfect sample for strontium isotope ratio measurements can be found. One should remember that every sample has the potential of giving a correct age when dating with strontium isotope ratios but special care has to be given. A detailed screening of every sample has to be done in order to proof the correctness and reliability of the strontium isotope ratio and the potentially deducted age.

Samples taken on the field should already be chosen wisely because e.g. aragonitic samples are very good indicators of low diagenetic impact. If a primary aragonitic structure is observed on the field, the possibilities to date the sample are potentially good.
Fossils with a calcium carbonate shell structure should show primary crystallization prisms. This primary structure can be checked later in laboratory with Scanning Electron Microscope (SEM) or cathodoluminescence.

Smalley *et al*. (1994) differentiate three categories of samples that can be used for SIS. A first category with high reliability of sample types susceptible to preserve a $^{87}Sr/^{86}Sr$ ratio includes belemnites, non-luminescent brachiopod shells, well-preserved tests of foraminifera in deep sea-sediment, red algae, massive anhydrite in marine evaporite and rudist bivalves. A second category with medium reliability of $^{87}Sr/^{86}Sr$ preservation contains luminescent brachiopod shells, thick-shelled bivalves (oysters) and conodonts with alteration traces. The third category includes all types of samples with a low reliability of strontium isotopic ratio conservation with highly altered conodonts, thin-shelled bivalves, fish teeth, echinoids, ammonoids, disseminated anhydrite, foraminifera tests in deeply buried sandstones, whole-rock samples of limestone and chalk. Echinoids are to be used with care; their High Magnesium Calcite (HMC) shell is more sensitive to dissolution processes. Meanwhile, it has been proven that whole rock samples and chalk may give correct strontium isotope ratios (McArthur, 1998; Bailey *et al.*, 2000; Li *et al.*, 2011).

Special care should be given when measuring strontium isotope ratios because strontium is very sensitive to alteration effects. These may include fluid-rock interactions with fluids of meteoric origin, diagenetic origin, tectonic circulation, metamorphic origin, which can have an impact on the original $^{87}Sr/^{86}Sr$ of a sample. A slight variation of strontium isotope ratios can have an important impact on the deduced ages and their subsequent interpretation and integration in a broader geological context. The most important part when preparing samples for strontium isotope ratios is to check if a sample can give a potentially trustful value, or not. Many authors have combined the strontium isotope ratio with screening methods in order to prove that their samples ratios reflect the original marine $^{87}Sr/^{86}Sr$ ratio. These measurements are in fact the most important part when working with $^{87}Sr/^{86}Sr$ because it validates the usefulness of the given ratio.

If a strontium isotopic ratio does not intersect with the curve in the pre-defined age interval, it may have different reasons: the initial age interval may have been wrongly or badly defined, the screening methods may not have revealed any trace of diagenetic effects, a contaminant may be present in the phase, occurring problems with the compiled curve (the original values from the selected authors might be wrong) and finally, in rare cases, local effects that may increase or lower the ratio. In this case, care has to be given, because no age can be defined.

2.2. **The strontium isotope ratio measurement**

Samples measured for strontium isotopic ratios have to undergo a chromatographic separation technique in order to avoid interferences, have a more reliable signal of ^{86}Sr and ^{87}Sr and consequently have the most suitable results for strontium isotope ratio dating (Charlier *et al.*, 2006; Vroon *et al.*, 2007, McArthur, 1998; Bailey *et al.*, 2000; Li *et al.*, 2011, amongst others). Vroon *et al.*, (2007) lists the advantages of chromatographic techniques to remove matrix and interfering elements such as ^{87}Rb, which interferes with ^{87}Sr, before measuring.

For relevant strontium isotope ratio dating, at least five digits have to be considered, the best would be to have a precision of 10^{-6} in order to have a better resolution.
In order to have a precision of at least 10^{-6}, a Thermal Ionization Mass Spectrometer (TIMS) device is currently the most suitable device for measuring $^{87}Sr/^{86}Sr$. The TIMS provides the expected analytical precision, and the cost/quality ratio is the most appropriate. Another appropriate choice is Multi Collector Inductively Coupled Plasma Mass Spectrometer (MC-ICP-MS) used in liquid mode on the separated Sr-fraction. This method tends to reach the precision obtained by TIMS analyses.
In-situ measurement of strontium isotope ratios by Laser Ablation (MC-LA-ICP-MS) are also intensively investigated and in future may have significant potentials (Vroon *et al.* 2007), however, at the moment difficulties with matrix effect and correcting for interfering ions limits the feasibility of this method for serious Sr-isotope dating.

2.3. **Contamination and Screening Methods**

Different types of contaminations are possible while working with strontium isotopes. These can be related to diagenetic alteration or the presence of interfering material. Also, the mixing of geological materials with different isotopic compositions is commonly occurring on the Earth surface and in its interior (Faure and Mensing, 2004).

If diagenetic alteration is related to the dissolution/reprecipitation mechanism of calcitic material, the original $^{87}Sr/^{86}Sr$ ratio is obliterated and the new isotopic composition will be the one of the diagenetic fluid that can be the circulating fluids, pore fluids or seawater (for submarine carbonate dissolution). As soon as a reprecipitation takes place, the $^{87}Sr/^{86}Sr$ ratio of the pore and circulating fluids is incorporated into the new mineral and this new ratio will not be representative of any deposition age. In the case of submarine reprecipitation, the $^{87}Sr/^{86}Sr$ ratio of the seawater of this period will be incorporated into the mineral structure and the $^{87}Sr/^{86}Sr$ ratio will give the age of the reprecipitation (if completely reprecipitated). The main issue is to know if the dissolution/reprecipitation mechanism is early or late and if it completely replaced the original $^{87}Sr/^{86}Sr$ signature. In the case of an early and total process, the obtained $^{87}Sr/^{86}Sr$ ratio will be close to the original marine ratio and the obtained age will then also be very close to the original one. Early dolomitization is a good example when early diagenetic process has not an important impact on the age deduction (Vahrenkamp *et al.*, 1988). If a late dissolution/reprecipitation mechanism occurred, it is impossible to conclude correct ages with $^{87}Sr/^{86}Sr$, but it might then e.g., give indications on the burial or cementation processes (Brigaud *et al.*, 2009).

The presence of an extraneous contaminant, e.g., clay mineral, celestite ($SrSO_4$) can also lead to erroneous values. This may be the case while working on samples with high porosity or hollow fossil shells (e.g., foraminifera), or even when working on whole rock material. In these cases, care has to be taken in order to avoid contaminating material that would considerably change the $^{87}Sr/^{86}Sr$ ratio. A small amount of contaminant can compromise the $^{87}Sr/^{86}Sr$ ratios (McArthur, 1994, Playa and Rosell, 2005 among others).

2.4. **Contamination**

McArthur (1998) explains that a contaminant present in a proportional ratio of only 1% of a sample can consequently alter a ratio. Of course, the origin of the contaminant has to be known, as it may highly increase or decrease the measured ratio. It is then essential to use the appropriate dissolution method in order to avoid the dissolution of a potential contaminant that could affect the strontium isotopic ratio.

In McArthur (1994) two types of plots show the effect of contamination on $^{87}Sr/^{86}Sr$, which are represented here by Figure 9 and Figure 10. Figure 8 shows a plot of the change in $^{87}Sr/^{86}Sr$ against the percentage of contaminant dissolved (considering the strontium isotope ratio of the analyzed material is 0.708000, a common value found in carbonates). It clearly shows the possible variations of strontium isotope ratios depending on the $^{87}Sr/^{86}Sr$ and the quantity of contaminant. The differences in $^{87}Sr/^{86}Sr$ can be drastic for an accurate age deduction with SIS, difference of up to 20×10^{-6} can be obtained whilst dissolving an amount of just 0.1% of a contaminant with $^{87}Sr/^{86}Sr$ of 0.800. Of course the value of a $^{87}Sr/^{86}Sr$ ratio of 0.800 is never observed in the ocean system but these are theoretical values of a potential contaminant in order to show the effects of an incorporated contaminant. The contaminant with ratios around 0.750 and 0.720 are more likely to be observed in samples. Dissolution of just 1% of contaminant in a carbonate sample with a strontium isotope ratio of 0.708000 can imply variations of up to 90×10^{-6} of the original strontium isotope ratio. Such variation may significantly influence the deducted age.

Figure 10 shows the strontium concentration of a contaminant against the $^{87}Sr/^{86}Sr$ of the contaminant. This figure highlights that every dissolved contaminant has an important impact on measured $^{87}Sr/^{86}Sr$ values. Depending on its strontium concentration and the amount of contaminant dissolution during the preparation, totally erroneous values for SIS may be generated (for a carbonate sample with a strontium isotope ratio of 0.708000).

It is important to notice that the presence of any contaminant can change the final $^{87}Sr/^{86}Sr$ value and so, the deducted age. The second important note is the dissolution method of a sample that has to be applied in order to avoid the dissolution of a contaminant. As shown above, a very low quantity of contaminant strontium dissolved during the sample preparation can have major consequences on the obtained ages and the interpretation of the results.

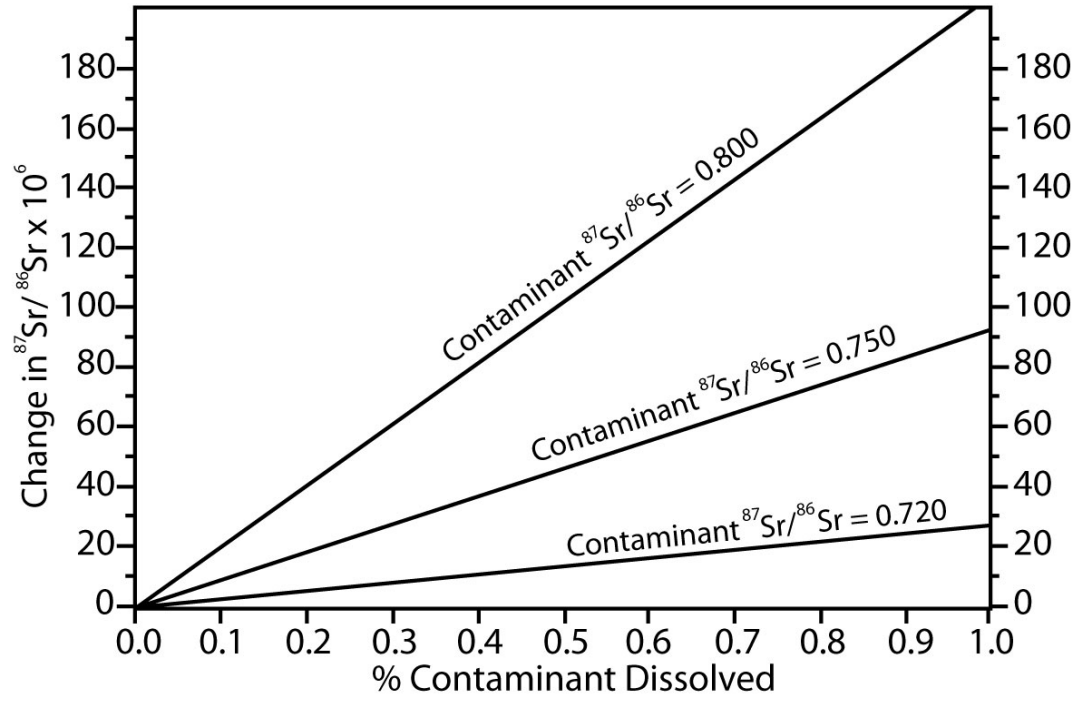

Figure 9: Change in $^{87}Sr/^{86}Sr$ of a sample contaminated by a second phase with $^{87}Sr/^{86}Sr$ values of 0.800, 0.750 and 0.720 for a carbonate target rock with a strontium isotope ratio of 0.708000 (from McArthur, 1994). A small amount of contaminant with a, in this case, very high strontium isotope ratio can considerably shift the target ratio.

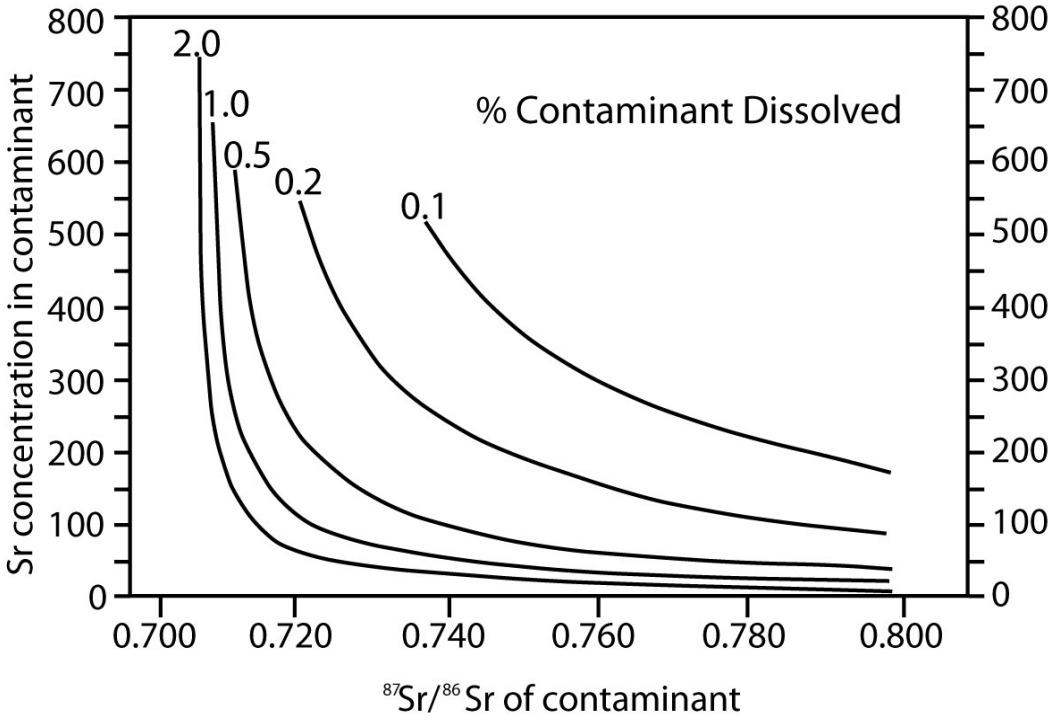

Figure 10: Plot of strontium concentration of contaminant phase against possible $^{87}Sr/^{86}Sr$ values for a carbonate target rock with a strontium isotope ratio of 0.708000 (from McArthur, 1994). A small amount of contaminant with a, in this case, very high strontium isotope ratio can considerably shift the target ratio.

2.5. **Sample disolution methods**

When working with strontium isotope ratios, the target mineral has to be separated avoiding any contamination from extraneous material, especially while working on whole rock analyses (Bailey et al., 2000, and references therein).
The easiest way of isolating the target mineral would be to physically separate it from the encasing rock. Often, a physical separation is not possible and the target mineral has to be isolated by chemical dissolution methods. The danger while working with acid attacks is to partially or completely dissolve an extraneous mineral that would affect the strontium isotope ratio from the target material. These dissolutions range from a first attack with a weak acid (McArthur, 1993a,b) to a total dissolution in strong acids (Hein et al., 1993 in Bailey et al., 2000). Some authors do a pre-leach in order to minimize the contamination (DePaolo *et al*., 1983; Ohde and Elderfield, 1992; McArthur *et al*., 1993a; Montanez *et al*., 1996 amongst others, in Bailey *et al.*, 2000). Bailey *et al.*, (2000) prove the effects of a wrong dissolution method and give a concrete step-by-step method in order to use an appropriate dissolution method. This method includes a pre-leach with weak acetic acid dissolving up to 40% of the sample and then dissolution of 30% of the sample in diluted acetic acid. If the entire carbonate sample was to dissolve, the residuum would affect the target minerals strontium isotope ratio, it is preferably to have about 10% of residuum left, which ensures only little contribution from silicate impurities.

Li *et al.*, (2011) presents a method that implies a pre-leach of about 30-40% of carbonates by acetic acid or hydrochloride acid and then dissolution of 30-40% of the subsequent carbonate with acetic acid. By using these two different phases it is then possible to consider a diagenetic trend. Again, the danger of this method is the partial or total dissolution of non-target minerals, which would again act as a contaminant and alter the strontium isotope ratio of the target mineral. However the leaching and dissolution methods have made their proofs in SIS, based on statistical work (Li *et al.*, 2011), and they may then be applied while working with bulk rock samples in order to have relevant results.

A recurrent problem that appears when preparation methods are presented is the sampling of the target mineral or fossil. Often, e.g. foraminifera or target minerals are sampled by manual or mechanical micro-drilling. In most cases, these samples are then considered as pure. This

may not be the case as it is impossible to have the required precision while hand drilling in order to guarantee a pure powder. Even when drilling with a computer-operated device, generally on fresh section of thin-section-counterparts, it is sometimes impossible to ensure a pure target sample because if there is no control on the 3 dimensional structure of the target mineral or fossil, the contamination cannot be quantified precisely.

2.6. **Sample screening**

There are various screening methods that should be performed in order to screen a sample and check if it is worth further preparation for strontium isotope measurements. The type of preparation depends on the samples and the dissolution method should be chosen wisely (Bailey *et al.*, 2000, Singh *et al.*, 1997, Veizer *et al.*, 1999; Frijia *et al.*, 2008; McArthur et al, 2006 among others).

When working with strontium isotope dating, every sample should be considered as altered or diagenetically modified. The main question to answer is to know which type of alteration the sample underwent and how the strontium isotopic ratio has probably varied. Of course, the best way to date with $^{87}Sr/^{86}Sr$ is to use samples where diagenetic effects are negligible and consequently where the original strontium isotope ratio is conserved.

2.6.1. Stable carbon and oxygen isotopic compositions

The carbon/oxygen stable isotopes composition gives hints on whether alteration has occurred in a closed or opened system, depending on the type of material and the sampling scale (McArthur, 1994).

In a closed system, if the reprecipitation occurs during burial, in conditions similar to the ones of oceanic seawater (especially temperature), the variations in $\delta^{18}O$ (stable oxygen isotopes) would not be distinguishable with other factors having an impact on the oxygen isotopic composition (Hudson and Andersen, 1989; McArthur, 1994).

In an open system, where the sample was exposed to meteoric water (with a different isotopic composition) that has replaced the pore fluid, variations in $\delta^{18}O$ are noticeable (this is the case for low temperatures). This may provide useful hints on the original values by back-tracking (McArthur, 1994). Figure 12 and Figure 13, show the stable isotopic values that should be

expected from different types of organisms (after Swart, 1993 and after Wefer and Berger, 1991). A first comparison of the obtained results with the values presented in and Figure 11 Figure 12 and Figure 13 may be helpful to assess alteration.

Burial and deep burial in pelagic sediments will also have an effect on the stable isotopic composition, because the water in deeply buried sediments can be up to 3 per mil more negative in $\delta^{18}O$ than seawater, making precipitated phases lighter. Furthermore, if the temperature is lower than the one of the seawater precipitated phases become heavier (Figure 12), introducing problems of assessing a correct diagenetic alteration (Lawrence, 1973, 1974; Lawrence *et al.*, 1975a,b; McArthur 1994).

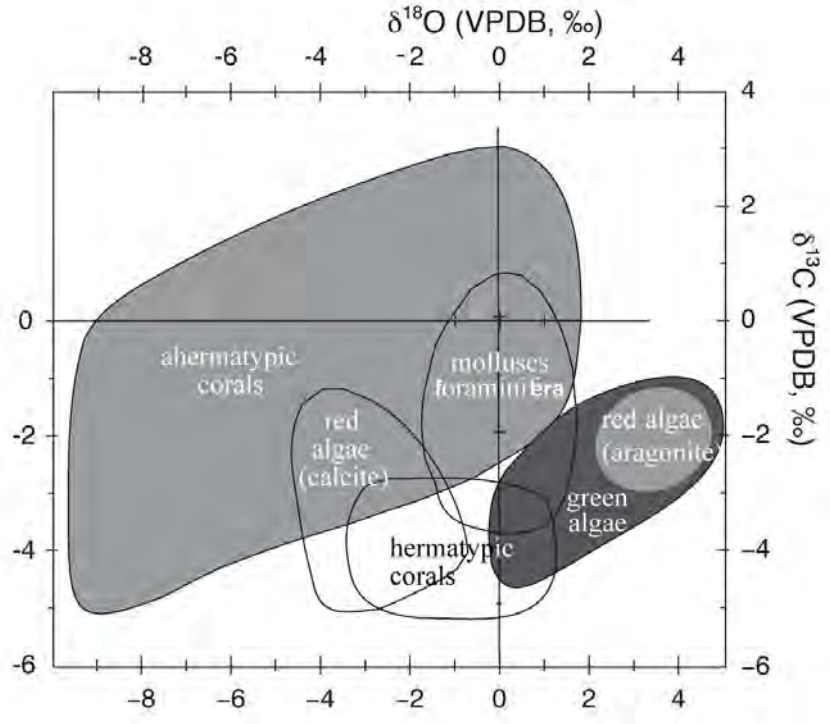

Figure 11: Isotopic fractionation of fossil calcareous types (after Swart et al., 1983). It can be useful to compare stable isotope results with existing ranges. When results are different from expected or predicted number, an alteration might have to be considered. Of course, every case study is unique, which has also to be considered.

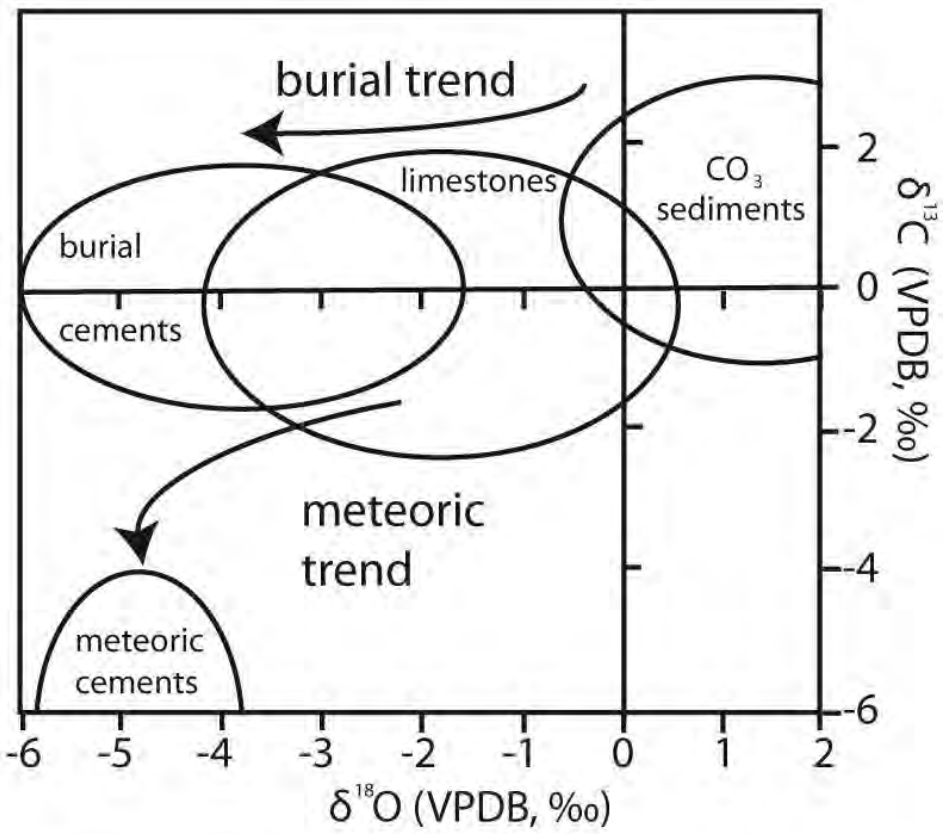

Figure 12: Stable isotopic variations with meteoric and burial diagenetic trends (after Knoerich and Mutti, 2006). This type of graph may show the diagenetic path a sample went through, again, every case study is unique, which has also to be considered.

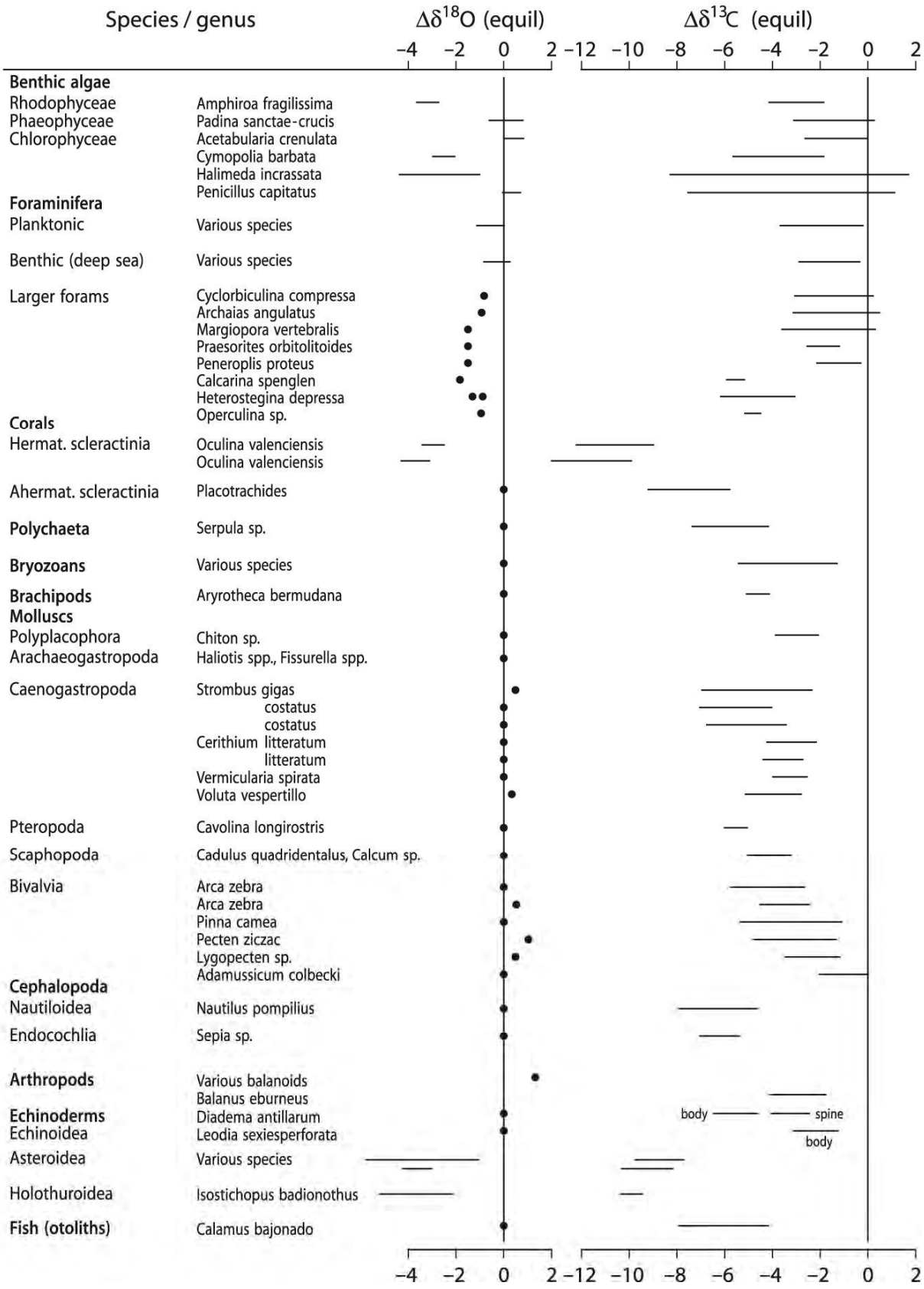

Figure 13: $\delta^{18}O$ and $\delta^{13}C$ differences from equilibrium isotope composition of extant calcareous species (after Wefer and Berger, 1991, in Hoefs 2009).

2.6.2. Chemical analyses, trace elements

An additional method would be to measure the concentration of trace and major elements in the samples. These trace and major elements e.g., Fe and Mn may show the alteration grade of a sample. Such elements including strontium, can easily be mobilized. Trace elements measured in sedimentary rocks and the acceptable concentrations often differ from one author to another. To verify the diagenetic alteration, the common idea for low-Mg calcite is a depletion in strontium concentrations and an increase in Fe and Mn concentrations (Al-Asam and Veizer, 1986, Steuber 1999, Steuber and Schlüter, 2012).

Reprecipitated low-Mg carbonates tend to be in equilibrium with interstitional fluids. The new values will be shifted towards those of the interstitional sea- or meteoric water (Brand and Veizer, 1980). This interstitial water is depleted in Sr^{2+}, Na^{+}, Mg^{2+} and has lower $\delta^{18}O$ and $\delta^{13}C$ values (Turekian, 1972). The reprecipitation process decreases the concentrations of Sr^{2+} and Na^{+} and increases the concentrations of Mn^{2+}, Fe^{2+} and Zn^{2+} in carbonate samples (Brand and Veizer, 1980).

In biogenic carbonates, the presence of Fe and/or Mn in high concentrations (>100 ppm of Fe, >100 ppm of Mn) might indicate diagenetic alteration, but in contrary if the concentrations are low, diagenesis cannot be excluded (McArthur, 1994).

But, these measurements should carefully be compared to the literature, because a sample can have a much higher original Fe or Mn concentration than the limit (around 200ppm) given in literature even if not altered. The criteria of low Fe and Mn concentrations cannot be used to quantify the degree of diagenetic alteration. Frijia and Parente (2008) explain that strontium concentrations > 800 ppm are a good indicator of low diagenetic alteration. The threshold of 800 ppm is based on the work of Steuber *et al.*, (2005), and it is linked to the difficulty of the application of conventional methods for his samples.

Proxies such as Sr/Ca or concentrations of Mg can also be used, but attention has to be given as every case study may show different ratios or concentrations which might still indicate a good sample for strontium isotope ratio measurements (McArthur, 1994, Brand, 1991, Carpenter *et al.*, 1991).

2.6.3. Cathodoluminescence

Cathodoluminescene (CL) is the most appropriate tool for looking at primary or secondary microstructures in fossils (Amieux, 1987, Elorza *et al.*, 2001, in Flügel 2010). It can be used while working on the petrography of both marine and non-marine carbonates (Marshall, l988, Barker and Kopp, 1991; Barbin *et al.*, 1991, in Flügel, 2010.) The main goals of using CL are the observation of diagenetic phases, the study of microstructures and the study of the diagenetic signature of a fossil or sample (Flügel, 2010; Ali, 1995) (Figure 14, Figure 15). For carbonate rocks, the Fe^{2+} acts as a quencher and Mn^{2+} as the main activator of cathodoluminescence (Marshall, 1988; Richter *et al.*, 2003; Boggs and Kinsley, 2006).
Note that Cathodoluminescence requires a thin section of the sample. Thus, Foraminifera e.g. that are picked cannot be observed through cathodoluminescence.

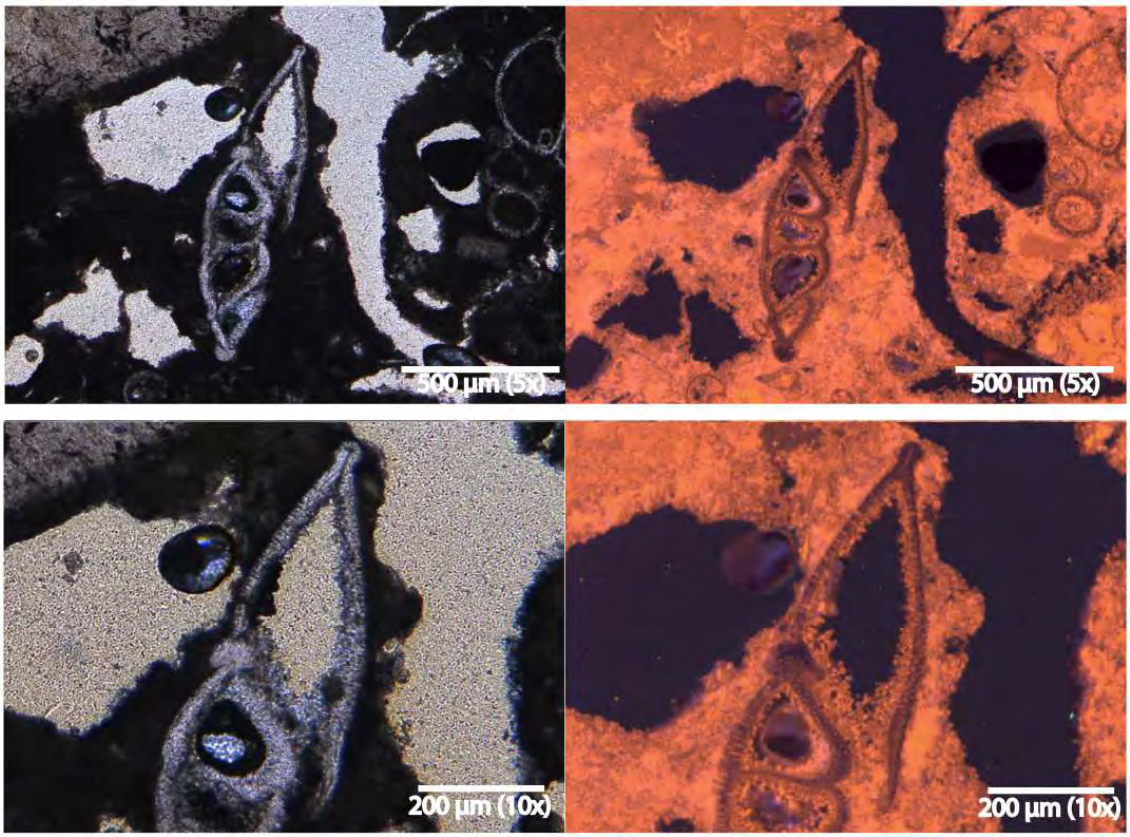

Figure 14: Example of samples observed with microscopy and CL. Cathodoluminescence shows a precipitated rim in the chambers of the foraminifera (very early marine diagenesis), matrix exhibits a bright orange luminescence because of the presence of Mn. In magnification 10x, dogtooth cements can be observed, also considered as an early diagenetic feature.

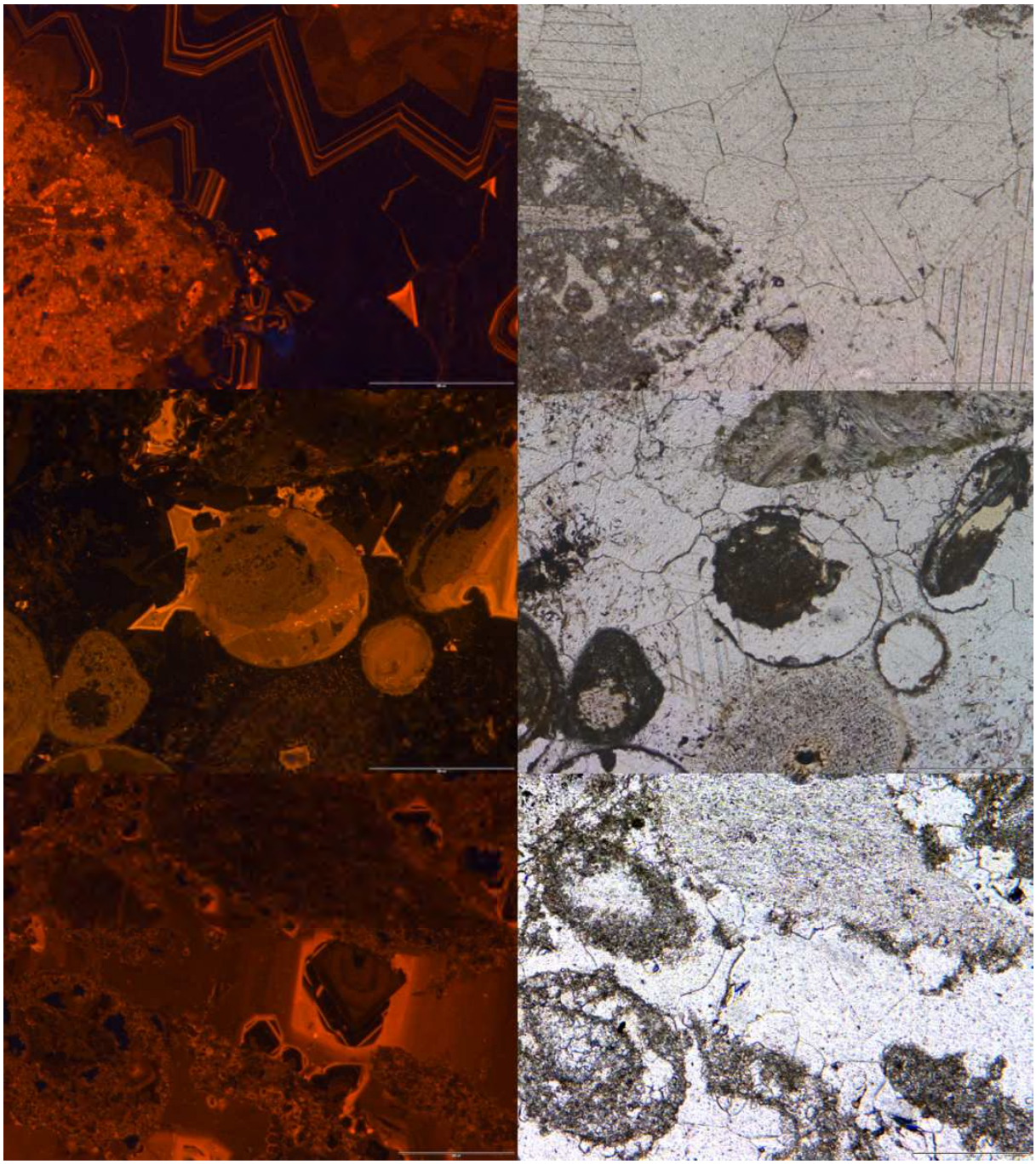

Figure 15: Example of diagenetic calcite cements in a limestone showing concentric orange–yellow bands of growth zonation (pictures kindly given by A. Godet).

2.6.4. Scanning Electron Microscope

The Scanning Electron Microscope (SEM), coupled to an Energy Dispersive Spectrometer (EDS) gives an insight of the crystalline structure of a fossil. McArthur (1994) mentions the difficulty of a non-expert to assess the preservation of original biomineralisation, since then, several publications allows making critical observations with a SEM, when comparing the own data with published data (e.g., Voigt *et al*., 2003). In Figure 16, a Pleistocene fossil coral structure is compared to a present coral one in order to check the preservation. Figure 17 shows a reprecipitated echinoderm shell and a highly dolomitized foraminifera test. EDS allows a first qualitative estimation of major element presence in the observed object. It is possible to check the presence of e.g., Fe, Mn, which can also indicate an alteration.

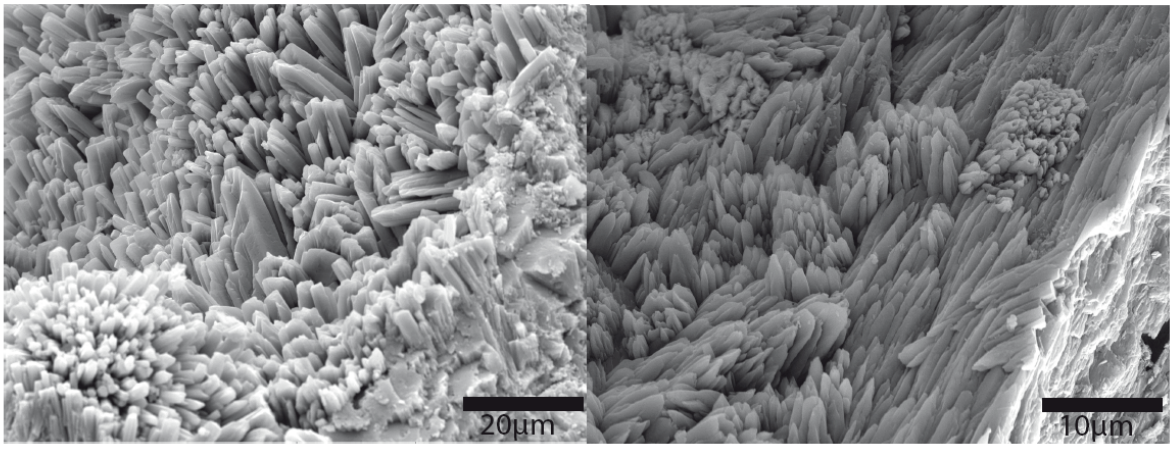

Figure 16: SEM pictures of a Pleistocene fossil coral (left) and a recent coral (right). Pictures were made in order to observe the primary structures and compare an ancient sample with a recent one.

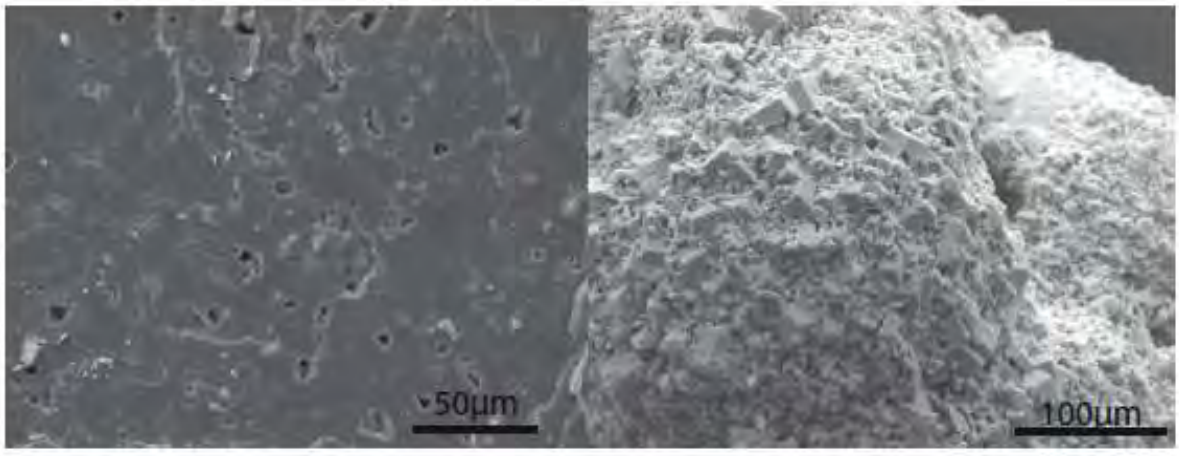

Figure 17: SEM picture of a diagenetically altered echinoid (left) and a dolomitized foraminifera (right). Both samples would be unsuitable for SIS.

2.6.5. The $^{87}Sr/^{86}Sr$ measurement

The $^{87}Sr/^{86}Sr$ measurement permits to discuss the preservation of a sample. First, one can compare the strontium isotope ratios of different materials from the same layer (Jones *et al.*, 1994). In fact when different samples from one layer show similar values, low diagenetic alteration may be considered. Thus, it is advised to measure strontium isotope ratios on e.g. microfossils and macrofossils, or e.g., calcite and aragonite because of the differences in robustness of the materials (Ludwig *et al.*, 1988, in McArthur, 1994).

The concordance of results may then suggest materials have retained their original $^{87}Sr/^{86}Sr$ (McArthur, 1994). The latter author also mentions that when $^{87}Sr/^{86}Sr$ ratios differ in a banc on different samples, it may be linked to the diagenetic alteration that has overwritten the $^{87}Sr/^{86}Sr$ signal. It should be nearly impossible to have the same value within a layer that has undergone diagenetic alteration. The consistency of strontium isotope ratios is then a useful indicator for the accuracy of the obtained $^{87}Sr/^{86}Sr$ ratios and the deducted ages.

2.7. How to handle the results from the screening

The screening of samples is unavoidable when doing SIS. The results given by microscopy, CL microscopy, SEM (EDS), major and/or trace elements and stable isotope analysis have to be considered all together in order to ensure the relevance and reliability of strontium isotope ratios.

Often, these methods make it possible to avoid diagenetically altered samples. On the contrary, even if screening makes it not possible to detect any alteration, the measured ratios may deviate from the original value and results should not be taken for granted.

The screening procedures are not only indicators of diagenesis but are also helpful for the interpretation of the final strontium isotopic ratio.

Not all the screening methods are requested on all samples. Normally if two to three of these methods are applied to a sample it already provides reliable evidences on the validity of a strontium isotopic ratio, considering that the ratio itself also gives hints on the quality of samples.

The combination of the strontium isotope ratio and the screening gives hints on how reliable the deducted ages are. If the aim of a work is to review the curve and have new input data in order to refine variations in the curve, only samples that prove absolutely pristine conservation have to be considered.
If the aim of a work is to date sedimentary sections or single spots in a stratigraphic column, errors on the strontium ratio are acceptable if they remain small and can be discussed.
One should always keep in mind that the strontium isotopic results do not show the questionability of the ratio itself (only the analytical error is represented) but the combination with the results of the screening does. It is not possible to quantify the error translated in ages but it can be put under discussion if results are reliable or not.

2.8. **Methods applied in this study**

In this work, strontium isotope ratios are not only used to date carbonate samples but the deduced ages make it possible to understand a regional tectonic history, whose evolution can been refined through new age constrains. In our case the isotope ratios are not always stratigraphically and paleontologically well constrained. However paleontological anchor points provide information on their approximate ages and hence the expected strontium ratio range can be set. Therefore, the term of Strontium Isotope Stratigraphy is not suitable; the term of $^{87}Sr/^{86}Sr$ age should be more appropriate (see Remark in 2.1).
In general, measurements on a same sample or layer were done twice. The obtained values were then compared to each other and a maximal difference was set, depending on the samples and localities, and considered as acceptable or not. In fact, the reproducibility of an analysis allows determining if a value can be accepted or rejected.

If two samples have no reproducibility, the two obtained values are not within their respective standard error or the age difference is large, it could mean that something has been missed or overseen during the screening, and sometimes analytical or geologic (e.g., reworking) problems have to be considered.
A choice would be to do a third analysis and compare the obtained value to the two previous ones. If it is close to one prior obtained ratio (within the standard error), one can discriminate the value that does not fit, (this suggests a potential correctness of 66%). If the third value

does not correspond to any of those measured before, one should assume that the sample is not valid for SIS.

If two measurements were close to each other (e.g., within their standard error), it would imply the obtained ratios are true ratios and an age can be deducted from each value or they may be averaged. However, diagenesis is often patchy (McArthur, 1998) and the strontium isotopic signal can, in some cases, be homogenized. If diagenesis has occurred, it should be revealed by various screening methods.

When dating with strontium isotopes, the first step is to select appropriate samples as discussed above and select samples in a stratigraphic order that makes sense for a geologic study.

If samples are selected along a section, it is not worth the trouble to date all the samples. First, the upper and lower limits of the section should be dated by strontium isotopes. Further measurements inside this interval would only confirm the relative age. A frequent mistake is to measure too much samples that just confirm what is already known without giving any more precisions. Meanwhile, if the aim of a work is to define relative sedimentation rates, it would be necessary to measure multiple points in this pre-defined time interval in order to be consistent on a work.

Of course it all depends on the precision that wants to be given to the ages, considering the errors of a dating curve and the analytical errors, that is directly translated into an age error.

Detailed field observations and notes are important: a single sample often does not give any hints of how a layer or outcrop looks like. Often dissolution/precipitation mechanisms can be observed around a sample in a layer, but cannot be described later on the fossil. A precise description of the diagenetic hints, which can be studied on a layer, may avoid some unnecessary collecting and preparation for sample screening and strontium isotopes measurements. The sampling strategy should always be done in accordance with the whole studied section, e.g., hiatus in sedimentation, condensate layers, erosion surfaces and faults have to be taken in account and might influence the sampling in the field.

2.9. **Conclusion**

In summary, SIS has proved its validity as a high-resolution method for dating carbonate rocks and fossils. The SIS method is also helpful for stratigraphic correlation and sedimentary studies. Nevertheless the points discussed above show the complexity of the SIS method and its limits for dating.

The screening methods presented in this Chapter are commonly accepted; they are highly recommended in order to assess the diagenetic alteration of the samples. However, care has to be taken with the results of the screening and samples have to be considered in their general sedimentary history. The results have to be interpreted wisely in order to conclude, correct ages of the samples. The combination of carbon and oxygen stable isotopes, cathodoluminescence, SEM, major and trace elements and the $^{87}Sr/^{86}Sr$ ratios themselves provide good indications on the diagenetic influence a sample underwent.

2.10. **References**

Al-Aasm, I.S., and Veizer, J., **1986**. Diagenetic stabilization of aragonite and low-Mg calcite, I.Trace elements in rudists. Journal of Sedimentary Petrology, 56, pp. 138-152.

Ali, M.Y., **1995**. Carbonate cement stratigraphy and timing diagenesis in a Miocene mixed carbonate-clastic sequence, offshore Sebah, Malaysia: constraints from cathodoluminescence, geochemistry, and isotope studies. Sedimentary Geology, 99, pp. 191-214.

Amieux, P., **1982**. La cathodoluminescence: méthode d'étude sédimentologique des carbonates. – Bull. Centre Rech. Explor.-Prof. Elf-Aquitaine, 6, pp. 437-483.

Bailey, T.R., McArthur, J.M., Prince, H., and Thirwall, M.F., **2000**. Dissolution methods for strontium isotope stratigraphy: whole rock analysis. Chemical Geology 167 pp. 313-319.

Banner, J.L. and Kaufman, J. **1994**. The isotopic record of ocean chemistry and diagenesis preserved in non-luminescent brachiopods from Mississippian carbonate rocks, Illinois and Missouri. Geological Society of America, Bull. 106, pp. 1074-1082.

Banner, J.L., **2004**. Radiogenic isotopes: systematics and applications to earth surface processes and chemical stratigraphy. Earth-Science Reviews 65, pp. 141-194.

Barbin, V., Ramseyer, K., Debenay, J.P., Schein, E., Roux, M., and Decrouez, D., **1991**. Cathodoluminescence of Recent biogenic carbonates: an environmental and otogenic fingerprint. Geological Magazine, 128, pp. 19-26.

Barker, C.E., and Kopp, A.C., **1991**. Luminescence microscopy and spectroscopy. Quantitative and qualitative applications. – SEPM Short Course, 25, 195 pp.

Barrera E., Baldauf J. and Lohmann K.C., **1993**. Strontium isotope and benthic foraminifer stable isotope results from Oligocene sediment at site 803. Proceedings of the ODP, Scientific Results,130, pp. 269-279.

Barrera, E.C., Savin, S.M., Thomas, E., and Jones, C.E., **1997**. Evidence for thermohaline-circulation reversals controlled by sea-level change in the latest Cretaceous. Geology, 25(8), pp. 715-718.

Barrera, E., and Savin, S.M., **1999**. Evolution of late Campanian-Maastrichtian marine climates and oceans. Geol. Soc. of America Special Paper 332, pp. 245-282

Berner, R.A., and Rye, D.M., **1992**. Calculations of the Phanerozoic strontium isotope record of the oceans from a carbon cycle model. Am. J. Sci. 292, pp. 136–148.

Bertram, C. J., Elderfield, H., Aldridge, R. J., and Morris, S. C., **1992**. $^{87}Sr/^{86}Sr$, $^{143}Nd/^{144}Nd$ and REEs in Silurian phosphatic fossils: Earth and Planetary Science Letters, v. 113,

pp. 239-249.

Boix, C., Frijia, G., Vicedo, V., Bernaus, J.M., Di Lucia, M., Parente M., and Caus, E., **2011**. Larger foraminifera distribution and strontium isotope stratigraphy of the La Cova limestones (Coniacian-Santonian, "Serra del Montsec", Pyrenees, NE Spain). Cretaceous Research 32, pp. 806-832.

Bralower, T.J., Fullagar, P.D., Paull, C.K., Dwyer, G.S., and Leckie, R.M. **1997**. Mid-Cretaceous strontium-isotope stratigraphy of deep-sea sections, Geological Society of America Bull., 109, pp. 1421-1442.

Brigaud, B., Durlet, C., Deconinck, J.-F., Vincent, B., Thierry, J., and Trouiller, A., **2009**. The origin and timing of multiphase cementation in carbonates: impact of regional scale geodynamic events on the Middle Jurassic Limestones diagenesis (Paris Basin, France) Sedimentary Geology, 222, pp. 161–180.

Brand, U., and Veizer, J., **1980**. Chemical diagenesis of a multicomponent carbonate system - 1: Trace elements. Journal of Sedimentary Petrology, 50, pp. 1219-1236.

Brand, U., **1991**. Strontium isotope diagenesis of biogenic aragonite and low-Mg calcite. Geological Society of America Bull., 101, pp. 377-390.

Brand, U., and Brenckle, P., **2001**. Chemostratigraphy of the Mid-Carboniferous boundary global stratotype section and point (GSSP), Bird Spring Formation, Arrow Canyon, Nevada, USA Palaeogeography, Palaeoclimatology, Palaeoecology, 165, pp. 321–347.

Brand, U., **2004**. Carbon, oxygen and strontium isotopes in Paleozoic carbonate components: an evaluation of original seawater-chemistry proxies. Chemical Geology 204, pp. 23-44.

Brass, G.W., **1976**. The variation of the marine 87Sr/86Sr ratio during Phanerozoic time: interpretation using a flux model. Geochimica et Cosmochimica Acta 40, pp. 721-730.

Bruckschen, P., Oesmann, S., and Veizer, J., **1999**. Isotope stratigraphy of the European Carboniferous. Proxy signals for ocean chemistry, climate and tectonics Chemical Geolology (Isotope Geoscience Section), 161, pp. 127–163.

Burke, W.H., Denison, R.E., Hetherington, E.A., Koepnick, R.B., Nelson, H.F., and Otto, J.B., **1982**. Variation of 87Sr/86Sr throughout Phanerozoic time. Geology 10, pp. 516–519.

Callomon, J., **2000**. On the proposed basal boundary stratotype (GSSP) of the Middle Jurassic Callovian Stage. GeoRes. Forum 6, pp. 41-54.

Capo, R.C., Stewart, B.W., and Chadwick, O.A., **1998**. Strontium isotopes as tracers of ecosystem process: theory and methods. Geoderma, 82, pp. 197-225.

Carpenter, S. J., Lohmann, K. C., Holden, P., Walter, L. M., Huston, T. J., and Halliday, A.N., **1991**. $\delta^{18}O$ values, $^{87}Sr/^{86}Sr$ and Sr/Mg ratios of Late Devonian abiotic calcite: implications for the composition of ancient seawater. Geochimica et Cosmochimica Acta, 55, pp. 1991–2010.

Charisi, S.D. and Schmitz, B., **1995**. Stable ($\delta^{13}C$, $\delta^{18}O$) and strontium ($^{87}Sr/^{86}Sr$) isotopes trough the Paleocene at Gebel Aweina, eastern Tethyan region. Palaeogeography, Palaeoclimatology, Palaeoecology, 116, pp. 103-129.

Charlier, B.L.A., Ginibre, C., Morgan, D., Nowell, G.M., Pearson, D.G., Davidson, J.P., and Ottley, C.J., **2006**. Methods for the microsampling and high-precision analysis of strontium and rubidium isotopes at single crystal scale for petrological and geochronological applications. Chemical Geology, 232, pp. 114-133.

Clemens, S. C., Farrell, J. W., and Gromet, L. P., **1993**. Synchronous changes in seawater strontium isotope composition and global climate. Nature 363, pp. 607–610.

Clemens, S. C., Gromet, L. P., and Farrell, J. W., **1995**. Artefacts in Sr isotope records. Nature, 373, p. 201.

Cummins, D.I. and Elderfield, H., **1994**. The strontium isotopic composition of Brigantian/late Dinantian seawater. Chemical Geology, 118, pp. 255-270.

Dash, E.J. and Biscaye, P.E., **1971**. Isotope composition of strontium in Cretaceous-Recent pelagic foraminifera. Earth Planet. Sci. Lett. 11, pp. 201-204.

Denison, R. E., Koepnick, R. B., Fletcher, A., Dahl, D. A., and Baker, M.C., **1993**. Re-evaluation of Early Oligocene, Eocene, and Paleocene seawater 87Sr/86Sr using outcrop samples from the U.S. Gulf Coast. Paleoceanography 8, pp. 101–126

Denison, R.E., Koepnick, R.B., Burke, W.H., Hetherington, E.A., and Fletcher, A., **1994**. Construction of the Mississippian, Pennsylvanian and Permian seawater $^{87}Sr/^{86}Sr$ curve. Chemical Geology (Isotope Geoscience Section) 112, pp. 145-167.

Denison, R. E., Koepnick, R. B., Burke, W. H., Hetherington, E. A., and Fletcher, A., **1997**. Construction of the Silurian and Devonian seawater 87Sr/86Sr curve. Chemical Geology, 140, pp. 109–121.

Denison, R. E., Koepnick, R. B., Burke, W. H., and Hetherington, E. A. **1998**. Construction of the Cambrian and Ordovician seawater 87Sr/86 Sr curve. Chemical Geology,152, pp. 325–340.

DePaolo, D.J., Kyte, F.T., Marshall, B.D., O'Neil, J.R., and Smit, J., **1983**. Rb–Sr, Sm–Nd, K–Ca, O, and H study of Cretaceous– Tertiary boundary sediments, Caravaca, Spain: evidence for an oceanic impact site. Earth Planetary Science Letters, 64, pp. 356–373.

DePaolo, D.J. and Ingram, B.L., **1985**. High-Resolution stratigraphy with Strontium isotopes. Science 227, pp. 938-941.

DePaolo D.J. and Finger K.L. **1991**. High resolution strontium isotope stratigraphy and biostratigraphy of the Miocene Monterey Formation, central California. Geological Society of America, Bull. 103, pp. 112-124.

Derry, L.A., and France-Lanord, C., **1996**. Neogene Himalaya weathering history and river $^{87}Sr/^{86}Sr$: impact on the marine Sr record. Earth Planet. Sci. Lett. 142, 59– 74.

Dia, A.N., Cohen, A.S., O'Nions, R.K. and Shackelton, N.J., **1992**. Seawater Sr isotope variation over the past 300 kyr and influence of global climate cycles. Nature, 356, pp. 786-788.

Diener, A., Ebneth, S., Veizer, J., and Buhl, D. **1996**. Strontium isotope stratigraphy of the Middle Devonian: brachiopods and conodonts. Geochimica et Cosmochimica Acta 60, pp. 639–652.

Ebneth, S., Shields, G.A., Veizer, J., Miller, J.F., and Shergold, J.H., **2001**. High-resolution strontium isotope stratigraphy across the Cambrian-Ordovician transition. Geochimica et Cosmochimica Acta, 65, pp. 2273-2292.

Edmond, J.M., **1992**. Himalayan tectonics, weathering processes, and the strontium isotope record in marine limestones. Science 258, 5088.

Elderfield, H., **1986**. Strontium isotope stratigraphy. Palaeogeography, Palaeoclimatology, Palaeoecology 57, pp. 71–90.

Elorza, J., Gomez Alday, J.J., and Olivero, E.B., **2001**. Environmental stress and diagenetic modifications in inoceramids and belemnites from the Upper Cretaceous, James Ross Basin, Antarctica. Facies, 44, pp. 227-242.

Evans, M.J., Derry, L.A., Ansderson S.P., and France-Lanord, C., **2001**. Hydrothermal source of radiogenic Sr to Himalayan rivers. Geology, 29, pp. 803-806.

Farrell, J. W., Clemens, S. C. and Gromet, L. P., **1995**. Improved chronostratigraphic reference curve of late Neogene seawater 87Sr/86Sr. Geology, 23, pp. 403-406.

Faure, G., Crocker, J.H., and Hurley, P.M., **1967**. Some aspects of the geochemistry of Sr and Ca in the Hudson Bay and the Great Lakes, Geochimica et Cosmochimica Acta, 31, pp. 451-461.

Faure, G., Assereto, R., and Tremba, E.L., **1978**. Strontium isotope composition of marine carbonates of Middle Triassic to Early Jurassic age, Lombardic Alps, Italy. Sedimentology, 25, pp. 523-543.

Faure, G., **1986**. Principles of Isotope Geology, second edition, John Wiley and Sons, New York, 589 p.

Faure, G., and Mensing. T.M., **2004**. Isotopes: Principles and applications, third edition, Wiley Edition, 928 p.

Flügel, E., **2010**. Microfacies of carbonate rocks: Analysis, Interpretation and Application. 2nd Edition, Springer, 1006 p.

Frijia, G. and Parente, M., **2008**. Strontium isotope stratigraphy in the upper Cenomanian shallow-water carbonates of the southern Apennines: Short-term perturbations of marine $^{87}Sr/^{86}Sr$ during the oceanic anoxic event 2. Palaeogeography, Palaeoclimatology, Palaeoecology 261, pp. 15-29.

Goldstein, S.J., and Jacobson, S.B., **1988**. Nd and Sr isotopic systematics of river water suspended material: Implications for crustal evolution. Earth and Planetary Science Letters, 87, pp. 359-265.

Hein, J.R., Yeh, H.-W., Gunn, S.H., Sliter, W.V., Benninger, L.M., and Wang, C.-H., **1993**. Two major Cenozoic episodes of phosphogenesis recorded in equatorial Pacific seamount deposits. Paleoceanography, 8, pp. 293–311.

Henderson, G. M., Martel, D. J., O'Nions, R. K., and Shackleton, N. J., **1994**. Evolution of seawater $^{87}Sr/^{86}Sr$ over the last 400 ka: the absence of glacial/interglacial cycles. Earth Planet. Sci. Lett. 128, pp. 643–651.

Hess, J., Bender, M.L. and Schilling, J.-G., **1986**. Evolution of the ratio of Strontium-87 to Strontium-86 in seawater from Cretaceous to present. Science 231, pp. 979-984.

Hess, J. L., Scott, D., Bender, M. L., Kennett, J. P. and Schilling, J. -G., **1989**. The Oligocene marine microfossil record: Age assessments using strontium isotopes. Paleoceanography, 4, 6, pp. pp. 655-679.

Hochard, C., Vérard, C., and Baumgartner, P.O., **2011**. Geodynamic evolution of the Earth over 600 Ma: implications for palaeo-climatic indicators. American Geophysical Union Fall Meeting (AGU), San Francisco, California, December 5–9, 2011.

Hodell, D.A., Benson, R.H., Kennett, J.P., and Bied, K.R.E., **1989a**. Stable isotope stratigraphy of latest Miocene sequences in northwest Morocco: the Bou Regreg section. Paleoceanography 4, pp. 467–482.

Hodell, D.A., Mueller, P.A., McKenzie, J.A. and Mead, G.A., **1989b**. Strontium isotope stratigraphy and geochemistry of the late Neogene ocean. Earth Planet. Sci. Lett. 92, pp. 165-178.

Hodell, D.A., Mead, G.A.,and Mueller, P.A., **1990**. Variation in the strontium isotopic

composition of seawater (8 Ma to resent): Implications for chemical weathering rates and dissolved fluxes to the oceans. Chemical Geology, 80, pp. 291-307.

Hodell, D.A., Mueller, P.A. and Garrido, J.R., **1991**. Variations in the strontium isotopic composition of seawater during the Neogene. Geology 19, pp. 24-27.

Hodell, D.A. and Woodruff, F., **1994**. Variations in strontium isotopic ratio of the seawater during the Miocene: Stratigraphic and geochemical implications. Paleoceanograpy 9, pp. 405-426.

Hoefs, J., **2009**. Stable Isotope Geochemistry. Sixth Edition. Springer, 293 p.

Holland, H.D., **1984**. The Chemical Evolution of the Atmospheres and Ocean. Princeton University, Princeton, N.J., 582 p.

Howarth, R.J., and McArthur, J.M., **1997**. Statistics for strontium isotope stratigraphy. A robust LOWESS fit to the marine Sr-isotope curve for 0 - 206 Ma, with look-up table for the derivation of numerical age. Journal of Geology, 105, pp. 441-456.

Hudson, J.D., and Andersen, T.F., **1989**. Ocean temperature and isotopic compositions through time. Transactions of the Royal Society of Edinburgh: Earth Science, 80, pp. 183-192.

Jenkyns, H. C., Paull, K., Cummins, D. I., and Fullagar, P. D. **1995**. Strontium-isotope stratigraphy of lower Cretaceous atoll carbonates in the mid Pacific Mountains. Proc. Ocean Drilling Prog. Sci. Results 143, pp. 89–97.

Jones, C.E., Jenkyns, H.C., and Hesselbo, S.P., **1994a**. Strontium isotopes in the Early Jurassic seawater. Geochimica et Cosmochimica Acta, 58, pp. 1285-1305.

Jones, C.E., Jenkyns, H.C., Coe, A.L. and Hesselbo, S., **1994b**. Strontium isotopic variations in the Jurassic Cretaceous seawater. Geochimica et Cosmochimica Acta, 58, pp. 3061-3074.

Jones, C.E., and Jenkyns, H.C., **2001**. Seawater strontium isotopes, oceanic anoxic events, and seafloor hydrothermal activity in the Jurassic and Cretaceous. Am. J. Sci. 301, pp. 112–149.

Karim, A., and Veizer, J., **2000**. Weathering processes in the Indus River Basin: implications from riverine carbon, sulphur, oxygen, and strontium isotopes. Chemical Geology, 170, pp. 153-177.Knoerich, A.C. and Mutti, M., **2006**. Epitaxial calcite cements in Earth history; a cooler-water phenomenon during aragonite-sea times? Geological Society Special Publications, 255, pp. 323-335

Kocsis, L., Osi, A., Vennemann, T., Trueman, C.N., and Palmer, M.R., **2009a**. Geochemical study of vertebrate fossils from the Upper Cretaceous (Santonian) Csehbánya

Formation (Hungary): Evidence for a freshwater habitat of mosasaurs and pycnodont fish. Palaeogeography, Palaeoclimatology, Palaeoecology, 280, pp. 532–542.

Kocsis, L., Vennemann, T.W., Hegner, E., Fontignie, D., and Tütken, T., **2009b**. Constraints on Miocene oceanography and climate in the Western and Central Paratethys: O-, Sr-, and Nd-isotope compositions of marine fish and mammal remains. Palaeogeography, Palaeoclimatology, Palaeoecology, 271, pp. 117–129.

Koepnick, R. B., Denison, R. E., Burke, W. H., Hetherington, E. A., and Dahl, D. A. **1990**. Construction of the Triassic and Jurassic portion of the Phanerozoic curve of seawater $^{87}Sr/^{86}Sr$. Chemical Geology (Isot. Geosci. Sect.), 80, pp. 327–349.

Koepnick R.B., Burke W.H., Denison R.E., Heatherington E.A., Nelson H.F., Otto J.B., and Waite L.E., **1985**. Construction of the Seawater 87Sr/86Sr curve for the Cenozoic and Cretaceous: supporting data. Chemical Geology (Isot. Geosc. Sect.), 58, pp. 55-81.

Korte, C., Kozur, H.W., Bruckschen, P., and Veizer, J., **2003**. Strontium isotope evolution of Late Permian and Triassic seawater. Geochimica et Cosmochimica Acta 67, pp. 47–62.

Kürschner, W., Becker , R.T., Buhl, D and Veizer, J. **1993**. Strontium isotopes in conodonts: Devonian-Carboniferous transition, the northern Rhenish Slate Mountains, Germany. Annales de la Société Géologique de Belgique, 115, pp. 595-621.

Lasaga, A.C., and Berner, R.A., **1998**. Fundamental aspects of quantitative models for geochemical cycles. Chemical Geology, 145, pp. 161–175.

Lawrence, J.R., **1973**. Interstitial water studies, Leg 15 - oxygen and carbon isotope variations in water carbonates and silicates from the Venezuela Basin (Site 149) and the Aves Rise (Site 148), Initial Report of Deep Sea Drilling Project, 20, pp. 891-899.

Lawrence, J.R., **1974**. Stable oxygen and carbon isotope variations in the pore waters carbonates and silicates, Sites 225 and 228, Red Sea, Initial Report of Deep Sea Drilling Project, 23, pp. 939-942.

Lawrence, J.R., Gieskies, J., and Anderson, T.F., **1975a**. Oxygen isotope material mass balance calculations, Leg 35, Initial Report of Deep Sea Drilling Project, 35, pp. 507-512.

Lawrence, J.R., Gieskies, J., and Broekcer, W.S., **1975b**. Oxygen isotope and cation composition of DSDP pore waters and the alteration of Layer II basalts. Earth and Planetary Science Letters, 27, pp. 1-10.

Li, D., Shields-Zhou, G.A., Ling, H.-F., and Thirwall, M., **2011**. Dissolution methods for strontium isotope stratigraphy: Guidelines for the use of bulk carbonate and

phosphorite rocks. Chemical Geology, 209, Issues 3-4, pp. 133-144.

Ludwig, K.R., Halley, R.B., Simmons, K.R., and Peterman, Z.E., **1988**. Strontium-isotope stratigraphy of Enewetak Atoll. Geology, 16, pp. 173-177.

Marshall, D.J., **1988**. Cathodoluminescence of geological materials. 146 pp., London (Unwin Hyman)

Martin, E.E. and McDougall, J.D., **1991**. Seawater Sr isotopes at the Cretaceous/Tertiary boundary. Earth and Planetary Science Letters, 104, pp. 166-180.

Martin, E.E., Macdougall, J.D., Herbert T.D., Paytan, A., and Kastner, M., **1995a**. Strontium and neodymium isotopic analyses of marine barite separates. Geochimica et Cosmochimca Acta, 59, pp. 1353-1361.

Martin, E.E. and Macdougal, J.D. (**1995b**): Sr and Nd isotopes at the Permian/Triassic boundary: A record of climate change. Chemical Geology, 125: 73-99.

Martin, E.E., Shackleton, N.J., Zachos, J.C., and Flower, B.P., **1999**. Orbitally-tuned Sr isotope chemostratigraphy for the late middle to late Miocene, Paleoceanography 14, pp. 74-83.

Martin, E.E., and Scher, H.D., **2004**. Preservation of seawater Sr and Nd isotopes in fossil teeth: bad new and good news. Earth and Planetary Science Letters, 220, pp. 25-39.

McArthur, J.M., **1994**. Recent trends in strontium isotope stratigraphy. Terra Nova, 6. p. 331-358.

McArthur, J.M., Thirlwall, M.F., Gale, A.S., Chen, M., and Kennedy, W.J., **1993a**. Strontium isotope stratigraphy in the Late Cretaceous: numerical calibration of the Sr isotope curve and intercontinental correlation for the Campanian, Paleoceanography 8, pp. 859-873.

McArthur, J.M., Thirlwall, M.F., Burnett, J., Kennedy, W.J., Gale, A.S., Mattey, D., and Lord, A.R., **1993b**. Strontium-isotope stratigraphy in the Late Cretaceous: a new curve, based on the English Chalk. In Hailwood, E., and Kid, R., eds. High resolution stratigraphy. Geol. Soc. Lond. Spec. Publ. 70, pp. 195–209.

McArthur, J.M., Kennedy, W.J., Chen, M., Thirlwall, M.F., and Gale, A.S., **1994**. Strontium isotope stratigraphy for Late Cretaceous time: Direct numerical calibration of the Sr isotope curve based on the US Western Interior. Palaeogeography, Palaeoclimatology, Palaeoecology, 108, pp. 95-119.

McArthur, J.M., Thirlwall, M.F., Engkilde, M., Zinsmeister, W.J., and Howarth, R.J., **1998**. Strontium isotope profiles across K/T boundary sequences in Denmark and Antarctica, Earth Planet. Sci. Lett. 160, pp. 179.192.

McArthur, J.M., **1998**. Strontium Isotope Stratigraphy. Unlocking the Stratigraphical Record: Advances in Modern Stratigraphy. Edited by P. Doyle and M.R. Bennet. John Wiley & Sons Ltd, Chapter 8.

McArthur, J. M., and Morton, M. **2000**. Strontium isotope stratigraphy of the Aalenian/Bajocian auxiliary stratotype point at Bearreraig, Isle of Skye, NW Scotland. GeoRes. Forum 6, pp. 137–144.

McArthur, J.M., Howarth, R.J., and Bailey, T.R., **2001**. Strontium isotope stratigraphy: LOWESS version 3: best fit to the marine Sr-isotope curve for 0–509 Ma and accompanying look-up table for deriving numerical age. J. Geol. 109, pp. 155-170.

McArthur, J.M., and Howarth, R.G., **2004**. Chapter 7 in: A Geologic Time Scale 2004, eds. Felix M. Gradstein, James G. Ogg, and Alan G. Smith. Cambridge University Press, pp. 96- 105.

McArthur, J.M., Rio D., Massari, F., Castradori, D., Bailey, T.R., Thirlwall, M., and Houghton, S., **2006**. A revised Pliocene record for marine-87Sr/86Sr used to date an interglacial event recorded in the Cockburn Island Formation, Antarctic Peninsula. Palaeogeography, Palaeoclimatology, Palaeoecology 242, pp. 126-136.

McArthur, J.M., Doyle, P., Leng, M.J., Reeves, K., Williams, C.T., Garcia-Sanchez, R., and Howarth, R.J., **2007**. Testing palaeo-environmental proxies in jurassic belemnites: Mg/Ca, Sr/Ca, Na/Ca, $\delta^{18}O$ and $\delta^{13}C$. Palaeogeography, Palaeoclimatology, Palaeoecology, 252 (3-4), pp. 464 - 480.

McCauley, S.E., and DePaolo, D.J., **1997**. The marine $^{87}Sr/^{86}Sr$ and $\delta^{18}O$ records, Himalayan alkalinity fluxes, and Cenozoic climate models. In: Ruddiman, W.F. (Ed.), Tectonic Uplift and Climate Change. Plenum, New York, pp. 427– 467.

McKenzie, J.A., Isern, A., Elderfield, H., Williams, A., and Swart, P.K., **1993**. Strontium Isotope dating of paleoceanographic, lithologic, and dolomitization events on the northeastern Australian margin, Leg 133. Proc. of the ODP, Scientific Results 133, pp. 489-498.

McKenzie, J.A., Hodell, D.A., Mueller, P.A., and Mueller, D.W., **1988**. Application of strontium isotopes to late Miocene - early Pliocene stratigraphy. Geology 16, pp. 1022-1025.

Mead, G.A., and Hodell, D.A., **1995**. Controls on the 87Sr/86Sr composition of seawater from the middle Eocene to Oligocene: Hole 689B, Maud Rise, Antarctica, Paleogeography 10, pp. 327-346.

Miller, K.G., Feigenson, M.D., Wright, J.D., and Clement, B.M. **1991**. Miocene isotope

reference section, Deep Sea Drilling Project Site 608: an evaluation of isotope and biostratigraphic resolution, Paleoceanography 6, pp. 33-52.

Miller, K.G., Feigenson, M.D., Kent, D.V., and Olson, R.K., **1988**. Upper Eocene to Oligocene isotope (87Sr/86Sr, $\delta^{18}O$, $\delta^{13}C$) standard section, Deep Sea Drilling Project Site 522, Paleoceanography 3, pp. 223-233.

Montañez I.P., Banner J.L., Osleger D.A., Borg L.E., and Bosserman P.J., **1996**. Integrated Sr isotope variations and sea-level history of Middle to Upper Cambrian platform carbonates: Implications for the evolution of Cambrian sea-water $^{87}Sr/^{86}Sr$: Geology, v. 24, pp. 917– 920.

Ohde, S., and Elderfield, H., **1992**. Strontium isotope stratigraphy of Kita-daito-jima Atoll, North Phillipines Sea: implications for Neogene sea-level change and tectonic history. Earth and Planetary Science Letters, 113, pp. 473–486.

Oslick, J.S., Miller, K.G., Feigenson, M.D., and Wright, J.D., **1994**. Oligocene-Miocene strontium isotopes: Stratigraphic revisions and correlations to an inferred glacioeustatic record. Paleoceanography, 9, pp. 327-443.

Palmer, M.R., and Elderfield, H., **1985**. Sr isotope composition of seawater over the past 75 Myr. Nature, 314, pp. 526–528.

Palmer,M.R.,and Edmond, J.M., **1989**. The strontium isotope budget of the modern ocean. Earth and Planetary Science Letter 92, pp. 11–26.

Palmer, M.R., and Osmond, J.M., **1992**. Controls over the Sr isotope composition of river water. Geochimica et Cosmochimica Acta, 56, pp. 2099-2111.

Paytan, A., Moore, W.S., and Kastner, M., 1996. Sedimentation rate as determined by ^{226}Ra activity in marine barite: Geochimica et Cosmochimica Acta, 60, pp. 4313–4319.

Paytan, A., Mearon, S., Cobb, K., and Kastner, M., **2002**. Origin of marine barite deposits: Sr and S isotope characterization. Geology, 30, pp. 747-750.

Peterman, Z.E., Hedge, C.E., and Tourtelot, H.A., **1970**. Isotopic composition of strontium in seawater throughout Phanerozoic time. Geochimica et Cosmochimica Acta 34, pp. 105-120.

Playa, E., and Rosell, L., **2005**. The celestite problem in gypsum Sr geochemistry: An evaluation of purifying methods of gypsiferous samples. Chemical Geology, 221, pp. 102-116.

Popp, N.B., Podosek, F.A., Brannon, J.C., Anderson, T.F., and Pier, J., **1986**. 87Sr/86Sr in Permo-Carboniferous seawater from the analyses of well preserved brachiopod shells. Geochimica et Cosmochimca Acta, 50, pp. 1321-1328.

Posner, A. S., Blumenthal, N. C., and Betts, F., **1984**. Chemistry and structure of precipitated hydroxyapatites. In: Phosphate Minerals (eds. J. O. Nriaga and P. B. Moore) pp. 330–350. Springer Verlag, Berlin.

Price, G.D., and Groecke, D.R., 2002. Strontium-isotope stratigraphy and oxygen- and carbon-isotope variation during the Middle Jurassic-Early Cretaceous of the Falkland Plateau, South Atlantic. Palaeogeography, Palaeoclimatology, Palaeoecology 183, pp. 209-222.

Prokoph, A., Shields, G.A., and Veizer, J., **2008**. Compilation and time-series analyses of a marine carbonate $\delta^{18}O$, $\delta^{13}C$, $^{87}Sr/^{86}Sr$ and $\delta^{34}S$ database through Earth history. Earth-Science Reviews 87, pp. 113-133.

Quing, H, Barnes C. R., Buhl, D., and Veizer, J., **1998**. The Sr isotopic composition of Ordovician and Silurian brachiopods and conodonts: relationships to geological events and implications for coeval seawater.

Quinn, T.M., Taylor, F.W., and Halliday, A.N., **1994**. Strontium-Isotopic dating of neritic carbonates and Bougainville Guyot (Site 831), New Hebrides island arc. Proc. of ODP, Scientific Results, 134, pp. 89-95.

Ray, J.S., Veizer, J., and Davis, W.J., **2003**. C, O, Sr and Pb isotope systematics of carbon sequences of the Vindhyan Supergroup, India: age, diagenesis, correlations and implications for global events. Precambrian Research, 121, pp. 103-140.

Raymo, M.E., Ruddiman,W.F., and Froelich, P.N., **1988**. Influence of late Cenozoic mountain building on ocean geochemical cycles. Geology 16, pp. 649–653.

Raymo, M.E., and Ruddiman, W.F., **1992**. Tectonic forcing of Late Cenozoic climate. Nature 359, pp. 117–122.

Raymo, M.E., **1994**. The Himalayas, organic carbon burial, and climate in the Miocene. Paleoceanography 9, pp. 399– 404.

Richter, F.M., Rowley, D.B., and DePaolo, D.J., **1992**. Sr isotope evolution of seawater: the role of tectonics. Earth Planet. Sci. Lett. 109, pp. 11– 23.

Richter, F.M., and Turekian, K.K., **1993**. Simple models for the geochemical response of the ocean to climatic and tectonic forcing. Earth Planet. Sci. Lett. 119, pp. 121– 131.

Ruppel, S. C., James, E. W., Barrick, J. E., Nowlan, G., and Uyeno, T. T., **1996**. High-resolution $^{87}Sr/^{86}Sr$ chemostratigraphy of the Silurian: Implications for event correlation and strontium flux. Geology, 24, pp. 831-834.

Shields, G.A., **2007**. A normalized seawater strontium curve: possible implications for Neoproterozoic-Cambrian weathering rates and the further oxygenation of the Earth.

eEarth, 2, pp. 35-42.

Singh, S.K., Triverdi J.R., Pande, K., Ramesh, R., and Krishnaswami, S., **1998**. Chemical and Strontium, Oxygen, and Carbon Isotopic Compositions of Carbonates from the Lesser Himalaya: Implications to the Strontium Isotope Composition of the Source Waters of the Ganga, Ghaghara, and the Indus Rivers. Geochimica et Cosmochimica Acta, 62, pp. 743-755.

Smalley, P.C., Higgins, A.C., Howarth, R.J., Nicholson, H., Jones, C.E., Swinburne, N.H.M., and Bessa, J., **1994**. Seawater Sr isotope variations through time: a procedure for constructing a reference curve to date and correlate marine sedimentary rocks. Geology 22, pp. 431– 434.

Steuber, T., **1999**. Isotopic and chemical intra-shell variations in low-Mg calcite of rudist bivalves (Mollusca-Hippuritacea): disequilibrium fractionations and late Cretaceous seasonality. International Journal of Earth Sciences, 88, pp. 551-570.

Steuber, T., Korbar, T., Jelaska, V., and Gusic., I., **2005**. Strontium-isotope stratigraphy of Upper Cretaceous platform carbonates of the island of Bra_c (Adriatic Sea, Croatia): implications for global correlation of platform evolution and biostratigraphy. Cretaceous Research 26, pp. 741-756.

Steuber. T., and Schlüter, M., **2012**. Strontium-isotope stratigraphy of upper Cretaceous rudist bivalves: Biozones, evolutionary patterns and sea-level change calibrated to numerical ages. Earth-Science reviews, 114, pp. 42-60.

Sugarman, P. J., Miller, K. G., Bukry, D., and Feigenson, M. D. **1995**. Uppermost Campanian- Maastrichtian strontium isotopic, biostratigraphic, and sequence stratigraphic framework of the New Jersey coastal plain. Geological Society of America Bull., 107, pp. 19–37.

Swart, P.K., **1983**. Carbon and Oxygen Isotope Fractionation in Scleractinian Corals: a Review. Earth-Science Reviews, 19, pp. 5 l- 80.

Vahrenkamp, V.C., Swart, P.K., and Ruiz, J., **1988**. Constraints and interpretations of $^{87}Sr/^{86}Sr$ ratios in Cenozoic dolomites, Geophysical Research Letters, v. 15, p. 385-388.

Vasiliev, I., Reichart, G.-J., Davies, G.R., Krijgsman, W., and Stoica, M., 2010. Strontium isotope ratios of the Eastern Paratethys during the Mio-Pliocene transition; Implications for interbasinal connectivity. Earth and Planetary Science Letters, 292, pp. 123–131.

Veizer, J., **1989**. Strontium Isotopes in seawater through time. Annual Review in Earth and

Planetary Sciences, 17, pp. 141-167.

Veizer, J. and Compston, W., **1974**. $^{87}Sr/^{86}Sr$ composition of seawater during the Phanerozoic. Geochimica et Cosmochimica Acta, 38, pp. 1461-1484.

Veizer, J., Buhl, D., Diener, A., Ebneth, S., Podlaha, O.G., Bruckschen, P., Jasper, T., Korte, C., Schaaf, M., Ala, D., and Azmy, K., **1997**. Strontium isotope stratigraphy: potential resolution and event correlation. Palaeogeography, Palaeoclimatology, Palaeoecology, 132, pp. 65–77.

Veizer, J., Ala, D., Azmy, K., Bruckschen, P., Buhl, D., Bruhn, F., Carden, G.A.F., Diener, A., Ebneth, S., Goddéris, Y., Jasper, T., Korte, C., Pawellek, F., Podlaha, O.G., and Strauss, H., **1999**. $^{87}Sr/^{86}Sr$, $\delta^{13}C$ and $\delta^{18}O$ evolution of Phanerozoic seawater. Chemical Geology 161, pp. 59-88.

Veizer, J., and MacKenzie, F.T., **2003**. Evolution of sedimentary rocks, in: Treatise of Geochemistry, edited by MacKenzie, F.T., Volume 7, Sediments, diagenesis and sedimentary rocks. pp. 369-407.

Vennemann, T.W., Hegner, E., Cliff, G., and Benz, G.W., **2001**. Isotopic composition of recent shark teeth as a proxy for environmental conditions. Geochimica et Cosmochimica Acta, 65, pp. 1583–1599.

Vérard, C., Hochard, C. and Baumgartner, P., **2011**. Geodynamic evolution of the Earth over 600 Ma: palaeo- topography & -bathymetry (from 2D to 3D). American Geophysical Union Fall Meeting, (AGU), San Francisco, California, December 5-9, 2011.

Vroon, P.Z., van der Wagt, B., Koorneef, J.M., and Davies, G.R., **2007**. Problems in obtaining precise and accurate Sr isotope analysis from geological materials using laser ablation MC-ICPMS. Analytical and Bioanalytical Chemistry, 2008, 390, pp. 465–476.

Wadleigh, M.A., and Veizer, J., **1992**. $^{18}O/^{16}O$ and $^{13}C/^{12}C$ in Lower Paleozoic brachiopods: isotopic composition of sea water. Geochimica et Cosmochimica Acta, 56, pp. 431-443.

Wefer, G., and Berger, W.H., **1991**. Isotope paleontology: growth and composition of extant calcareous species. Marine Geology 100, pp. 207–248.

Wenzel, B., **1997**. Isotopenstratigraphie silurischer Abfolgen und deren palaeozeanographische Interpretation: Erlanger Geologische Abhandlungen, v. 129, 117 p.

Whittaker, S.G., and Kyser, T.K., **1993**. Variations in the neodymium and strontium isotopic composition and REE content of molluscan shells from the Cretaceous Western Interior seaway. Geochimica et Cosmochimica Acta 57, pp. 4003-4014.

Wickam, F.E., **1948**. Isotope ratios: a clue to the age of certain marine sediments, Journal of Geology, 56, pp. 61-66.

Witkowski, F.W., Blundell, D.J., Gutteridge, P., Horbury A.D., Oxtoby, N.H., and Qing, H., **2000**. Video cathodoluminescence microscopy of diagenetic cements and its application. Marine and Petroleum Geology, 17, pp. 1085-1093.

Zachos, J.C., Berggren, W.A., Aubry, M.-P., and Mackensen, A., **1992**. Isotopic and trace element geochemistry of Eocene and Oligocene foraminifers from site 748, Kerguelen Plateau. Proceedings of Ocean Drilling Program, Scientific Results, 120, pp. 839–854.

Zachos, J.C., Opdyke, B.N., Quinn, T.M., Jones, C.E., and Halliday, A.N., **1999**. Early Cenozoic glaciation, Antarctic weathering, and seawater $^{87}Sr/^{86}Sr$: is there a link? Chemical Geology, 161, pp. 165–180.

3. Methods

As mentioned in Chapter 2, various methods can be applied in order to screen samples prior to the strontium isotopic composition measurement. Screening methods applied during this thesis are explained below, they consist of Scanning Electron Microscopy, Stable Carbon and Oxygen Isotope Geochemistry, Trace elements and Cathodoluminescence. Results obtained through these methods are commonly accepted as reliable for assessing alteration and diagenetic features of a sample. In order to have to most precise strontium isotope ratios, the $^{87}Sr/^{86}Sr$ measurements were done on a Thermal Ionization Mass Spectrometer.

3.1. Scanning Electron Microscope (SEM)

All SEM-images were taken at the University of Lausanne (UNIL) using a Tescan Mira LMU Scanning Electron Microscope (SEM) operated at 20kv and ~25mm working distance. In addition, the presence of Fe and Mn was checked by Energy Dispersive Spectrometry (EDS). Representative samples were observed with SEM in order to assess the diagenetic alteration of the samples. The samples were withdrawn from the encasing rock and underwent an acid attack (HCl 10%) for a few seconds in order to clean it from calcitic debris and reveal the structure of the shell.

3.2. Stable Carbon and Oxygen Isotope Geochemistry

Carbon and oxygen isotope compositions of the samples and standards were determined with a Gasbench II coupled to a Thermo Finnigan Plus XL Isotope Ratio Mass Spectrometer (IRMS) at the Stable Isotope Laboratory of the UNIL following the method of acid digestion at 70°C (Spötl and Vennemann, 2003). Isotopic compositions of carbonate are reported in the δ-notation relative to VPDB (Vienna Peedee Belemnites). The analytical precision for this method is generally better than ±0.1‰ for O and C isotopes.

3.3. Cathodoluminescence

The cathodoluminescence analyses were carried out at the Institut de Géologie et Paléontologie at the University of Lausanne on an OPEA Cold cathode luminescence model. The images were captured using an Olympus BX51WI with a digital CC12 camera. A vibration isolation table has been added for improved high magnification imaging.

Cathodoluminescence allows distinguishing primary biogenic carbonate minerals form diagenetic overgrowths, because of their differences in trace element content, namely Fe and Mn (Baumgartner-Mora and Baumgartner 1994). In this study, cathodoluminescence was used for the observation of diagenetic phases, cementation, microstructures and eventual diagenetic signature in the fossils and rocks.

3.4. Inductively Coupled Plasma Mass Spectrometer (ICP-MS) – Trace elements

The concentrations of Mn, Fe and Sr were determined on a quadrupole spectrometer (Elan 6100 DRC).

The quadrupole spectrometer Elan 6100 DRC is used in applications that do not require the lowest possible detection limit. These applications include the analysis of a wide variety of natural solutions and dissolved solid samples (mine tails, natural and underground waters, carbonates). During this study, samples were dissolved in acetic acid in order to determine the concentrations of Mn, Fe and Sr in liquid mode.

3.5. Thermal Ionization Mass Spectrometer (TIMS) – Strontium isotope ratios

Samples for Chapter 4 and Chapter 6 were measured on TIMS at the Geneva Laboratory. Between 30 and 50 mg of powdered carbonate samples (Inocerams) were dissolved in 2.2 M acetic acid. Sr separation was carried out using columns with Sr-spec resin following the method of Kindler *et al.* (2011). Sr was loaded on single Re filaments with a Ta oxide solution and measured at a pyrometer-controlled temperature of 1470°C in static mode on a Thermo TRITON mass spectrometer (Section of Earth and Environmental Sciences, University of Geneva) on Faraday cups using the virtual amplifier design to cancel out biases in gain calibration among amplifiers. $^{87}Sr/^{86}Sr$ values were internally corrected for fractionation using a $^{88}Sr/^{86}Sr$ value of 8.375209. Raw values were further corrected for external fractionation by a value of +0.034‰, determined by repeated measurements of the

SRM987 standard ($^{87}Sr/^{86}Sr$ = 0.710248). External reproducibility of the $^{87}Sr/^{86}Sr$ ratio of the SRM987 standard for >100 measurements is 6 ppm.
For Sr isotope ratio measurements, sample surfaces were systematically mechanically abraded in order to sample only the good preserved, deeper calcite prisms and avoid any contamination by exposed surfaces.

Samples for Chapter 5 were measured for strontium isotopes at GEOMAR Helmholtz Centre for Ocean Research in Kiel, Germany. Typically 5-10mg of carbonate powder weighted into 1.5ml centrifuge tubes were dissolved in 0.5ml of 2.5N HCl at room temperature. After centrifugation the chromatographic procedures followed those of Hoernle et al. (2008). Isotope analyses were carried out in static multi-collection mode on a Thermo Finnigan TRITON-TI thermal ionization mass spectrometer (TIMS) at GEOMAR using a TaCl5 emitter on Rhenium single filaments. Sr isotopic ratios were normalized within run to $^{86}Sr/^{88}Sr$ = 0.1194 and errors are reported as 2 sigma of the mean. NBS987 standard measured along with the samples gave $^{87}Sr/^{86}Sr$ values of 0.710240 ± 0.000009 (n=10) and was normalized to $^{87}Sr/^{86}Sr$ = 0.710250 to monitor the longterm variation of NBS987 on this TIMS. Total Sr chemistry blanks were 50-100pg and thus considered negligible.

Interlaboratory bias was determined by measuring the same sample at Geneva and Kiel laboratory. In the latter laboratory, the test sample gave a strontium isotope ratio of 0.707311 ± 0.000003. The same sample yielded average strontium isotope result of 0.707308 ± 0.000003. The deviation being within the standard error, no supplementary calculation was applied.

The strontium isotope ratios vs. numerical age determined in “SIS LOOK-UP TABLE: Version 4: 08 / 04”, (Howarth and McArthur, 1997; McArthur *et al.*, 2001), are normalized to a NBS987 ratio of 0.710248. Because the values measured in this study were normalized to a ratio of 0.710250, a -0.000002 was applied to all the strontium isotope ratios.

4. $^{87}Sr/^{86}Sr$ analyses in Upper Cretaceous Formations of the Nicoya Peninsula North-Western Costa Rica

4.1. Introduction

The main aim of this study is to precise, reafirm and specify ages of the Nambi Formation, the Piedras Blancas Formation and the Quebrada Pavas Member on the Nicoya Peninsula by means of $^{87}Sr/^{86}Sr$ and so better constrain the tectonic evolution of the actual Nicoya Peninsula.

These formations have been dated by Flores (2003), Bandini *et al.*, (2008) and Andjic (2011). Flores (2003) presented a chronostratigraphic chart, which has been modified by Bandini *et al.*, (2008) (Figure 20) and will be partly completed with the data obtained in this study.

Because of the lack of datable outcrops in the studied area we decided to measure Sr isotope ratios of the samples. Furthermore, we did not have any other age constrains except from foraminifera and radiolaria assemblages. Radiolaria assemblages often give approximate ages (long intervals) of Late Cretaceous formations from Costa Rica because radiolarian biozones are not very well defined and sometimes contradicting in the Late Cretaceous (Bandini *et al.*, 2008).

The samples presented in this chapter were collected during two field campaigns during July 2008 and February-March 2010. In the inland, outcrops are rare and consequently, sampling is sparse.

The local weather with one dry and one raining season may have a major impact on the weathering of the outcrops. Good samples are hard to find and even well preserved samples may be subject to chemical weathering. Also, the abundant presence of basaltic and detrital material in this region might influence the Sr isotope ratio. As presented in Chapter 2, already small amounts of extraneous contaminant may considerably shift the Sr isotope ratio. Nevertheless, we collected samples in order to confirm and/or widen the existing datings in the region. The samples are composed of *Inoceramus* shells which, through their thick shell ma be resistant to alteration and diagensis and therefore represent the most suitable samples for $^{87}Sr/^{86}Sr$ isotope dating.

4.2. **Geographic and geologic setting**

The studied area, the Nicoya Peninsula, is located in North-West Costa Rica and covers a surface of around 7200 km^2. It borders the Pacific Ocean to the West and the Nicoya Golf Area to the East. The northern part of the Peninsula is located in the Guanacaste province and the southern part in the Puntarenas province.

The Panamean Microplate, which corresponds to the actual occidental CLIP *s.s.*, is a part of the Caribbean tectonic plate (Kerr *et al.*, 1996; Pindell *et al.*, 2006; Buchs, 2008; Baumgartner *et al.*, 2008). It is characterized by a large number of terranes, plateaus and seamounts, which are accreted in the fore-arc basin and can partially be observed in the field (Buchs, 2008). The ages of the accreted parts are variable: rocks with oceanic affinity and of Jurassic to Tertiary age are exposed in certain terranes whose origin is not related to the CLIP *s.s.* (Baumgartner & Denyer, 2006 ; Denyer *et al.*, 2006 ; Tournon & Bellon, 2009 ; Denyer & Gazel, 2009 ; Buchs *et al.*, 2009 ; Buchs *et al.*, 2010). The major eruption activity of the CLIP took place during a Turonian to Coniacian period. Rocks that are older than this age cannot have their origin in the CLIP (Baumgartner *et al.*, 2008).

The Panamean Microplate is bordered by the Mesquito Composite Oceanic Terrane (MCOT) in the North-West (Baumgartner *et al.*, 2008 ; Flores, 2009). This terrane is characterized by the presence of mafic and ultra-mafic rocks and radiolarite of an Late Triassic, Jurassic and Early Cretaceous age and by a collision of an intra-oceanic arc and a continental arc during Jurassic times. The Panamean Microplate is characterized by. Late Cretaceous or younger basaltic basements, that have been associated with oceanic plateaus such as the CLIP. The studied area lies between the Panamean Microplate and the MCOT (Figure 18). After Baumgartner *et al.* (2008) this zone represents the border between the MCOT and the CLIP *s.s.* and corresponds to the association of plateaus with an ages older than formation of the CLIP *s.s.*.

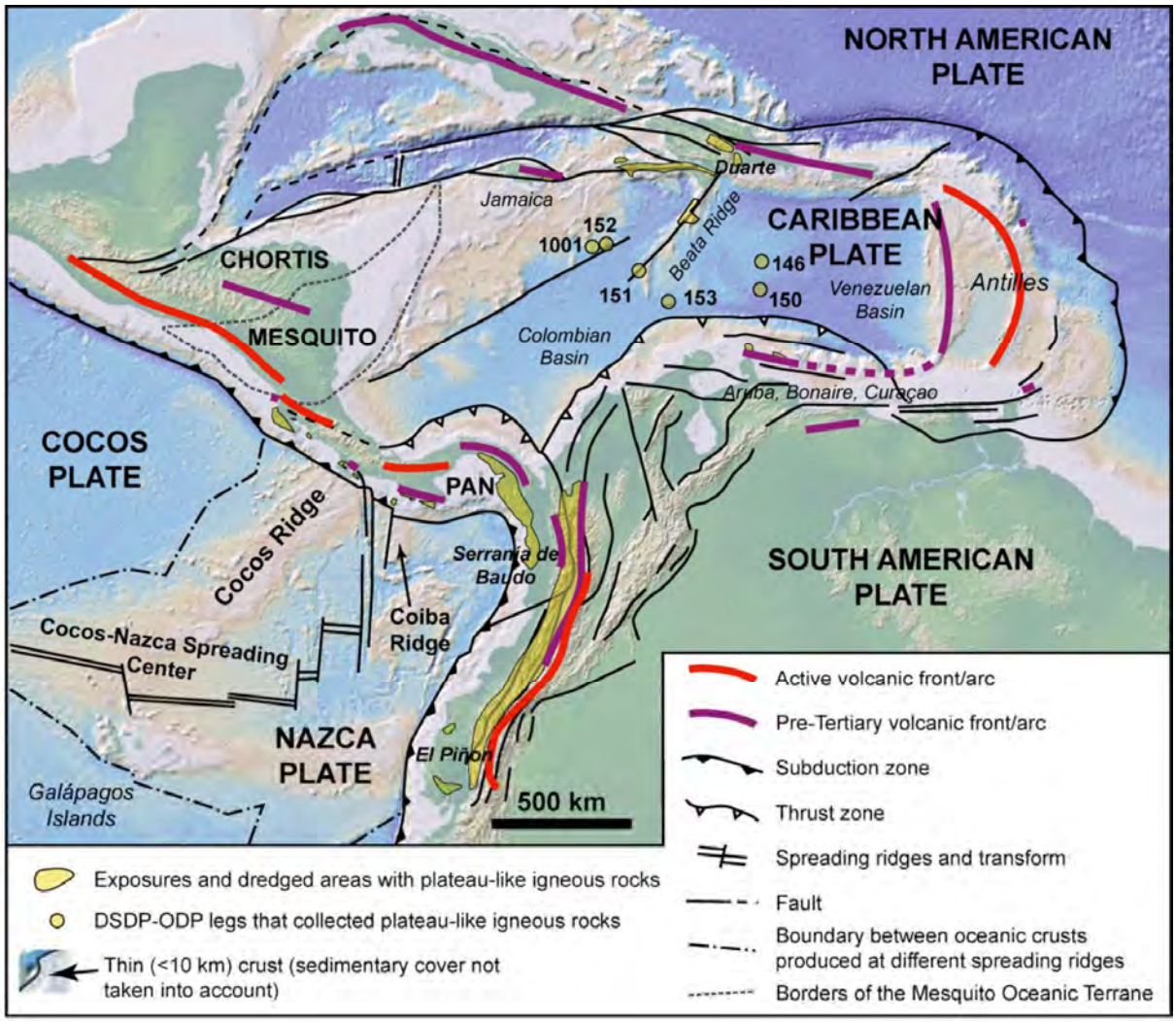

Figure 18: Tectonic and terrane map of Central America (Buchs *et al.*, 2010). The Nicoya Peninsula is located on the northwestern pacific coast of Costa Rica, on the subduction zone of the Cocos Plate under the Caribbean tectonic plate.

Flores (2006) and Bandini *et al.*, (2008) distinguish 3 different terranes in this region, the Matambù Terrane, the Manzanillo Terrane and the Nicoy Complex.

The Matambù Terrane, which includes the Loma Chumico, the Sabana Grande and the Nambì Formations. A 10 Ma gap can be observed between the Loma Chumico and Sabana Grande Formation (Figure 19, Figure 22).

The siliceous sediments of pre-Campanian age include 5 different formations. Formations that were studied during this work are written in bold.

- The Loma Chumico Formation is characterized by bituminous and pelagic sediments of Albian age with a maximum thickness of 90m (Azéma *et al.*, 1979 ; Flores, 2003 ; Flores *et al.*, 2003a). This is the oldest formation on the Nicoya Peninsula. It has been

dated by the presence of *Neokentroseras* sp. (Azéma *et al.*, 1979). The contacts with the basement or other formations are unconformable (Figure 19, Figure 22).

- The Sabana Grande Formation consists in hemipelagic and turbiditic sediments. These lithologies have been dated to a Coniacian to Middle Campanian age and reach a thickness of about 250m (Flores, 2003 ; Flores *et al.*, 2003a ; Bandini *et al.*, 2008) (Figure 19, Figure 22).
- The **Nambì** Formation is described as a hemipelagic and turbiditic formation with a Coniacian to Middle Campanian age (Bandini *et al.*, 2008). This formation indicates the erosion of a basaltic basement. Its maximum thickness reaches 130 meters (Flores *et al.*, 2003a). This formation gradually switches to the **Piedras Blancas** Formation. The Piedras Blancas Formation has a Early Coniacian age ($^{87}Sr/^{86}Sr$ age by Flores *et al.*, 2003a). Radiolarians dated this formation to a Coniacian to Maastrichtian age (Bandini *et al.*, 2008) (Figure 19, Figure 22).

The Manzanillo Terrane characterized by an arc-derived series (Berrugate Formation) (Flores *et al.*, 2003a) associated to a mafic oceanic plateau basement (Figure 19, Figure 22).

- The Berrugate Formation corresponds to fore-arc series. It is mainly composed of greenish tuffitic and volcanoclastic turbidites of metric size (Flores, 2003; Flores *et al.*, 2003a). This formation has only been described in the Golf of Nicoya, its age is Coniacian to Early Campanian, based on radiolarian age (Bandini *et al.*, 2008) (Figure 19, Figure 22).

The Nicoya Complex has been defined in Denyer and Baumgartner (2006) as a basaltic sequence older than Lower Campanian-Santonian, composed of olivine tholeiites that occur as massive and pillow flows, dykes and haylocalstic pillow breccias (Figure 19, Figure 20).

- Radiolarites can only be observed in the in North-West of the Nicoya Peninsula, their ages range from middle Jurassic to Late Cretaceous (Denyer and Baumgartner, 2006). These rocks show important deformations and are intruded by basalts and gabbros. The ages of these gabbros are younger than the radiolarites and/or have ages corresponding to the age of the CLIP *s.s.* (Sinton *et al.*, 1997 ; Hauff *et al.*, 2000). Some basalts of an Early Cretaceous age also occur (Hoernle *et al.*, 2004).

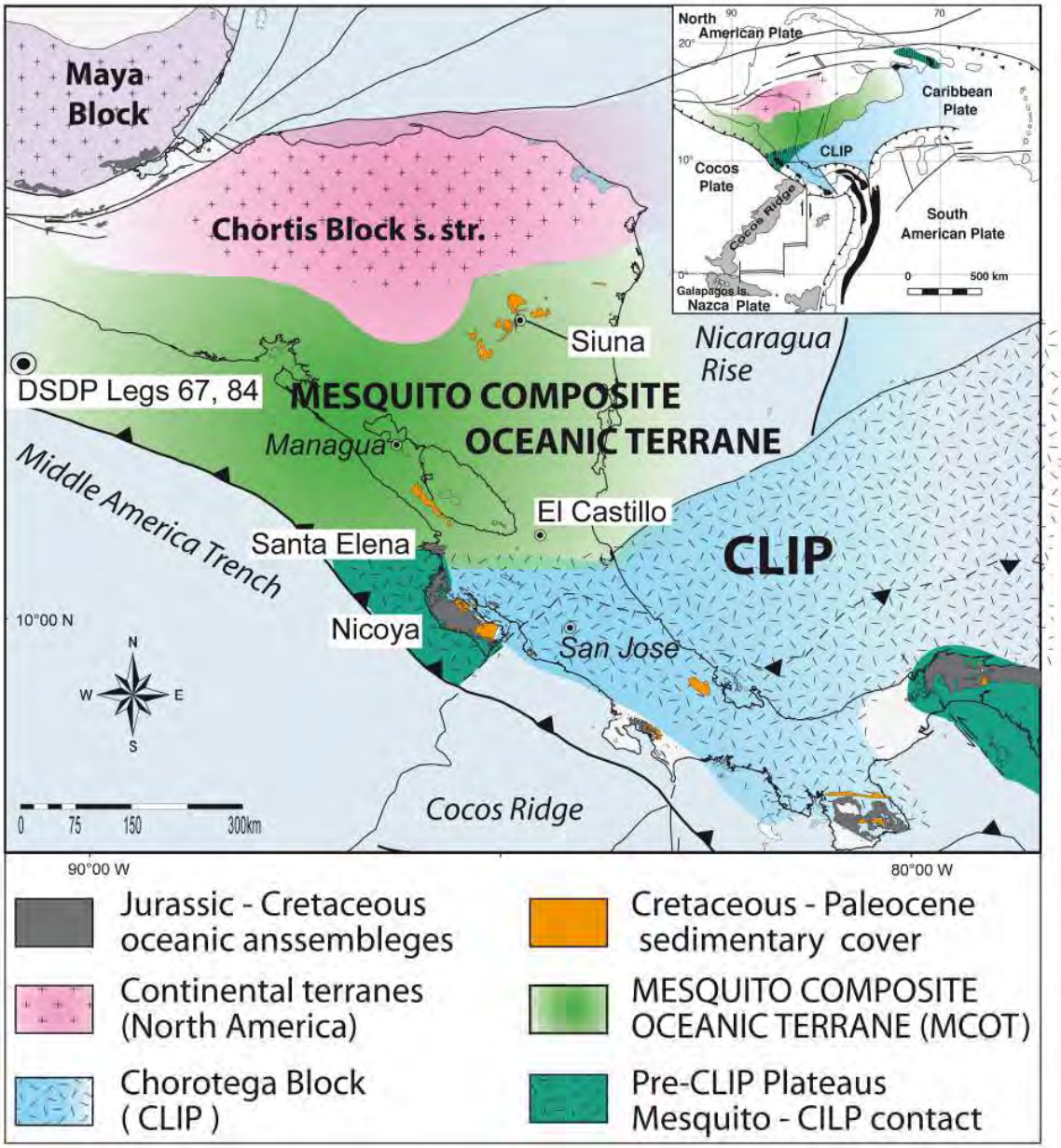

Figure 19: Terrane Map of the Nicoya Peninsula, North-West Costa Rica. On the Nicoya Peninsula, one can observe the Matambù Terrane in the west, the Nicoya Complex to the North and the Manzanillo Terrane to the East. Further North, the Santa Helena Peninsula with the Mesquito Composite Oceanic Terrane (MCOT), (not relevant for this study).

The overlap sequence is characterized by two distinct series. The first series is characterized by siliceous hemipelagic rocks with turbidites of a pre-Middle Campanian age, associated to the mafic rocks and one overlap sequence of a Middle Campanian-Paleocene age. Carbonate rocks characterize the latter, which includes reefal, neritic and hemipelagic facies with turbidites. Contacts between the different formations are generally tectonic or discordant and

sedimentary contacts with the basement are rare. The overlap sequence comprises the following formations:

- The Barbudal Formation shows shallow water volcanoclastic conglomerates reaching 50m in thickness (Rivier, 1983 ; Seyfried & Sprechmann, 1985 ; Flores, 2006). This formation only occurs on the eastern part of the Nicoya Peninsula (Flores, 2003). It is dated to Middle-Late Campanian through the presence of *Pseudorbitoides israelskyi* (Seyfried & Sprechmann, 1985) (Figure 19, Figure 22).
- The Coyolito Formation is described as an alternation of calciculites and hemipelagic arenites of about 200m (Flores *et al.*, 2003b). This formation has not been directly dated but Flores *et al.*, (2003b) suggest an Early to middle Campanian age based on its stratigraphic position (Berrugate and El Viejo Formation) (Figure 19, Figure 22).
- The El Viejo Formation is caracterized by neritic and recifal limestones and arenites, set on the slope of a carbonate platform and reaches a thickness of 150m (Seyfried & Sprechmann, 1985 ; Jaccard *et al.*, 2001 ; Flores, 2003). The age of this formation is Campanian – Maastrichtian age according to Pons & Schmidt-Effing (1989a,b) because of the presence of *Globotruncanita calcarata* and based on rudists. Middle Campanian to Maastrichtian age has been assigned to this formation by Flores (2003) and Bandini *et al.* (2008) (Figure 19, Figure 22).
- The **Piedras Blancas** Formation is composed of hemipelagic limestones and described as rich in globotruncanids with a thickness of 250m (Flores *et al.*, 2003a). Its age is described as Middle-Late Campanian to Late Maastrichtian (Galli & Schmidt-Effing, 1977; Di Marco *et al.*, 1995; Flores *et al.*, 2003a (Figure 19, Figure 20, Figure 22).
- The Curù Formation shows alternating arenites and lutites. The turbiditic characteristics indicate the erosion of a volcanic structure (Denyer *et al.*, 2005). The age of this formation has been assigned to Maastrichtian - Late Paleocene by Astorga (1987) and to Early Paleocene by Bandini *et al.*, (2008). The Curù Formation reaches a thickness of about 1500m (Astorga, 1987) (Figure 19, Figure 22).
- Flores *et al.*, (2007a) name the base of the Curù Formation the **Quebrada Pavas Member.** According to them, this 20m -50m thick sequence is characterized by highly erosional but short event at the Late Maastrichtian. It is described as sandstone (centimetric to metric layers) with conglomeratic lenses composed by rounded clasts

of basalts, radiolarites, siliciferous lutites and angular clasts of pink and white calcilutite. This unit shows parallel plane and cross laminations. It is unconformably overlying the Piedras Blancas Formation and conformably overlain by centimetric brownish lutites of the Curù Formation (Figure 19, Figure 21, Figure 22).

- The Descartes Formation consists in alternating volcanoclastic and turbiditic carbonate layers, with a thickness of about 2000m (Astorga, 1987; Denyer *et al.*, 2005). Astorga (1987) suggests an Late Paleocene to Late Eocene/Early Oligocene age for this formation, whereas Flores (2003) and Bandini *et al.*, (2008) suggest an Late Paleocene age (Figure 19, Figure 22).
- The Barra Honda Formation is characterized by micritic boundstones, packstones and sparitic grainstones with presence of algae, sponges, bryozoaria and foraminifera (Jaccard & Münster, 2001 ; Jaccard *et al.*, 2001 ; Flores *et al.*, 2003b). The thickness of this formation reaches 350m (Flores *et al.*, 2003b). The age is assigned to the Late Paleocene, based on Sr isotope dating and larger foraminifera (Jaccard & Münster, 2001) (Figure 19, Figure 22).

Figure 20: Outcrop of the hemipelagic limestones of the Peidras Blancas Formation (N 10°2.468'; W085°19.000'). DecieInoceramus shells are thick and presumably well conserved.

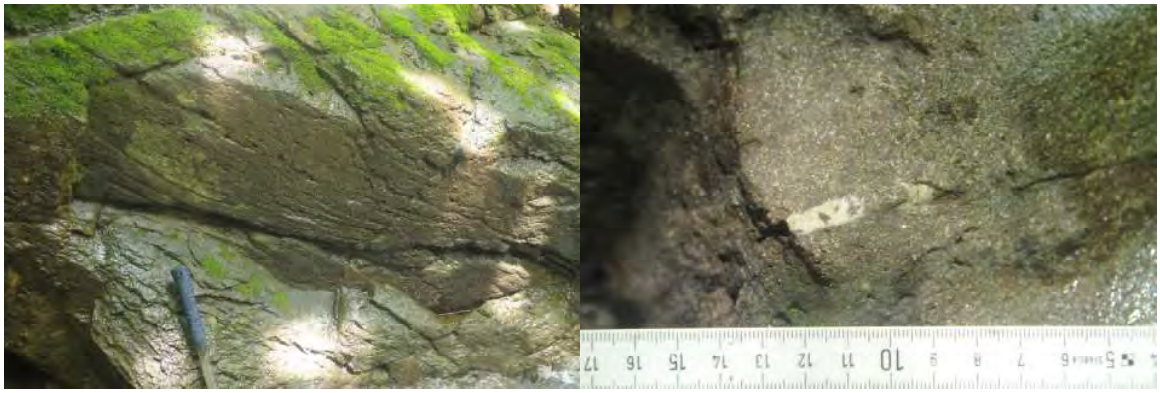

Figure 21: Outcrop of the Quebarda Pavas Member (N 10°1.900'; W085°19.120'). Th picture on left shows the Members lenses. On left, thick Inoceramus shells appear as fractured.

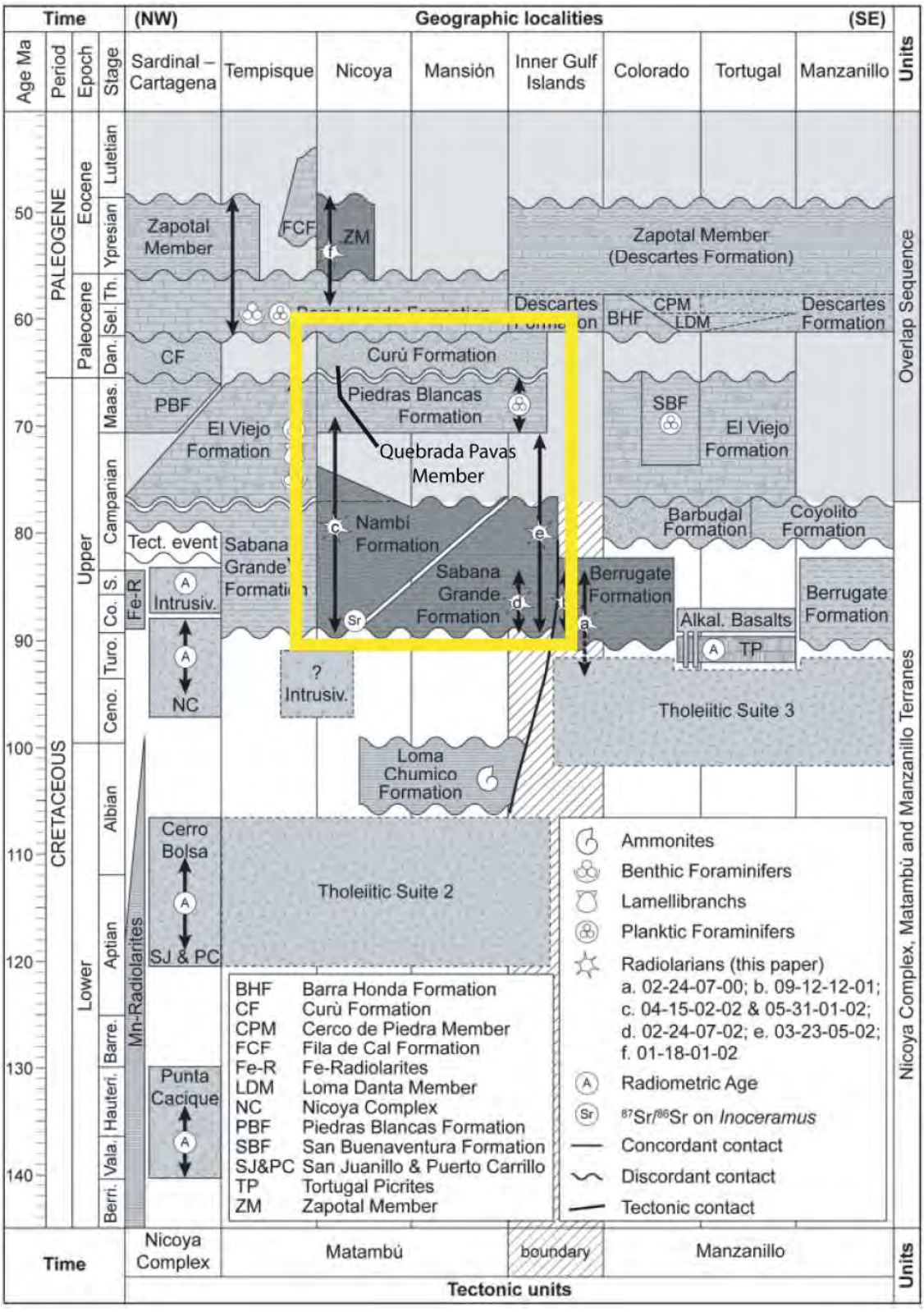

Figure 22: Chronostratigraphic chart after Bandini *et al.*, (2008) (modified after Flores, 2003). The Formations studied in this Thesis are the Nambì Formation, the Quebrada Pavas Member and the Piedras Blancas Formation. These formations are dated bay radiolarian assemblages and planctic foraminifera. Note that one single strontium isotope age (Coniacian) has been assigned at the base of the Nambì Formation.

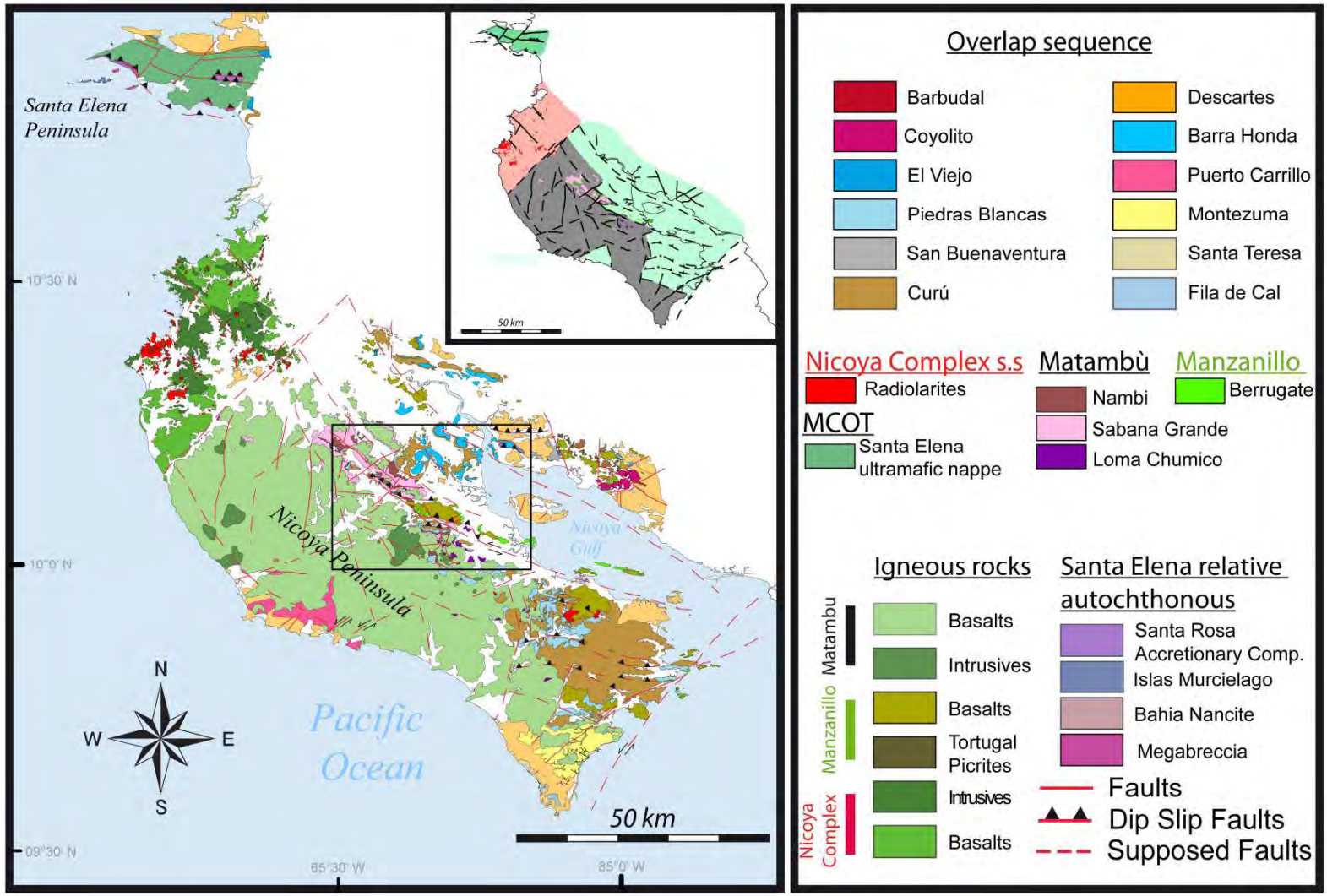

Figure 23: Geologic map of the Nicoya Peninsula. Note that the directions of faults have only been assigned when known. Faults without any direction are supposed faults. The original map is from Flores, (unpublished), modified by Andjic *et al.,* (in progress).

4.3. **Samples and Localities**

As the outcrops are sparse and often inaccessible, only few samples could be selected for Sr isotope ratio measurements. A first selection of samples was done on the field with hand lens. We selected *Inoceramus* fossils, which are the most suitable fossils for Sr isotope ratio measurements found in the studied formations; their occurrence is, in some outcrops, abundant.

Inoceramid bivalves are distributed in all palaeolatitudes and were abundant in various palaeoenvironments and palaeobathymetries from Permian to late Cretaceous times (Gòmez-Alday et al., 2008, Waterhouse, 1970, Ward et al., 1991; MacLeod, 1994; Keller, 2001). The extinction of these bivalves is accepted to be related to a global oceanic circulation change where dense, warm, deep-ocean waters were replaced by, cold oxygen-rich waters (Saltzmann *et al.*, 1982; Barron *et al.*, 1984; Barrera and Huber, 1990; Huber, 1990; Thomas, 1990, Gòmez-Alday *et al.*, 2004, 2008). The gigantism of Inoceramids is believed to be an antipredatory strategy (Elorza and Garcia-Garmilla, 1998).

Through their thick shell, Inoceramids are reltaively resistent to diagenetic alteration and provide valuable results, even though their use as a chemostratigraphic tool (Gòmez-Alday *et al.*, 2004, 2008) and palaeoenvironmental indicator (Kumagae et al., 2011) is put under discussion. Furthermore, Inoceramids have a complex shell structure with three different shell layers (Inner-, Middle- and Outer Shell Layer (ISL, MSL, OSL)) where the Inner Shell Layer has a nacreous aragonitic structure (Wright, 1987; Whittaker *et al.*, 1987; Pirrie and Marshall, 1990). Calcite prisms diameter notably decrease from the ISL towards the OSL (Elorza and Garcia-Garmilla, 1998).

The samples for the Piedras Blancas Formation were collected west of Santa Rita (N 10°2.468'; W085°19.000'), close to the outcrop of the samples of the Quebrada Pavas Member (N 10°1.900'; W085°19.120'). Samples of the Nambi Formation were collected along the Nicoya-Santa Cruz road (N10°13.083'; W085°31.099') (Figure 23, Figure 24).

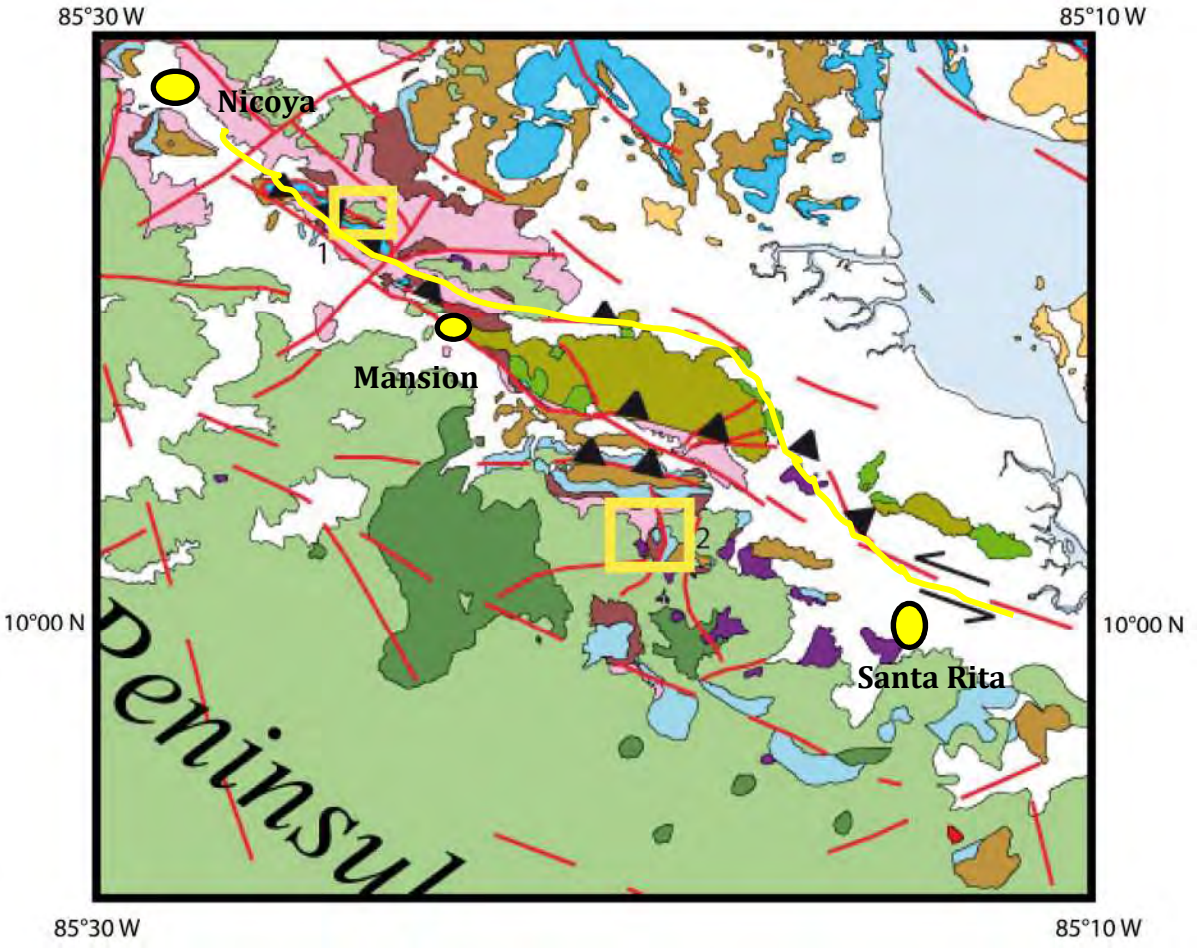

Figure 24: The yellow squares show the localisation of the samples on the geological map. The original map is from Flores, (unpublished), modified by Andjic *et al.*, (in progress). Samples of the Nambi Formation were collected along the Nicoya-Santa Cruz road (Yellow line) (Square 1), samples for the Piedras Formation and Quebrada Pavas Member were collected west of Santa Rita (Square 2). (For legend see Figure 21).

4.4. **Results**

Scanning Electron Microscope

SEM pictures reveal if the primary structure of the shell calcite has been conserved. The calcite prisms on the surface of the *Inoceramus* shell show evidences of alteration (Figure 25B, 25C, 25D). The inside mineral structure show that prisms are well preserved and minor alteration is observed and typical inter-prism boundaries can be seen (Figure 26A, 26A). Fractured prisms show inter-prism pits (Figure 26B, 26C, 26D), which may be due to carbonate dissolution or the loss of organic filaments (Marshall, 1990).

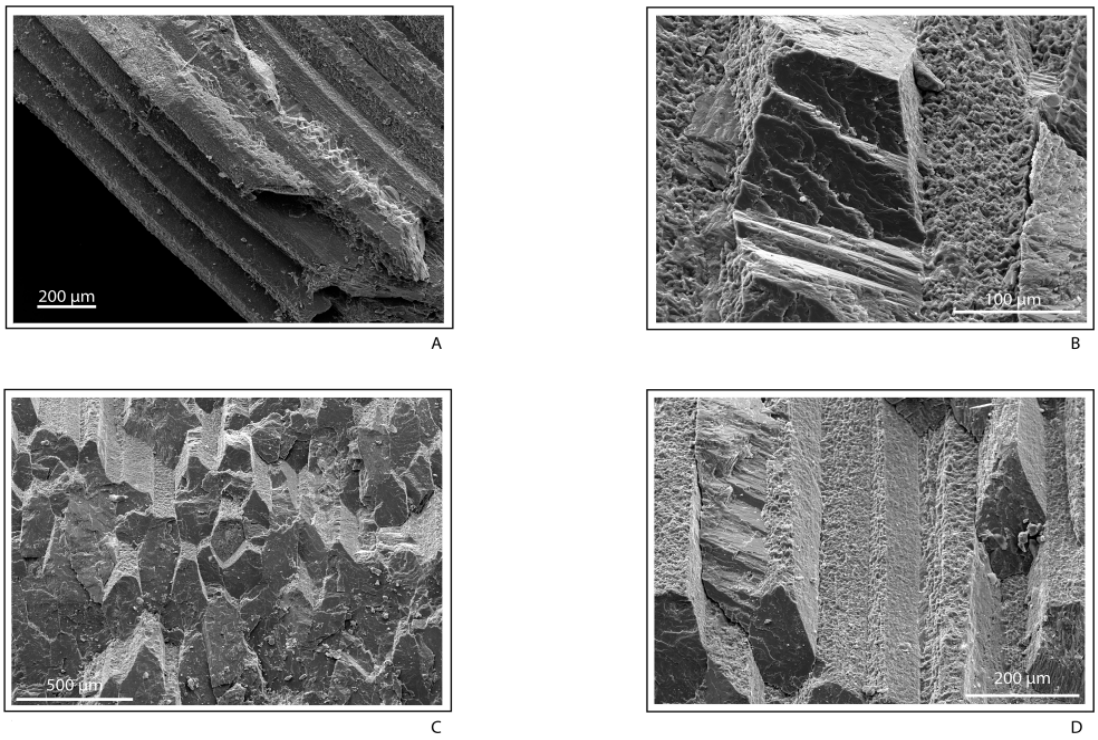

Figure 25: SEM images of *Inoceramus* shell from Nambì Formation (1-22-08-02 I). A: General overview of *Inoceramus* shell. B: Calcite prism showing light alteration. C: Perpendicular view on calcite prisms. D: Surface alteration of calcite prisms.

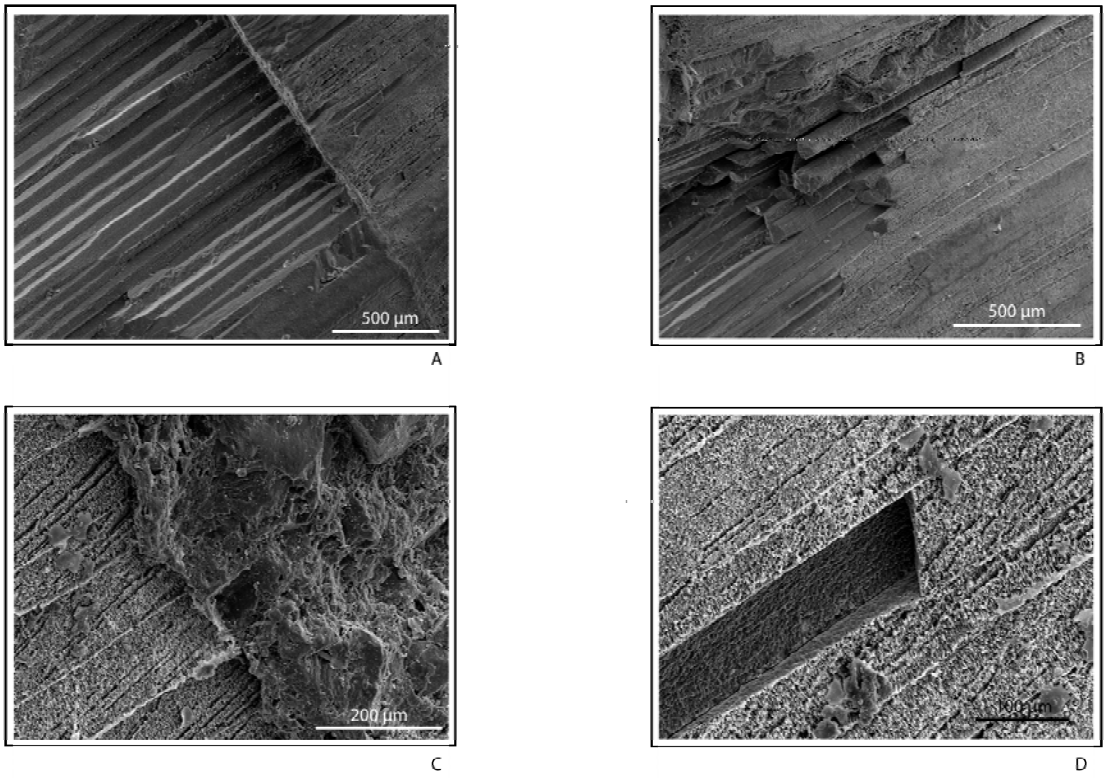

Figure 26: SEM images of *Inoceramus* shell from Quevrada Pavas Member (PA-08-019). A: 2 zones can be observed, Upper right, the altered surface prisms, lower left, unaltered prisms. B: General overview of the calcite prisms. C: Encasing rock on right, prisms with interprism infill on left. D: General overview of altered prisms.

Stable Isotopes

For the Nambì Formation, samples yield values varying between 0.0‰ and 0.3‰ for $\delta^{13}C$ and between -5.3‰ and -7.1‰ for $\delta^{18}O$ (Figure 27, Table 16 (Appendix II)).

For the Piedras Blancas Formation the measured samples yielded values ranging from 1.3‰ - 2.0‰ $\delta^{13}C$ and $\delta^{18}O$ values ranging from -5.4‰ to -5.9‰ (Figure 27, Table 16 (Appendix II)).

The isotopic composition for the samples from the Quebrada Pavas Member ranges from 2.3‰ -2.7‰ for carbon and from -2.4‰ to -2.8‰ for oxygen (Figure 27, Table 16 (Appendix II)).

One can observe a slight positive carbon isotopic shift (0.0‰ to 2.7‰) and a clear negative change for oxygen isotopes from the Quevrada Pavas Member to the Nambi Formation (from -2.4‰ down to -7.1‰).

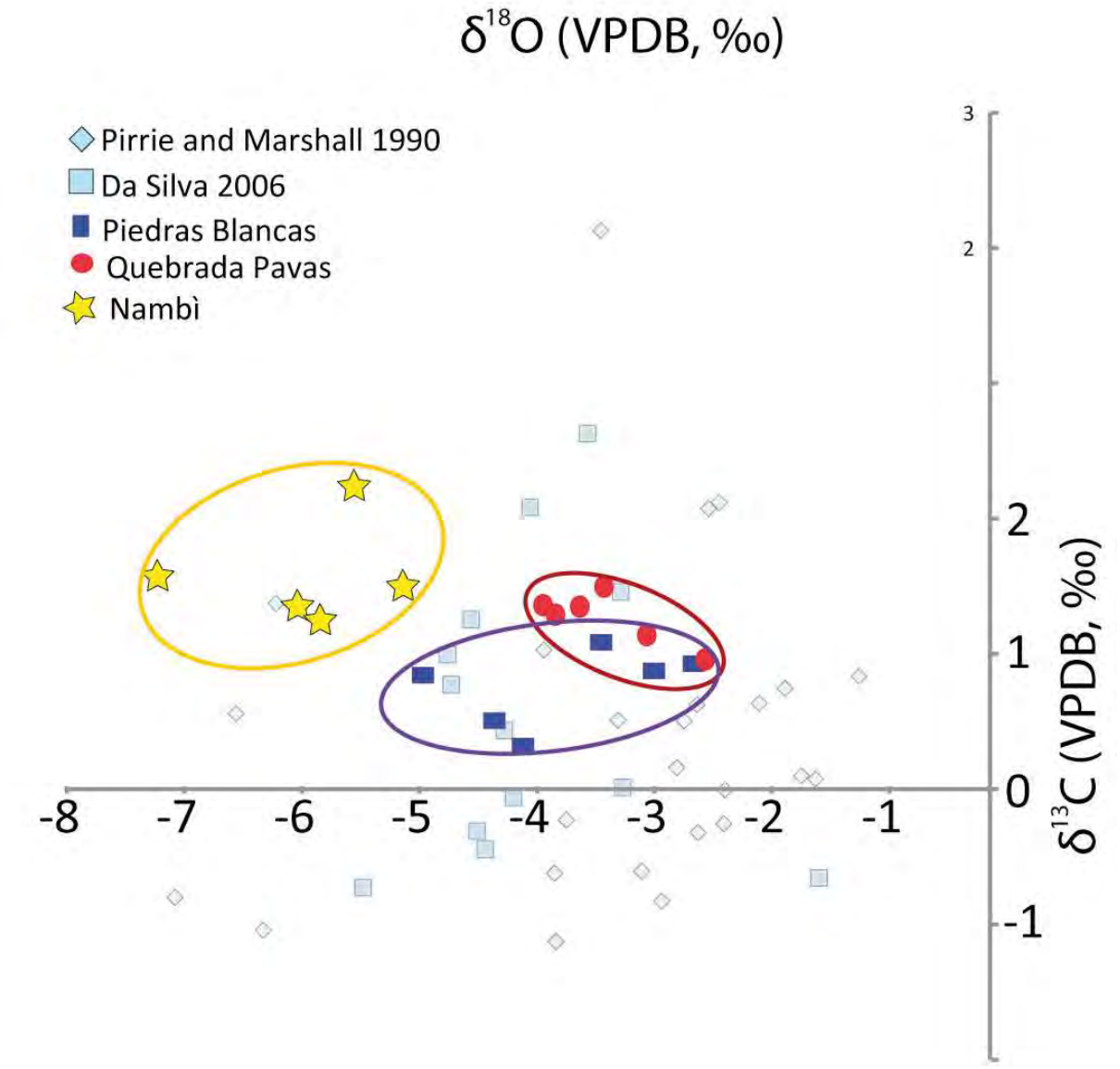

Figure 27: Plot of stable isotopes. Diamonds: Pirrie and Marshall, 1996; Squares Da Silva, 2006. These studies show the ranges of stable isotopic composition of altered *Inoceramus* samples. The *Inoceramus* samples of this study are within these ranges.

Cathodoluminescence

Samples from the Nambì Formation and the Piedras Blancas Formation show a yellowish to light reddish luminescence (Figure 28). The prisms of the calcitic shells may reveal their original shape. Along the boarder of the prisms, a yellowish luminescent material appears. In the Nambì and Piedras Blancas Formations, broken prisms are present in the host rock.

Samples from the Quebrada Pavas member show darker *Incocreamus* prisms (compared to the samples of the Nambi and Piedras Blancas Formations). Inner (ISL), middle (MSL) and outer (OSL) shell layers can be clearly distinguished (Figure 26, E +F).

A few badly preserved planktonic foraminifera have been observed in thin section with transmitted light, fortunately the cathodoluminescence technique revealed some tests of planktonic foraminifera in the Piedras Blancas Formation. The foraminifera are described in the discussion below.

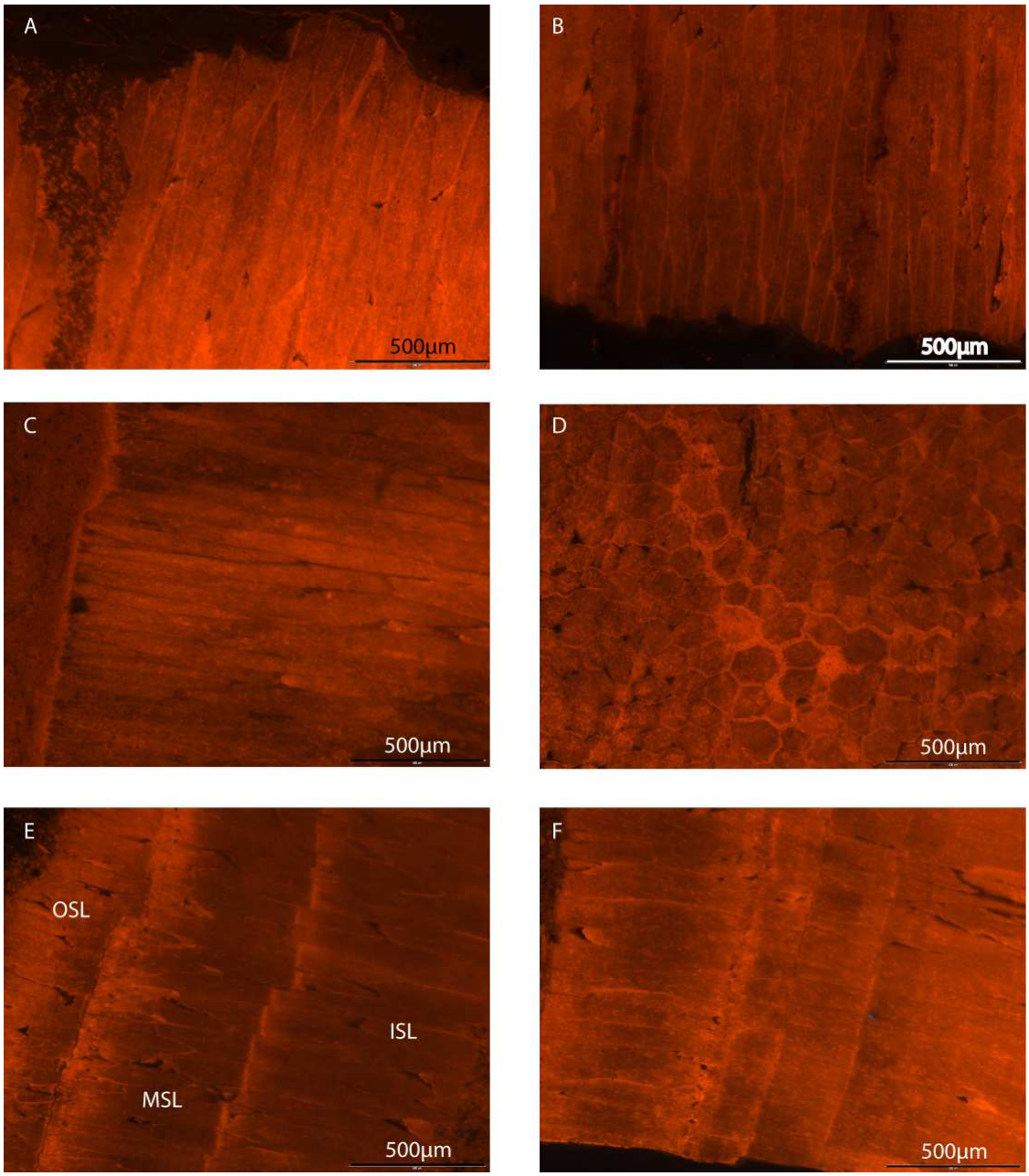

Figure 28: CL pictures of Inoceramid shells. (A+B; Nambì Formation) A: Prismatic structure of Inoceramid shell. Fracture with infill from the encasing rock. Interprism infill with yellowish luminescence B: Prismatic structure of the OSL. (C+D; Piedras Blancas) C: Prismatic structure of the OSL. Luminescent colors appear to be patchy. D: Perpendicular cut through the calcite prisms with yellowish luminescent interprism infill. (E+F; Quebrada Pavas Member) E+F: Complete structure of the shell; from OSL to ISL. Growth lines appear more luminescent than prisms. Shell in F is more luminescent than in E, maybe due to different diagenetic effects.

Trace elements

Because of their thin structures, no distinction of the shell layer could be made; in fact one powder was divided in three parts used for all three geochemical analyses (including $^{87}Sr/^{86}Sr$). The obtained results are then directly linked to the Sr isotope analyses.

The Inoceramids from the Nambì Formation, Piedras Blancas Formation and the Quebrada Pavas Formation show various ranges of Mn and Fe and low Sr concentrations. The results presented in Table 1, are average values obtained for the Inoceramids expressed in ppm. The high concentrations of Mn and Fe combined with the relatively low concentrations of Sr indicate alteration by diagenetic fluid.

	Mn (ppm)	Fe (ppm)	Sr (ppm)
Nambi	5312	1966	92
Piedras Blancas	748	1791	210
Quebrada Pavas Member	568	1135	220

Table 1: Average concentrations of Mn, Fe and Sr of *Inocemramus* shell samples. Samples show high concentrations in Mn and Fe and low concentrations of Sr. This combination shows the samples underwent diagenetic alteration, especially because of low Sr concentrations. Samples from Quebrada Pavas Member and Piedras Blancas Formation show better results than the samples of the Nambi Formation. The concentrations are average values obtained by the measurement of two Inoceramid samples from the same locality and that were measured for strontium isotope ratios (Nambì: 3 samples VU-08-22I, 1-22-08-02 I, 2-24-08-02 I ; Quebrada Pavas: 2 samples PA-08-019, 6-23-08-02 I, Piedras Blancas: 1 sample PA-08-021).

4.5. $^{87}Sr/^{86}Sr$ results and ages

The presented data show good reproducibility of the Sr isotope measurements. Multiply sampling and repeated analyzes of the same samples are also within their respective standard error.

The Sr isotope ratios range from 0.707296 to 0.707763 (Table 2), (Figure 29), which define an age younger than Turonian and older than Late Maastrichtian (Howarth and McArthur, 1997; McArthur *et al.*, 2001).

The Nambì Formation reveals ages ranging from Late Turonian (94.00 Ma – 94.30 Ma) to Late Cenomanian (87.05 Ma - 97.75 Ma). In this formation we could also date intermediate samples to a Lower Turonian age (Table 2), (Figure 29).

The selected samples for $^{87}Sr/^{86}Sr$ from the Piedras Blancas Formation yielded a Late Campanian age (72.90 Ma - 74.35 Ma), (Table 2), (Figure 29).

The Sr isotope ratios allow dating the Quebrada Pavas from Late Campanian (71.85 Ma - 72.2 Ma) to Lower Maastrichtian (67.00 Ma - 72.25 Ma) (Table 2), (Figure 29).

Sample Name	Formation	$^{87}Sr/^{86}Sr$	2SE	Age (Ma)
1-22-08-02 I	Nambì	0.707323	0.000006	88.90-89.25 or 91.80-91.95
1-22-08-02 III	Nambì	0.707320	0.000012	88.85-89.25 or 91.95-92.55
3-26-06-04 I	Nambì	0.707296	0.000006	89.40-89.95
3-26-08-04 II	Nambì	0.707306	0.000048	88.10-90.10
VU-08-22I	Nambì	0.707379	0.000006	87.10-87.70 or 94.00-94.25
VU-08-22II	Nambì	0.707379	0.000014	87.05-87.75 or 93.85-94.30
2-24-08-02 I	Nambì	0.707298	0.000008	89.65-89.95 or 90.00-90.85
2-24-08-02 II	Nambì	0.707300	0.000006	89.35-89.7 or 90.15-90.80
2-24-08-02 III	Nambì	0.707305	0.000014	89.05-89.95 or 90.55-91.40
PA-08-021 I	Piedras Blancas	0.707654	0.000014	72.9-74.35
PA-08-021 II	Piedras Blancas	0.707657	0.000008	73.00-74.05
PA-08-021 III	Piedras Blancas	0.707660	0.000004	73.3-73.75
PA-08-019	Quebrada Pavas	0.707717	0.000004	71.20-71.85
PA-08-16	Quebrada Pavas	0.707763	0.000046	67.00-71.95
6-23-08-02 I	Quebrada Pavas	0.707706	0.000004	71.75-72.10
6-23-08-02 II	Quebrada Pavas	0.707699	0.000004	71.85-72.25
PA-08-021 B	Piedras Blancas	0.707585	0.000008	87Sr/86Sr of encasing rock
VU-08-22B	Nambì	0.706550	0.000006	

Table 2: Sr isotopic results with Standard error and deducted ages after (Howarth and McArthur, 1997; McArthur *et al.*, 2001). For the Nambì Formation, note that the inversion of the curve occurs at 90.00 an that the limit between Turonian and Coniacian is situated at 89.27 Ma (ages from the TS2004). Note that all the measurements have been done on Inoceramid shell samples, except PA-08-021B and VU-08-22 B; these results correspond to the strontium isotope ratio of the encasing rock.

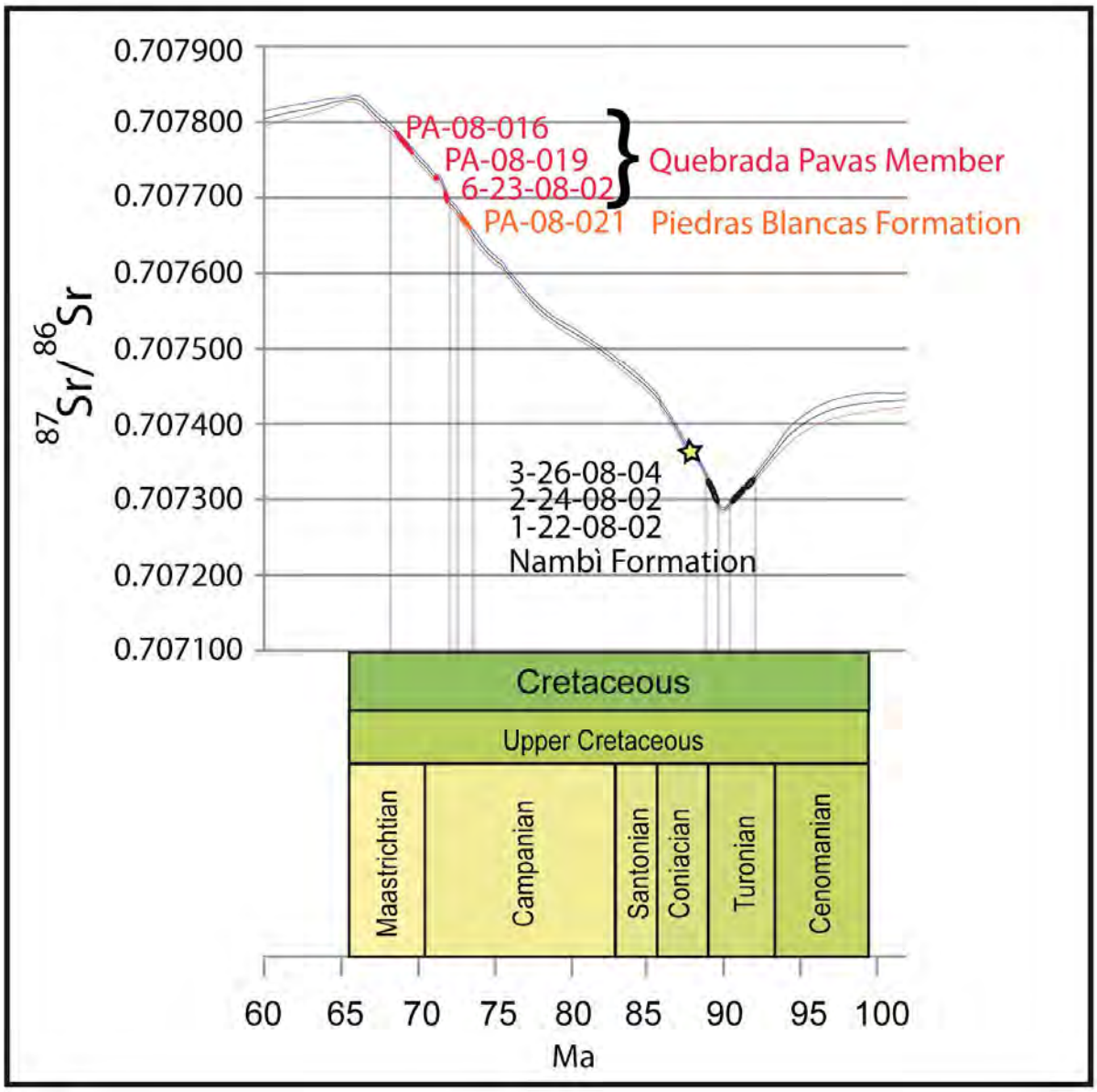

Figure 29: Strontium isotope ratios plotted on $^{87}Sr/^{86}Sr$ curve by Howarth and McArthur, 1997; McArthur *et al.*, 2001. Samples from the Nambì Formation cluster around Turonian-Coniacian ages. Because no further information permits to assign better age constrains, two possible ages have been considered in this study. A sample from the Piedras Blancas Formation yielded a Late Campanian age for this Formation. Samples from the Quebrada Pavas Member show Maastrichtian ages. The yellow star marks the Strontium isotope age obtained by Flores *et al.* (2003a).

4.6. Discussion

Screening results

The oxygen isotope composition of the samples from the Nambi and Piedras Blancas Formations (Nambì, $\delta^{18}O$ between -5.3‰ and -7.1‰, Piedras Blancas $\delta^{18}O$ between -5.4‰ and -5.9‰) indicate they were influenced by diagenesis and underwent more alteration when compared to samples from the Quebrada Pavas Formation ($\delta^{18}O$ between -2.4‰ and -2.8‰).
The carbon and oxygen stable isotope results are comparable to the isotopic compositions described for *Inoceramus* by Pirrie and Marshall, (1990) and Da Silva, (2006) (Figure 26). Saltzmann and Barron (1982), consider *Inoceramus* to precipitate their shell in equilibrium with the oxygen isotopic composition of ambient waters.
They invoke that well-preserved Inoceramus should present isotopic compositions ranging from 1.1‰ to -2.6‰ for $\delta^{18}O$ and from 1.9‰ to -1.3‰ for $\delta^{13}C$.
Pirrie and Marshall (1990) present results that are close to those from this study and mentions that palaeoenvironmental conditions may influence the isotopic composition. This work is based on a diagenetic study on Inoceramids. Gòmez-Alday *et al.*, (2008), also measured similar stable isotope values, which they interpret as burial diagenesis. They also proof an increase of Sr isotope ratios with depletion in $\delta^{18}O$ values in their samples, which might be due to the presence of transformed clay minerals.

Cathodoluminescence shows the same trend than stable isotope composition. In the Quebrada Pavas Member, the selected Inoceramids show less bright luminescence than in the two other formations, which is limited to the external borders of the shell. Prisms belonging to the MSL and ISL seem to have undergone less important diagenetic effects (Figure 28).

From the screening results, two groups of samples can be distinguished. Samples from the Nambì and Piedras Blancas Formations appear to be more altered than the samples of the Quebrada Pavas Member. This is evidenced by the SEM and cathodoluminescence microscopy but also by the oxygen isotopes, which are more negative for Nambì and Piedras Blancas Formations than for the Quebrada Pavas Formation. Additionally low concentrations of Sr combined with the low $\delta^{18}O$ is may be linked to a late meteoric alteration of the Inoceramid shells.
Inoceramids from the Quebrada Pavas Formation seem to have a relatively better preservation, but the $\delta^{18}O$ values may be also linked here to some meteoric water contribution. However

cathodoluminescence and SEM microscopy also indicate better preservation of the original structure. Consequently, the Sr isotope ratios obtained for Quebrada Pavas may have a higher reliability than the two other studied formations.

Gòmez-Alday *et al.*, (2008) mention a possible misleading interpretation of chemostratigraphic results on *Inoceramus* shells, even if cathodoluminescence, major and trace element contents and stable isotopic data indicate just a slight alteration. This does not exclude *Inoceramus* shells to provide good Sr isotopic ages. The luminescent material that is present between the calcite prisms is considered as the pathway for diagenetic fluids (Elorza and Garcia-Garmilla, 1998).

Micropaleonological age of Piedras Blancas sample

In cathodoluminescent light a thin section of the Piedras Blancas Formation revealed the presence of foraminifera such as *Globigerinoides*, *Heterohelix* and abundant fragments of *Globotruncana*, as fragments of globotruncanids which under transmitted light are poorly visible or remain completely undetected. We have distinguished flat forms with 2 keels such as *Globotruncana gr. linneiana*. One single keeled form can be determined under CL as *Globotruncanita cf. orientalis*. Some triserial tests with globular chambers increasing in size as added are determined as *Guembelitria sp*. forms under CL. The genus *Globigerinoides* is very abundant in the studied section, *Globigerinoides cf. prairiehillensis* is the most abundant form. There is only one well-defined specimen of *Globlotruncana ventricosa* (Figure 28). This assemblage indicates a Campanian - Maastrichtian age (Foraminifera determined by C. Baumgartner-Mora). This range unfortunately does not restrain the age of the Piedras Blancas Formation better than the age presented by Bandini *et al.*, (2008).

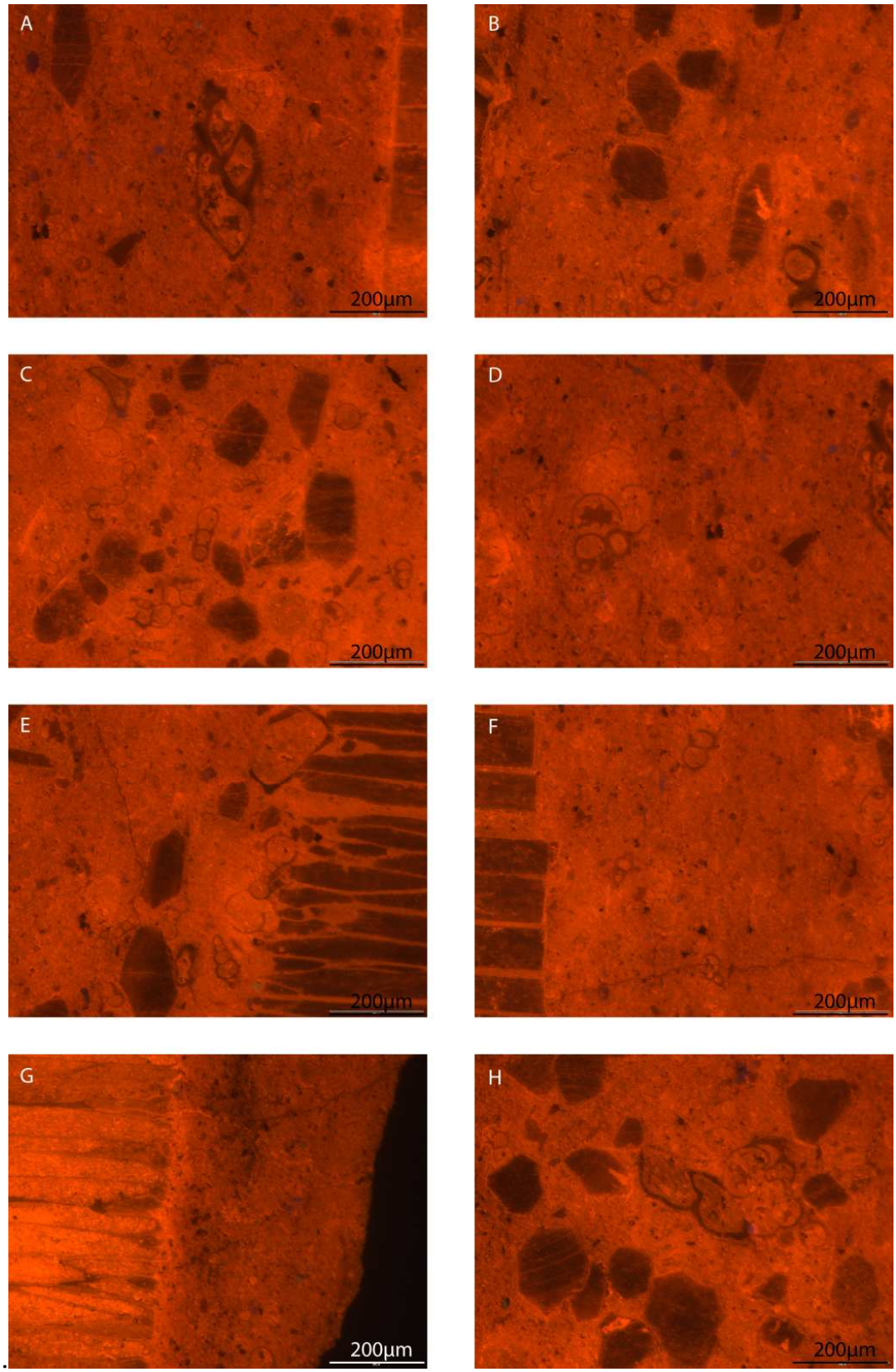

Figure 30: Foraminifera were revealed by cathodoluminescence microscopy in a sample from the Piedras Blancas Formation (PA-08-021 I). A: *Globotruncanita* cf. *orientalis* B: Prisms of the *Inoceramus* shells in encasing rock. C: Prisms of *Inoceramus* shell with foraminifera in encasing rock, presence of *Globigerinoides* cf. *prairiehillensis.* D: *Guembelitria* sp E: Shell of Inoceramid and shell fragments, the shell calcite is less luminescent than the encasing rock presence of *Globigerinoides* sp G: *Inoceramus* shell that has the same bright luminescence than the encasing rock. H: monokeeled *Globotruncanids.*From the foraminifera assemblage, a Campanian-Maastrichtian age was assigned.

4.7. **Contamination**

Strontium isotope ratios were measured on the encasing rocks in order to check for a potential contamination during the preparation of the sample. The mass balance formula used for calculcations is the following:

$$\left(^{87}Sr/^{86}Sr\right)_m = \frac{\left(^{87}Sr/^{86}Sr\right)_s (C)_s F_s + \left(^{87}Sr/^{86}Sr\right)_c (C)_c (1-F_s)}{C_m}$$

(after Banner and Hanson, 1990)

(where C=concentration, F=fraction, m=measured, c=contaminant, s=sample)

The mass balance formula after Banner and Hanson, (1990), expresses the relation between the measured strontium isotope ratio and concentration, and the samples' and contaminants' ratio and concentration. It appears that the measured strontium isotope ratio is depending of the concentration in strontium and the ratio of strontium isotope ratios of the sample and the contaminant.

Sample VU-08-022B (encasing rock of the Nambì Formation) yielded a value of 0.706550, while the ratio on the *Inoceramus* itself was 0.707379 (VU-08-22I and VU-08-22II). Calculations show that, if we consider 1% of contaminant in the system, the original value would have been 0.707387, for a 2% contamination it would have been 0.707395. (The strontium concentration in the encasing rock has been estimated to be close to the one of the Inoceramid shell). This shows that a major shift of strontium ratios is only possible with a major input of contaminant. In other terms, as a slight contamination cannot be discarded, the real value of the Inoceramid shell might be slightly higher, resulting in ages that are barely younger than those presented here. Even though a 2% contamination is considered (see Chapter 2), the calculated ages would not result in a false interpretation, as they would be at 86.80 Ma at its youngest. This contamination would result in a slightly wrong age determination of the Inocermus shell, shifted by less than 0.5 Ma towards younger ages.

Strontium isotope ratio of encasing rock from the Piedras Blancas Formation was also analysed for Sr-ratio (sample PA-08-021B). The encasing rock revealed a ratio of 0.707585. The *Inoceramus* shell showed an average ratio of 0.707657. Again, if we consider a 1% contamination the original value should have been 0.707657, a 2% contamination would mean an original value of 0.707658. A physical contamination, which would occur during the sampling on the *Inoceramus* can, for this specific sample, be considered as negligible.

Sample VU-08-022 (Nambi Formation) shows relatively high differences in strontium isotope ratios between the host rock and the fossil sample, which would suggest a low interaction between the shell and the encasing rock. For sample PA-08-22 (Piedras Blancas Formation), the ratios of the encasing rock and the fossil are very close to each other. This may be due to a homogenization of the geochemical properties through the presence of diagenetic fluids (Chapter 2).

4.8. **Age constrains**

The carbon and oxygen isotopes measured on samples from the Nambì and Piedras Blancas Formations did confirm they underwent alteration processes. Cathodoluminescence and SEM observation revealed secondary crystallization of the *Inoceramus* shells. In general, sample alteration gets more significant with the age of the samples. Nevertheless, the samples measured for $^{87}Sr/^{86}Sr$ gave comforting age results. The obtained ages all lie within the ages defined by micropaleontologic ages.

Bandini *et al.*, (2008) dated the upper member of the Nambì Formation to a Coniacian to middle Campanian age. Flores *et al.*, (2003b), dated an *Inoceramus* sample from this formation to a Coniacian age. As a result, we might have $^{87}Sr/^{86}Sr$ ages that should be older than Coniacian to early Maastrichtian, as we collected samples from the lower, turbiditic member of the Nambì Formation. In this outcrop, *Inoceramus* shells are pluri-decimetric in size show fragmentation, which is interpreted as related to post sedimentary tectonics The samples for the Nambì Formation have all been collected from the same outcrop (±50m wide), which through its turbiditic characteristics has probably sedimentated, in a geological point of view, very quickly. We therefore assume the $^{87}Sr/^{86}Sr$ ratios have to show ages that form a cluster with a relatively short age range.

Furthermore, the $^{87}Sr/^{86}Sr$ results, which are ranging between 0.707287 and 0.707426, will automatically have two different age ranges (Figure 29). There is no geological certainty that indicates a Turonian rather than a Coniacian age for the dated samples of the Nambì Formation.

From the various samples studied for the Nambì Formation, sample VU-08-022 shows a Strontium isotope ratio that deviates from 3 other samples measured for this outcrop. In fact, the samples 1-22-08-02, 3-26-06-04I, and 2-24-08-02, with an average strontium isotope ratio of 0.707307 (total of 7 measurements), cluster well. In contrary, sample VU-08-22 showed an average strontium ratio of 0.707379. The deviation of the strontium isotope ratio for the sample VU-08-022 from this average value ($+71x10^{-6}$) can explained by the different positions within the outcrop or the incorporation of contaminant.
Furthermore, for Sabana Grande Formation the age ranges have been revised without dating a sample from the latter one. This formation, which is conformably overlain by the Nambì Formation, has also been attributed to a Late Turonian-Early Coniacian to Middle Campanian age range.

The Piedras Blancas Formation contains Inoceramid shells, of which one has yielded a $^{87}Sr/^{86}Sr$ ratio of Late Campanian age. This age is in the interval assigned by Galli & Schmidt-Effing, (1977), Di Marco *et al.*, (1995), Flores *et al.*, (2003a). Only one sample for this formation has been measured during this study (the Sr isotope ratio indicate an age of 72.9-74.35 Ma), but other samples, which could date the top of the Piedras Blancas Formation, are waiting to be measured.

The Quebrada Pavas Member bears Inoceramid shell fragments, which have been dated to a very late Campanian to Maastrichtian age, with strontium isotope ratios ranging from 0.707699 to 0.707763). This member is composed of sandstones and conglomerates and can be defined as "molasse-like". In fact, Flores *et al.*, (2007a) also point out the high erosion, which occurred during a very short lapse of time that gave birth to this unit. The age of the Inoceramids of the Curù Formation may therefore not be contemporaneous with the sedimentation but may indicate the age of the eroded/reworked rocks.
Furthermore, the overlying Curù Formation, characterized by turbiditic arenites and lutites, shows no sedimentary similarities with the Quebrada Pavas Member. Because of these

arguments, the Quebrada Pavas Member may be separated from the Curù Formation and may be considered as a formation by itself.

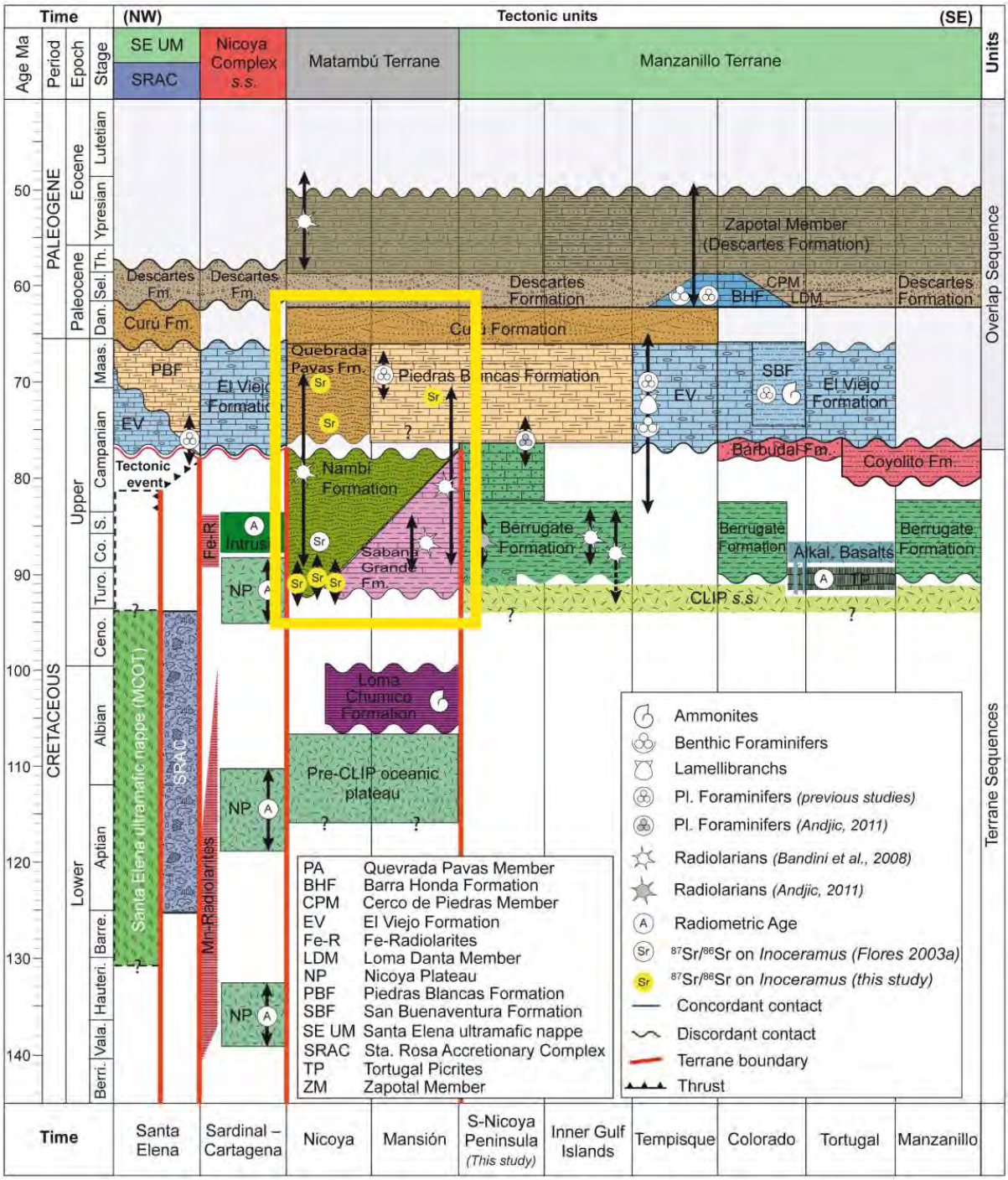

Figure 31: Chronostratigraphy of the Nicoya Peninsula, chart after Flores (2003), Bandini et al., (2008), Andjic, (2011), modified. The strontium isotope ages obtained through this study are shown in yellow circles. The samples from the Nambì Formation, which have two possible ages, are marked by yellow circles with an arrow defining the total age range. The base of the Nambì Formation has been modified to a Turonian age.

4.9. Problems that have to be considered in the age interpretations

In Sr isotope stratigraphy it is assumed that a steep curve will provide better age constrains because of the quick variation of the Sr isotopic ratio (McKenzie et al., 1988; Hodell et al., 1989a; Hodell et al., 1994; Veizer et al., 1999; McArthur et al., 2001; Vasiliev et al., 2010), which is the case for the Late Cretaceous.

During the Late Cretaceous, from the Coniacian to the Late Maastrichtian, Sr isotopic ratios vary in a range between 0.707286 and 0.707830 (Howarth and McArthur, 1997; McArthur *et al.*, 2001). In other words, the Sr isotope ratio increases by $5{,}44 \times 10^{-4}$ in a time interval of ~25 Ma, which implies an average variation of 22×10^{-6}/Ma.

The priory defined ages are not well constrained because of the non-existence of biozonations in the Late Cretaceous (Bandini *et al.*, 2008). If the age constrain is wide, it will allow to have wider ranges of Sr isotope ratios, which will fall into the right time interval but the age given by the effective ratio may be biased.

Results of $^{87}Sr/^{86}Sr$ isotopes for the Quebrada Pavas Formation have a higher reliability than the results of the Piedras Blancas and the Nambì Formation. These results can be accepted as true ages, but the results for the two latter formations can be discussed as following.

The age of the Piedras Blancas Formation is described as Middle-Late Campanian to Late Maastrichtian (Galli & Schmidt-Effing, 1977; Di Marco et al., 1995; Flores et al., 2003a). In other means, this formation covers a time interval of approximately 12.5 Ma, which, consequently means that any Sr isotope ratio between 0.707555 and 0.707830 (Howarth and McArthur, 1997; McArthur *et al.*, 2001), will provide comparable results.

The Nambì Formation is dated by radiolarians, which give this formation a Coniacian to middle Campanian age (Bandini *et al.*, 2008). This case is worse than for Piedras Blancas, because every isotopic ratio in a range between 0.707830 and 0.707286 can be considered as valid.

From the various screening results, one can assume that the samples from the 3 studied formations underwent diagenetic alteration. Furthermore, the presence of volcanic material, sometimes in proximity of the collected samples, and the detrital origin of the beds may be a source of contaminant, which may alter the Sr isotope ratio and lead to biased interpretations. As described in Chapter 2, the presence of contaminant in a very small proportion may

already highly influence the Sr isotope ratio. The presence of a contaminant with a volcanic origin may lower the ratio. This may not be excluded, because the volcanic activity in this region is well known and has played a major role in defining the geochemical signature of the sediments (Andjic, 2011). This may have a major effect on the chemistry of fossils found in sandstones, which, independently of their geochemical signature often present high interstitial porosity that facilitates the movements of pore fluids.

On the other hand, if the diagenesis occurred in a marine environment, very quickly after the sedimentation, one can assume that the interacting fluids may have a marine late Cretaceous Sr isotope signature, which is, as seen in Figure 29, nearly constantly increasing until the late Maastrichtian. The age derived, would then be the age of the diagenesis, mixed with the original Sr marine ratio, which would be younger than the age belonging to the Inoceramids. This assumption is only true if the diagenetic replacement is older than Late Maastrichtian. If it occurred later, there is no control on the shift of the Sr isotope ratios because the Sr isotope signature of a post Maastrichtian diagenesis could again shift the ratio into a unknown direction, the obtained isotopic ratio would again just be a mix a the original Sr marine ratio and the one of the diagenesis age (if it occurred with interaction of marine fluids).

The screening results showed that alteration and diagenesis could not be excluded, which will undeniably have an influence on the Sr isotopic ratio. The ratio may have varied and is then not representative of the former marine Sr isotopic composition. Elorza and Garcia-Garmilla, (1998) have encountered similar problems with their samples and concluded Inoceramid shells were to be used carefully in order to date with Sr isotopes.
At least, in this study, from the results obtained on the encasing rocks, the interaction of a physical contaminant with the *Inoceramus* shell can be considered as negligible.

4.10. **Conclusion**

On the Nicoya Peninsula sediments from the Nambi Formation, Piedras Blancas Formation and Quebrada Pavas Formation were dated by the means of strontium isotope ratios measured in Upper Cretaceous *Inoceramus* shell fragments. Results have shown average $^{87}Sr/^{86}Sr$ values of 0.707322 (Turonian-Coniacian) for the Nambi Formation 0.707654 (middle late Campanian) for the Piedras Blancas Formation and 0.707721 (late Campanian-Maastrichtian) for the Quebrada Pavas Formation.

The abundant presence of detrital components in the studied formations constitutes a difficulty to strontium isotope dating. In fact, the fossil bearing sediments can easily contaminate the target fossil with strontium mobilized from basalts during diagenesis and thus the obtained strontium isotope ratios may be influenced significantly and so will the obtained ages, this could not be quantified during this study. Therefore, the obtained age results can be considered as reliable for the dating of the studied formations but the ages may not be considered as absolute. Mass balance calculations show the effect of contamination of the $^{87}Sr/^{86}Sr$ isotope ratio by the encasing rock during the sample preparation can be considered as negligible.

Also, the new and precise age assignments allow for more precision in the chronostratigraphic chart of the sedimentary and tectonic evolution of the Nicoya Peninsula, providing a better insight on the evolution of this region.

4.11. References

Andjic, G., 2011. Sédimentation pélagique et détritique d'arc du Crétacé supérieur dans le nord - ouest du Costa Rica (Côte Pacifique, Sud de l'Amérique Centrale). Master Thesis, University of Lausanne.

Astorga, A., **1987**. El Cretácico Superior y el Paleógeno de la vertiente pacífica de Nicaragua meridional y Costa Rica septentrional: Origen, evolución y dinámica de las cuencas profundas relacionadas al margen convergente de Centroamérica. Lic. Thesis, University of Costa Rica, 1- 115.

Bandini, A. N., Flores, K., Baumgartner, P. O., Jackett, S.-J. & Denyer, P., **2008**. Late Cretaceous and Paleogene Radiolaria from the Nicoya Peninsula, Costa Rica: a tectonostratigraphic application. Stratigraphy, 5, 3-21.

Barrera, E., Huber, B.T., **1990**. Evolution of Antarctic bottom waters during the Maastrichtian, foraminifer oxygen and carbon isotope ratios, ODP Leg 113. Initial Reports Proccedings Ocean Drilling Program, 113, pp. 813-828.

Barron, E.J., Saltzman, E., Price, D.A., **1984**. Occurrence of *Inoceramus* in the South Atlantic and oxygen isotope palaeotemperatures in Hole 530A. Initial Reports Deep Sea Drilling Project 75, pp. 893-904.

Baumgartner, P.O. & Denyer, P., **2006**. Evidence for middle Cretaceous accretion at Santa Elena Peninsula (Santa Rosa Accretionary Complex), Costa Rica. Geologica Acta, 4 (1/2), 179–191.

Baumgartner, P.O., Flores, K., Bandini, A.N., Girault, F. & Cruz, D., **2008**. Upper Triassic to Cretaceous radiolaria from Nicaragua and northern Costa Rica – the Mesquito composite oceanic terrane. Ofioliti, 33, 1–19.

Baumgartner-Mora, C., Baumgartner, P.O., **1994**. Shell structure of fossil foraminifera studied by cathodoluminescence. European Microscopy and analysis, issue 28.

Buchs, D. M., **2008**. Late Cretaceous to Eocene geology of the South Central American forearc area (southern Costa Rica and western Panama): Initiation and evolution of an intra-oceanic convergent margin. PhD thesis, Université de Lausanne, 1 - 230.

Calvo, C., **1998**. Kretazische Subduktions-prozesse in Südzentralamerika. Profil, 15, 1-161.

Da Silva, S., **2006**. Investigation of Cretaceous Molluscan Shell Material for Isotopic Integrity: Examples and Implications from the Baculites compressus/cuneatus

Biozones (Campanian) of the Western Interior Seaway. University of Florida, Master Thesis, 211 pp.

Denyer, P., & P.O. Baumgartner, **2006**. Emplacement of Jurassic-Lower Cretaceous radiolarites of the Nicoya Complex (Costa Rica). *Geologica Acta*, *4*, 203-218.

Denyer, P., Montero, W. & Flores, K., **2005**. Apuntes sobre la geologia de la hojas Golfo y Berrugate, Costa Rica. Revista Geológica de América Central, 32, 99-108.

Di Marco, G., Baumgartner, P.O. & Chanell, J.E.T., **1995**. Late Cretaceous-early Tertiary paleomagnetic data and a revised tectonostratigraphic subdivision of Costa Rica and western Panama. Geological Society of America Special Paper, 295, 1-27.

Elorza, J., Garcîa-Garmilla, F., **1998**. Palaeoenvironmental implications and diagenesis of inoceramid shells (Bivalvia) in the mid-Maastrichtian beds of the Sopelana, Zumaya and Bidart sections (coast of the Bay of Biscay, Basque Country). Palaeogeography, Palaeoclimatology, Palaeoecology, 14, pp. 303–328.

Flores, K., **2003**. Propuesta tectonoestratigráfica de la región septentrional del golfo de Nicoya, Costa Rica. Licenciatura thesis, University of Costa Rica, 1-176.

Flores., K., Denyer, P. & Aguilar, T., **2003a**. Nueva propuesta estratigráfica: Geología de las hojas Matambú y Talolinga, Guanacaste, Costa Rica. Revista Geológica de América Central, 28, 131-138.

Flores, K.., Denyer, P. & Aguilar, T., **2003b**. Nueva propuesta estratigráfica: Geología de la hoja Abangares, Guanacaste, Costa Rica. Revista Geológica de América Central, 29, 127-136.

Galli, C. & Schmidt-Effing, R., **1977**. Estratigrafía de la cubierta sedimentaria supra-ofiolitica cretácica de Costa Rica. Cienc. Tec., 1, 87-98.

Gòmez-Alday, J.J., Lòpez, G., Elorza, J., **2004**. Evidence of climatic cooling at the Early/Late Maastrichtian boundary from inoceramid distribution and isotopes. Sopelana sections, Basque Country, Spain. Cretaceous Research, 25, pp. 649-668.

Gòmez-Alday, J.J., Cruz Zuluaga, M., Elorza, J., **2008**. $^{87}Sr/^{86}Sr$ ratios in inoceramids (Bivalvia) and carbonate matrix as indicators of differential diagenesis during burial. Early Maastrichtian Bay of Biscay sections (Spain and France). Potential use for chemostratigraphy? Cretaceous Research, 29, pp. 563-576.

Hauff, F., Hoernle, K., van den Bogaard, P., Alvarado, G. & Garbe Schoenberg, D., **2000**. Age and geochemistry of basaltic complexes in western Costa Rica; contributions to the geotectonic evolution of Central America, Geochemistry, Geophysics, Geosystems - G 3.

Hodell, D.A., Benson, R.H., Kennett, J.P., Bied, K.R. E., **1989**. Stable isotope stratigraphy of latest Miocene sequences in northwest Morocco: the Bou Regreg section. Paleoceanography 4, p. 467–482.

Hodell, D.A., Benson, R.H., Kent, D.V., Boersma, A., Bied, K.R.-E., **1994**. Magnetostratigraphic, biostratigraphic, and stable isotope stratigraphy of an Upper Miocene drill core from the Salé Briqueterie (northwest Morocco): a high-resolution chronology for the Messinian stage. Paleoceanography 9, p. 835–855.

Hoernle, K., Hauff, F. & van den Bogaard, P., **2004**. 70 m.y. history (139-69 Ma) for the Caribbean large igneous province. *Geology, 32*, 697-700.

Howarth, R.J., and McArthur, J.M., **1997**. Statistics for strontium isotope stratigraphy. A robust LOWESS fit to the marine Sr-isotope curve for 0 - 206 Ma, with look-up table for the derivation of numerical age. Journal of Geology, 105, pp. 441-456.

Huber, B.T., **1990**. Maastrichtian planktonic foraminifera biostratigraphy of the Maud Rise (Weddell Sea, Antarctica); ODP leg 113 holes 689B and 690C. Proceedings of the Ocean Drilling Program, Scientific Results, 113, pp. 489-513.

Jaccard, S. & Münster, M., **2001**. Etude géologique multidisciplinaire de la plateforme de Barra Honda (Guanacaste): sédimentologie, isotopes stables du strontium, du carbone, de l'oxygène et contexte géodynamique. Travail de diplôme, Université de Lausanne.

Jaccard, S., Münster, M., Baumgartner, P.O., Baumgartner-Mora, C. & Denyer, P., **2001**. Barra Honda (Upper Paleocene – Lower Eocene) and El Viejo (Campanian - Maastrichtian) carbonate platforms in the Tempisque area (Guanacaste, Costa Rica). Revista Geológica de América Central, 24, pp. 9-28.

Kauffman, E.G., Harries, P.J., Meyer, C., Villamil, T., Arango, C., Jaecks, G., **2007**. Paleoecology of giant Inoceramidae (*Platyceramus*) on a Santonaian (Cretaceous) seafloor in Colorado. Journal of Paleontology, 81 (1), pp. 64-81.

Keller, G., **2001**. The end-Cretaceous mass extinction in the marine realm: year 2000 assessment. Planetary and Space Science, 49, pp. 817-830.

Kerr, A.C., Tarney, J., Marriner, G.F., Nivia, A., Klaver, G.T. & Saunders, A.D., **1996**. The geochemistry and tectonic setting of late Cretaceous Caribbean and Colombian volcanism, Journal of South American Earth Sciences, 9, pp. 111-120.

Kindler, P., Godefroid, F., Chiaradia, M., Ehlert, C., Eisenhauer, A., Frank, M., Hasler, C.-A., Samankassou, E., **2011**. Discovery of Miocene to lower Pleistocene deposits on Mayaguana, Bahamas: evidence for recent active tectonism on the North American

margin. Geology, v. 39/6, 523-526.

MacLeod, K.G., **1994**. Bioturbation, inoceramid extinction, and mid-Maastrichtian ecological change. Geology, 22, pp. 139-142.

McArthur, J.M., Howarth, R.J., Baieley, T.R., 2001. Strontium isotope stratigraphy: LOWESS version 3: best fit to the marine Sr-isotope curve for 0–509 Ma and accompanying look-up table for deriving numerical age. J. Geol. 109, p. 155-170.

McKenzie, J.A., Hodell, D.A., Mueller, P.A., Muller, D.W., 1988. Application of strontium isotopes to late Miocene–early Pliocene stratigraphy. Geology 16, p. 1022–1025.

Pindell, J.L., Kennan, L., Stanek, K.P., Maresch, W.V., & Draper, G., **2006**. Foundations of Gulf of Mexico and Caribbean evolution: Eight controversies resolved. Geologica Acta, 4, 89–128.

Pindell, J.L., & Kennan, L., **2009**. Tectonic evolution of the Gulf of Mexico, Caribbean and northern South America in the mantle reference frame: an update, *in* James, K., Lorente, M.A., & Pindell, J., eds., Origin and evolution of the Caribbean Region: Geological Society of London, Special Publication, 328, 1–55.

Pirrie, D., Marshall, J.D., **1990**. Diagenesis of *Inoceramus* and Late Cretaceous paleoenvironmental geochemistry, a case study from James Ross Island, Antarctica. Palaios, 5, pp. 336-345.

Pons, J., Schmidt-Effing, R., **1998a**. Caribbean rudist fauna from the pacific coast of Costa Rica.- Contribution to geology, University of West Indies, Jamaica (Congreso).

Pons, J. & Schmidt-Effing, R., **1998b**. Upper Cretaceous rudists from Guanacaste province, Costa Rica, Central América.- Terra Nostra, 16. 124-125.

Saltzmann, E.S., Barron, E.J., Price, D.A., 1982. South Atlantic Cretaceous paleotemperatures from DSDP cores. Palaeogeography, Palaeoclimatology, Palaeoecology 40, pp. 167-181.

Seyfried, H. & Sprechmann, P., **1985**. Acerca de la formación del puente-istmo Centroamericano Meridional, con énfasis en el desarrollo acaecido desde Campanénse al Eoceno. Revista Geológica de América Central, 2, 63-87.

Sinton, C.W., Duncan, R.A. & Denyer, P., **1997**. Nicoya Peninsula, Costa Rica: A single suite of Caribbean oceanic plateau magmas. *Journal of Geophysical Research-Solid Earth, 102*, 15507-15520.

Thomas, E., **1990**. Late Cretaceous through Neogene deep-sea benthic foraminifers (Maud Rise, Weddell Sea, Antarctica), ODP leg 113 holes 689B and 690C. Proceedings of the Ocean Drilling Program, Scientific Results, 113, pp. 571-594.

Vasiliev, I., Reichart, G.-J., Davies, G.R., Krijgsman, W., Stoica, M., 2010. Strontium isotope ratios of the Eastern Paratethys during the Mio-Pliocene transition; Implications for interbasinal connectivity. Earth and Planetary Science Letters, 292, pp. 123–131.

Veizer, J., Ala, D., Azmy, K., Bruckschen, P., Buhl, D., Bruhn, F., Carden, G.A.F., Diener, A., Ebneth, S., Goddéris, Y., Jasper, T., Korte, C., Pawellek, F., Podlaha, O.G., Strauss, H., **1999**. $^{87}Sr/^{86}Sr$, $\delta^{13}C$ and $\delta^{18}O$ evolution of Phanerozoic seawater. Chemical Geology 161, pp. 59-88.

Ward, P.D., Kennedy, W.J., MacLeod, K.G., Mount, J., **1991**. End-Cretaceous molluscan extinction patterns in Bay of Biscay K/T boundary sections, two different patterns. Geology, 19, pp. 1181-1184.

Waterhouse, J.B., **1970**. Permoceramus, a new inoceramid bivalve from the Permian of eastern Australia. New Zealand Journal of Geology and Geophysics, 13, pp. 760-766

5. $^{87}Sr/^{86}Sr$ study of shallow water carbonates from the Hess Rise, Caribbean Sea

5.1. Introduction

The samples of this chapter where collected by Prof. Peter O. Baumgartner who participated as a guest to the Cruise No. 81, LEG 2B on the MS-Meteor. The cruise took place from March 11 to April 21 2010 from Willemstad (Netherlands Antilles) to Bridgetown (Barbados). The cruise was realized in the frame of a research project of the IFM-Geomar (Kiel) named: CLIP - Origin of the Caribbean Large Igneous Province (CLIP) in connection with the geodynamic evolution of the Central Caribbean. (Cruise managers: Reinhard Werner, Kaj Hoernle, Folkmar Hauff from the IFM-Geomar in Kiel).
During LEG 2B a total of 28 dredges were carried out in 17 days. 15 of these dredges recovered magmatic rocks, 4 volcaniclastics, 17 sedimentary rocks and 3 manganese and iron oxides (Werner *et al*., 2010).
All the basic data on samples presented in this chapter is from the Cruise Report (Werner *et al*., 2010). This includes all the data about the sampling locations, the samples collected, the sediment echo sounding and the Muliti-Beam underwater maps. No Remotely Operated Vehicle (ROV) could be used during this Leg because of technical issues.

This chapter focuses on some sedimentary rocks collected during the scientific cruise. Priority was given to the shallow water carbonates. With the measurement of $^{87}Sr/^{86}Sr$ ratios in these samples, we intend to assess the sedimentary and tectonic history of this region.
The cruise report presents all the types of rocks collected. A first macroscopic description was done on board by Prof. Peter O. Baumgartner. More detailed data was given by Baumgartner and Mora-Baumgartner, 2010. This second description was based on ~100 thin sections and included a facies and a micro-paleontological part for age determinations.
Furthermore, deep-sea drillings have been carried out in this region (DSDP and ODP). In order to assemble all available data on the sedimentary features, the observations made on the samples from the cruise and the results obtained from the drillings are summarized below.

5.2. Nomenclature of samples

It is important to note how samples are named in order to avoid confusion in the following chapter. Samples are first named after the vessel and the cruise number. This is followed by the number of the sampling site. The last two digits correspond to the samples number in the dredge.

Finally, some of the samples have a last single digit in brackets, which corresponds to the number of the thin section from a sample. E.g., M81-123-45 (6) would have to be read as following: Meteor Cruise 81, sampling site 123, sample 45, thin section number 6. In order to facilitate the reading, dredge sites might be referred to as DR-123 (example).

5.3. Geographic and geologic setting

The Hess Escarpment and Beata Ridge are located on the Caribbean tectonic plate (Figure 32). They both limit the Colombian Basin: the Hess Escarpment and the Beata Rise separate it from the Nicaragua Rise to the west and the Venezuelan Basin to the east, respectively. The Colombian Basin is limited to the south by Colombian, Panamean and Costa Rican territories. To the north the basin is bordered by the Island of Hispaniola. In the literature, the northern part of the Colombian Basin is sometimes referred to as the Haiti-Basin or Haiti sub-basin (Figure 32).

The Colombian Basin has been studied by various authors and because it is under water-columns reaching depths of 3000-4000 m, the only way to obtain samples and data is core - drilling, seismic data, and/or, as in our case, dredging.

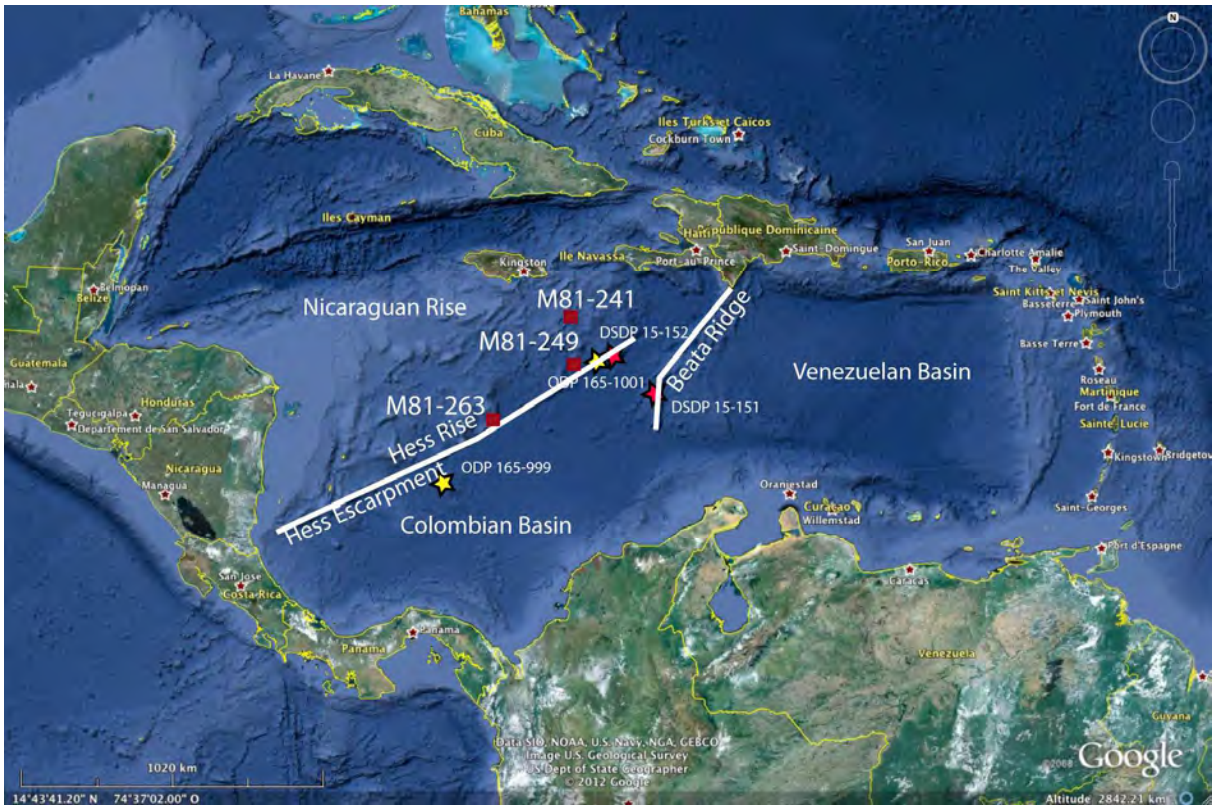

Figure 32: Localization map of the Hess Escarpment and Beata Ridge (yellow stars correspond to ODP sites and red stars to DSDP sites). The red squares correspond to the dredging locations where strontium isotope ratios could be obtained. (Map from Google Earth).

The basement of the Colombian Basin is formed by a thickened oceanic crust, the Cretaceous Caribbean oceanic plateau (Bowland and Rosencrantz, 1988), which is nowadays known as the Caribbean Large Igneous Province (CLIP) (Coffin and Eldholm, 1991, 1992). The first sediments overlying the basement are characterized by an accumulation of upper Cretaceous pelagic deposits. These sediments have been correlated with units from the neighboring Venezuelan Basin. Above, a large volume of clastic sediments represents a second depositional episode, which ranges from Eocene to Miocene age. These hemipelagic sediments are overlain by late Miocene to present sediments.

From seismic data, the upper surface of the oceanic plateau is described as smooth and has been correlated to a Late Cretaceous seismic horizon of the Venezuelan Basin (Saunders et al, 1973) and the Late Cretaceous mafic basement of southern Central America (Saunders *et al.*, 1973; Bowland and Rosencrantz, 1988; Bowland, 1993). Lu and McMillen (1982) describe two seismic facies in the deep Colombian Basin, namely a pelagic facies and a turbidite facies. The source for volcanic material that is present in the westernmost Colombian basin is probably located in southern Central America (Edgars *et al.*, 1973; Zimmerman, 1982).

The Hess Rise, which has a rectangular shape, represents a fault-bounded block. After Sigurdsson *et al.* (1997), the benthic foraminiferal assemblage indicates shallow water depths during the emplacement of the Hess Rise, emplacement that was followed by rapid subsidence. The Hess Rise is about 2000 m shallower than the abyssal plain of the Colombian basin. The origin of the crust north of the escarpment remains unclear. Two hypotheses have been emitted, one considering it as part of the Chortis block, the other one assumes a relation to the CLIP based on geochemical results of basaltic lavas recoered from DSDP Site 152 (Edgar *et al.,* 2007). The central Hess Escarpment is characterized by seamounts and NNE-SSW and NNE-SSE trending ridge structures (Figure 32). These seamounts and ridges are thought to be remains of volcanic islands, which subsided and were eroded to sea level (Werner *et al.,* 2010). The Tertiary shallow water samples recovered in this region indicate a subsidence of about 1600 - 1800 m (Werner *et al;* 2010, Huenecke, 2010), in view of their present position. The southwestern Hess Rise is characterized by a massive guyot-type seamount (80 x 40 km at its base) and a rough morphology (a guyot-type seamount is characterized by steep sides and gentle dome-like tops) (Meschede *et al.*, 2010). From multi-beam mapping it appears that the Beata Rise shows longitudinal structures and the Hess Escarpment more circular structures (Meschede *et al.*, 2010). They indicate the possibility that the Beata Rise and Hess Escarpment are transtensive structures that result from a E-W extension of the Caribbean tectonic plate. Parasound profile data of the sediments in the Beata area show a graben structure and extensional faults. A detailed analysis of these structures is being prepared. Meschede *et al.* (2010), emit the hypothesis that the seamounts, which once were ocean island volcanoes related to the Caribbean Flood Basalt event (around 90 Ma) with a probable second phase around 77 Ma, were eroded to sea level during their subsidence. This hypothesis is confirmed by shallow water carbonates of a platform that began to grow on the margins of these leveled volcanic seamounts (Hueneke, 2010). This erosion gave them their gentle dome-like tops. The major subsidence of about 1600 - 1800 m of this region is the response of the extension of the central Caribbean, which is related to a north-south compression of the CLIP between the Americas (Figure 33). Smaller structures were revealed by the Parasound, which according to their magnetic intensity were interpreted as a younger, maybe post-erosional volcanic phase (second phase of the CLIP around 77 Ma or younger, Meschede *et al.*, 2010).

The shallow water sediments studied in this Chapter may help assigning an age and rate of the subsidence in this region. After Hueneke (2010), the carbonate platforms formed on top of the seamounts and then drowned by submergence below the photic zone and thus below the zone

of maximum carbonate production in warm water conditions. For Hueneke, a backstepping and reorientation of the platform margins occurred during the subsidence, which is consistent with a general lack of volcanic rocks in the dredges carried out on seamount caps. The back-stepping results in a modification of the flat topped plateau into a mounded plateau, which indicates a gradual subsidence or submergence below the wave action and finally a complete drowning of the carbonate platform (Hueneke, 2010).

The drowning of carbonate platforms are complex case studies because the single eustasy would not hamper the growing of a carbonate platform, which can respond very quickly to sea-level rise (Schlager, 1981). It must be related to another factor that may have helped in stopping the platform growth. These can be a major relative sea-level rise before drowning, a lateral overgrowth due to steep slopes, an increase of clastic contribution, an increase of nutrients that would prevent the carbonate-producing fauna from sunlight and thus make photosynthesis impossible, or a modification in water currents that would affect the carbonate factory (Schlager, 2005, Schlager *et al,* 1981, Wilson *et al.*1998, Mutti *et al,* 2005, Camoin *et al.*, 1998, Sattler *et al.*, 2009). For instance, demise of a platform in Oligocene times may be related to major oceanic changes during the Oligocene, related to a general global cooling reflected by the appearance of continental ice-sheets in Antarctica, a major sea-level fall and global shifts in the distribution and intensity of precipitations (Zachos *et al.*, 1999, Mutti *et al*., 2005).

Interestingly, in the neighboring Nicaragua Rise, Mutti *et al., (*2005), studied shallow water carbonates and present a model for the drowning of a large carbonate platform (megabank) due to pulsed subsidence changes, a first one from 21 - 25 Ma and a second one from 8-16 Ma (Cunningham, 1998, in Mutti *et al,* 2005). Droxler *et al,* (1992) suggest a breaking up of part of the megabank during the middle Miocene leading to a change in the Caribbean currents: the opening of the intra-Caribbean gateway initiated the Caribbean Current and intensified the Gulf Stream (Droxler *et al,* 1998, Mutti *et al.*, 2005).
Seismic profiles from Mutti *et al.* (2005) show tilted blocks, which form a drowning unconformity overlain by middle Miocene periplatform sediments (which is another mechanisms than for the seamounts). They date the drowning of the platform to a middle Oligocene age, with partial break-up a part of individual banks until the late early Miocene.

This study focuses principally on the $^{87}Sr/^{86}Sr$ measurements of the shallow water sediments recovered during the M81-2A/B cruise, but another aim is to date the beginning of the drowning. The study of Mutti *et al.* (2005) is therefore essential and may serve as a reference model, even though the samples from this study have been collected on seamounts. The only difference with the mega bank then is the basement on which the platform grows, but these seamounts with their platforms are subject to the same regional subsidence setting, even though the effect of the subsidence can have local variations. $^{87}Sr/^{86}Sr$ measurements may provide key elements for the timing of the subsidence activity.

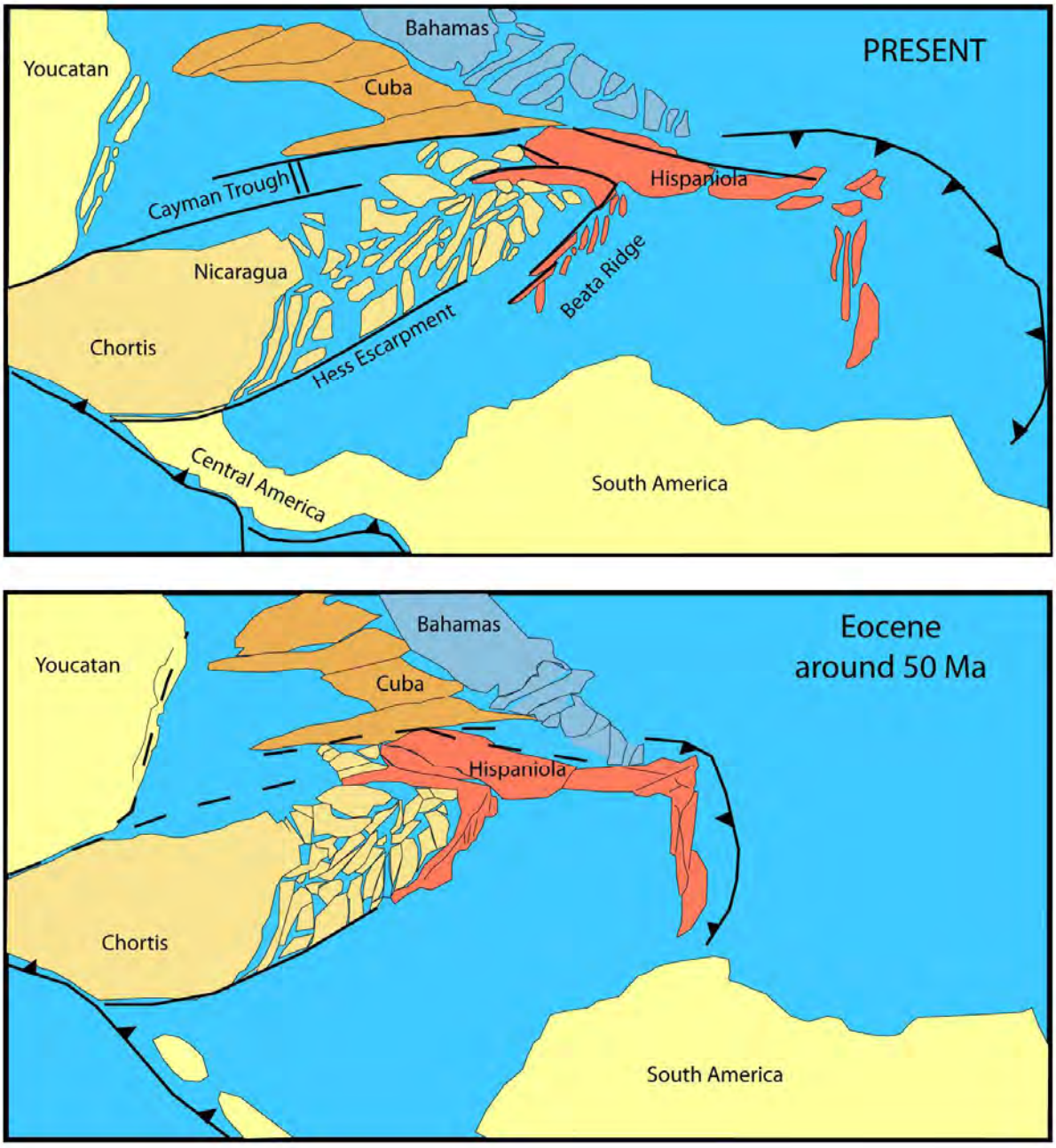

Figure 33: Model of the E-W extension of the Caribbean tectonic plate proposed by Meschede et al. (2010). The upper image shows the present situation, the blocks correspond to underwater blocks as seen of today. The lower image corresponds to an Eocene situation. This model is based on the "Inter-Amrican model" for the Caribbean tectonic plate after Meschede et al. (2010). It only shows morphologic features, not geologic terranes.

5.4. **Samples**

After first observations with the microscope and preliminary stable isotope results, samples were selected in order to proceed to Sr isotope measurements. Samples have been selected in order to compare $^{87}Sr/^{86}Sr$ values with paleontological ages of shallow water facies carbonates given by Baumgartner and Baumgartner-Mora (2010). Ten samples were selected for Sr isotope investigations, from the dredging sites DR-241, DR-245, DR-249 and DR-263 (Figure 32).

Because the samples are hard rocks, separating bioclasts or target fossils from the host rock is impossible. Therefore, samples were micro-drilled, targeting bioclasts such as algae, corals or foraminifera. The presence of a potential contaminant can therefore not be excluded and the $^{87}Sr/^{86}Sr$ ratios obtained by the samples has to be considered as bulk powder. Examples of target fossils are shown in (Figure 36, Figure 37, Figure 38).

Samples with ferromanganese crusts were avoided, as they would probably have Sr isotopic ratios that are shifted by the contamination of these crusts. Such samples are very unlikely to provide useful Sr isotopic ratios (Vonder Haar *et al.*, 1995).

Type	Station	Location	Content summary	on bottom		off bottom		depth (m)	
				lat °N	long °E	lat °N	long °E	max	min
DR	M81-241	Hess Escarpment North	lava, volcaniclastics, sedimentary rocks	16,805	75,642	16,802	75,635	1,705	1,111
DR	M81-245	Hess Escarpment North	sedimentary rocks, manganese	16,379	75,886	16,381	75,881	927	632
DR	M81-249	Hess Escarpment North	sedimentary rocks	15,990	75,514	15,997	75,506	3,159	2,645
DR	M81-263	Hess Escarpment South-West	sedimentary rocks	14,336	77,616	14,336	77,615	1,196	1,025

Table 3: Localizations and details on the sampling localities. Note that because the samples are dredged, position of the dredge (on bottom) and a position of the vessel (off bottom) are indicated.

5.5. **Results**

Stable Oxygen and Carbon Isotope Geochemistry

Powders were withdrawn from the thin section counterpart using a diamond micro-drill.
The stable isotopes yield values between -2.2‰ and +3.1‰ (VPDB) for oxygen and between +0.6‰ and +2.6‰ (VPDB) for carbon. Only sample 249-1-3 has oxygen stable isotope composition that would suggest alteration with $\delta^{18}O$ of -2.2‰ and -1.9‰ (VPDB) (Figure 34, Table 4). Otherwise, neither of the samples shows values that could correspond to a meteoric influence and therefore an exposure to freshwater may be excluded. The values fit well with the ranges proposed by Knoerich and Mutti (2003), (Chapter 2).

Sample	$\delta^{13}C$ VPDB (‰)	$\delta^{18}O$ VPDB (‰)
M81-241-15.5	0.6	0.3
	0.7	0.5
M81-241-18.5	2.6	-0.6
	2.6	-0.5
M81-241-19	1.2	0.2
	1.7	3.1
M81-249-1-3	2.3	-2.2
	2.5	-1.9
M81-263-1	1.5	0.2
	1.4	0.2
	1.6	0.5
M81-263-2	1.7	-0.5
	1.7	-0.8
M81-263-8	1.8	2.1
	1.6	1.6
	1.7	1.9
M81-263-9	1.7	0
	1.5	0

Table 4: Stable Carbon and Oxygen isotope geochemistry results of samples used for strotium isotope measurements.

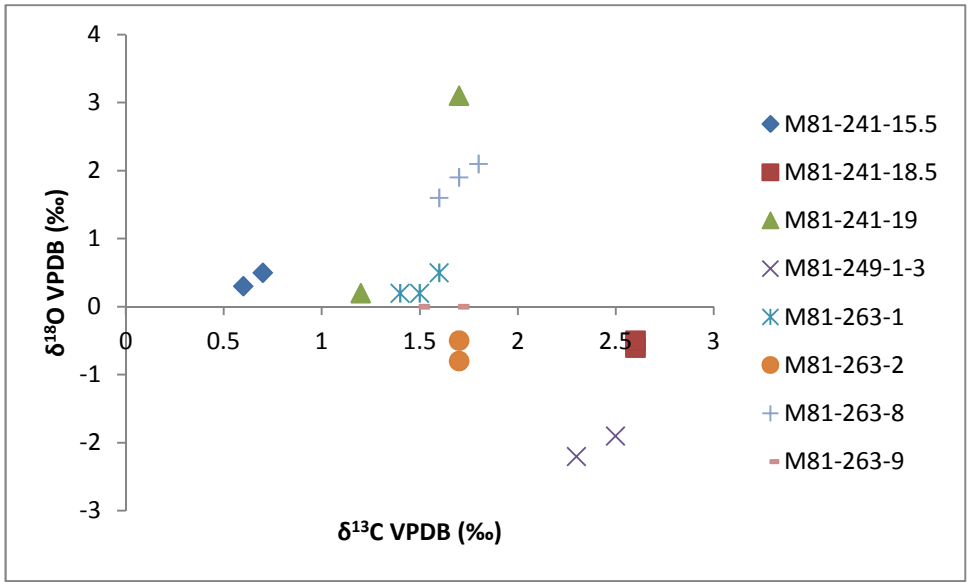

Figure 34: Stable carbon and oxygen isotope geochemistry of the samples selected for strontium isotope measurements.

Cathodoluminescence and trace elements

Thin sections were observed with cathodoluminescence in order to check if secondary diagenetic phases are present. For carbonate rocks, the Fe^{2+} acts as a quencher and Mn^{2+} as the main activator of cathodoluminescence (Marshall, 1988; Richter *et al.*, 2003; Boggs and Kinsley, 2006). In addition to the observations made by cathodoluminescence, Mn, Fe and Sr concentrations were measured in liquid mode using an ICP-MS device.

Sample M81-241-15 and M81-241-18 showed crystallization of a secondary phase of cement. Cathodoluminescence also revealed a reddish luminescence (Figure 35).

Isopachous calcitic crystals seem to have grown as a secondary phase inside the porosity.

The porosity cavities show a light dissolution on their rim. This could be the proof of another distinct dissolution phase. The outside boarder of foraminifera show a light luminescence, which may be related to an early cementation process.

These samples were selected for further Sr isotopic analysis despite the presence of a secondary phase; the obtained Sr isotopic ratio might be close to the original marine value. Also, the presence of secondary cementation could mean the samples might have been exposed to freshwater conditions.

Samples M81-241-19, M81-263-3 and M81-263-8 showed very low to no luminescence (under the same conditions of sample M81-241-15/18). Furthermore, the samples have probably never been exposed to reducing conditions, under which Mn^{2+} and Fe^{2+}would have been incorporated. For these samples, during the deposition and the subsidence, conditions were probably always well oxygenized. From cathodoluminescence we assume that the

samples are pristine and did not undergo any reprecipitation process. The observations made by cathodoluminescence are therefore a further proof of very low to no alteration process. Also, regarding trace elements, results for all the samples are very constant, with Mn < 25 ppm, Fe concentrations of 450-600 ppm and Sr concentrations of 250-300 ppm (even for the samples M81-241-15/18), these concentrations are in agreement with studies done on shallow water carbonates (Flügel, 2010, Bausch, 1968, amongst others).

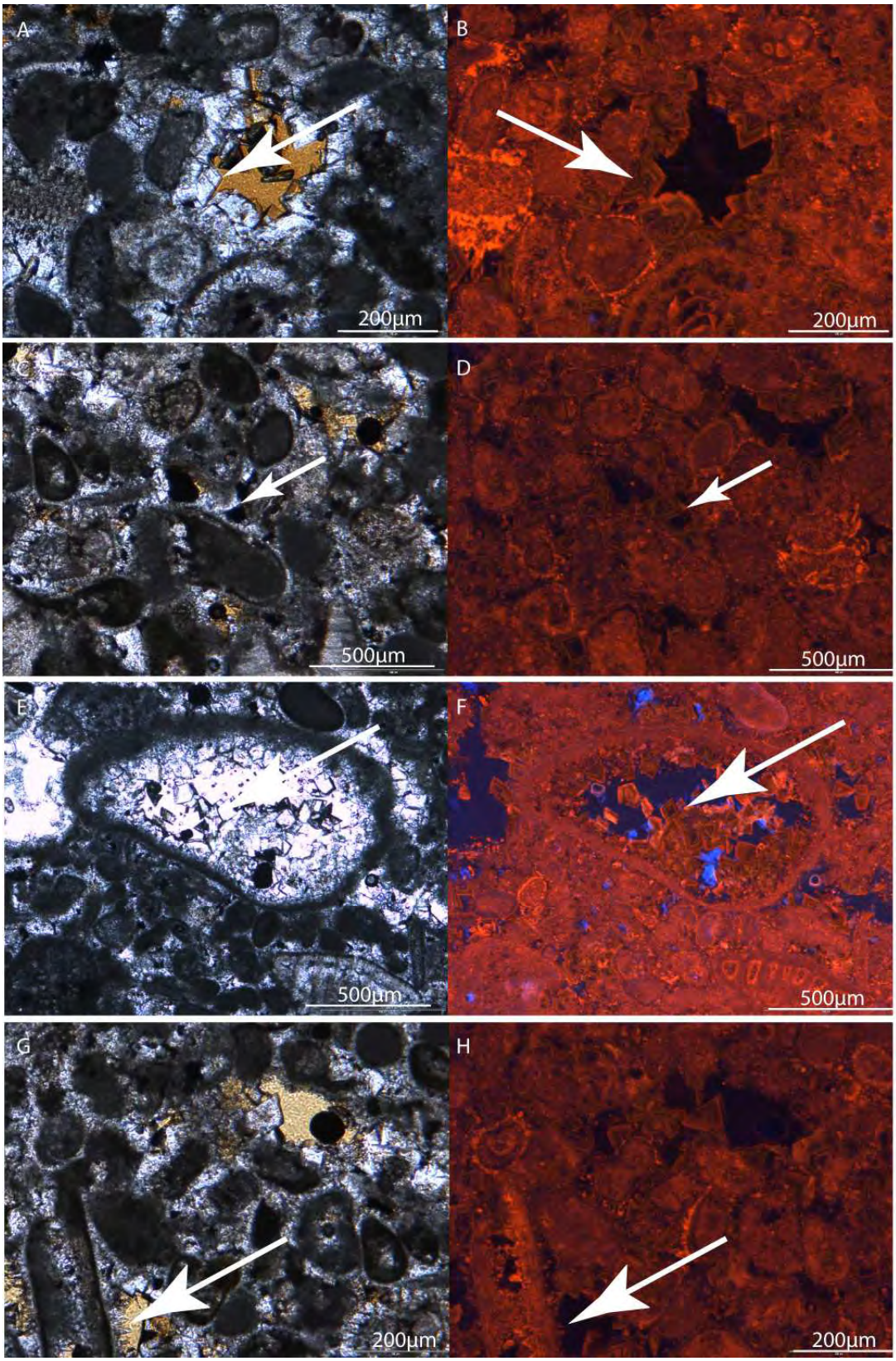

Figure 35: This plate shows cathodoluminescent images of the samples from site M81-241. (A-D = M81-241-15.5; E-H = M81-241-18.5). Arrows highlight isopachous crystal growth A, B, C, D and the cement infill of primary posority (E, F, G, H).

5.6. $^{87}Sr/^{86}Sr$ results and ages combined with micropaleontologic ages

In order to facilitate the reading, results from strontium isotope analyses have been combined with the paleontological descriptions of the samples.

Northern Hess Escarpment/Lower Hess Rise

At Station DR-241, big blocks of massive carbonates were recovered. These blocks contained the following sediments: cross-stratified washed carbonate sands, reefal limestones, lagoonal carbonate wackestones, pelagic limestones. The carbonate samples also contain larger foraminifera that are constrained to an Eocene-Oligocene age (Baumgartner and Baumgartner-Mora, 2010). Sample M81-241-15 yielded strontium isotope values of 0.707941 and 0.707972. These values show an intra-sample heterogeneity, but the corresponding ages of 29.95 Ma, respectively 30.95 Ma (both Rupelian age). Sample M81-241-18 revealed strontium isotope ratios of 0.707850 and 0.707847 (Table 5, Figure 39). These two ratios are within the S.E. of the sample and can therefore be qualified as very reliable. The strontium ages are 33.20 Ma and 33.25 Ma respectively (both early Rupelian). The strontium isotope results for sample M81-241-19 showed very large intra-sample variations. The first analyses yielded a value of 0.708149, the second one a ratio of 0.709140 (Table 5, Figure 39). The first value indicates an age of 25.40 Ma (both Chattian age). The second ratio corresponds to a strontium age close to modern seawater (1.00 Ma); both values have consequently been excluded. Sample M81-241-24 yielded strontium isotope ratios of 0.709181 and 0.709186 (Table 5, Figure 39). These results were not taken into consideration, as these ratios are higher than the strontium isotope ratios of recent seawater (0.709174). Some of the collected samples showed fractures with a pelagic infill. The presence of *Orbulina universa* was detected in these infills, suggesting a middle Miocene age or younger (Baumgartner and Baumgartner-Mora, 2010).

Station DR-245 revealed Mn-encrusted and bored limestone samples of shallow water origin. It contains coral fragments and larger benthic foraminifera including *Lepidocyclina chaperi*, *Lepidocyclina pustulosa* ssp., *Lepidocyclina tournori*, *Lepidocyclina gubernacula* and *Homotrema* sp. This fossil assemblage indicates a Late Eocene-Oligocene age (Baumgartner and Baumgartner-Mora, 2010). Sample M81-245-3, show high strontium isotope ratio

differences with one ratio of Chattian age (27.3 Ma) for a ratio of 0.708083, and one Aquitanian age (22.7 Ma) for a ratio of 0.708270 (Table 5, Figure 39).

The dredge of station DR-249 contained 5-10 cm bedded light yellowish gray pelagic limestones. Zoophycus trace fossils indicate a bathyal environment. The presence of *Globotruncanita calcarata, Globotruncana bulloides, Globotruncana ventricosa, Globotruncana arca* suggests a Late Campanian age (75-70 Ma, Baumgartner and Baumgartner-Mora, 2010).

For sample M81-249-1-3, one ratio could not be used because of an analytical problem. The measurement procedure was aborted early. The second measurement yielded a strontium isotope ratio of 0.707778, which corresponds to an age of 68.85 Ma (earliest Maastrichtian) (Table 5, Figure 39).

South-Western Hess-Escarpment/ Hess Rise

This region features an Early to Middle Campanian pelagic sediments covering a slightly older basaltic basement. In this area, shallow water carbonates with facies and ages similar to the ones from the North-Western Lower Hess Rise were recovered (Baumgartner and Baumgartner-Mora, 2010).

The shallow water carbonates in this region indicate a photic environment because of the presence of larger benthic foraminifera and rhodoliths (Baumgartner and Baumgartner-Mora, 2010).

The lithofacies of these limestones includes bioclastic limestones and rhodolitic boundstones.

In general, the bioclastic limestones show the presence of *Lepidocyclina pustulosa, Nummulites macquarveri?, Operculina dia, Fabiania cassis, Fabiania* ssp., which indicate a Eocene-Oligocene age (Baumgartner and Baumgartner-Mora, 2010).

Sample M81-263-9 contains *Lepidocyclina pustulosa*, *Lepidocyclina macdonaldi, Asterocyclina asterisca*, *Asterocyclina* sp., and planktonic foraminifera such as *Orbulinoides* sp. and *Globogerinateka* sp., suggesting a late Middle Eocene or Priabonian age (Baumgartner and Baumgartner-Mora, 2010).

Furthermore, pelagic wackestones are highly bored and contain a deep dwelling community of brachiopods, echinoids and branching deep-water corals. Planktonic foraminifera in the

matrix yielded an age younger than Middle Miocene (Baumgartner and Baumgartner-Mora, 2010).

Sample M81-263-1 provided strontium isotope ages of 23.9 Ma and 23.1 Ma (Chattian age) with strontium isotope ratios of 0.708196 and 0.708238, respectively. The Sr-age models are considered as reliable because they are very close to each other. Sample M81-263-2 yielded strontium isotope ratios of 0.707967 and 0.707938, which corresponds to an age of 30.40 Ma and 31.05 Ma respectively. These numerical ages define a Rupelian age for this sample (Table 5, Figure 39).

Sample M81-263-8 shows large offsets between the two obtained Sr isotope ratios, with strontium isotope ratios of 0.708173 and 0.708322, indicating ages of 24.55 Ma and 21.9 Ma respectively, and was therefore eliminated from the selection.

Sample M81-263-9 exhibits two good strontium isotope results and corresponding ages. The measured ratios yielded values of 0.708007 and 0.707966, which both indicate a Rupelian age (29.3 Ma and 30.45 Ma).

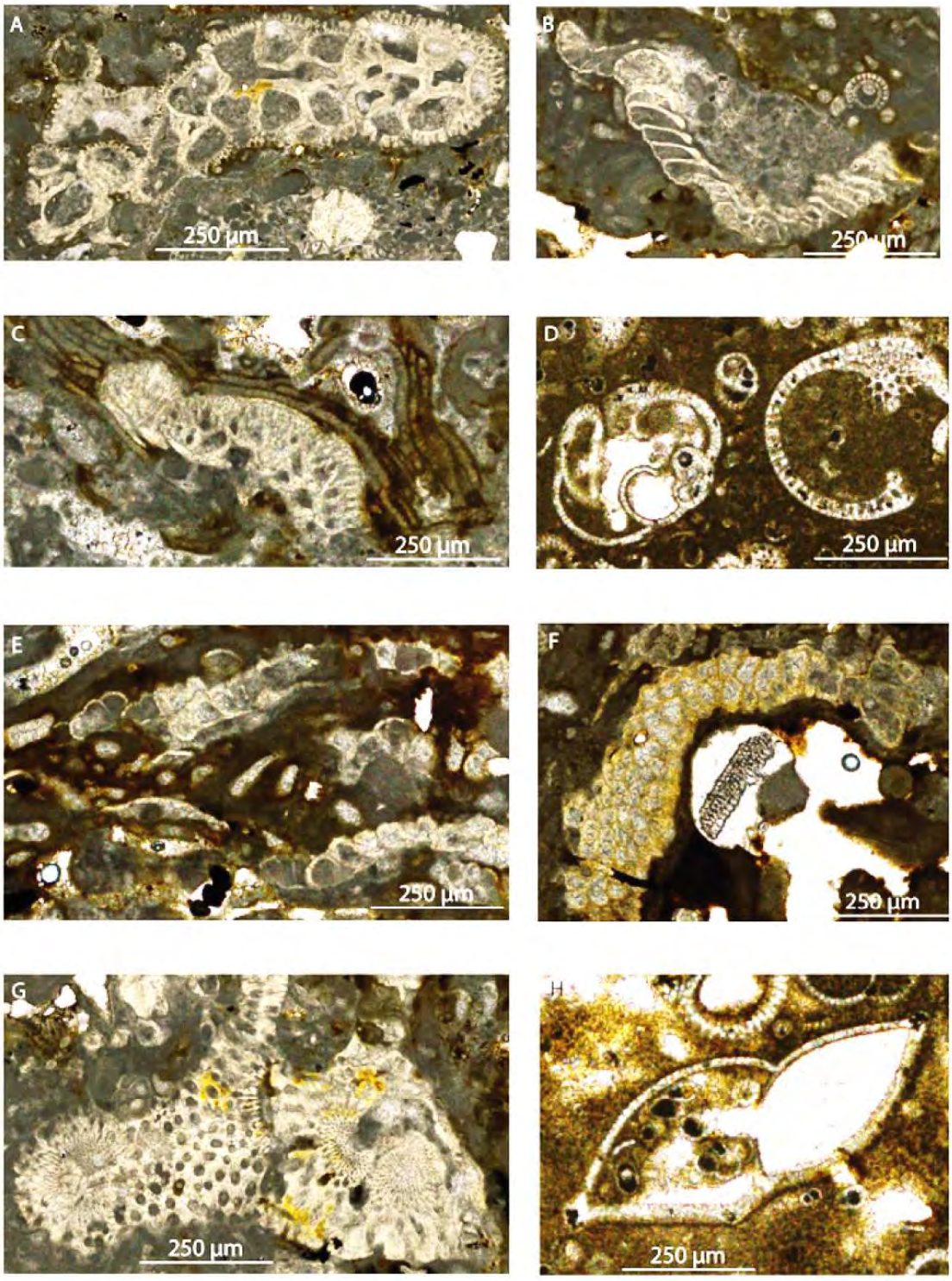

Figure 36 : A. Incrusting foraminifer, B. Eofabiania sp., C. Fabiania cf. cubensis, D. Globigerinoides sp., E-F calcareous bioclastes (algae), G. Bryozoan, H. Rotalid planktonic foraminifer. (A, B, G : sample M81-263-9 (3), C-E : sample M81-263-9 (4), D, F, H : sample M81-293-9(2)).

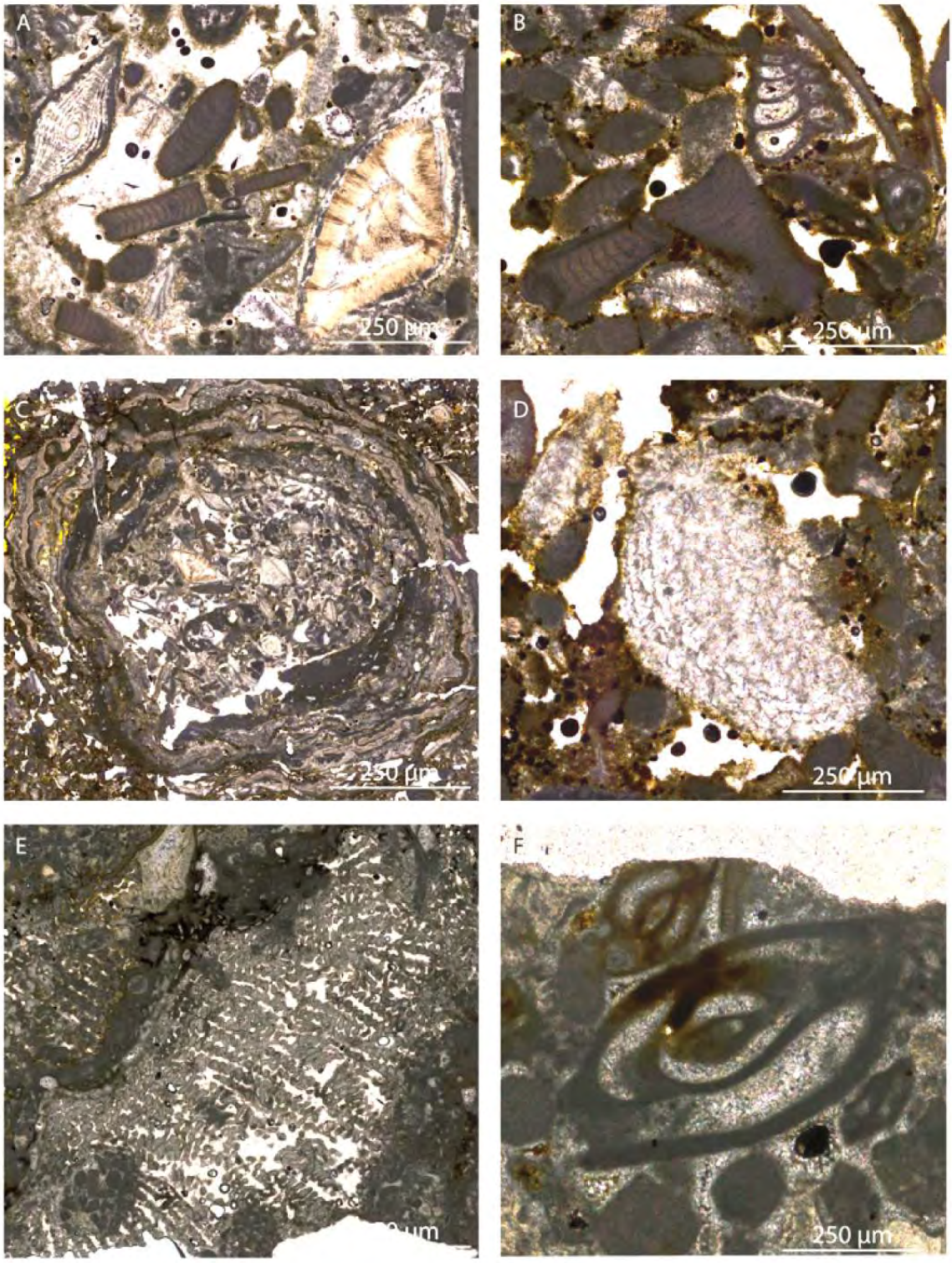

Figure 37 : ***Amphistegina*** **sp., B ,** ***Lithothanium*** **sp. and microbenthic foraminifera, C algal oncoid with** ***Amphistegina ssp in center*****., D Fragment of** ***Sphaerogypsina sp*****., E. poritid coral fragment, F** ***Miolidid*****. (A-D : sample M81-263-1, E,F : sample M81-263-9).**

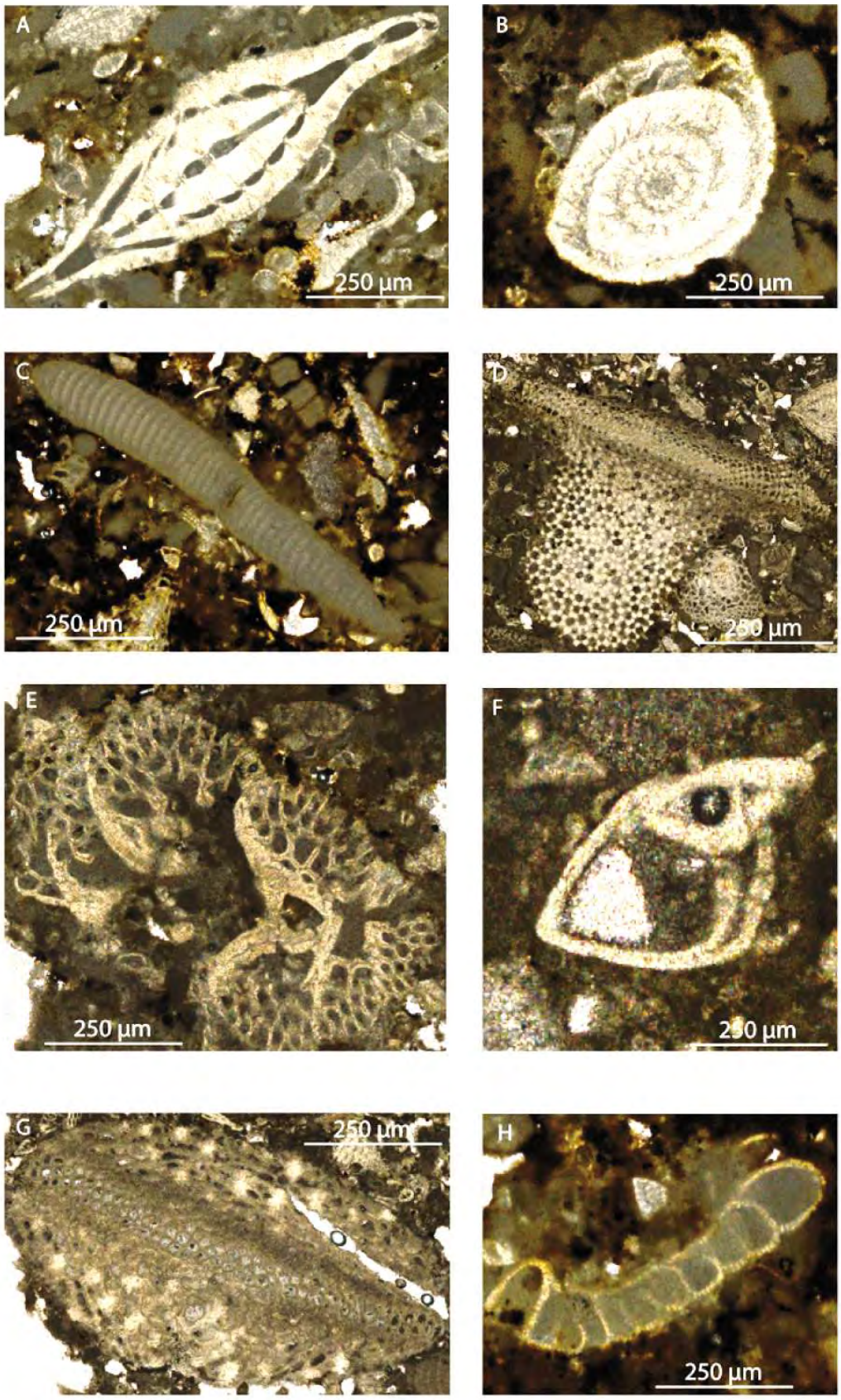

Figure 38 : *Nummulites sp.* , B. *Amphistegina sp.* C. Lithothanium, D. Fragment of cf. *Lepidocyclina sp.* E. Incrusting foraminifer. F. *Rotalid.*, G. *Lepidocyclina sp.* H. Fragment of microbenthic foraminifer? (A, B, C, H : sample M81-263-8 (8), D, E, F, G : sample M81-263-8 (7)).

Sample	$^{87}Sr/^{86}Sr$	2 S.E.	Numerical age (Ma)	Foraminifera age (Ma)
M81-241-15.5 (1)	0.707941	0.000003	30.90 - 31.65	Eocene - Oligocene
M81-241-15.5 (2)	0.707972	0.000003	29.95 - 30.70	
M81-241-18.5 (1)	0.707850	0.000003	33.00 - 33.45	
M81-241-18.5 (2)	0.707847	0.000004	33.05 - 33.50	
M81-241-24.5I	0.709181	0.000004	above recent	
M81-241-24.5II	0.709186	0.000003	above recent	
M81-245-3 (1)	0.708083	0.000003	intrasample heterogeneity	
M81-245-3 (2)	0.708270	0.000003	intrasample heterogeneity	
M81-249-1-3 (2)	0.707778	0.000004	68.80 - 69.05	75-70
M81-263-1 (1)	0.708196	0.000003	24.00 - 24.40	Eocene-Oligocene
M81-263-1 (2)	0.708238	0.000003	23.05 - 23.40	
M81-263-2 (1)	0.707967	0.000003	30.10 - 30.85	
M81-263-2 (2)	0.707938	0.000004	30.90 - 31.75	
M81-263-8 (1)	0.708173	0.000003	intrasample heterogeneity	
M81-263-8 (2)	0.708322	0.000003	intrasample heterogeneity	
M81-263-9 (1)	0.708007	0.000003	29.15 - 29.60	not younger than Priabonain
M81-263-9 (2)	0.707966	0.000003	30.35 - 30.85	

Table 5: Strontium isotope ages and the paleontological ages of the samples. The ages obtained by strontium isotopes are within these ranges (except sample M81-263-9) and can therefore be used for further discussion. Ages according to (Howarth and McArthur, 1997; McArthur *et al.*, 2001).). As the measurements were done on powders taken from the samples, these have to considered as bulk samples. Sample M81-263-8 showed high intra-sample heterogeneity and sample M81-241-24.5 yielded strontium isotope ratios that are above recent. These two samples are not considered for further interpretation.

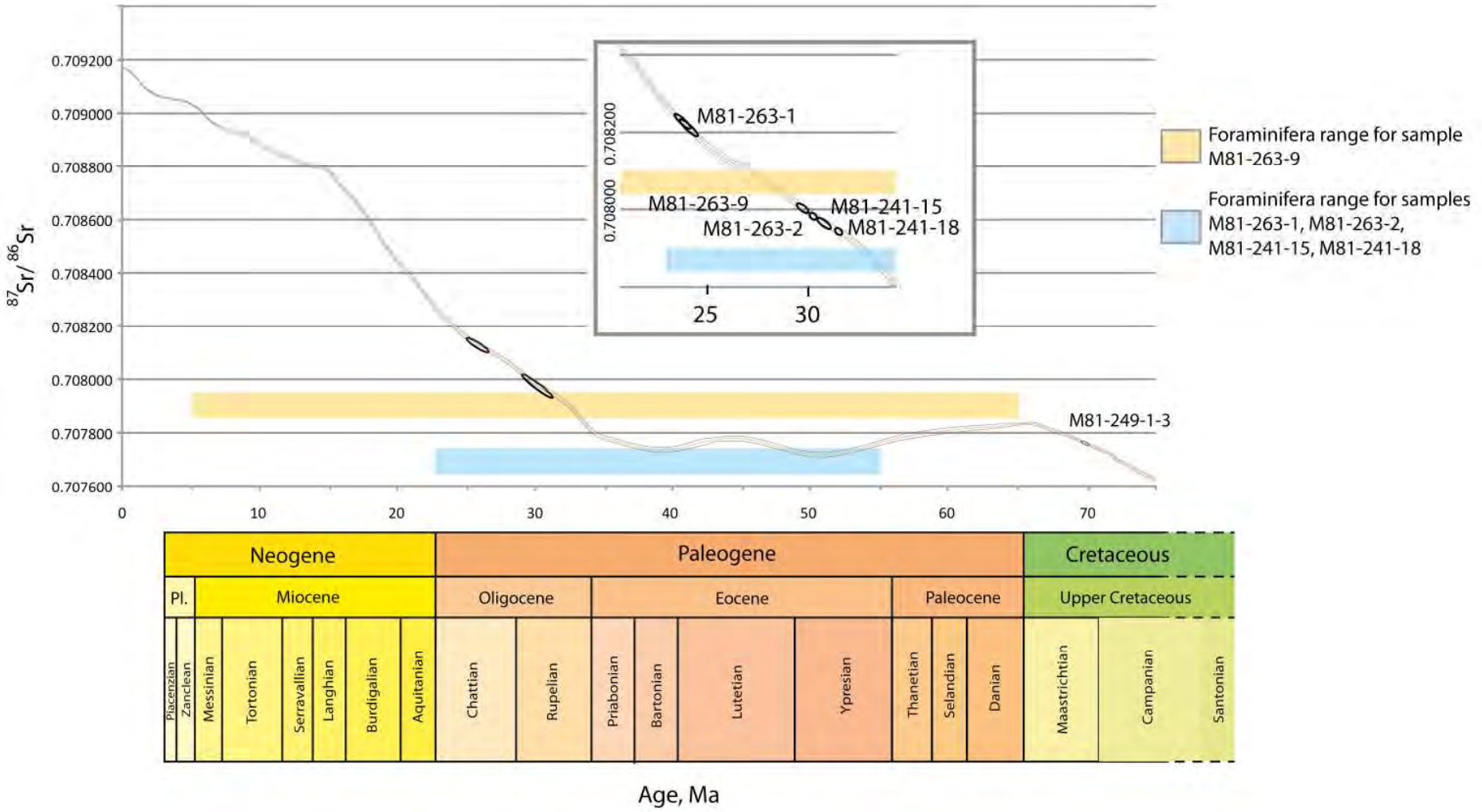

Figure 39: Strontium isotope results plotted on LOWESS curve from McArthur. All the significant values cluster in the Oligocene (Rupelian for samples M81-241-15, M81-241-18, M81-263-2, M81-263-9), (Ages determined by Baumgartner and Baumgartner-Mora, 2010, c.f Chapter 4.5.3.). Sample M81-263-1 shows a Chattian age. The yellow and blue bars show the age interval given by foraminifera ages.

5.7. Discussion

A difficulty is introduced by the absence of a continuous stratigraphy. It is therefore impossible to study a detailed section but every sample has to be considered independently because there is no control over relative positions of the samples, which means no information on mass accumulation rates. Even the presence of ash layers which could contaminate the samples with extremely low values cannot be clarified. A problem of these samples is related to the diagenetic processes that take place in seawater. Their original Sr isotope ratio might be overprinted by a secondary phase which could be affected by a marine Sr isotope ratio with a value comprised between the original ratio and the ratio of present-day marine waters (0.709174).

From the strontium isotope results it is possible to observe two distinct clusters of ages, one cluster at an age of around 29.00 Ma - 33.25 Ma (Rupelian) and a second cluster at an age of around 23.00 Ma - 25.00 Ma (Chattian). Furthermore, most of the strontium isotope ages are in accordance with the ages predicted by foraminiferal assemblages.
One test sample of pelagic limestone (M81-249-1-3) was Sr-dated to an age of 68.95 Ma (Early Maastrichtian). This sample was used in order to cross check a pelagic sample, that is more probable to maintain its strontium isotope ratio, and so test the reproducibility of the method. According to the foraminiferal assemblages, this sample is dated to the Campanian stage. Considering the limit of Maastrichtian and Campanian at 70.60 Ma, the sample must have undergone a slight alteration process (also shown by stable carebon and oxygen isotope geochemistry).

From the trace element results, the iron concentrations might be interpreted as the presence of iron oxide in cements, which has no effect on cathodoluminescence. These results may only be considered as indicative as a different dissolution method has been used for these powders than for the strontium isotope measurements on TIMS. Nevertheless, these values should be very close to the real concentrations.

Furthermore, various samples showed a realitvely high intrasample heterogeneity (samples 245-3, and 263-8), these results are therefore not used for further interpretation. This may be

due to the presence of Mn crusts. A small contamination of theses crusts may already considerably shift the Sr isotope ratio (VonderHaar *et al*, 1995), therefore, a contamination during powder preparation may have occurred. Another possibility would be a contamination by cements, which could not be avoided during the drilling of sample powders.

From the results presented above, two hypotheses can be assumed, which are presented here.

Hypothesis 1

For the samples from the dredge 241, Eocene-Oligocene ages were expected from foraminiferal assemblages. Sr-age models are within this interval, since they are within the Rupelian-Chattian interval.
Samples from the dredge 263 showed foraminiferal assemblages of Eocene - Oligocene age. Again, the ages obtained by strontium isotope ratios lay within this interval, with Rupelian (Early Oligocene) and Chattian (Upper Oligocene) ages. The Sr isotope ages can therefore be accepted as correct. Only sample M81-263-9, which should be constrained to the Eocene, also shows Rupelian ages, therefore, one could tend to statistically exclude sample M81-263-1 because it is the only sample that showed Chattian age, although the screening of this sample did not show that this particular sample should present erroneous results.

Hypothesis 2

All the samples cluster in the early Oligocene (Rupelian), except for sample M81-263-1, which shows a late Oligocene (Chattian) age. On the first sight this might be considered as the true ages because the samples are constrained by foraminifera to Eocene-Oligocene age. Only sample M81-263-9, which is constrained by foraminifera to a middle-late Eocene age shows conflicting strontium isotope ages. This suggests that all the obtained strontium isotope ages might have been shifted to a higher strontium isotope ratio by the contribution of one specific component of the rock, which results in younger ages.
The study refocused on the infill of the original porosity because all samples are packstones or grainstones and their original porosity in the samples is relatively high. Petrographic observations allow estimating the percentage of cements that fills the original porosity. Also, the presence of these cements might be the reason of the intra-sample heterogeneity of the

strontium isotope ratios, which, if incorporated into the powder measured for strontium isotope ratios in different quantities might differently affect the measured ratios.
During the Eocene (55.80 Ma - 33.90 Ma), the strontium isotope reference curve is relatively flat (Howarth and McArthur, 1997; McArthur *et al.*, 2001), with an average ratio of 0.707747 for the entire Eocene, and 0.707757 if only the middle-late Eocene interval is considered. One can imagine that an input of a strontium isotope ratio that is much higher can easily shift the measured ratio towards higher ratios and consequently younger ages.

5.8. Cement contamination

The idea consists of dating the cement, which interacts as a contaminant on the measured $^{87}Sr/^{86}Sr$ ratio. Cathodoluminescence and microscopy analyses of these samples show cements characteristic for an emersion suggesting the platform demise is due a major sea-level fall. Also, dissolution around the primary porosity can be observed, supporting this early phase of emersion. This dissolution can lead to cements with relatively low Sr concentrations. The cement that is present on the pore walls would then be the witness of the re-entering of the platform into the ocean water. It is assumed that the cement is of younger age than the sample itself, which is supposed to be of Eocen age. This would mean, as only an increase of strontium isotope ratios from the Eocene-present can be observed (Figure 39), that the cements $^{87}Sr/^{86}Sr$ would be higher than the ratio that has been measured. The cement may therefore have a ratio that is comprised between an age younger than Eocene and the present day ratio. (The cement could be of Middle Miocene to present age because of the presence of *Orbulina universa*, as this age cannot be clearly constrained, a maximum range is considered). The proportion of cement present in the samples is estimated by thin section analyses. An original average strontium isotope ratio for the samples of 0.707747 ± 0.000025 is assumed (the value of 0.707747 is an average value for the Eocene, as strontium isotope ratios do not vary significantly during this period). The target is to calculate the strontium isotope ratio of the cement and assign an age to the obtained ratio. Because the samples are considered as bulk rock, relative cement proportion was evaluated by microscopy. This proportion has been used in the calculations in order to establish a potential strontium isotope ratio of the cement and obtain an age.

These considerations may permit to calculate the strontium isotope ratio of the cements, by considering their estimated proportion in the samples, the measured strontium isotope ratios and the possible original value deducted from the paleontological ages.

The mass balance formula after Banner and Hanson, (1990), expresses the relation between the measured strontium isotope ratio and concentration, and the samples' and contaminants' ratio and concentration. The measured strontium isotope ratio is depending of the concentration in strontium and the ratio of strontium isotope ratios of the sample and the contaminant.

$$\left(^{87}Sr/^{86}Sr\right)_m = \frac{\left(^{87}Sr/^{86}Sr\right)_s (C)_s F_s + \left(^{87}Sr/^{86}Sr\right)_c (C)_c (1-F_s)}{C_m}$$

(Where C=concentration, F=fraction, m=measured, c=contaminant, s=sample)

The concentration of Sr being unknown in the cements, they had to be estimated, although they can vary significantly (Banner, 1995). As there is no certainty of these concentrations, calculations showed that for sample M81-241-15, a Sr concentration of the cement above 100 ppm would result in a strontium isotope ratio of the cement that is lower than the Sr isotope ratio of modern sea water and so have a deducted $^{87}Sr/^{86}Sr$ age. For sample M81-241-18, the threshold to have a Sr isotope ratio lower than modern sea water is at 73ppm and for sample M81-263-9 it would be at 335 ppm (Figure 40 A).

If the concentration of the cement and the concentration measured on the sample equal each other it implies that the measured Sr concentration (C_m), the original sample Sr concentration (C_s) and the Sr concentration of the contaminant (C_c) have no effect on the Sr isotope ratio of the cement.

The mass balance calculations are relatively complex, because the assumed Sr concentration of the cement has a direct impact on the Sr concentration of the sample; these two concentrations are inversely proportional. This is due to fact that a relatively high Sr concentration in the cement implies a very low Sr concentration in the sample. These concentrations are not representative of shallow water marine carbonates (Chapter 2). Calculations show that if the Sr concentrations in the cement are considerably higher, their

resulting Sr isotope ratio will tend towards the measured Sr isotope ratio, if it is assumed the cement is not older than Middle Miocene (*Orbulina universa*), Sr concentrations of the cement reach about 220 ppm (Figure 40), if the cement is not older than very Early Miocene, Sr concentrations would reach up to 270 ppm (which is higher than the samples Sr isotope ratio, condition that has been considered impossible in the assumptions), (Figure 40). In general, for a known fraction of contaminant: the higher the concentration of Sr in the cement, the lower the concentration of Sr in the sample, the lower its resulting Sr isotope ratio, the older it's age would be (close to the measured ratio). An example of this calculation is shown in Figure 40 A+B, where the different mass balance calculations show that the Sr isotope ratio of the cement depends on the fraction of cement present in the measured sample and its concentration.

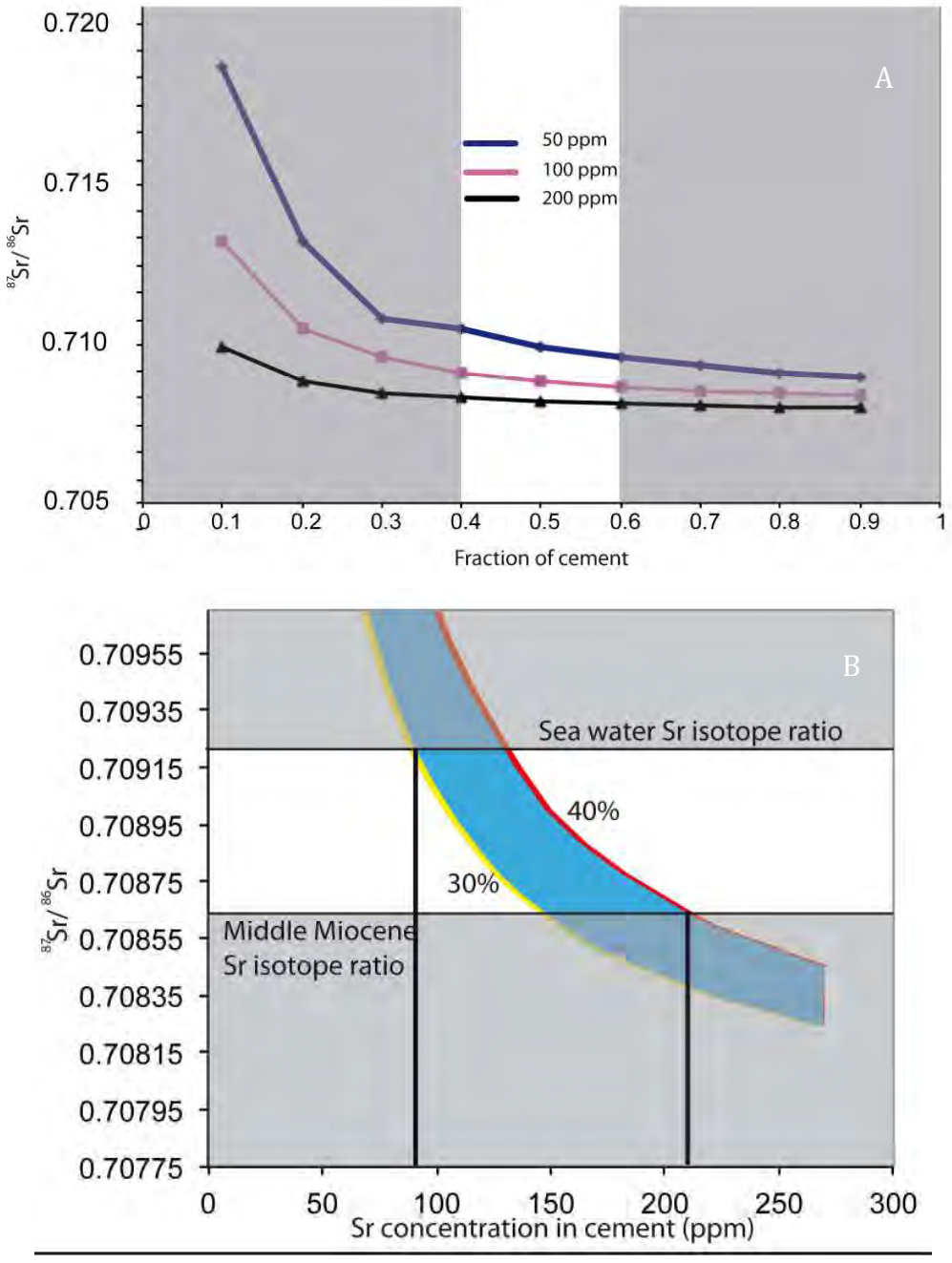

Figure 40: A: Mass balance calculations for samples M81-241-15. This graph shwos the possible variations of the cement Sr isotope ratio in function of its concentration and fraction. Note that for this sample, the fraction of cement has been estimated to 30%-40%. The calculated Sr isotope ratios for cement concentrations of 50 ppm, 100ppm and 200ppm are represented. B: The mass balance calculations permit to have a maximal and minimal concentration vs. Sr isotope ratio curve. A samples Sr isotope ratio should be comprised in between the modern marine seawater ratio and the Middle Miocene Sr isotope ratio (*Orbulina universa*). This graph shows for which concentrations the Sr isotope ratios are in an acceptable range. It shows that only samples with a concentration in between ~95 ppm and ~205 ppm, valid for cement fractiosn between 30% (yellow line) and 40 % (red line), can have Sr isotope ratios comprised between modern marine seawater ratio and the Middle Miocene Sr isotope ratio.

Sample	average $^{87}Sr/^{86}Sr$ of the sample	estimated cement presence
M81-241-15	0.707957	30%-40%
M81-241-18	0.707849	20%-25%
M81-263-9	0.707988	10%-15%

Table 6: This table shows the average strontium isotope ratios of the samples and the presence of cement in the initial porosity. The results of the calculations show the strontium isotope ratio of the cement according to the percentage of cement presence in the samples.

The samples from the site M81-241 showed that these cements have calculated values that can be representative for the early Miocene while having “reasonable” Sr concentrations (higher than 100, lower than 210).

It is important to note that an extremely low value has been taken into account for the samples of site 241, in order to show the "worst case scenario". If the sediments were of very late Eocene, or very early Oligocene age (with ratios > 0.707747), the drowning would be shifted towards older ages.

Nevertheless, lacking a proof that the concentrations and the Sr isotope ratios are correct, it suggests further studies on this specific cement.

For sample 263-9, the same calculation has been applied. In general, samples from dredge site 263 showed very low to no luminescence, characteristic of a “normal” marine, well oxygenated diagenetic signal and no secondary crystallization phase was observed. The cement has been assumed to represent a primary phase. The calculated strontium isotope ratios for the cements of these samples have been calculated with the estimated percentage of cement presence and Sr concentration, in the same way than for samples from the dredge site 241. Results for sample M81-263-9 show that the $^{87}Sr/^{86}Sr$ ratios of these cements are higher than the present marine ratio (>0.709174), when calculating with cement Sr concentrations of around 150 ppm. In fact, even with a Sr concentration of cements equal to the measured concentration of the sample, the Sr isotopic ratio of the cements lies above recent marine waters. (The only possibility to lower considerably the Sr isotope ratio of the cement would be to have high Sr concentrations or to have a fraction of cement that is more consequent). Calculations show that in order to have a modern sea water Sr ratio for the cement, the Sr

concentration should be at least at 330 ppm, which is more 4x more than the concentration calculated for samples M81-241-15 and M81-241-18.

Furthermore, foraminifera of sample M81-263-9 revealed a late Eocene age. Strontium isotope ratios resulted in a Rupelian (early Oligocene) age. This could be linked to reworking, a parameter that has been overseen during screening, or to the analytical procedure. Reworking may have been the best candidate to explain such anomalous age: on DSDP site 150, which is located in the extended vicinity of the dredge stations, Bolli and Silva (1973) mentioned reworked Eocene foraminifera in Oligocene sediments, although no physical evidence of reworking could be observed for sample M81-263-9.

Also, the $^{87}Sr/^{86}Sr$ ratios were measured on a coral, whose aragonite replacement by calcite has probably shifted the ratios values towards younger ages. A general overprint of the samples may also have occurred. The timing of this overprint cannot be certified, because the resulting strontium isotope ratios would only show biased strontium ratio values. Hypothetically, the overprint might have occurred during the early Miocene as seen for samples M81-241-15/18.

Sample M81-263-8 shows a relatively wide intrasample heterogeneity in the strontium isotope results. This can also be explained by the presence of cements that interferes as a contaminant in the measured ratio, similar to samples M81-263-9. (There is no control on the quantity of contamination by cement during the sample preparation, neither its strontium isotope ratio).

5.9. Conclusion and outlook

The ages obtained for site DR-241 show a possible bias of the strontium isotope results by the presence of secondary cement, which acts as a contaminant. For site DR-263, the obtained ratios are highly probable to reflect the original marine ratios. Also, for site DR-241, a possible date of the immersion of the sediments could be determined. Unfortunately, age datings of the volcanic rocks of the carbonate platforms substratum are lacking to support this hypothesis. Nevertheless, the results of these dating are expected during 2013, their ages will be very helpful in order to assign reliable ages and to emit a general tectonic history of this region of the Caribbean Tectonic Plate. Only the combination of the ages obtained from the

seamounts and from the studied carbonates can help defining the timing and the intensity of the tectonic activity.

In order to complete this study, it would be useful to make a complete paleontological study of the thin sections, which would allow showing the whole spectra of paleontological ages. Also much more detailed strontium isotope analyses on the cements and separately on the bioclasts (avoiding contamination by the cements) would provide further information on their ages and origin. Unfortunately, even in areas where these cements are very abundant, it is nearly impossible to separate them from the host rock without avoiding a contamination and it would be recommendable to do this *in situ*.

5.10. References

Banner, J.L., **1995**. Application of trace element and isotope geochemistry of strontium to studies of carbonate diagenesis. Sedimentology, vol. 42, Issue 5, pp. 805-824.

Baumgartner and Baumgartner-Mora, **2010**. Chapter 5.5, Sedimentary Rocks pp. 29-34; in Meteor-Berichte 11-8, CLIP - Origin of the Caribbean Large Igneous Province (CLIP) in connection with the geodynamic evolution of the Central Caribbean 78 pp.

Bausch, W.M., **1968**. Outlines of distribution of strontium in marine limestone. In:Muller, G. Friedman, G.M. (eds): Recent developments in carbonate sedimentology- Central Europe, 106-115. Berlin-Heidelberg. New York Springer

Bice, D.M., Stewart, K.G., **1990**. The formation and drowning of isolated carbonate seamounts: tectonic and ecological controls in the Northern Apennines. Special publications of international Association of Sedimentologists, 9, pp. 145-168.

Bolli, H.M., Silva, I.P., **1973**. 10. Oligocene to recent planktonic foraminifera and stratigraphy of the LEG 15 sites in the Caribbean Sea. DSDP Volume XV, Special Studies.

Bowland, C. L,, **1984**. Seismic stratigraphy and structure of the western Colombian Basin, Caribbean Sea [M.A. thesis]: Austin, Texas, University of Texas at Austin, 247 p.

Bowland, C. L-, and Rosencrantz, E., **1988**. Upper crustal structure of the western Colombian Basin, Caribbean Sea: Geological Society of America Bulletin, 100, p. 534-546.

Camoin, G.F., Arnaud-Vanneau, A., Bergersen, D.D., Enos, P., Ebren, Ph., **1998**. Development and demise of mid-oceanic carbonate platforms, Wodjebato Guyot (NW Pacific). Special publications of international Association of Sedimentologists, 25, pp. 39-67.

Coffin, M.F., Eldholm, O., **1991**. Large Igneous Provinces: JOI/USSAC Workshop Report. The University of Texas at Austin Institute for Geophysics Technical Report 114: 79 pp.

Coffin, M.F., and Eldholm, O., **1992**. Volcanism and continental break-up: a global compilation of large igneous provinces Geological Society, London, Special Publications, 1992, 68, pp. 17-30

Edgar, N. T., Saunders, J. B., Bolli, H. B., Boyce, R. E., Donnelly, T. W., Hay, W. W., Maurrasse, F., Prell, W., Premoli-Silva, I., Riedel, W. R., Schneidenmann, N., **1973**. Site 154, *in* Edgar, N. T., and others, Initial reports of DSDP Leg 15: Washington, D.C., U.S. Government Printing Office, p. 407-471.

Flügel, E., **2010**. Microfacies of carbonate rocks: Analysis, Interpretation and Application. 2nd Edition, Springer, 1006 p.

Hoernle, K., Abt, D.L., Fischer, K.M., Nichols, H., Hauff, F., Abers, G.A., van den Bogaard, P., Heydolph, K., Alvarado, G., Protti, M., Strauch, W., **2008**. Arc-parallel flow in the mantle wedge beneath Costa Rica and Nicaragua. Nature 451, pp. 1094-1097.

Howarth, R.J., and McArthur, J.M., **1997**. Statistics for strontium isotope stratigraphy. A robust LOWESS fit to the marine Sr-isotope curve for 0 - 206 Ma, with look-up table for the derivation of numerical age. Journal of Geology, 105, pp. 441-456.

Hueneke, H., **2010**. Chapter 5.7, Morphology of the Seamounts from a Sedimentological Perspective pp. 38-39; in Meteor-Berichte 11-8, CLIP - Origin of the Caribbean Large Igneous Province (CLIP) in connection with the geodynamic evolution of the Central Caribbean 78p.

Lu, R. S., and McMillen, K. J., **1982**. Multichannel seismic survey of the Colombia Basin and adjacent margins, *in* Watkins, J. S., and Drake, C. L., eds., Studies in continental margin geology: American Association of Petroleum Geologists Memoir, 34, p. 395-410.

Meschede, M., Huenecke, H., Bartsch, C., Sperl., Hoernle, K., Werner, R., **2010**. Chapter 5.6 Geomorphological Observations, pp. 34-37; in in Meteor-Berichte 11-8, CLIP - Origin of the Caribbean Large Igneous Province (CLIP) in connection with the geodynamic evolution of the Central Caribbean 78 pp.

Mutti, M., Droxler, A.W., Cunningham, A.D., 2005. Evolution of the Northern Nicaragua Rise during the Oligocene–Miocene: Drowning by environmental factors. Sedimentary Geology, 175, pp. 237–258.

Sattler, U., Immenhauser, A., Schlager, W., Zampetti, V., **2009**. Drowning history of a Miocene carbonate platform (Zhujiang Formation, South China Sea). Sedimentary Geology, 219, pp. 318-331.

Saunders, J. B., Edgar, N. T., Donnelly, T. W., and Hay, W. W., **1973**. Cruise synthesis, *in* Edgar, N. T., and others, Initial reports of DSDP Leg 15: Washington, D.C., U.S. Government Printing Office, p. 1071-1111.

Schlager, W., **1981**. The paradox of drowned reefs and carbonate platforms. Geological Society of America Bulletin, 92, pp. 197-211.

Schlager, W., **2003**. Benthic carbonate factories of the Phanerozoic. International Journal of Earth Science, 92, pp. 445-464.

Sirgudsson, H., Leckie, R.M., Acton, G.D., **1997**. Proceedings of the Ocean Drilling Program,

Initial Report, 165.

Spötl, C., Vennemann, T., **2003**. Continuous-flow isotope ratio mass spectrometric analysis of carbonate minerals. Rapid Communications in Mass Spectrometry, 17, p. 1004-1006.

Vonder Haar D.L., Mahoney J.J., McMurtry G.M, **1995**. An evaluation of strontium isotopic dating of ferromanganese oxides in a marine hydrogenous ferromanganese crust. Geochimica et Cosmochimica Acta, 59, p. 4267-4277.

Werner, R., Hoernle, K., Hauff, F., Maicher, D., Conrad, C., Seidel, E., Krüger, U., Loose, P., Sperl., D., **2010**. Chapter 5.4, Magmatic Rock Sampling Summary, pp. 28-29; in Meteor-Berichte 11-8, CLIP - Origin of the Caribbean Large Igneous Province (CLIP) in connection with the geodynamic evolution of the Central Caribbean 78pp.

Wilson, P.A., Jenkyns, H.C., Elderfield, H., Larson, R.L., **1998**. The paradox of drowned carbonate platforms and the origin of Cretaceous Pacific guyots. Nature, 392, pp. 889-894.

Zachos, J.C., Opdyke, B. N., Quinn, T.M., Jones, C. E., Halliday, A.N., **1999**. Early Cenozoic glaciation, Antarctic weathering, and seawater $^{87}Sr/^{86}Sr$: is there a link? Chemical Geology, 161, pp. 165-180.

Zimmerman, H. B., **1982**. Lithologies stratigraphy and clay mineralogy of the western Caribbean and eastern equatorial Pacific, *in* Prell, W. L., and others, Initial reports of DSDP Leg 68: Washington, D.C., U.S. Government Printing Office, p. 383-396.

6. $^{87}Sr/^{86}Sr$ data from La Désirade, Guadeloupe France

6.1. Introduction

Sr isotope ratios are a very powerful and precise tool to date carbonates rocks and fossils. The residence time of Sr of about 10^6 years is far longer than the mixing time of the ocean waters, which is around 10^3 years; Sr isotope ratios are then considered to be the same worldwide for a given time, (Burke *et al.*, 1982; De Paolo & Ingram, 1985; Elderfield, 1986; McArthur 1994; Smalley *et al.*, 1994; Veizer *et al.*, 1997; in Frijia & Parente, 2008; Prokoph *et al.*, 2008, Hodell *et al.*, 1991). Because Sr is incorporated in carbonates and in biominerals when precipitated in seawater, it is then possible to date carbonate samples with strontium isotopes (McArthur, 1994 amongst others).

The generally steep appearance of the $^{87}Sr/^{86}Sr$ curve for the last 50 My suggests a very high potential in Strontium Isotope Stratigraphy (SIS) for this time period (McKenzie *et al.*, 1988; Hodell *et al.*, 1989a; Hodell *et al.*, 1994; Veizer *et al.*, 1999; Mc Arthur *et al.*, 2001; Vasiliev *et al.*, 2010). An explanation for this steep increase in $^{87}Sr/^{86}Sr$ ratios is believed to be mostly due to the uplift and weathering of the Himalayan chain (Hodell *et al.*, 1990), but this is sometimes doubted (McArthur 1998; Banner, 2004). Nevertheless, the worldwide Sr ratio variations are in good agreement with the evolution of the length of the collision zones (Hochard *et al.*, 2011) and the volume of mountains (Vérard *et al.*, 2011).

SIS is very useful for the late Neogene, as a general increase in $^{87}Sr/^{86}Sr$ is observed, with a range of higher precision during the Messinian to Zanclean (6.0 Ma to 4.5 Ma) interval and a range with lower precision during a Late Miocene (8.0 Ma - 6.0 Ma) and Pliocene (4.5 Ma - 2.5 Ma) due to the variations in the $^{87}Sr/^{86}Sr$ curve slope (Hodell *et al.*, 1990). Combined with the data of McArthur *et al.* (2006), the curve has the necessary precision in order to calculate ages with high precision.

In this work we present new Late Neogene- Quaternary Sr isotope data from well preserved calcareous fossil samples from La Désirade in order to better constrain the tectonic evolution of this island. It is known that La Désirade underwent tectonic uplift and subsidence (Bouysse *et al.*, 1990), which may be better constrained through SIS. In this time interval subsidence and uplift is difficult to determine, since the record of high glacio-eustatic sea level variations

during the Late Miocene to Pleistocene interferes with the record of tectonic subsidence and uplift.

6.2. Island Morphology

La Désirade is a small (2x 12 km) island located East of Grande Terre and Basse Terre, the main Islands of the Guadeloupe Archipelago in the Lesser Antilles Arc (Figure 41).
The northern coast is characterised by up to 200 meters high cliffs (Figure 41, Figure 44), whereas more gentle slopes characterize the southern side, where terraces are present. Local landslides can also be observed. Between the "Pointe du Souffleur" and Beauséjour a major landslide is present along the main road (Figure 41).
The Island is characterized by its tabular shape, with a maximum elevation of 276 meters at the "Grande Montagne". A major normal fault (Desert Fault) crosses the Island of La Désirade and splits it into two parts. A smaller western part around Beauséjour and a major eastern part called Plateau de "La Montagne" (Figure 41), which gives the tabular shape to the Island. The Plateau de la Montagne is cut into 3 blocks by 2 normal faults.

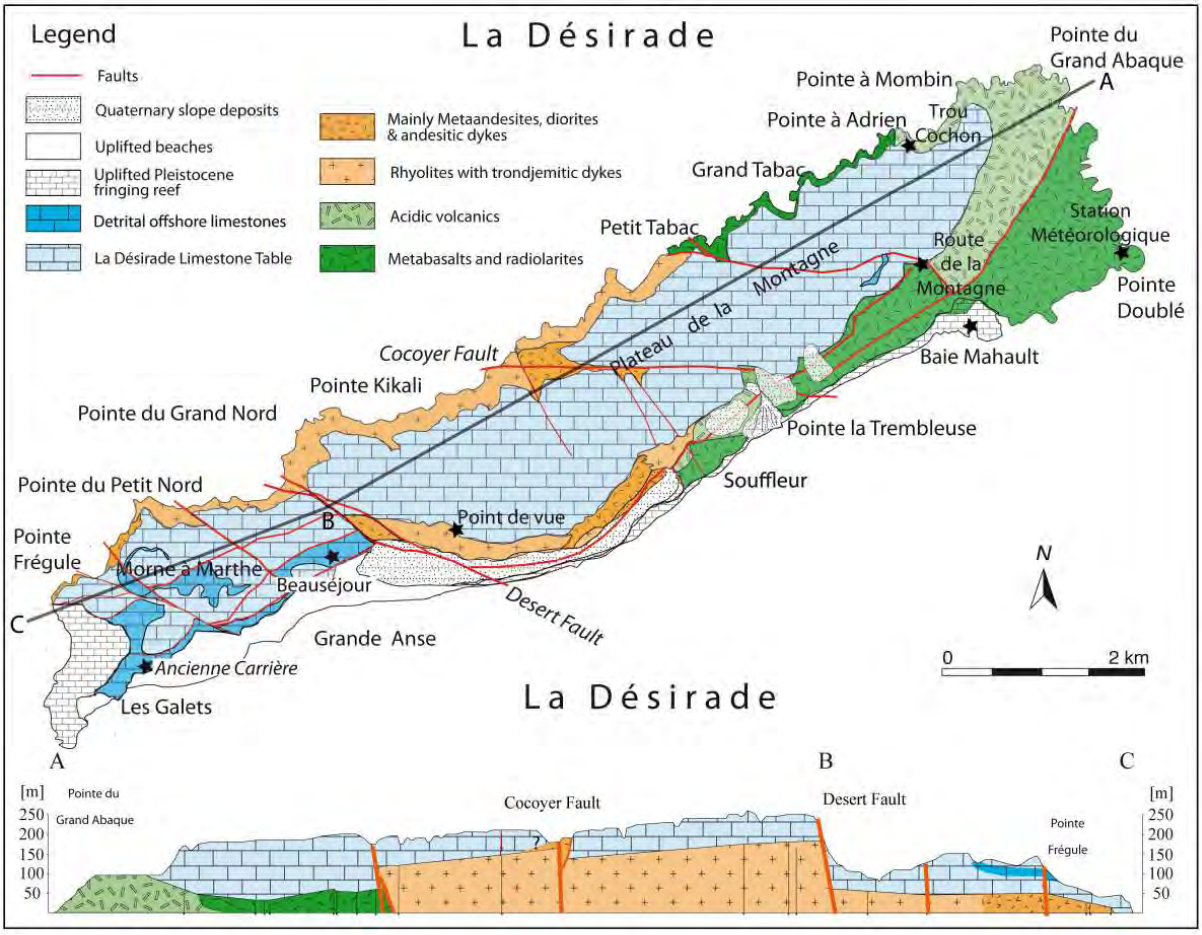

Figure 41: Geologic map of La Désirade (Baumgartner-Mora & Baumgartner, 2011, modified) with section A-B-C, Elevations of the basement/limestone contact were measured by laser rangefinder and GPS-localisation along the north coast of La Désirade Island. Light gray vertical lines correspond to measured heights. The section through the Island corresponds to the view towards South. Section ABC at the same horizontal scale than the geologic map, vertically exaggerated.

6.3. **Geological setting**

La Désirade is an outer forearc high located about 100km westward to the trench where Atlantic crust is currently subducted under the Caribbean Plate (at around 2cm/y) (Figure 42). The island is located on the "Banc des Vaisseux", west of the Karukera Spur (Figure 42, Figure 43). To the North, the La Désirade Escarpment reaches a depth of 4700m in a continuous slope (Bouysse *et al.*, 1990) (Figure 43). The Karukera Spur is separated from the "Banc des Vaisseux" by a major normal fault (Figure 43). According to Feuillet *et al.*, (2004) a general westwards tilting of the Guadeloupe Archipelago can be observed.

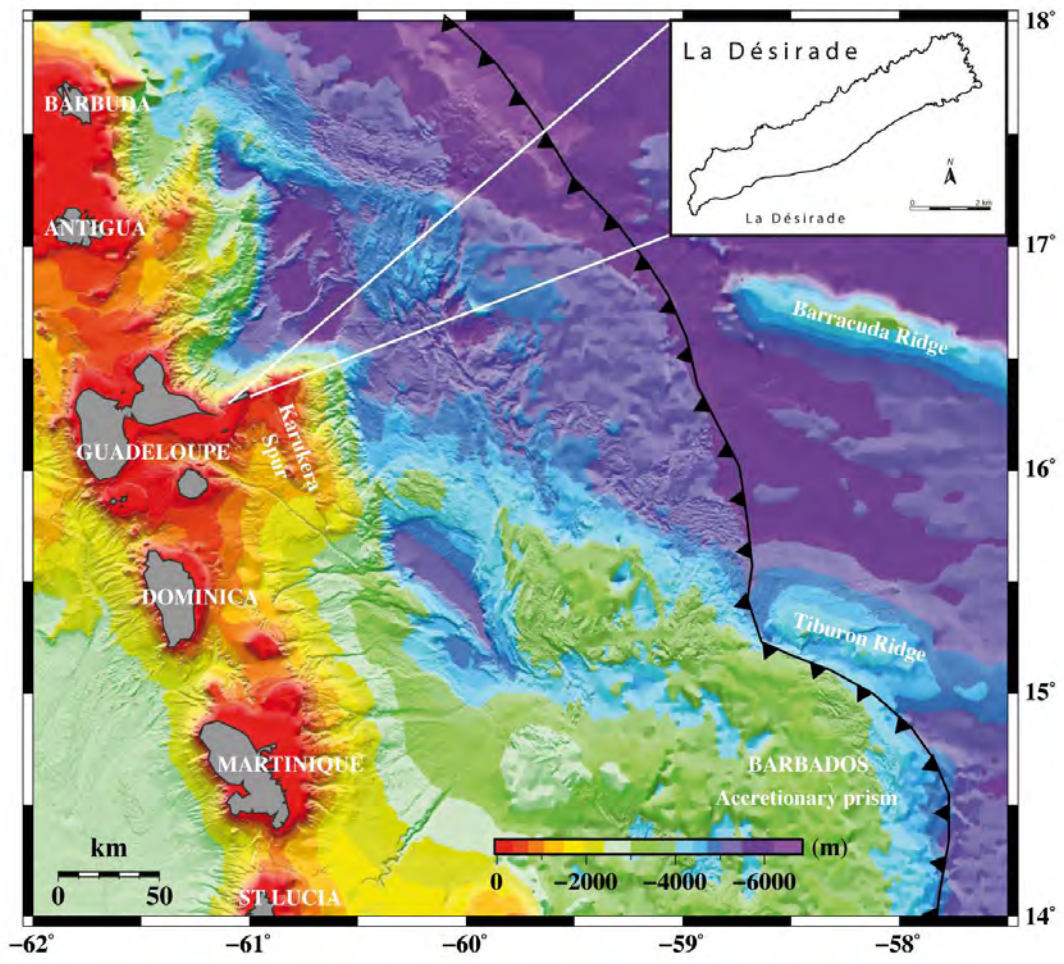

Figure 42: Localisation of La Désirade, close to the subduction trench on the Karukera Spur. Bathymetric map modified after Evain *et al.* (2011). La Désirade located is about 150km west of the Lesser Antilles Subduction zone.

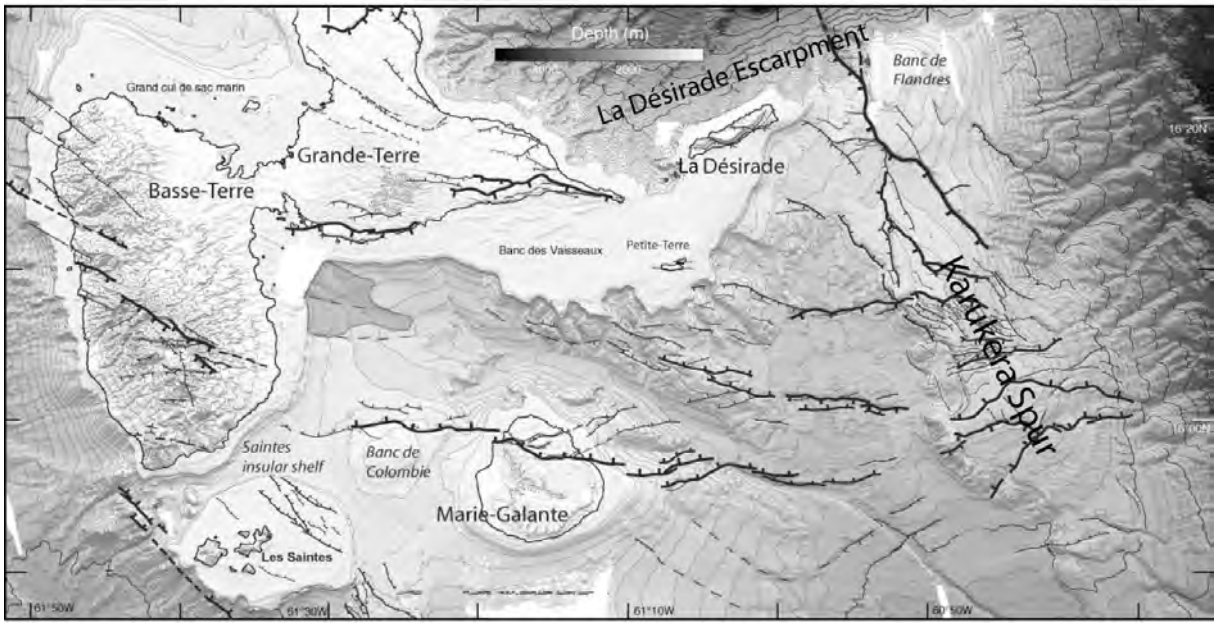

Figure 43: High resolution Bathymetry of the Guadeloupe Archipelago (from Twain). This map shows La Désirade is placed west of the Karukera spur which shows NW-SE and E-W oriented faults.

La Désirade Island, together with Grande Terre and Marie-Galante Island are part of the "Calcareous Lesser Antilles". This edifice is characterized by Neogene-Quaternary carbonate platforms that formed on top of an extinct and eroded Tertiary outer arc and is subaerially exposed due to Quaternary uplift. Basse Terre to the west with the Souffrière Volcano is part of the modern volcanic arc, active since the Burdigalian (Early Miocene), (Bouysse and Westercamp 1988).

La Désirade was mapped for the first time by Fink (1970), then by Westercamp (1980). More recently we have mapped the whole island (Baumgartner-Mora & Baumgartner, 2011) (Figure 41). Westercamp (1980) differentiates in his geological outcrop descriptions two late Pliocene formations: the "table calcaire" that forms the limestone plateau of the Montagne and the Morne à Marthe and the "calcaires meubles organo-détritiques" that form the low hills around Morne à Marthe in W- Désirade (W of Beauséjour, Ancienne Carrière, and les Galets); (Figure 41). In this work, the "table calcaire" will be refered to as Limestone Table (LT), and the "calcaires meubles organodétritiques" to Detrital Offshore Limestone (DOL).

For Westercamp (1980) the LT corresponds to a reef in place. It is represented by biomicrites and biosparites in which coral debris and melobesian red algae dominate. Based on the presence of rare larger foraminifera in the LT such as *Amphistegina* and few peneroplids, associated with rare planktonic foraminifera he concludes on a lower to/or middle Pliocene "parareefal" facies.

The DOL are described as loose limestone with fine texture composed of bioclastic carbonate. Westercamp (1980) interprets these formations as coeval, but of a more open marine environment, beneath the reef "in place" of the LT. More recently, La Désirade carbonates are compared to the Early Pliocene reefal carbonates of Marie Galante (Andreieff *et al.*, 1983).

Several, more recent studies stress the very important pre-Pliocene uplift necessary to bring the Désirade basement into shallow water. For instance Bouysse and Westercamp (1990) developed a model in which the attempted subduction and final underplating of a buoyant aseismic ridge resulted in the >2 km uplift documented in La Désirade. According to them, this event also caused the extinction of the pre-Miocene outer arc and the initiation of the Miocene to Recent inner arc.

A few authors dated La Désirade carbonate rocks by foraminifera. The ages do not vary significantly between authors, but there is considerable uncertainty. Barrabé (1953) compared the La Désirade limestone with those of Grande Terre and considered a Miocene age by facies

analogies. Westercamp (1980) dated the carbonate rocks as early Pliocene. Münch *et al.* (2011) consider the carbonate rocks of La Désirade to be at most of Zanclean (Early Pliocene) age, and finally Baumgartner-Mora & Baumgartner (2011) conclude a latest Miocene to early Pliocene age based on a new study of planktonic foraminifera of the detrital offshore limestones. The difference in ages is mostly due a redefinition of the Mio-Pliocene boundary (Wade *et al.*, 2011). Sr isotope ratios may be used to date and correlate the rocks of La Désirade with oceanic sections studied in great detail both for planktonic foraminifera and Sr-isotopes. It is then possible to produce Sr isotope ages with a relatively high precision for the La Désirade carbonate rocks.

Baumgartner-Mora and Baumgartner (2011) point out the presence of a basal conglomerate which overlays the volcanic basement. All the lithologies of the basement can be found as clasts in this conglomerate. The presence of rounded cobbles to boulders proves a high-energy environment, which we interpret as the reason of the flat-surfaced shape of the La Désirade basement. This surface is cut by normal faults, which create the differences in elevation of the basement. Furthermore, the presence of a paleosoil at the "Trou Cochon" suggests the basement had been emerged. Neither timing nor the origin of this paleosoil could be determined. (Figure 41, Figure 44, Table 7).

The timing of the activity of the normal faults cutting La Désirade into blocks cannot be precised. A syn- or post-depositional activity is probable because the limestone thickness varies along the different blocks, and furthermore, geomorphological properties indicate that the faults may still be active as valleys are carved into the limestone above the faults of the basement (Figure 41).

6.4. **Samples and Localities**

Marine Sr isotope ratios are best preserved in fossils that consist of primary biogenic calcite (McArthur, 1994). Measurements on foraminifera may be difficult, as they are small and sometimes filled with contaminants such as clay and diagenetic calcite (McArthur, 1998). If samples are collected from carbonate-rich layers, these problems can be avoided, because altered carbonate may show similar Sr ratios as the surrounding carbonates (McArthur, 1998). Bulk rock samples from lithified limestone may yield marine Sr-values of the time of the early diagenesis, if no exchange between the carbonates and detrital minerals that may contain

very different Sr-ratios occurred (McArthur *et al.*, 1994, McArthur *et al.*, 1998, Bailey *et al.*, 2000, Singh *et al.*, 1997). For the Désirade carbonates, the geographical proximity of the volcanic arc active since the Burdigalian (today: La Soufrière volcano on Basse Terre) is a potential source of contaminants. The presence of ash layers in the stratigraphic record could have an effect on $^{87}Sr/^{86}Sr$ ratios of bioclasts and early cements (see Chapter 2).

The samples used in this work include well-preserved microfossils (foraminifera) and macrofossils (corals) that could give representative $^{87}Sr/^{86}Sr$ results.
Aragonitic fossil samples, such as corals and gastropods, also have a very high potential in Sr isotope dating when primary aragonite is preserved. A first observation in the field allows checking the presence of primary aragonitic structure. Samples that show replacement textures, such as coarse sparite crystals, were eliminated.
We intended to sample a complete stratigraphic transect through the Limestone Table. The best locality to do so is the "Route de la Montagne", where the sequence is thickest and probably most complete, and outcrops are mostly accessible (samples DES025I and II, DES029I and II).

Detrital Offshore Limestone

Samples were collected on the W-side of La Désirade, in Beauséjour (BSJI and BSJII) in the DOL in order to observe if differences in age of the DOL and the LT appear (Figure 41).

Limestone Table

For the LT, samples were collected in the probably most complete stratigraphic outcrop of La Désirade, east of "Trou Cochon" (Figure 41, Figure 44, Table 7). Unfortunately, this outcrop is of difficult to access. Samples from the "Trou Cochon" have not been analysed for $^{87}Sr/^{86}Sr$ because of the presence of dolomite in the samples. At the "Grand Abaque" (samples GRAEI and GRAEII) (Figure 41, Table 7) a well preserved rhodolite has been collected a few meters above the contact with the basaltic basement. Other samples were collected at the "Point de

Vue" (samples DES035I, II and III) on the geological top of the LT, on the south side of the Island, above the locality of Beauséjour (Figure 41, Table 7).

Fringing Reefs and Beach Rock

A beach rock has been sampled, at the "Station Météorologique" at the far south-east of La Désirade (D4043AII). (The meteorological station is built on the terrace formed by the beach rock). Because a beach rock is formed with the interaction of marine and freshwater and its cements can have a marine origin, it suggests a possibility of dating by Sr isotope ratios. Freshwater Sr might act as a contaminant, but the presence of carbonate rocks with similar ages will not provide a Sr source that is much different from the sea-water ratio of the timing of the creation of the beach-rock. Also, no rivers have been observed on the Island, this would mean that the Sr is recycled through dissolution from preexisting limestone with an older age.
At the Baie Mahault Bay, coral samples have been taken from a fossil reef (BBMAI and BBMAII) (Figure 41, Table 7).
Along the mountain road a contact layer between the volcanic basement and a fringing reef can be observed, this contact layer is characterized by a fine-grained conglomerate. We have not observed big boulders or pebbles and the presence of marine algae which suggest a marine depositional environment. Therefore we consider this conglomerate different from the base conglomerates found elsewhere on the island. We suggest the emplacement of the fringing reef on a palaeotopography that was characterized by a volcanic substratum. (The same situation can be observed nowadays along the easternmost coastline of La Désirade Island, close to the waste disposal). A fossil echinoid shell and a fossil coral were sampled from the first layers above the conglomerate (RMECHI, RMECHII, RMOI and RMOII) (Figure 41).

Unfortunately, the reef cap on the far-east summit of the LT did not yield well-preserved corals. The outcrops show an abundance of corals but they did not reveal any measurable samples, as corals are highly altered and no aragonitic mineralogy is preserved.

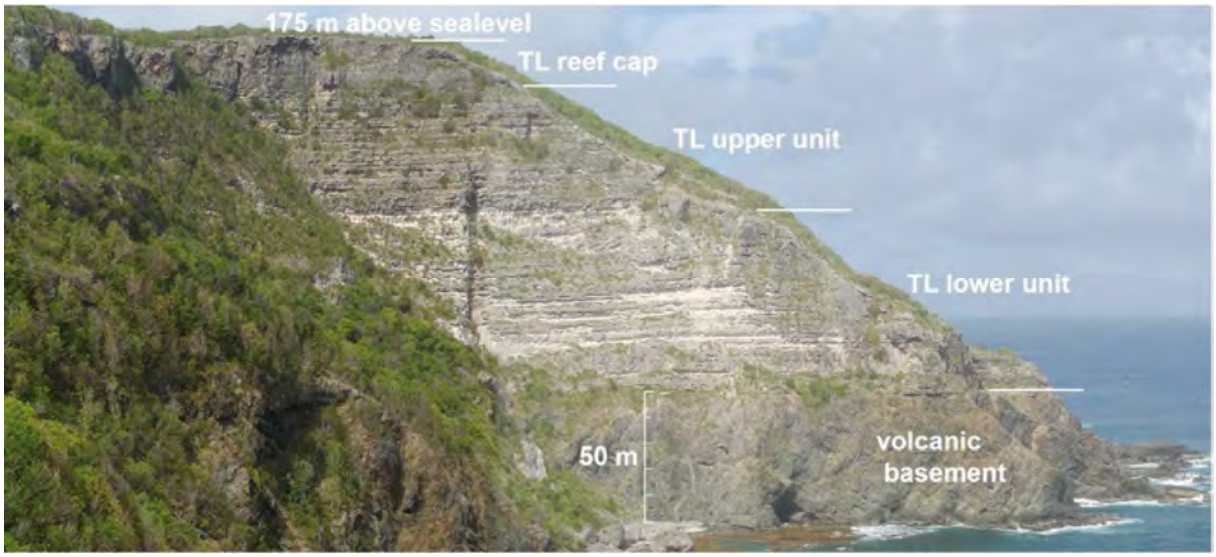

Figure 44: View of Trou Cochon. This locality shows the most complete section of La Désirade, the volcanic basement, the complete Limestone Table and the reef cap can be observed (from Baumgartner-Mora and Baumgartner, 2011).

Location	GPS Coordinates	
Baie Mahault	19°19'43.00 N	61°00'49.00W
RMECH	16°19'49.00 N	61°01'11.10 W
Algae Cluster	16°20'23.50 N	61°01'18.90 W
Station Météo	16°20'06.20 N	61°00'08.00 W
Mountain Road	16°20'06.20N	61°01'18.00 W
Point de vue	16°18'38.00 N	61°03'30.00 W
Beauséjour	16°18'10.00 N	61°04'45.00 W
Ancienne Carrière	16°18'00.00 N	61°05'10.00 W

Table 7: GPS Coordinates of the sampling localities

6.5. Methods

All small samples (e.g. foraminifers, gastropods, corals echinoids, red algae) were first rinsed in pure water in order to wash away all the impurities. The samples were then treated in an ultrasonic bath in order to detach all hard cement on the fossils. If organic matter was present, the samples were washed with H_2O_2. Powders were collected on dry samples with a micro-drill that was cleaned with 10% HCl and ultrapure water between every sampling in order to avoid any contamination.
In order to check the preservation of the samples, the methods presented in Chapter 3 were applied.

6.6. Results

Scanning Electron Microscope

Samples were observed through SEM in order to check the preservation of the fossils. Crystallization of secondary minerals was used as a criterion in order to eliminate a sample for Sr isotope measurements. Presence of Mn or Fe was constrained through EDS analyses. Only samples presenting no apparent secondary minerals were selected. Figure 45 shows bad preservation of fossil samples, on altered echinoderm and a dolomitized foraminifer. This dolomitization might have happened during early diagenesis in mixed meteoric/marine waters. In fact the outcrops of the northern coast of the island are subject to the climatic erosion as it is exposed to winds, rain and seawater spray.
Figure 46 shows the preservation of a recent coral (*Diploria clivosa*) vs. a sample from the Mountain Road used for Sr age determination. No significant differences can be observed. Both pictures show acicular aragonite, which is probably related to an early cementation process in a marine-phreatic environment (Sayani *et al.*, 2012). Because the diagenesis can be characterized as early, the obtained age defining Sr isotope ratios might not vary much from the original marine Sr ratio.

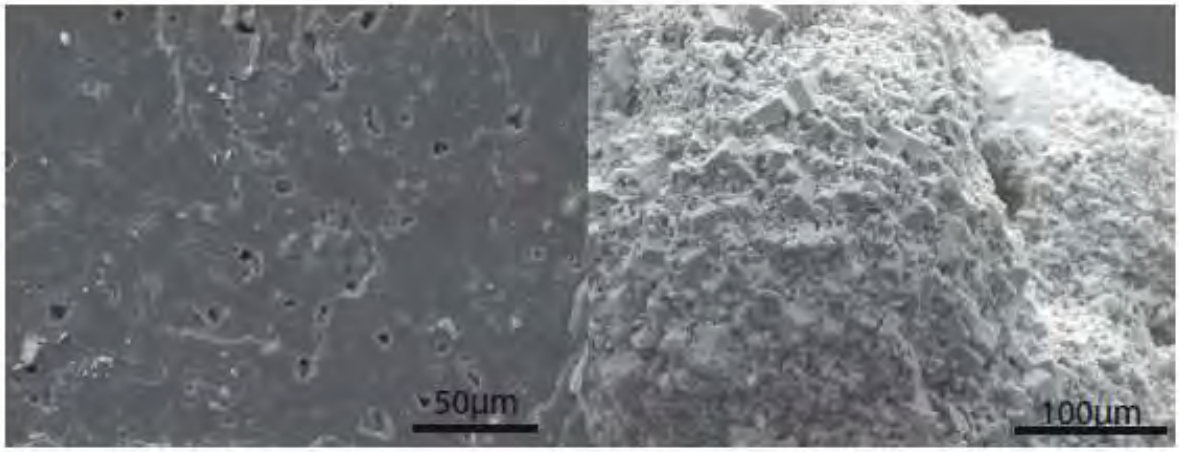

Figure 45: SEM pictures of badly preserved samples. On left, diagenetically altered echinoid shell. On right, completely dolomitized foraminifera shell.

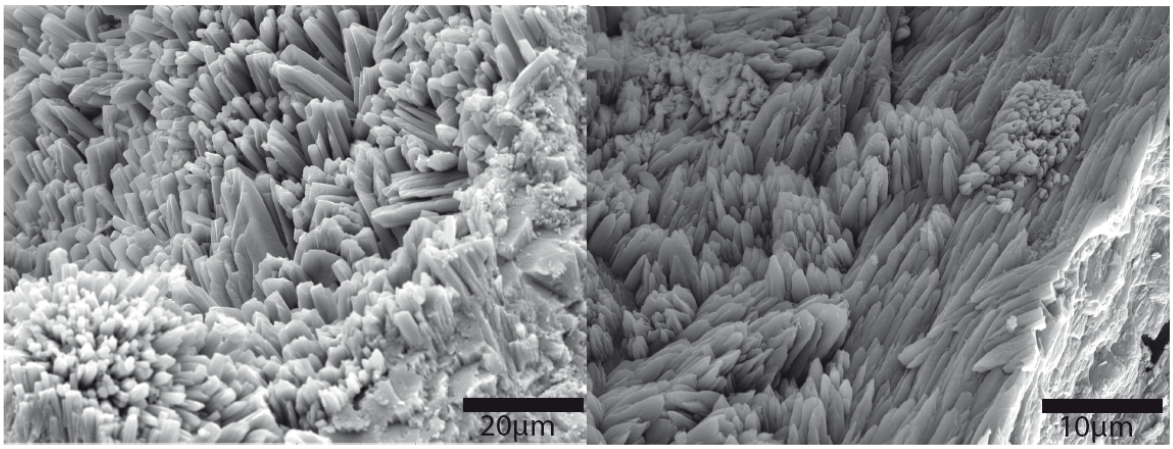

Figure 46: SEM images of coral samples. On left, a recent coral (*Diploria clivosa*). On right a fossil coral selected for Sr isotope measurements. No significant differences can be observed. Both images show acicular aragonite, related to a marine diagenetic environment, (Sayanai *et al.*, 2012; Flügel, 2010).

Stable carbon and oxygen isotope geochemistry

Measurements were made on whole well preserved foraminifera, coral and red algae fragments. For foraminifera samples, the stable isotopes yield values between -0.73‰ and -2.67‰ for oxygen and between -1.04‰ and -4.09‰ for carbon (Table 8, Figure 47). For coral samples, the oxygen isotope composition is in between -1.95‰ and -3.70‰ and carbon isotopic values are between 0.18‰ and 1.29‰ (Table 8, Figure 47). Echinoid samples yielded carbon isotope values between -8.00‰ and -8.50‰ and oxygen isotope compositions of -3.30‰ and -3.50‰. Most of the results appear to be acceptable for the $^{87}Sr/^{86}Sr$ measurements. The echinoid samples show very negative oxygen isotope compositions,

maybe related to diagenetic effects due to its High Magnesium Calcite shell which is more sensitive to dissolution processes (Chapter2).

Sample Name	Description	Locality	Formation	$\delta^{13}C$ ‰ (VPDB)	$\delta^{18}O$ ‰ (VPDB)
BSJI	Bulk Rock	Beauséjour	DOL	-2.7	-0.7
BSJII	Bulk Rock	Beauséjour			
DES025I	Foraminifera	Carrière route de la	LT	-1.42	-2.03
DES025II	Foraminifera	montagne	LT	-3.12	-2.43
DES029I	Foraminifera	Carrière route de la	LT	-4.09	-2.20
DES029II	Foraminifera	montagne	LT	-3.88	-2.67
DES035I	Foraminifera	Point de vue	LT	-2.17	-1.90
DES035II	Foraminifera		LT	-1.04	-0.73
DES035III	Foraminifera		LT		
GrAEI	Red Algae	Grand Abaque	LT	-0.9	1.3
GrAEII	Red Algae		LT		
RM0I	Coral	Mountain Road	Fringing Reef	1.06	-3.69
RM0II	Coral		Fringing Reef	1.19	-3.70
BBMA2I	Coral	Baie Mahault Bay	Fringing Reef	0.26	-1.95
BBMA2II	Coral		Fringing Reef	0.18	-2.15
D4043AII	Beach Rock (Bulk)	Meteorological station		-1.10	-3.60
ECHI	Echinoid	Mountain Road	Fringing Reef?	-8.00	-3.30
ECHII	Echinoid		Fringing Reef?	-8.50	-3.50

Table 8: Stable isotopic composition of the samples from La Désirade. Results are presented according to the geologic origin of the samples.

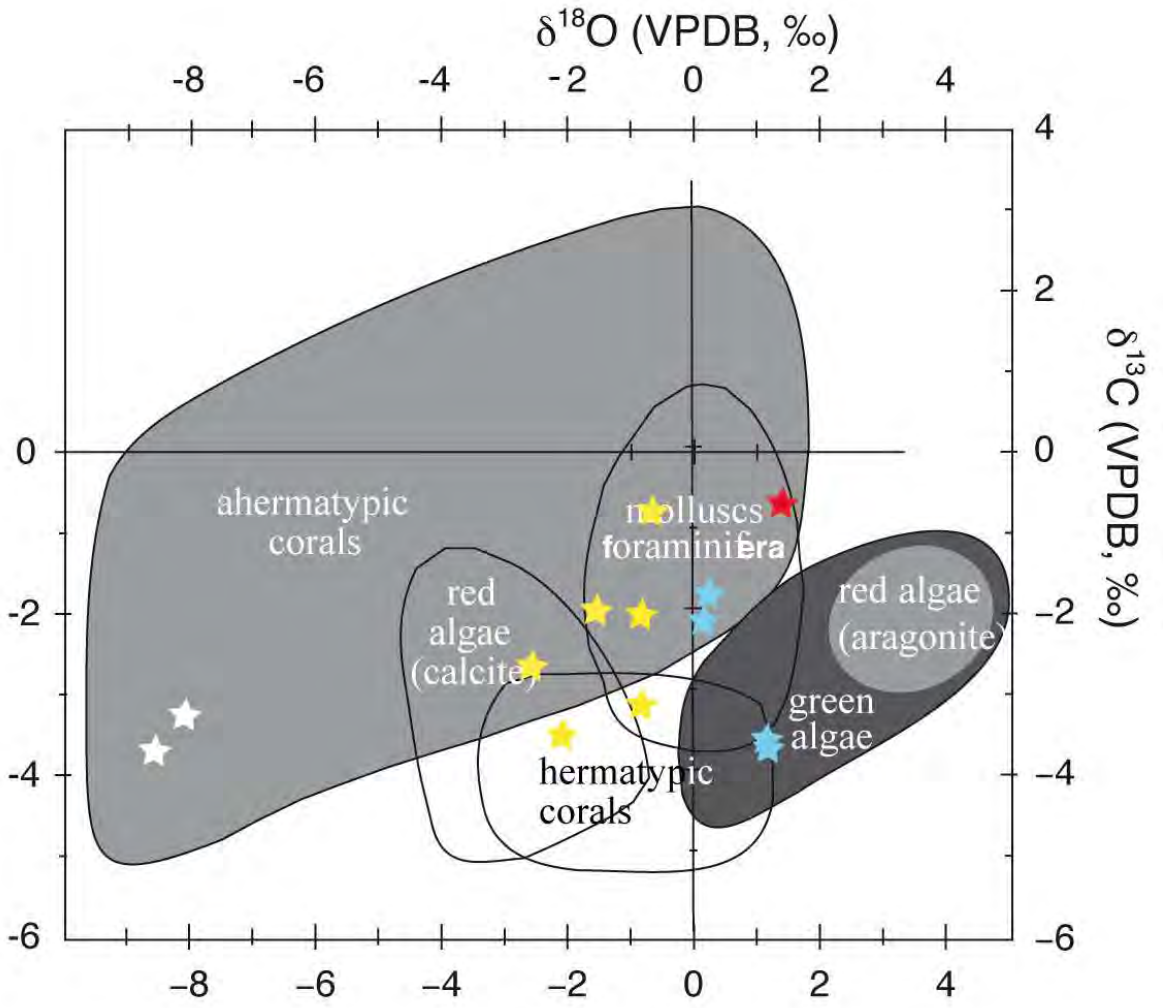

Figure 47: Stable isotopic composition of various groups of calcareous organisms (Swart, 1983 modified), with stable isotopic compositions of the samples used for this study (Yellow stars: Foraminifera, Blue stars: Coral, Red star: red algae, White stars: echinoid).

Cathodoluminescence

Cathodoluminescene on thin sections from the DOL at the "Ancienne Carrière" (sample BSJ) showed that foraminifera shells are largely covered by overgrowth cements (Figure 48). The general luminescence of the thin sections is dull. Furthermore, the internal parts of the shells show secondary cements, which might indicate that this sample has been exposed to fresh water. This sample was measured for Sr isotopes, by micro-drilling the thin section counterpart. Even though we focused on the foraminifera shells that are well preserved a contamination by secondary cements cannot be avoided, hence these $^{87}Sr/^{86}Sr$ results are considered as bulk rock analyses.

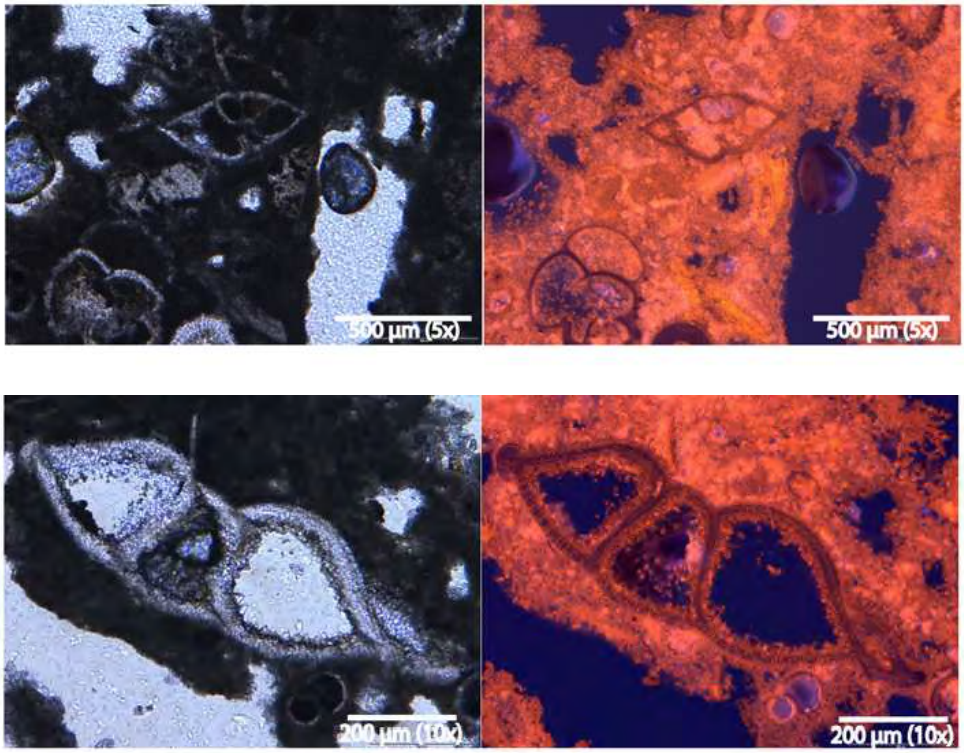

Figure 48: Transmitted light on left vs. cathodoluminescence on right of sample AC-2 from the "Ancienne Carrière". Cathodoluminescence shows a secondary phase on the inside of foraminifera. General appearance of cathodoluminescence pictures show diagenetic alteration and presence of Mn.

$^{87}Sr/^{86}Sr$ Results and ages

All measured $^{87}Sr/^{86}Sr$ ratios range between 0.708992 and 0.709146 with a standard error (S.E.) of 1-3x10^{-6}. The reproducibility of the values is good (Table 9, Figure 49). On a first approach, these ratios correspond to the values that are expected from samples from the Late Neogene according to Howarth and McArthur, (1997) and McArthur *et al.* (2001).

A bulk rock measurement (BSJI & BSJII) analyzed on a single block found in the DOL yield a latest Miocene to early Pliocene age (5.15-5.80 Ma) (Table 9, Figure 49).

In the Limestone Table, two major clusters of $^{87}Sr/^{86}Sr$ can be separated (Table 9, Figure 49). Firstly, the base of the section was dated to a very early Zanclean (early Pliocene) to Zanclean age (5.35-4.05 Ma) (Table 9, Figure 49). Secondly, in the top of the LT $^{87}Sr/^{86}Sr$ indicate a Late Piacenzian to Early Gelasian age (Late Pliocene to Early Pleistocene) (Table 9, Figure 49).

Samples of two fringing reefs and one of beach-rock were measured for $^{87}Sr/^{86}Sr$. The fringing reef on the Mountain Road was dated to a late Calabrian to early Ionian age (0.60-

1.05 Ma) (Table 9, Figure 49). The beach rock at the Meteorological station was dated at an age of 0.27-0.55 Ma (Table 9, Figure 49). Another reef at the Baie Mahault bay was dated at an age of 0-0.36 Ma.

The echinoid samples (RMECHI and RMECHII) yielded two strontium isotope ratios of 0.708992 and 0.709107. This intra-sample heterogeneity does not allow concluding reliable strontium isotope ages.

Sample Name	Type	Locality	Formation	$^{87}Sr/^{86}Sr$	2 S.E.	Age (Ma)
BSJI	Bulk Rock	Beauséjour	DOL	0.709013	0.000004	5.50-5.80
BSJII	Bulk Rock	Beauséjour	DOL	0.709025	0.000004	5.15-5.55
DES025I	Foraminifera	Carrière route de la montagne	LT	0.709076	0.000002	2.15-2.45
DES025II	Foraminifera		LT	0.709075	0.000004	2.35-2.55
DES029I	Foraminifera	Carrière route de la montagne	LT	0.709067	0.000004	2.40-2.95
DES029II	Foraminifera		LT	0.709075	0.000006	2.05-2.65
DES035I	Foraminifera	Point de vue	LT	0.709047	0.000004	4.05-4.85
DES035II	Foraminifera		LT	0.709047	0.000004	4.05-4.85
DES035III	Foraminifera		LT	0.709047	0.000004	4.05-4.85
GrAEI	Algae Cluster	Grand Abaque	LT	0.709031	0.000004	4.95-5.35
GrAEII	Algae Cluster		LT	0.709030	0.000004	5.00-5.30
RM0I	Coral	Mountain Road	Fringing Reef	0.709144	0.000008	0.6-1.05
RM0II	Coral		Fringing Reef	0.709146	0.000006	0.65-1.0
BBMA2I	Coral	Baie Mahault Bay	Fringing Reef	0.709170	0.000004	0-0.36
BBMA2II	Coral		Fringing Reef	0.709175	0.000006	0-0.3
D4043AII	Coral	Meteorological station	Beach Rock	0.709163	0.000004	0.27-0.55
RMECHI	Echinoid	Mountain Road	Fringing Reef	0.708992	0.000004	5.95-6.15
RMECHII	Echinoid		Fringing Reef	0.709107	0.000006	1.30-1.60

Table 9: $^{87}Sr/^{86}Sr$ ratios of the studied samples, with their locality and belonging formation. and their according ages ranges after Howarth and McArthur, 1997; McArthur et al., 2001.

Figure 49: Strontium isotope results plotted on LOWESS curve after Howarth and McArthur, 1997; McArthur *et al.*, 2001. Age clusters for the Upper and Early Limestone Table can be observed. Samples from the base of the Limestone table appear to be early Pliocene in age and samples the top of the Limestone table cluster in the very Late Pliocene - early Pleistocene. Fringing reefs are also presented on this curve.

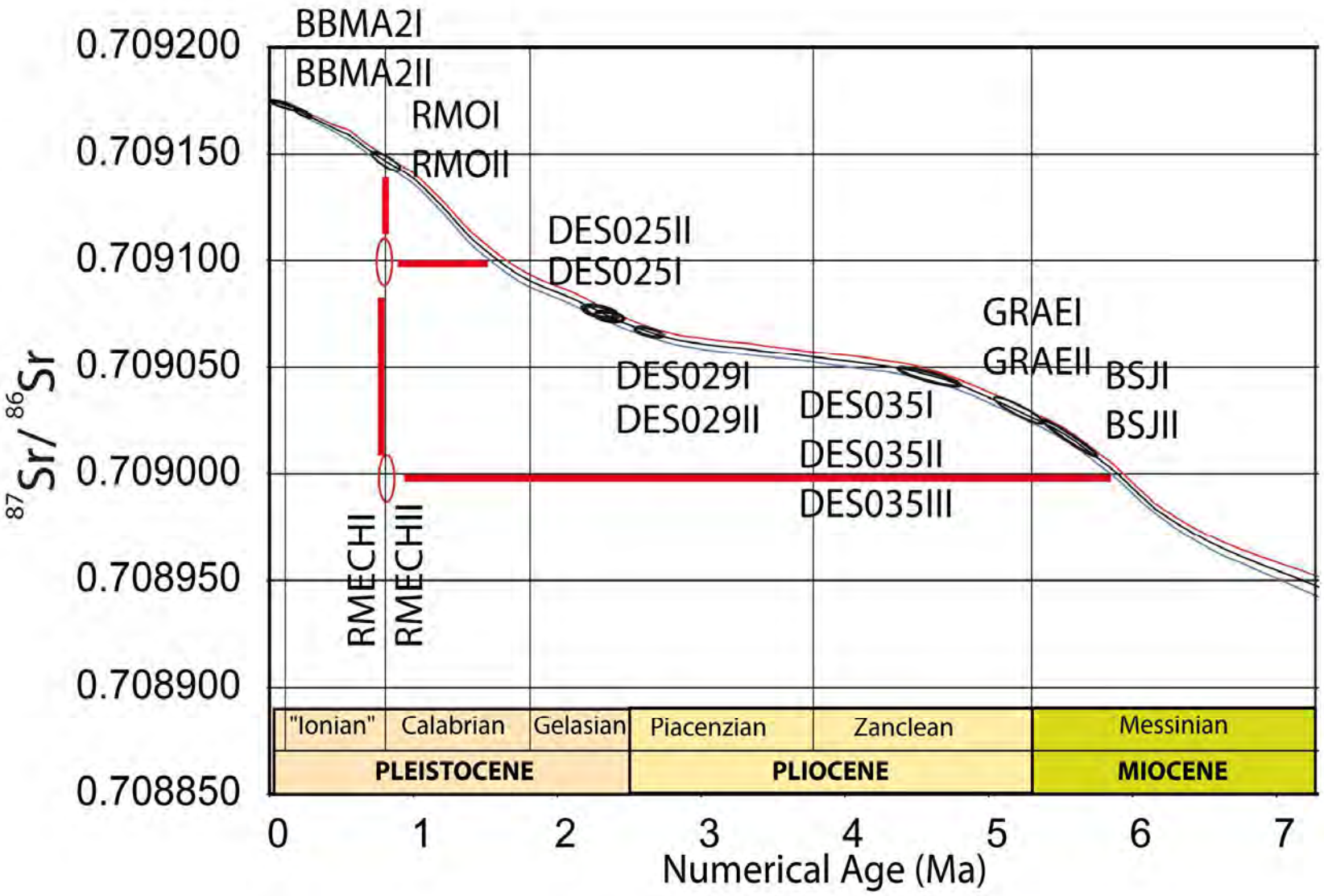

6.7. Discussion

Screening

Results from the screening methods show that the samples underwent no or just slight alteration and only minor diagenetic processes are epxected. This is comforted by the stable carbon and oxygen isotope geochemistry and the different results obtained by SEM and cathodoluminescence microscopy. Consequently, the $^{87}Sr/^{86}Sr$ ratio may be biased by this alteration but the variations may be considered as negligible.

In a general context, the dissolution-precipitation process may not vary the ratios significantly. The $^{87}Sr/^{86}Sr$ ratio of carbonates that are dissolved is incorporated during the reprecipitation process. The ratio may not vary significantly because of the very close ages of the surrounding sediments (McArthur, 1998). Furthermore the foraminifera that are present in the sediments show ages similar to the ages obtained by $^{87}Sr/^{86}Sr$.

No clear stratigraphic indications of ash layers were observed in the field. As explained in Chapter 2, their presence should considerably shift the Sr isotope ratio towards lower values.

In order to avoid contaminated samples, caution was given during the sampling. Furthermore, the screening of the samples prior to the strontium isotope ratio measurements has clarified this problem. Any sample showing the presence of dolomite was discarded for further analyses.

Detrital Offshore Limestone

A bulk rock $^{87}Sr/^{86}Sr$ measurement (BSJI & BSJII) done in a single block from the DOL yields a latest Miocene to early Pliocene age (5.15-5.80 Ma). We determined the presence of, *Globorotalia limbata*, *Globorotalia multicamerata*, *Globorotalia menardii s.l.*, *Globigerinoides sacculifer* and members of the *Globorotalia menardii* group in this sample. This assemblage indicates a rather imprecise interval from Late Miocene to Pliocene, which is in agreement with the Sr dating. In addition, the latest Miocene to early Pliocene age determined by (Baumgartner-Mora & Baumgartner, 2011) in the Ancienne Carrière corresponds well with our data. The latter constrain the planktonic foraminifera to the latest

Miocene/early Pliocene (lower zone N19), because of the presence of *Sphaeroidinella dehiscens, Globorotalia plesiotumida* and *Globoroatia merotumida* (dating based on the work of Wade *et al*. (2011)). This would be the oldest sample we dated on La Désirade and confirms the ages given to the DOL by Baumgartner-Mora & Baumgartner, 2011.

The Limestone Table

A rhodolite (GrAE) from the Grand Abaque was dated as very Early Zanclean (Early Pliocene), (4.95-5.35 Ma). This sample is located just few meters above the contact with the basal conglomerate and might so date the very beginning of the sedimentation of the LT.
A sample from the "Point de vue" (DES035) yielded a Zanclean (Early Pliocene) age, ranging from 4.05 - 4.85 Ma. This outcrop is located around 20 m above the contact with the basement.
Measurements done on foraminifera (DES025, DES029) from the Mountain Road quarry, yielded ages ranging from 2.05 - 2.95 Ma, which corresponds to an Upper Piacenzian (Upper Pliocene) to Gelasian (Early Pleistocene) age.
The echinoid samples (RMECHI and RMECHII) have strontium ages of about 1.30-1.60 Ma and 5.95-6.15 Ma. This can be interpreted in two different ways. The samples' ages do not correspond to the age of other samples taken in this location, the sample is diagenetically altered and the age resulting from the strontium isotope ratios cannot be used. Another interpretation would be to consider this samples age as reliable. The sample was collected from a loose limestone, below the contact between the conglomerate and the lower limestone table. This sample could therefore show the age of the beginning of the sedimentation of the limestone table on the eastern part of La Désirade. However, carbon and oxygen stable isotope composition showed the sample underwent a diagenetic process. The strontium isotope results of these samples should therefore not be considered in the final age model.
All samples measured for the Limestone Table, give a good age resolution good indications about the general age range. The difficulty lies in the fact that normal faults separate the Island into 4 blocks. Consequently, samples were selected carefully in order to avoid the dating of two identical layers. In the field, it is difficult to find indications on the exact stratigraphic position, except the elevation above the conglomerate and the distance to the top of the island. The top of the Limestone Table, namely the reef cap has not been dated by strontium isotope ratios, coral samples seemed highly altered and were therefore not sampled.

Fringing reefs

Mountain Road

On the Mountain Road (Figure 49, Table 9) a major reef, at a level of about 70 m, has been dated to a late Calabrian to early Ionian age (0.60-1.05Ma) (sample RMO).

"Station météorologique"

We also dated a Late Pleistocene corals (D4043A) near the "Station Meteorologique" (0.27-0.55 Ma) (Figure 49, Table 9). These corals are reworked in a beach rock like outcrop that is today about 20m above the sea level. The ages may then give at oldest, the real ages of the corals and at youngest the formation of the beach rock. As beach rocks are quickly formed in intra-tidal and/or vadose environment the obtained age may then not vary significantly. The beach rock was probably formed during the MIS-11, when the sea level was high and close to the present one (Bowen, 2010, Waelbroeck, 2002).

Baie Mahault

The reef at the east part of Baie Mahault Bay (BBMA), (Figure 49, Table 9) revealed an age of 0.00-0.36 Ma. This age probably corresponds to the Eemian interglacial event where the sea-level was 4-6m above present levels (Overpeck *et al.*, 2006; Feuillet *et al.*, 2004).

Interpretation

The paleontological ages determined by Baumgartner-Mora & Baumgartner, (2001) indicate the approximate age ranges for $^{87}Sr/^{86}Sr$. Most of the presented results can, by comparing, be assumed as reliable ages as the Sr ages are in the foraminifera's interval ages.
Our results show various interesting age data on the studied carbonate layers. We can clearly couple our $^{87}Sr/^{86}Sr$ results with the biostratigraphic ages of ours samples. Foraminiferal assemblages (Baumgartner-Mora, 2011) showed a late Miocene to Early Pliocene age of samples of the Ancienne Carrière. $^{87}Sr/^{86}Sr$ ages of samples from the same layers show a

latest Miocene to earliest Pliocene age as well. We would like to point out the possibility of a Late Miocene sedimentation which can accord to the emplacement of carbonate platforms in the fore-arc setting on the top of a ancient (Oligo? - Miocene) abandoned arc mentioned by Bouysse *et al.*, (1990).

Cornée *et al.*, 2011, describe Grande Terre and/or Marie-Galant to be source of the carbonates of the DOL at Ancienne Carrière The timing of these sedimentary events should be post-Miocene, as some debris with a late Miocene age (BSJI and BSJII) have been observed within the Detrital Offshore Limestone on the field. This idea can even more be explained by the sedimentary onlaps of dunes (Cornée *et al.*, 2011) showing the presence of the limestone table was prior to the sedimentation of the DOL, especially in Ancienne Carrière.

The $^{87}Sr/^{86}Sr$ ages of the Limestone table fit stratigraphically even if on some places very big gaps in ages are observed, this is for two main reasons. The first one is the accessibility of the outcrops on the field and the second one is the glacio-eustatic sea level variations that have a big impact on the sedimentary record. As facies do not vary significantly, sedimentary structures show wave influenced and tidal environments, and sea level falls may erode some parts, it is sometimes impossible to observe an erosional surface, which may mislead us as we may wrongly conclude on a continuous sedimentation.

Tectonic history of La Désirade Island

The combination of the $^{87}Sr/^{86}Sr$ results of the fringing reefs allows constraining the Neogene tectonics of the island. The sea-level curve and data used from Miller et al., (2005) provide a complete sea level curve for our time interval and so, make conclusions on the tectonic uplift of La Désirade (Figure 50).

The three dated outcrops that can help solving this problem are the Baie Mahault reef, the beach-rook at the "Station Météorologique" and the Mountain Road reef (Figure 41). Their actual positions above the recent sea level are +6m, +20m and +70m respectively (Figure 50).

The emplacement of these reefs is believed to have occurred during sea level high stands. If the emplacement took place during low stands, the lowest reefs would still be immerged.

At the Baie Mahault, a reef outcrops at around 2 to 6 m above present sea-level. The ages measured on coral samples range from 0.00 - 0.36 Ma. According to Feuillet et al. (2004), these reefs have an Eemian age, which goes along with our Sr isotope age. As the sea-level

was 4-6m above present levels (Overpeck et al., 2006) during Eemian times, this would mean that there has been a maximal uplift rate of ~0-3.2 cm/ky. Feuillet et al. (2004) mentions Eemian reefal terraces on la Désirade that reach from 2m up to 9m above the present sea level. This would imply an uplift rate (considering La Désirade is still uplifted) of ~ 0-5.6 cm/ky. The data of Battistini et al. (1986) suggest a same uplift rate (Figure 50).

The late Pleistocene beachrock (0.27-0.55 Ma; when sea level was close to recent sea level), dated at the "Station Météorologique", at an altitude of approximately 20 m, imply a tectonic uplift rate of ~ 4.1-5.7 cm/ky. If considering only the MIS-11 highstand, it would suggest a rate of ~5cm/ky.

The reef of the Mountain Road yielding an age of 0.60-1.05 Ma, is today located at an altitude of approximately 70 m. According to the estimated sea-levels of Miller et al. (2005), a +25 m around 0.945 Ma marks the highstand during this 0.60-1.05 Ma time period. This suggests a calculated uplift of ~5 cm/ky (Figure 50).

The presented results led us to conclude that the uplift rate should average around 5cm/ky, assuming a constant and still ongoing uplift of La Désirade. The differences of the elevations of the Eemian reefs can be explained by original submarine relief and/or by differential uplift of fault blocks (Figure 41). Depending on which block these reefs are observed, their relative altitude may differ (Figure 41, Figure 50).

La Désriade basement was uplifted close to the sea surface in a wave dominated environment. Sea level oscillated around a long-term constant level from 10 Ma to 7 Ma; we consider this the period the abrasion of the basement took place, becoming the flat regular surface it is today. Big boulders, which can be observed in the conglomerate, were formed at that time (Baumgartner-Mora and Baumgartner, 2011). In a second phase, the volcanic basement had to undergo a major subsidence prior to the uplift in order to provide accommodation space to the carbonate sediments (Figure 50).

The oldest sediments dated on La Désirade were sampled just a few meters above the limit between the LT and the conglomerate yielded an age of 4.95 Ma - 5.35 (Figure **49**, Figure 50, Table 9).

This date may define the beginning of the subsidence of La Désirade basement. The uplift of La Désirade has then probably started around 2.2 Ma, while the basement had reached a depth

of 80-100 m below sea level. We dated sediments of the summit of the LT to an age of 2.25 Ma - 2.7 Ma, which correlates well the approximate timing of the tectonic emersion of La Désirade (Figure 49, Figure 50, Table 9).

The reef cap above the LT could not be dated through a conventional method but after this model, the formation of the reef cap might have occurred during a 2.0 -2.25 Ma time period (early Pleistocene), during the last major highstand (Figure 49, Figure 50, Table 9).

The obtained values are in accordance with the uplift derived by the data of Battistini *et al.* (1986), who also dated Eemian reefs. However, the uplift rates are approximately 10 times inferior to the uplift rates given by Feuillet *et al.* (2004) for Marie-Galante, Grande Terre and La Désirade. Feuillet *et al.* (2004) consider a major westward tilting of the Guadeloupe archipelago. They deduct the uplift rates by correlations of various fringing reefs and reefs on Marie-Galante, Grande-Terre and La Désirade. They therefore conclude, by reef composition analogy, that the reef cap of La Désirade emerged at approximately 300 ky to be uplifted to an altitude of 276m. Even if coral assemblages are the same, the frequent glacio-eustatic sea-level variations make it impossible to clearly correlate reefs by their assemblage. Furthermore, the reef cap is not present at the highest point of La Désirade. In fact, the reef cap is only present in the easternmost part of La Désirade at elevations that of around 170m. Finally, La Désirade and Basse-Terre, even if very close to each other have probably had a different tectonic history. Also, the presence of numerous faults in this region would probably not allow a general linear westward tilting.

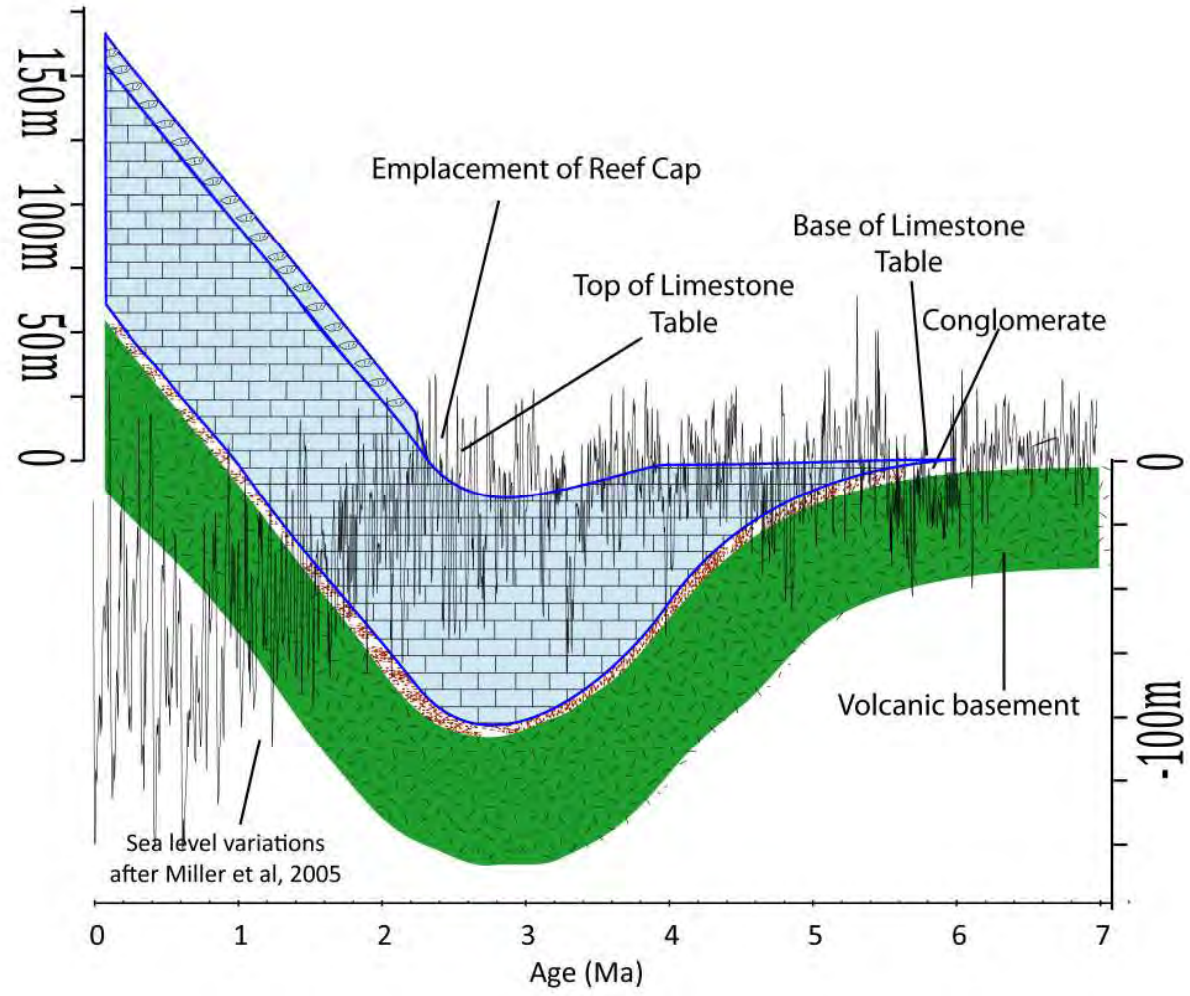

Figure 50: Subsidence/uplift path of La Désirade according to the data of this work, combined with the sea-level curve of Miller *et al.*, 2005. The volcanic basement may have been eroded during an average stable marine sea level. In order to create the accommodation space for the sedimentation of the carbonates, the basement must have undergone a subsidence, which has been followed by a major tectonic uplift. Light blue lines define the limits between the various facies limits. The uplift rate has been considered as constant at 5 cm/ky.

6.8. **Conclusion**

Through this study, it has been possible to date the ages of the Limestone Table. Age ranges from very Early Pliocene to Pleistocene were defined, which helped in solving the remaining questions on the sedimentology of shallow water carbonates of La Désirade.

The age assignments given by the $^{87}Sr/^{86}Sr$ ratios allow determining a tectonic path of La Désirade Island, which shows that a subsidence prior to the uplift that raised the island to its actual position had to occur in order to have enough accommodation space for the sediments. Average uplift rates of 5cm/ky have been determined through the dating of samples from different localities of La Désirade.

6.9. References

Andreieff, P., **1987**. Géologie de L'arc insulaire des Petites Antilles, et evolution Géodynamique de l'Est-Caraïbe. Thèse de Doctorat D'Etat ès Sciences, pp. 1-359.

Bailey, T.R., McArthur, J.M., Prince, H., and Thirwall, M.F., **2000**. Dissolution methods for strontium isotope stratigraphy: whole rock analysis. Chemical Geology 167 pp. 313-319.

Banner, J.L., **2004**. Radiogenic isotopes: systematics and applications to earth surface processes and chemical stratigraphy. Earth-Science Reviews 65, pp. 141-194.

Barrabé, F., Andreieff, P., 1984. Sedimentation et tectonique plio-quaternaires compares de Marie Galante et de Grande Terre (Goudeloupe): Géodynamique in principaux résultats scientifiques et techniques du BRGM, p.97.

Battistini, R., F. Hinschberger, C. T. Hoang, and M. Petit **1986**. La basse Terrasse corallienne (Ee´mien) de la Guadeloupe: Morphologie, datation $^{230}Th/^{234}U$, néotectonique, Revue de Géoomorphologie Dynamique, 35, p. 1 – 10.

Baumgartner-Mora, C., Baumgartner, P.O., **1994**. Shell structure of fossil foraminifera studied by cathodoluminescence. European Microscopy and analysis, issue 28.

Baumgartner-Mora, C., Baumgartner, P.O., **2011**. Latest Miocene-Pliocene Larger Foraminifera and depositional environments of the carbonate bank of La Désirade Island, Guadeloupe (French Antilles). Revue de micropaléontologie, 54, p.183-205.

Boggs, S., Krinsley, D., **2006**. Application of cathodoluminescence imaging to the study of sedimentary rocks. Cambridge University Press. 177 p.

Bouysse, P., Westercamp, D., **1988**. Effets de la subduction de rides océaniques sur l'évolution d'un arc insulaire : l'exemple des Petites Antilles. Geologie de la France 2/3, p. 3–38.

Bouysse, P., Westercamp, D., **1990**. Subduction of Atlantic aseismic ridges and Late Cenozoic evolution of the Lesser Antilles island arc. Tectonophysics 175, p. 349–390.

Bowen, D.Q., **2010**. Sea level 400 000 years ago (MIS 11): analogue for present and future sea-level?, Climate of the Past, 6, pp. 19-29.

Burke, W.H., Denison, R.E., Hetherington, E.A., Koepnick, R.B., Nelson, H.F., and Otto, J.B., **1982**. Variation of 87Sr/86Sr throughout Phanerozoic time. Geology 10, pp. 516–519.

Cornée, J.-J., Corsini, M., Lardeaux, J.-M. and Münch, P., **2011**. La Désirade Excursion. In: 19th Caribbean Geological Conference, Le Gosier, 21-26 March 2011, Guadeloupe,

26 pp.

DePaolo, D.J. and Ingram, B.L., **1985**. High-Resolution stratigraphy with Strontium isotopes. Science 227, pp. 938-941.

Elderfield, H., **1986**. Strontium isotope stratigraphy. Palaeogeography, Palaeoclimatology, Palaeoecology 57, pp. 71–90.

Evain, M., Galve, A., Charvis, P., Laigle, M., Kopp, H., Bécel, A., Gallart, J., **2011**. Structure of the Lesser Antilles subduction forearc and backstop from 3D seismic refraction tomography. Tectonophysics.

Farrell J.W., Clemens S.C., Gromet L.P., **1995**. Improved chronostratigraphic reference curve of Neogene seawater $^{87}Sr/^{86}Sr$. Geology v. 23, no.5; p. 403-406.

Fink, L.K., 1970. Field guide to the island of La Desirade with notes on the regional history and development of the Lesser Antilles island arc. International Field Institute Guidebook to the Caribbean Island-Arc System, 287-302.

Feuillet, N., Tapponnier, P., Manighetti, I., Villemant, B., King, G.C.P., **2004**. Differential uplift and tilt of pleistocene reef platforms and quaternary slip rate on the Morne-Piton normal fault (Guadeloupe, French West Indies). J. Geophys. Res., 109, BO2404.

Frijia, G. and Parente, M., **2008**. Strontium isotope stratigraphy in the upper Cenomanian shallow-water carbonates of the southern Apennines: Short-term perturbations of marine $^{87}Sr/^{86}Sr$ during the oceanic anoxic event 2. Palaeogeography, Palaeoclimatology, Palaeoecology 261, pp. 15-29.

Gill, I., Olson, J.J., Hubbard, D.K., **1995**. Corals, paleotemperature records, and the aragonite-calcite transformation. Geology, 23, pp. 333-336.

Hochard, C., Vérard, C. and Baumgartner, P.O., **2011**. Geodynamic evolution of the Earth over 600 Ma: implications for palaeo-climatic indicators. American Geophysical Union Fall Meeting (AGU), San Francisco, California, December 5–9, 2011.

Hodell, D.A., Benson, R.H., Kennett, J.P., Bied, K.R. E., **1989a**. Stable isotope stratigraphy of latest Miocene sequences in northwest Morocco: the Bou Regreg section. Paleoceanography 4, p. 467–482.

Hodell, D.A., McKenzie, J.A., Mead, G.A., **1989b**. Strontium isotope stratigraphy and geochemistry of the late Neogene ocean. Earth Planet. Sci. Lett. 92, p. 165–178.

Hodell, D.A., Mueller, P.A., Garrido, J.R., **1991**. Variations in the strontium isotopic composition of seawater during the Neogene. Geology 19, p. 24–27.

Hodell, D.A., Benson, R.H., Kent, D.V., Boersma, A., Bied, K.R.-E., **1994**. Magnetostratigraphic, biostratigraphic, and stable isotope stratigraphy of an Upper

Miocene drill core from the Salé Briqueterie (northwest Morocco): a high-resolution chronology for the Messinian stage. Paleoceanography 9, p. 835–855.

Howarth, R.J., and McArthur, J.M., **1997**. Statistics for strontium isotope stratigraphy. A robust LOWESS fit to the marine Sr-isotope curve for 0 - 206 Ma, with look-up table for the derivation of numerical age. Journal of Geology, 105, pp. 441-456.

Kindler, P., Godefroid, F., Chiaradia, M., Ehlert, C., Eisenhauer, A., Frank, M., Hasler, C.-A., Samankassou, E., **2011**. Discovery of Miocene to lower Pleistocene deposits on Mayaguana, Bahamas: evidence for recent active tectonism on the North American margin. Geology, v. 39/6, 523-526.

Marshall, D. J., **1988**. Cathodoluminescence of Geological Materials, Boston, Unwin Hyman.

McArthur, J.M., Kennedy, W.J., Chen, M., Thirlwall, M.F., and Gale, A.S., **1994**. Strontium isotope stratigraphy for Late Cretaceous time: Direct numerical calibration of the Sr isotope curve based on the US Western Interior. Palaeogeography, Palaeoclimatology, Palaeoecology, 108, pp. 95-119.

McArthur, J.M., **1998**. Strontium Isotope Stratigraphy. Unlocking the Stratigraphical Record: Advances in Modern Stratigraphy. Edited by P. Doyle and M.R. Bennet. John Wiley & Sons Ltd, Chapter 8.

McArthur, J.M., Howarth, R.J., Bailey, T.R., **2001**. Strontium isotope stratigraphy: LOWESS version 3: best fit to the marine Sr-isotope curve for 0–509 Ma and accompanying look-up table for deriving numerical age. J. Geol. 109, p. 155-170.

McArthur, J.M. & Howarth, R.G., 2004. A Geologic Time Scale **2004**, eds. Felix M. Gradstein, James G. Ogg, and Alan G. Smith. Cambridge University Press, p. 96-105.

McArthur, J.M., Rio D., Massari, F., Castradori, D., Bailey, T.R., Thirlwall, M., Houghton, S., **2006**. A revised Pliocene record for marine-$^{87}Sr/^{86}Sr$ used to date an interglacial event recorded in the Cockburn Island Formation, Antarctic Peninsula. Paleogeography, Plaeoclimatology, Paleoecology 242, p. 126-136.

McKenzie, J.A., Hodell, D.A., Mueller, P.A., Muller, D.W., **1988**. Application of strontium isotopes to late Miocene–early Pliocene stratigraphy. Geology 16, p. 1022–1025.

Miller K.G., Kominz, M.A., Browning J.V., Wright J.D., Mountain G.S., Katz M.E., Sugarman P.J., Cramer, B.S., Christie-Blick N., Pekar, S.F., **2005**. The Phanerozoic Record of Global Sea-Level Change. Science 310, pp. 1293-1298.

Münch, P., Melinte, M., Quillévéré, F., Verati, C., Cornée, J-J., Lebrun, J-F., De Min, L., Demory, F., Randriansolo, A., Léticée, J., Marié, L., **2011**.Tectonostratigraphy of the

Pliocene-Pleistocene carbonate platforms of the Guadeloupe Archipelago, Lesser Antilles fore-arc. Abstract, 19ème Confórence Géologique de la Caraïbe.

Overpeck, J.T., Otto-Bliesner, B.L., Miller, G.H., Muhs, D.R., Alley, R.B., Kiehl, J.T., **2006**. Paleoclimatic Evidence for Future Ice-Sheet Instability and Rapid Sea-Level Rise. Science, 311, pp. 1747-1750.

Prokoph, A., Shields, G.A., and Veizer, J., **2008**. Compilation and time-series analyses of a marine carbonate $\delta^{18}O$, $\delta^{13}C$, $^{87}Sr/^{86}Sr$ and $\delta^{34}S$ database through Earth history. Earth-Science Reviews 87, pp. 113-133.

Richter, D. K., Th. Götte, J. Götze, and R. D. Neuser, **2003**. Progress in application of cathodoluminescence (CL) in sedimentary petrology. Mineralogy and Petrology, 79, pp. 127–66.

Sayani, H. R., Cobb, K. M., Cohen, A. L., Crawford Elliot, W., Nurhati, I. S., Dunbar, R. B., Rose, K. A., Zaunbrecher, L. K., **2012**. Effects of diagenesis on paleoclimate reconstructions from modern and young fossil corals. Geochimica et Geocosmica Acta, 75, pp. 6361-6373.

Singh, S.K., Triverdi J.R., Pande, K., Ramesh, R., and Krishnaswami, S., **1998**. Chemical and Strontium, Oxygen, and Carbon Isotopic Compositions of Carbonates from the Lesser Himalaya: Implications to the Strontium Isotope Composition of the Source Waters of the Ganga, Ghaghara, and the Indus Rivers. Geochimica et Cosmochimica Acta, 62, pp. 743-755.

Smalley, P.C., Higgins, A.C., Howarth, R.J., Nicholson, H., Jones, C.E., Swinburne, N.H.M., and Bessa, J., **1994**. Seawater Sr isotope variations through time: a procedure for constructing a reference curve to date and correlate marine sedimentary rocks. Geology 22, pp. 431– 434.

Spötl, C., Vennemann, T., **2003**. Continuous-flow isotope ratio mass spectrometric analysis of carbonate minerals. Rapid Communications in Mass Spectrometry, 17, p. 1004-1006.

Swart, P.K., **1983**. Carbon and Oxygen Isotope Fractionation in Scleractinian Corals: A review. Earth-Science Reviews, 19, pp.51-80.

Vahrenkamp, V.C., Swart, P.K., and Ruiz, J., **1988**, Constraints and interpretations of $^{87}Sr/^{86}Sr$ ratios in Cenozoic dolomites, Geophysical Research Letters, 15, p. 385-388.

Vasiliev, I., Reichart, G.-J., Davies, G.R., Krijgsman, W., Stoica, M., **2010**. Strontium isotope ratios of the Eastern Paratethys during the Mio-Pliocene transition; Implications for interbasinal connectivity. Earth and Planetary Science Letters, 292, pp. 123–131.

Veizer, J., Buhl, D., Diener, A., Ebneth, S., Podlaha, O.G., Bruckschen, P., Jasper, T., Korte,

C., Schaaf, M., Ala, D., and Azmy, K., **1997**. Strontium isotope stratigraphy: potential resolution and event correlation. Palaeogeography, Palaeoclimatology, Palaeoecology, 132, pp. 65–77.

Veizer, J., Ala, D., Azmy, K., Bruckschen, P., Buhl, D., Bruhn, F., Carden, G.A.F., Diener, A., Ebneth, S., Goddéris, Y., Jasper, T., Korte, C., Pawellek, F., Podlaha, O.G., Strauss, H., **1999**. $^{87}Sr/^{86}Sr$, $\delta^{13}C$ and $\delta^{18}O$ evolution of Phanerozoic seawater. Chemical Geology 161, pp. 59-88.

Vérard, C., Hochard, C. and Baumgartner, P., **2011**. Geodynamic evolution of the Earth over 600 Ma: palaeo- topography & -bathymetry (from 2D to 3D). American Geophysical Union Fall Meeting, (AGU), San Francisco, California, December 5-9, 2011.

Wade, B.S., Pearson, P.N., Berggren, W.A. and Pälike, H., **2011**. Review and revision of Cenozoic tropical planktonic foraminiferal biostratigraphy and calibration to the geomagnetic polarity and astronomical time scale: Earth Science Reviews, v. 104, p. 111-142.

Waelbroeck, C., Labeyrie, L., Michel, E., Duplessy, J.C., McManus, J.F., Lambeck, K., Balbon, E., Labracherie, M., **2002**. Sea-level and deep water temperature changes derived from benthic foraminifera isotopic records, Quaternary Science Reviews, 21, pp. 295–305.

Werner, R., Hoernle, K., Hauff, F., (Eds.) **2010**. Meteor-Berichte 11-8, CLIP - Origin of the Caribbean Large Igneous Province (CLIP) in connection with the geodynamic evolution of the Central Caribbean.

Westercamp, D., **1980**. La Désirade, carte géologique à 1:25 000 et notice explicative. In: Service géologique national. Bureau de Recherche Géologique et Minière, Orléans, France.

Westercamp, D., Andreieff, P., Bouysse, P., Mascle, A., Baudron, J.C., **1985**. Géologie de l'Archipel des Grenadines. Documents du Bureau de Recherche Géologique et Minière 92, p. 1–197.

7. General Conclusions

In Chapter 4 ($^{87}Sr/^{86}Sr$ analyses in Upper Cretaceous Formations of the Nicoya Peninsula North-Western Costa Rica, it was possible to:

- Assign additional age constrains on the Piedras Blancas and Quebrada Pavas Formations
- Extend the age of the base of the Nambi Formation
- Show that even if the screening results might sometimes be "bad", the measured strontium isotope ratio can indicate a correct age
- Confirm ages of radiolarian assemblages, even though these ages are not representative for a radiolarian biozone

In Chapter 5 ($^{87}Sr/^{86}Sr$ study of shallow water carbonates from the Hess Rise, Caribbean Sea) it was possible to:

- Date the shallow water carbonates of the Hess Rise to a Rupelian and Chattian age
- Give a possible age of the beginning of the subsidence in the northern Hess Rise

In Chapter 6 ($^{87}Sr/^{86}Sr$ data from La Désirade, Guadeloupe France) it was possible to:

- Date precisely the sediments of the Limestone Table with strontium isotopes
- Date two different fringing reefs and a beach rock with strontium isotopes
- Based on the strontium isotope results, suggest a new subsidence/uplift history of La Désirade Island

The results obtained through this PhD Thesis show that strontium isotope dating is a powerful asset for carbonate rock and fossil dating. The revealed strontium isotope results permit to have a better understanding of the sedimentary and tectonic evolution of geologically complex situations.
During this thesis, where sediments of different facies, type and age were studied, the limits of strontium isotope dating have been reached. This is related to the fact of not having

complete sections that are dated with SIS, and therefore, samples are sparse. The only control of ages is the relative position of the samples. This has shown to work well in Chapter 6.

Even though evidence for geochemical alteration and weathering has been spotted (Chapter 4 and 5), the obtained results are within the age ranges priory defined by siliceous and carbonate micorplancton. The results can therefore be considered as usefull, but may not be used to assign ages to radiolarian assemblages.

It has also been shown that the general aspect of the strontium isotope curve can have relevant consequences on the interpretations of the strontium isotope results, namely the problematic age determination when working close to a major trend change in the strontium isotope curve (Figure 51). This has been the case for the Turonian rocks studied in Chapter 4. During this study, it was also shown that a steep curve might provide a better resolution of the derived ages (Chapter 4 and 6), but on the contrary it can be misleading during interpretations. A general flat aspect of the strontium isotope curve can also influence the interpretation of data, as exact age determinations are not possible. Nevertheless, this study shows that an interpretation of results can be discussed by considering all the parameters that influence age assignments, which are the aspect of the curve, the precision of the strontium isotope ratios and the presence of contaminants.

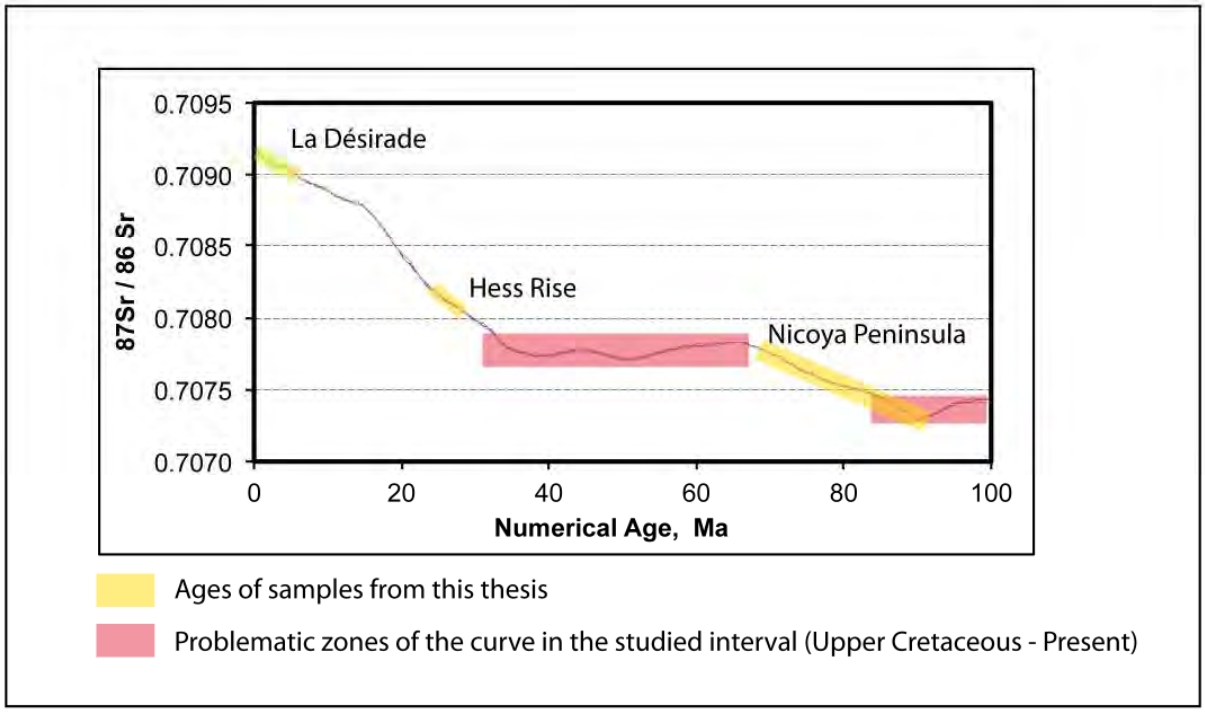

Figure 51: Strontium isotope ratio curve of the total age range of the samples studied in this thesis (Nicoya Peninsula - Upper Cretaceous; Hess Rise - Eocene - Oligocene; La Désirade - very late Miocene - Quaternary) (shown in yellow). The pink boxes highlight the problems of strontium isotope ratio dating due to the general aspect of the curve (multiple ages during Upper Cretaceous and multiple ages plus flat curve during late Cretaceous - late Eocene).

8. Annexes

APPENDIX I

Abstracts

SwissSed 2011 Fribourg

Late Cretaceous pelagic and arc-derived sedimentation in the S-Nicoya Peninsula, Costa Rica

Goran Andjic , Philippe J.N. Weber, Peter O. Baumgartner & Maria I. Sandoval Gutierrez

Institut de Géologie et Paléontologie, Anthropole-Dorigny, Université de Lausanne, 1015 Lausanne, Switzerland

Outcrops of the Nicoya area represent a collage of Mesozoic oceanic terranes that became assembled during the latest Cretaceous-Paleogene. Three units have been recognised: (1) the Nicoya Complex s. str., a highly deformed mélange of pre-Campanian plateau-like igneous rocks that extruded and intruded into Middle Jurassic to Santonian Ribbon Radiolarites; (2) the Matambu Terrane, a pre-Albian oceanic basement covered by hemipelagic/turbiditic Late Cretaceous sediments, and (3), the Manzanillo Terrane, a pre-Turonian oceanic basement covered by Coniacian-early Campanian arc-derived deep-water sequences, cropping out in the eastern Nicoya Peninsula and on the eastern side of the Nicoya Gulf. This study focuses on pre-Campanian pelagic/hemipelagic and arc-derived siliceous deposits cropping out in the southern Nicoya Peninsula. New paleontological and geochemical data suggest that these sequences are no older than Coniacian. The Late Cretaceous radiolarian-bearing siliceous mudstones discussed here imply that these outcrops belong to the late Turonian- early Campanian Berrugate Formation and not to the Albian Loma Chumico Formation as thought by previous authors. Green decimetric, fine-grained tuffaceous turbidites of dacitic to rhyolitic composition may represent a distal equivalent of the plurimetric mass flows of the type area of the Berrugate Formation in the Nicoya Gulf. Incompatible element patterns normalized to primitive mantle yield characteristic island arc signatures with relative Nb-,Ti-, and P- depletions and Pb-enrichments, identical to those from the Berrugate mass flows. The occurence of the Berrugate Formation in the southern part of the Nicoya Peninsula indicates that this area is in paleogeographic continuity with the Gulf area and belongs to the Manzanillo Terrane. The Manzanillo Terrane represents a paleo-fore-arc setting that receives sediments from a Late Cretaceous (Late Turonian- early Campanian) island arc, that predates the late Campanian-Maastrichtian Golfito island arc, and was located east of the modern Nicoya Gulf. This arc is probably buried beneath the Neogene- Recent volcanic arc.

Poster Presentation SwissSed 2011 Fribourg

$^{87}Sr/^{86}Sr$ and foraminiferal data, and sedimentology of the Late Miocene – Pliocene cyclic carbonates of La Désirade (Guadeloupe, France)

Weber Philippe J.N.*., Baumgartner-Mora Claudia*, Baumgartner Peter O.*

Institut de Géologie et de Paléontologie, Anthropole-Dorigny, Université de Lausanne, 1015 Lausanne, Switzerland

La Désirade is a small island located E of Grande Terre and Basse Terre, the main islands of the Guadeloupe Archipelago in the Lesser Antilles Arc (Fig. 1a,b). La Désirade is an "outer forearc high" located immediately west of the trench where Atlantic crust is presently subducted under the Caribbean Plate. La Désirade, together with Grande Terre and Marie-Galante form part of the "Calcareous Lesser Antilles" characterized by Neogene-Quaternary carbonate platforms that formed on top of an extinct and eroded Tertiary outer arc and have become subaerially exposed due to Late Pliocene-Quaternary uplift. So far, the Désirade "Limestone Table" (LT) has been considered as a Plio-Quaternary reefal deposit. However, the prominent feature of this up to 140 m thick formation is its rhythmic bedding of alternating marly / tuffaceous / dolomitic and winnowed bioclastic carbonate layers. To the west of the island "detrital offshore limestones" occur in the low-lying hills. They represent alternating offshore marls, tuffs amd channelled mass flow deposits.

We have studied the biochronology of both benthic and planktonic foraminifera and measured 87Sr/86Sr ratios of selected biogenic shells such as aragonitic gasteropods, echinoderms and foraminifera, chosen for their good preservation confirmed by SEM and cathodoluminescence, to avoid results affected by diagenesis.

Planktonic foraminifera of the "detrital offshore limestones" constrain its age to the late Miocene/early Pliocene (lower zone N19), while 87Sr/86Sr ratios clearly cluster in the latest Miocene.

For the LT $^{87}Sr/^{86}Sr$ ratios from the base of the section cluster at the base of the Pliocene, while the top the rhythmic carbonates reveals values corresponding to a late middle to late Pliocene age. The latter measurements were mostly done on benthic and planktonic formainifera and bulk rock samples. These ages permit to determine the approximate sedimentation rate of the LT and to constrain the Neogene vertical tectonics of the island. We have also dated Pleistocene terraces that are in an unconformable contact along paleocliffs with the Mio-Pliocene sediments and occur up to a few tens of m above present sea-level. The future work will consist in a new field campaign in order to search samples, which could give us more information on intermediate ages.

The history of the carbonates begins with the initial tectonic uplift and erosion of the Jurassic igneous basement of La Désirade, that must have occurred at latest in late Miocene times, when sea-level oscillated around a long term stable mean. The rhythmic deposition of the Désirade Limestone Table can be explained by synsedimentary subsidence in a context of rapidly oscillating sea-level due to precession-driven (19-21 kyr) glacio-eustatic sea-level changes during the latest Miocene/earliest Pliocene - middle Pliocene. Except for a so far undated thin reef cap present at the eastern edge of the LT, no other in-place reefal constructions have been observed in the LT. The "detrital offshore limestones" of western Désirade are interpreted as below wave base gravity deposits that accumulated beneath a steep fore-reef slope. They document the mobilization of carbonate material including Larger Foraminifera on an adjacent carbonate platform by storms and their gravitational emplacement as debris and grain flows. The provenance of both the reefal carbonate debris

and the tuffaceous components redeposited in the carbonates of La Désirade must be to the west, i. e. the carbonate platforms of Marie Galante and Grande Terre.
Pre-late Miocene uplift, Pliocene subsidence and late Pliocene-Peistocene emergence (up to 200 m) and westward tilting must be the result of repeated subduction of buoyant ridges along the Caribbean trench located just offshore La Désirade.

Caribbean Geological Congress (CGC) 2011, **Oral Presentation**

A slightly modified version of this presentation was given at the "Journée des jeunes chercheurs" at the University of Lausanne" in 2011 (no call for abstracts).

$^{87}Sr/^{86}Sr$-ratios, foraminifera and sedimentology of the Late Miocene – Pliocene cyclic carbonates of La Désirade (Guadeloupe, France)

Philippe, J.,N. Weber, Claudia Baumgartner-Mora, Peter O. Baumgartner.

Institut de Géologie et Paléontologie, Anthropole-Dorigny, Université de Lausanne, 1015 Lausanne, Switzerland
Philippe.Weber2@unil.ch

The “Limestone Table” (LT) of La Désirade has been considered as a Plio-Quaternary reefal deposit. However, the prominent feature of this <140 m thick formation is its rhythmic bedding of alternating marly/tuffaceous/dolomitic, and winnowed bioclastic carbonate layers. To the west of the island the “detrital offshore limestones” represent alternating offshore marls, tuffs and channelled mass flow deposits, that accumulated below wave base beneath a steep fore-reef slope. They document the mobilisation of carbonate material on an adjacent platform by storms and their gravitational emplacement. The provenance of both the reefal carbonate debris and the tuffaceous components must be to the west, i. e. Marie Galante and Grande Terre.
Planktonic foraminifera of the “detrital offshore limestones” give a latest Miocene/early Pliocene age (lower zone N19), while $^{87}Sr/^{86}Sr$-ratios cluster in the latest Miocene. For the LT $^{87}Sr/^{86}Sr$-ratios from the base of the section cluster in the earliest Pliocene, while the top gives a late middle to late Pliocene age. These ages constrain the Neogene vertical tectonic movements of the island. We have also dated Pleistocene terraces that are in an unconformable contact along paleocliffs with the Mio-Pliocene sediments.
The history of the carbonates begins with initial tectonic uplift and erosion of the Jurassic igneous basement. It occurred before late Miocene times, when sea-level oscillated around a long term stable mean. The rhythmic deposition of the LT can be explained by synsedimentary subsidence during rapidly oscillating, precession-driven (19-21 kyr) glacio-eustatic sea-level in the latest Miocene/earliest Pliocene-middle Pliocene. Except for a thin reef cap at the eastern edge of the LT, no in-place reefal constructions occur in the LT. Pre-late Miocene uplift, Pliocene subsidence and late Pliocene-Pleistocene emergence (up to 200 m above modern sea-level), and westward tilting must be the result of repeated subduction of buoyant ridges along the Caribbean trench located offshore La Désirade.

Proceedings of 13th INTERRAD - A conference on Fossil and Recent Radiolarians

http://www.ugr.es/~lodogher/InterRad13/Proceedings%2013th%20Interrad.pdf

Recent radiolarian distribution in the Equatorial Eastern Pacific

Erika BALDESSIN1, Peter O. BAUMGARTNER1, Philippe WEBER1 & Marc PICHERAL2
1) Institut de Géologie et Paléontologie, Université de Lausanne, Bâtiment Anthropole-Dorigny, CH 1015 Lausanne, Switzerland.
erika.baldessin@unil.ch
peter.baumgartner@unil.ch
philippe.weber.2@unil.ch
2) CNRS/UPMC, UMR 7093, Laboratorie d'Océanographie de Villefranche, Observatoire Océanologique, La Darse F-06234, Villefranche-sur-Mer Cedex 4, France.
picheral@obs-vlfr.fr

The Equatorial Pacific Ocean is characterized by a complex current situation (Fig. 1): Off Nicaragua and Costa Rica, the incoming Equatorial Counter current (ECC) turns north to become North Equatorial Current (NEC) under the influence of trade winds that cross the Central American Isthmus. Along the coasts of Peru and Ecuador the northward directed Peru Current (PC) turns westwards to become the South Equatorial Current (SEC) in the vicinity of the Galápagos Islands. These different current systems generate upwelling that induces high surface productivity and turn the region into a very interesting place to study radiolarian faunal distribution (Molina-Cruz, 1977). The objective of the work is to characterize radiolarian assemblages, as complete as possible, in surface sediments under each water mass by a multivariate taxon-quantitative study.
During summer 2010, the Geomar research expedition SO208 PLUMEFLUX, on board the German research vessel Sonne, covered this specific area, allowing to sample surface sediments directly from the ocean floor. The first Leg sailed in the region off Costa Rica and Nicaragua, while Leg 2 took place near Galápagos Islands (Fig. 1). Sediments were collected with a multicorer MUC (Fig. 2) which sampled the top 30 cm of bottom sediments. Bulk sediment samples were collected at various depths in the cores. In the laboratory these subsamples were treated with diluted HCl and H_2O_2 to remove carbonate and organic matter, respectively, and fauna slides were made with the whole residue. The fauna slides were scanned with the Olympus VS110 system that allows scanning of entire fauna slides (hundreds of individual images are taken at 2–3 images/s by a CCD camera and stitched together in real time), including a Z-stack for extended depth of focus. Entire slides make up to 400 megapixels. For final processing we used a pixel size of about 1.4 µm. Whole images were analysed in Image J with ZooProcess to obtain thumbnails of individual objects. The Plankton Identifier (PkID) software, developed by the Observatoire océanologique in Villefranche-sur-Mer (Gorsky et al., 2010), allows a semi-automatic classification of objects in the slides. A learning set is produced by manual validation which allows to optimize prediction of fossil groups. Mulivariate statistics will be applied to the results of this image analysis. This project is still going on. More results will be available in 2012.

References

• Gorsky, G., Ohman, M.D., Picheral, M., Gasparini, S., Stemmann, L., Romagnan, J.B., Cawood, A., Pesan, S., Garcia-Coman, C. & Prejger, F. 2010. Digital zooplankton analysis using the ZooScan integrated system. *Journal of Plankton Research*, 32(3): 285–303.

• Molina-Cruz, A. 1977. Radiolarian assemblages and their relationship to the oceanography of the subtropical S.E. Pacific. *Marine Micropaleontology*, 2(4): 315–352.

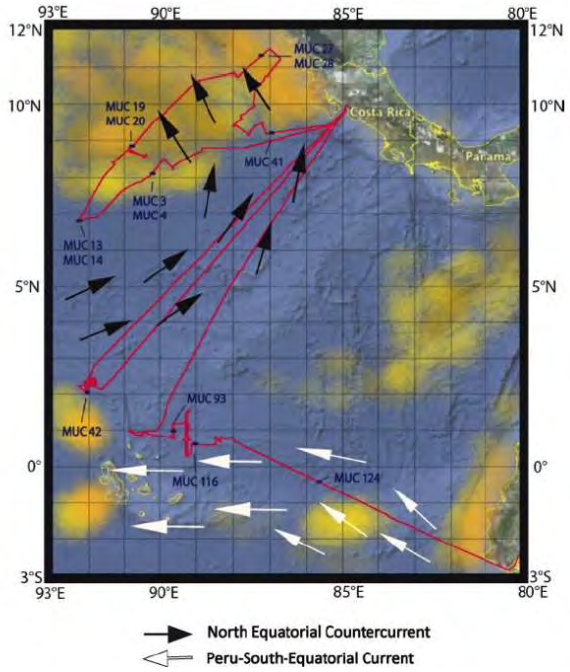

Figure 1. Track and localisation of the sampling stations during the expedition Sonne 208.

Figure 2. TV-Multicorer MUC.

Late Cretaceous Radiolaria of the Berrrugate Formation (Nicoya Peninsula, Costa Rica): Contemporaneous arc volcanism and plateau formation in terranes off the W-edge of the Caribbean Large Igneous Province.

Goran ANDJIC, Peter O. BAUMGARTNER, Philippe WEBER, Claudia BAUMGARTNER-MORA & María SANDOVAL-GUTIÉRREZ

Institut de Géologie et Paléontologie, Université de Lausanne, Bâtiment Anthropole-Dorigny, CH 1015 Lausanne, Switzerland.

goran.andjic@unil.ch, peter.baumgartner@unil.ch, philippe.weber.2@unil.ch , claudia.baumgartner@unil.ch, mariaisabel.sandovalgutierrez@unil.ch

Outcrops of the Nicoya Peninsula and Gulf area represent a collage of Mesozoic oceanic terranes that became assembled during the latest Cretaceous–Paleogene along the western edge of the Caribbean Plate (Fig. 1). Three units have been recognised (Flores, 2006; Bandini et al., 2008): (1) the Nicoya Complex s. str., a highly deformed mélange of pre-Campanian plateau-like igneous rocks that extruded and intruded into Middle Jurassic to Santonian Ribbon Radiolarites; (2) the Matambu Terrane, a pre-Albian oceanic basement covered by hemipelagic/turbiditic Late Cretaceous sediments, and (3) the Manzanillo Terrane, a pre-Turonian oceanic basement intruded by the Turonian Tortugual picritic suite. The Manzanillo Terrane is regarded as the westernmost outcrop of the Caribbean Large Igneous Province s.s (CLIP *s.s.*) is covered by Coniacian–early Campanian arc-derived deep-water sequences, cropping out in the eastern Nicoya Peninsula and on the eastern side of the Nicoya Gulf. This formation contains diverse and well-preserved radiolarian assemblages presented here. We studied hemipelagic, tuffitic siliceous mudstones of the lower Berrugate Formation in the southeast Nicoya Peninsula (Fig. 1). Eight samples from 4 different sections yielded moderately to well-preserved assemblages that contain several tens of morphotypes. Since the biochronology of the Late Cretaceous is not yet resolved on a global scale, we have used stacked ranges from several authors for each species to obtain the possible “full” range. The concurrent range of all species in each sample defines its biochronologic age. Most samples contain several species that have their first appearance in the Coniacian, such as Alievum gallowayi, A. praegallowayi, Theocampe sallilum, and Pseudoaulophacus floresensis. On the other hand, some samples seem to be restricted to the Coniacian–early Santonian by the presence of A. praegallowayi, while others may range up to the Late Santonian by the presence of Crucella cachensis, Hemicryptocapsa polyhedra, and Praeconocaryomma californiaensis. These radiolarian ages, as well as the presence of Globotruncana calcarata in the conformably overlying Piedras Blancas pelagic limestone Formation indicate, that the studied hemipelagic, arc-derived sediments belong to the Berrrugate Formation and range in age from the Coniacian to the early–middle Campanian. Earlier authors included the studied outcrops off S-Nicoya with the Albian Loma Chumico Formation (Calvo & Bolz, 1994). The assignment of the sampled sections in the southern Nicoya Peninsula to the Berrugate Formation is also based on lithological and geochemical arguments. We measured several sections that show green tuffaceous/siliceous turbidites similar to those described by Flores (2006). These green decimetric beds of dacitic to rhyolitic composition correspond to fine-grained tuffaceous turbidites, which may represent a distal equivalent of the plurimetric mass flow beds outcropping in the type area of the Berrugate Formation in the Nicoya Gulf.

Incompatible element patterns normalized to primitive mantle yield characteristic island arc signatures with relative Nb-,Ti-, and P- depletions and Pb-enrichments, are identical to those from the Berrugate Formation mass flows (Flores 2006). The occurence of the Berrugate Formation in the southern part of the Nicoya Peninsula indicates that this area is in paleogeographic continuity with the Gulf area and belongs to the Manzanillo Terrane. The Manzanillo Terrane represents a palaeo fore-arc setting that is affected by a Late Cretaceous (Coniacian–early Campanian) island arc source that predates the late Campanian–Maastrichtian Golfito island arc (Buchs et al., 2010) and was located east of the modern Nicoya Gulf. This island arc is probably buried beneath the Neogene–Recent volcanic arc. The "Berrugate" arc represents the oldest island arc associated with the western edge of the CLIP *s.s.* Very similar radiolarian assemblages recovered from plateau-like settings (e.g. Nicoya Complex *s.s.*) underline the synchronicity of ongoing plateau formation and island arc volcanism in different terranes. The chronology of island arc development along the western edge of the CLIP *s.s.* suggests that the subduction beneath it started during the Turonian?–Coniacian, in its northwestern part ("Berrugate" arc). Then, the subduction zone progressively propagated further to the SE (Golfito, Azuero, Darien).

References

• Bandini, A.N., Flores, K., Baumgartner, P.O., Jackett, S.-J. & Denyer, P. 2008. Late Cretaceous and Paleogene Radiolaria from the Nicoya Peninsula, Costa Rica: a tectonostratigraphic application. *Stratigraphy*, **5**: 3–21.

• Buchs, D.M., Arculus, R.J.. Baumgartner, P.O., Baumgartner-Mora, C. & Ulianov, A. 2010. Late Cretaceous arc development on the SW margin of the Caribbean Plate: Insights from the Golfito, Costa Rica, and Azuero, Panama, complexes. *Geochemistry, Geophysics, Geosystems*, **11**: 1–35.

• Calvo, C. & Bolz, A., 1994. Der älteste kalkalkaline Inselbogen-Vulkanismus in Costa Rica: Marine Pyroklastika der Formation Loma Chumico (Alb bis Campan). *Pro'l* **7**: 235–264.

• Flores, K. 2006. Jurassic–Late Cretaceous oceanic crustal terranes and arc-derived sediments south Chortis Block (NE Nicaragua to NW Costa Rica). Preliminary results of two key areas: Nicoya Peninsula and Siuna District. Unpublished DEA thesis, University of Lausanne 107 p.

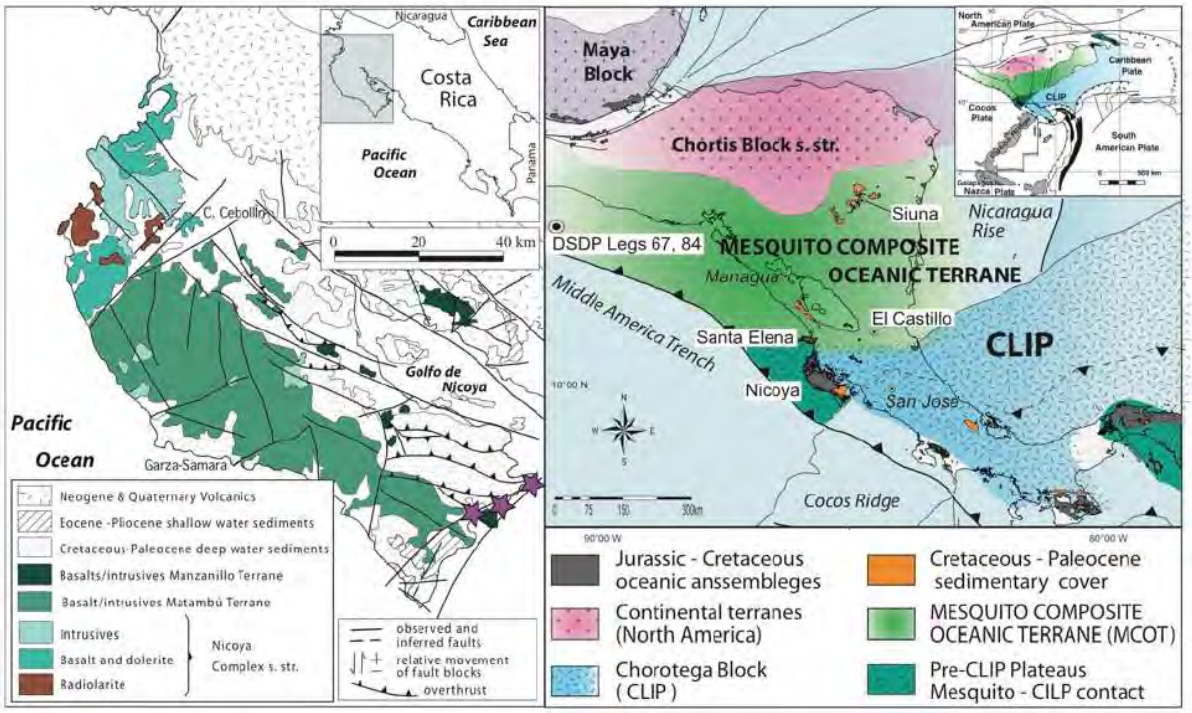

Figure 1. Left: Geologic map of the Nicoya Peninsula indicating the major geologic units and sample localities (stars). Right: Tectonic map of the W-Caribbean Plate.

European Geosciences Union General Assembly 2012, Vienna

87Sr/86Sr-ratios, foraminiferal data and sedimentology of the Latest Miocene – Pliocene cyclic carbonates of La Désirade (Guadeloupe, France)

Philippe, J.,N. Weber, Claudia Baumgartner-Mora, Peter O. Baumgartner

Institut de Géologie et Paléontologie, Anthropole-Dorigny, Université de Lausanne, 1015 Lausanne, Switzerland

La Désirade is a small island located E of Grande Terre and Basse Terre, the main islands of the Guadeloupe Archipelago in the Lesser Antilles Arc. La Désirade is an "outer forearc high" located immediately west of the trench where Atlantic crust is presently subducted under the Caribbean Plate.

The "Limestone Table" (LT) of La Désirade has been considered as a Plio- Quaternary reefal deposit. However, the prominent feature of this <140 m thick formation is its rhythmic bedding of alternating marly/tuffaceous/dolomitic, and winnowed bioclastic carbonate layers. To the west of the island the "detrital offshore limestones" represent alternating offshore marls, tuffs and channelled mass flow deposits, that accumulated below wave base beneath a steep fore-reef slope. They document the mobilisation of carbonate material on an adjacent platform by storms and their gravitational emplacement. The provenance of both the reefal carbonate debris and the tuffaceous components must be to the west, i.e. Marie Galante and Grande Terre.

We have studied the biochronology of both benthic and planktonic foraminifera and measured 87Sr/86Sr ratios of selected biogenic shells such as aragonitic gasteropods, corals, echinoderms and foraminifera. Preservation has been controlled by SEM, cathodoluminescence, carbon/oxygen isotopes and XRF to avoid diagenetically altered samples.

Planktonic foraminifera of the "detrital offshore limestones" give a latest Miocene/early Pliocene age (lower zone N19), while $^{87}Sr/^{86}Sr$ ratios cluster in the latest Miocene-earliest Pliocene, depending on the calibration applied. For the LT $^{87}Sr/^{86}Sr$ ratios from the base of the section cluster in the earliest Pliocene, while the top gives a late middle to late Pliocene age. These ages constrain the Neogene vertical tectonic movements of the island. We have also dated Pleistocene terraces and fringing reefs that are in an unconformable contact along paleocliffs with the Mio-Pliocene sediments.

In the lower unit of the LT, sedimetary environments alternate between below wave base, muddy carbonates documenting glacioeustatic highstads, and wavebedded, winnowed bioclastic carbonates representing lowstands. In the upper LT unit synsedimentary, tectonic subsidence must have decelerated, resulting in a different sedimentation pattern: Bioclastic limestones probably represent highstand separated by emersion/erosion surfaces resulting from lowstands. A cyclostratigraphic study in the LT has been attempted, but gave unreliable results so far. Erosion/non-deposition indicate that the depositional cycles of the LT are unreliable recorders of both the frequency and the amplitude of orbitally driven sea-level fluctuations.

The history of the carbonates begins with initial tectonic uplift and erosion of the Jurassic igneous basement. It occurred before late Miocene times, when sealevel oscillated around a long term stable mean. The rhythmic deposition of the LT can be explained by synsedimentary subsidence during rapidly oscillating, precession-driven (19-21 kyr) glacio-eustatic sea-level in the latest Miocene/earliest Pliocene-late Pliocene. Except for a thin reef cap at the eastern edge of the LT, no in-place reefal constructions occur in the LT.

Unfortunatley, samples from the reef cap were all severely altered and no 87Sr/86Sr ratios were measured. Pre-late Miocene uplift, Pliocene subsidence and late Pliocene-Pleistocene emergence (up to 200 m above modern sealevel), and westward tilting must be the result of repeated subduction of buoyant ridges along the Caribbean trench located offshore La Désirade.

APPENDIX II

GEOCHEMICAL ANALYSES

Lab N.	Sample	low	high	$^{87}Sr/^{86}Sr$	2 S.E.	$^{87}Sr/^{86}Sr$ FC		Locality
Sr5275	PA-08-019 I	0.707528	0.707615	0.707560	0.000086	0.707572	90 cycles	Quebrada Pavas
Sr5276	PA-08-019 II	0.707706	0.707764	0.707723	0.000058	0.707735	160 cycles	Quebrada Pavas
Sr5277	PA-08-016 I	0.707700	0.707743	0.707709	0.000044	0.707721	200 cycles	Quebrada Pavas
Sr5278	PA-08-016 II	0.707533	0.707690	0.707600	0.000156	0.707612	80 cycles	Quebrada Pavas
Sr5281	VU-08-022 I	0.707170	0.707348	0.707247	0.000178	0.707259	160 cycles	Nambi
Sr5282	VU-08-022 II	0.707124	0.707311	0.707206	0.000188	0.707217	60 cycles	Nambi
Sr5284	VU-08-022 IV	0.707466	0.707514	0.707478	0.000048	0.707490	200 cycles	Nambi
Sr5285	VU-08-022 V	0.707542	0.707650	0.707584	0.000108	0.707596	120 cycles	Nambi
Sr5286	VU-08-022 VI	0.707329	0.707369	0.707337	0.000040	0.707349	200 cycles	Nambi
Sr5337	PA-08-021 I	0.707647	0.707661	0.707652	0.000014	0.707654	200 cycles	Piedras Blancas
Sr5338	PA-08-021 II	0.707654	0.707661	0.707656	0.000008	0.707657	200 cycles	Piedras Blancas
Sr5339	PA-08-021 III	0.707658	0.707662	0.707659	0.000004	0.707660	200 cycles	Piedras Blancas
Sr5404	1-22-08-02 I	0.707302	0.707313	0.707295	0.000012	0.707307	200 cycles	Nambi
Sr5405	1-22-08-02 II	0.707321	0.707325	0.707312	0.000004	0.707323	200 cycles	Nambi
Sr5406	1-22-08-02 III	0.707347	0.707352	0.707337	0.000004	0.707349	200 cycles	Nambi
Sr5407	3-26-06-04 I	0.707293	0.707299	0.707284	0.000006	0.707296	200 cycles	Nambi
Sr5408	3-26-08-04 II	0.707282	0.707330	0.707294	0.000048	0.707306	200 cycles	Nambi
Sr5409	Alctz I	0.707280	0.707292	0.707274	0.000012	0.707286	200 cycles	Alcatraz
Sr5410	Alctz II	0.707307	0.707323	0.707303	0.000016	0.707315	200 cycles	Alcatraz
Sr5411	Obessu	0.709046	0.709051	0.709037	0.000004	0.709049	200 cycles	Desirade
Sr5412	Upa. Des.	0.709000	0.709004	0.708990	0.000004	0.709002	200 cycles	Desirade
Sr5413	Animas	0.707661	0.707666	0.707652	0.000004	0.707664	200 cycles	Desirade
Sr5414	Oursin	0.708990	0.708994	0.708980	0.000004	0.708992	200 cycles	Desirade
Sr5415	Oursin	0.709104	0.709110	0.709095	0.000006	0.709107	200 cycles	Desirade

Table 10: Strontium isotope ratio analyses, Costa Rica and La Désirade (Geneva Laboratory).

Lab N.	Sample	low	high	$^{87}Sr/^{86}Sr$	2 S.E.	$^{87}Sr/^{86}Sr$ FC		Locality
Sr5416	1-22-08-02 I	0.707320	0.707327	0.707311	0.000006	0.707323	200 cycles	Nambi
Sr5417	1-22-08-02 II	0.707249	0.707258	0.707241	0.000008	0.707253	200 cycles	Nambi
Sr5418	1-22-08-02 III	0.707315	0.707326	0.707308	0.000012	0.707320	200 cycles	Nambi
Sr5419	6-23-08-02 I	0.707705	0.707708	0.707694	0.000004	0.707706	200 cycles	Qubrada Pavas
Sr5420	6-23-08-02 II	0.707697	0.707701	0.707687	0.000004	0.707699	200 cycles	Qubrada Pavas
Sr5421	2-24-08-02 I	0.707294	0.707303	0.707286	0.000008	0.707298	200 cycles	Nambi
Sr5422	2-24-08-02 II	0.707298	0.707303	0.707289	0.000006	0.707300	200 cycles	Nambi
Sr5423	2-24-08-02 III	0.707298	0.707312	0.707293	0.000014	0.707305	200 cycles	Nambi
Sr6039	DES025I	0.709077	0.709080	0.709079	0.000002	0.709076	200 cycles	Desirade
Sr6040	DES025II	0.709076	0.709080	0.709078	0.000004	0.709075	200 cycles	Desirade
Sr6041	DES029I	0.709069	0.709072	0.709070	0.000004	0.709067	200 cycles	Desirade
Sr6042	DES029II	0.709074	0.709081	0.709078	0.000006	0.709075	200 cycles	Desirade
Sr6043	PNI	0.709042	0.709047	0.709045	0.000006	0.709042	200 cycles	Desirade
Sr6044	DES030I	0.709050	0.709059	0.709055	0.000008	0.709052	200 cycles	Desirade
Sr6045	DES035I	0.709048	0.709052	0.709050	0.000004	0.709047	200 cycles	Desirade
Sr6046	DES035II	0.709048	0.709051	0.709050	0.000004	0.709047	200 cycles	Desirade
Sr6047	DES035III	0.709048	0.709052	0.709050	0.000004	0.709047	200 cycles	Desirade
Sr6048	4602I	0.709041	0.709045	0.709043	0.000004	0.709040	200 cycles	Desirade
Sr6049	4602II	0.709014	0.709020	0.709017	0.000006	0.709014	200 cycles	Desirade
Sr6050	J3-3	0.709053	0.709057	0.709055	0.000004	0.709052	200 cycles	Desirade

Table 11: Strontium isotope ratio analyses, Costa Rica and La Désirade (Geneva Laboratory).

Lab N.	Sample	low	high	$^{87}Sr/^{86}Sr$	2 S.E.	$^{87}Sr/^{86}Sr$ FC		Locality
Sr6247	CrM0I	0.709080	0.709085	0.709083	0.000002	0.709059	200 cycles	Desirade
Sr6248	CRM0II	0.709088	0.709096	0.709092	0.000008	0.709068	200 cycles	Desirade
Sr6249	RM0I	0.709164	0.709172	0.709168	0.000008	0.709144	200 cycles	Desirade
Sr6250	RM0II	0.709167	0.709173	0.709170	0.000006	0.709146	200 cycles	Desirade
Sr6251	BBMA2I	0.709210	0.709220	0.709215	0.000010	0.709191	200 cycles	Desirade
Sr6252	BBMA2II	0.709199	0.709205	0.709202	0.000006	0.709178	200 cycles	Desirade
Sr6253	GrAEI	0.709053	0.709056	0.709055	0.000004	0.709031	200 cycles	Desirade
Sr6254	GrAEII	0.709052	0.709056	0.709054	0.000004	0.709030	200 cycles	Desirade
Sr6255	BSJI	0.709035	0.709039	0.709037	0.000004	0.709013	200 cycles	Desirade
Sr6256	BSJII	0.709047	0.709050	0.709048	0.000004	0.709025	200 cycles	Desirade
Sr6257	D4043AI	0.709192	0.709201	0.709196	0.0000010	0.709172	200 cycles	Desirade
Sr6258	D4043AII	0.709185	0.709189	0.709187	0.000004	0.709163	200 cycles	Desirade

Table 12: Strontium isotope ratio analyses, La Désirade (Geneva Laboratory).

Lab N.	Sample	low	high	$^{87}Sr/^{86}Sr$	2 S.E.	$^{87}Sr/^{86}Sr$ FC		Locality
Sr5581	AC 04 01	0.709102	0.709134	0.709106	0.000032	0.709118	200 cycles	Desirade
Sr5582	AC 04 02	0.709138	0.709151	0.709132	0.000012	0.709144	200 cycles	Desirade
Sr5583	AC 04 03 II	0.709017	0.709037	0.709015	0.000020	0.709027	200 cycles	Desirade
Sr5584	AC 04 03 II	0.709073	0.709090	0.709069	0.000018	0.709081	200 cycles	Desirade
Sr5585	AC 04 04	0.708966	0.708972	0.708957	0.000006	0.708969	200 cycles	Desirade
Sr5586	AC 04 05	0.709004	0.709014	0.708997	0.000010	0.709009	200 cycles	Desirade
Sr5587	AC 04 06	0.709039	0.709048	0.709031	0.000010	0.709043	200 cycles	Desirade
Sr5588	Panama	0.707305	0.707336	0.707309	0.000032	0.707321	200 cycles	Rio Güerito

Table 13: Strontium isotope ratio analyses, La Désirade and Panama (Geneva Laboratory).

Lab N.	Sample	$^{87}Sr/^{86}Sr$	2SE	Locality
U1	241-15.5 (1)	0.707943	0.000003	Hess
U2	241-15.5 (2)	0.707974	0.000003	Hess
U3	CoySrInoS	0.707343	0.000003	Coyolito
U4	MUC13SS1	0.707349	0.000003	Murcielago
U5	241-18.5 (1)	0.707852	0.000003	Hess
U6	241-18.5 (2)	0.707849	0.000004	Hess
U7	263.2S1	0.707649	0.000003	Playa Camaron
U8	263.2S2	0.707606	0.000004	Playa Camaron
U9	241-19.5 (1)	0.708151	0.000004	Hess
U10	241-19.5 (2)	0.709142	0.000004	Hess
U11	CM314I	*0.707159*	*0.000007*	Playa Mangle
U12	CM314II	*0.706909*	*0.000007*	Playa Mangle
U13	245-3 (1)	0.708085	0.000003	Hess
U14	245-3 (2)	0.708272	0.000003	Hess
U15	CM373I	0.707767	0.000004	Damas
U16	CM373II	0.707759	0.000004	Damas
U17	249-1-3 (1)	*0.707863*	*0.000016*	Hess
U18	249-1-3 (2)	0.707780	0.000004	Hess
U19	CM356I	0.707718	0.000003	Fila de Cal
U20	CM356II	0.707715	0.000003	Fila de Cal
V1	1572I	0.707729	0.000003	Punta Cuevas
V2	1572II	0.707717	0.000003	Punta Cuevas
V3	263-1 (1)	0.708198	0.000003	Hess
V4	263-1 (2)	0.708240	0.000003	Hess
V5	PA0821B	0.707585	0.000004	Piedras Blancas
V6	VU0822B	0.706550	0.000003	Nambi
V7	263-2 (1)	0.707969	0.000003	Hess
V8	263-2 (2)	0.707940	0.000004	Hess
V9	EF12I	0.707460	0.000004	St. Barth

Lab N.	Sample	$^{87}Sr/^{86}Sr$	2SE	Locality
V10	EF12II	0.707465	0.000002	St. Barth
V11	263-8 (1)	0.708175	0.000003	Hess
V12	263-8 (2)	0.708324	0.000003	Hess
V13	CM316I	0.706879	0.000003	Mangle
V14	CM316II	0.707862	0.000004	Mangle
V15	263-9 (1)	0.708009	0.000003	Hess
V16	263-9 (2)	0.707968	0.000003	Hess
V17	1571I	0.707735	0.000003	Malpais
V18	1571II	0.707698	0.000004	Malpais
V19	241-24.5I	0.709183	0.000004	Hess
V20	241-24.5II	0.709188	0.000003	Hess

Table 14: Strontium isotope ratio analyses, Hess Rise (Kiel Laboratory).

Sample M81-	$\delta^{18}C$ **VPDB**	$\delta^{18}O$ **VPDB**	
265-1	2.0	1.6	
263-9	1.7	0.4	
	1.7	2.7	
263-9	1.7	0.0	
263-9	1.5	0.0	
	1.6	0.4	
265-2	1.6	1.6	
265-3	1.6	1.9	
263-8	1.8	2.1	
	1.6	1.6	
263-8	1.7	1.9	
241-27.5	-3.3	-2.7	too small
	-3.7	-2.2	
263-1	1.5	0.2	
263-1	1.4	0.2	
	1.6	0.5	
263-2	1.7	-0.5	
263-2	1.7	-0.8	
242-1.8	2.7	1.1	
	2.7	2.9	
242-1.8	2.7	2.0	
242-1.6	1.7	2.9	
242-1.6	1.6	3.1	
263-4	2.2	4.2	
249-1-3/3	2.3	-2.2	
249-1-3/3	2.5	-1.9	
249-8 TS 3/3	2.1	-1.8	
249-8 TS 3/3	2.1	-1.9	
	2.1	-2.5	too small
249-7-2/3	2.5	-2.1	
249-1 M3	2.5	-2.1	
249-1 M3	2.5	-2.1	

Sample M81-	$\delta^{18}C$ **VPDB**	$\delta^{18}O$ **VPDB**	
249-8 TS 1/3	2.3	-1.5	
249-8-TS-1/3	2.2	-1.9	
	1.9	-2.6	too small
249-11	2.3	-1.6	
249-11	2.4	-1.5	
249-2-2/2	2.3	-2.5	
249-2-2/2	2.3	-2.5	
249-7-1/3	2.2	-1.9	
	2.2	-2.2	too small
249-2-1/2	2.3	-2.5	
249-2-1/2	2.3	-2.6	
249-7-2/3	2.2	-2.0	
249-7-3/3	2.3	-1.9	

Table 15: Stable isotope analyses, Hess Rise

Sample	$\delta^{18}C$ **VPDB**	$\delta^{18}O$ **VPDB**
STD1	1.9	-1.7
STD2	2.0	-1.6
CoySrInoS	2.1	-4.9
CoySrInoSS	1.5	-5.0
263.2S1	1.5	-3.3
263.2SS1	1.8	-3.5
263.2S2	1.9	-3.7
263.2SS2	1.9	-3.7
263.2B1	1.9	-3.8
263.2B2	2.2	-2.9
CRNi02S	-0.2	-4.1
CRNi02SS	0.0	-2.7
PA-08-022-I	2.7	-2.8
STD3	2.0	-1.7
MUC13S1	3.4	-4.2
MUC13SS1	3.8	-4.0
VU-08-022-I	1.8	-5.9
VU-08-022-IV	2.0	-5.6
VU-08-022-V	1.8	-5.8
VU-08-022-VII	1.7	-5.4
VU-08-022-B	1.3	-7.1
PA-08-022-II	2.6	-2.5
PA-08-022-III	2.5	-2.4
PA-08-022-B	2.3	-3.3
STD4	2.0	-1.8
1-22-08-02-S	0.0	-5.4

Table 16: Stable isotope analyses, Hess Rise, Costa Rica